2016-2

Daylighting and Thermo-Electrical performance of an Autonomous Suspended Particle Device Evacuated Glazing

Aritra Ghosh
Technological University Dublin

Daylighting and thermo-electrical performance of an autonomous suspended particle device evacuated glazing

Aritra Ghosh BTech. MSc

The thesis submitted for the degree of Doctor of Philosophy

Supervisors: Prof Brian Norton and Prof Aidan Duffy

School of Civil and Structural Engineering

Dublin Institute of Technology

February 2016

Abstract

Suspended particle device (SPD) glazing is an AC powered switchable glazing. PV powered SPD evacuated (vacuum) glazing was proposed with the potential of reducing the heating demand, cooling demand and artificial lighting demand of a building.

To achieve an autonomous SPD vacuum glazing, semi empirical simulation and outdoor characterisation was explored in this thesis. Transmission of SPD glazing (area 0.058 m^2) varied from 5% when opaque to 55% when transparent in the presence of 110 V, 0.07 W AC supply was characterised in outdoor test cell in Dublin. The SPD glazing has variable spectral transmission in the presence of variable applied voltage, with high transmission in the near infrared between 700 to 1100 nm. 30% transparent SPD glazing in a particular room configuration provided a constant 4% daylight factor with acceptable glare.

Use of a 0.34 m^2 vertical photovoltaic (PV) panel was investigated to self-power (autonomous) an SPD glazing system. The dynamic behaviour of the PV-powered SPD glazing gave good switching times that would maintain occupant comfort. It was observed that SPD material inside a glazing unit absorbs solar radiation giving a high glazing surface temperature. For this SPD glazing alone, the overall heat transfer coefficient (U-value) was found to be 5.9 W/m^2K typical of a single glazing. A SPD switchable double-glazing, was found to have a *U*-value of 1.99 W/m^2K. A vacuum glazing was attached to the SPD glazing was found to have a *U*-value of 1.14 W/m^2K.

Declaration

I certify that this thesis which I now submit for examination for the award of PhD, is entirely my own work and has not been taken from the work of others, save and to the extent that such work has been cited and acknowledged within the text of my work. This thesis was prepared according to the regulations for postgraduate study by research of the Dublin Institute of Technology and has not been submitted in whole or in part for another award in any other third level institution. The work reported on in this thesis conforms to the principles and requirements of the DIT's guidelines for ethics in research.

DIT has permission to keep, lend or copy this thesis in whole or in part, on condition that any such use of the material of the thesis be duly acknowledged.

Signature _____ Date _____

Dedicated to my Parents, sisters

Acknowledgments

First I would like to take the opportunity and express my sincerest appreciation to my supervisors Prof Brian Norton and Prof Aidan Duffy for all of their endless support, knowledge and encouragement throughout the past four years.

I would like to extend my gratitude to all staff members in the FOCAS Research Institute, School of Civil and Structural Engineering of DIT and Dublin Energy Lab for their full cooperation and help, and big thanks to FOCAS for proving excellent research facilities.

I want to thank my loving parents (Uma Sankar Ghosh and Jyotsna Ghosh) and sisters (Chandreyee Mallick and Atreyee Dutta) who have supported and encouraged me in whatever I have chosen to do. I remain grateful to Prof Tapas Mallick, Dr Partha Dutta, Prof Gauri Sankar Ghosh and Dr Malini Sen for their endless support.

Special thanks to Sanchari Konar for her unconditional support, love and encouragement at times when things were crazy.

I would like to say a huge thanks to Dr Rajiv Kumar Mishra, Dr Subhash Chandra, Dr Hind Ahmed, Vivek Tomar, Sukrat Kashyap, Dr Shyam for their technical and non-technical advice and assistance.

I would like to acknowledge the Graduate Research Education Programme of the Higher Education Authority, for providing PhD Scholarship

Finally, this work would not have been possible without the help, great support and encouragement of all my friend and colleagues. Special thanks go to, Moutrisha Das, Ananya Hazra, Shreya Roy Chowdhury, Piyali Roy ,Vanessa Araujo Leao Moraes, Hoda Akbari, Iftekhar Hussain, Sabade Gul , Minna Khalid , Arghyadip Ghosh, Sayantani Ghosh, and Itziar Moya Ramos.

List of abbreviations

AC	Alternating current
BGI	British glare index
DC	Direct current
DF	Daylight factor
DGI	Daylight glare index
DGP	Daylight glare probability
DOD	Depth of discharge
DSSC	Dye sensitized solar cell
EC	Electrochromic
EU	European Union
IEA	International energy association
LC	Liquid Crystal
LSC	Luminescent solar concentrator
LPSP	Loss of power supply probability
NZEB	Net zero energy building
NIR	Near infra radiation
SHGC	Solar heat gain coefficient
SE	Transmitted solar energy through glazing
SOC	State of charge
SPD	Suspended particle device
SPD-double	Suspended particle device –double
MoWiTT	Mobile Window Thermal Test facility

OPV	Organic photovoltaic
PASSYS	Passive Solar Systems and Component Testing
PCM	Phase change material
PV	Photovoltaic
UDI	Useful daylight index
UGR	Unified glare index
U value	Overall heat transfer coefficient
USA	United States of America
UV	Ultraviolet
VCP	Visual comfort probability

Table of contents

List of figures

List of tables

Nomenclature

A_{wall}	Total area of interior surface of test cell (m^2)
A_w	Aperture area of window (m^2)
A_i	Anisotropy index
C_{air}	Heat capacity of air (kJ/kgK)
C_{water}	Heat capacity of water (kJ/kgK)
DF	Daylight factor
DGI	Daylight glare index
DGI_N	New daylight glare index
d_g	Thickness of glazing pane (m)
E_v	Vertical plane external illuminance (lux)
$E_{v,neag}^{in}$	Vertical illuminance near the glazing (lux)
$E_{V,win}^{in}$	Glazing illuminance (lux)
$E_{V,adp}^{in}$	Adaptation illuminance (lux)
F1	Circumsolar brightening coefficient
F2	Horizon brightening coefficient
GI	Glare index
h_0	Heat transfer coefficient from glazing outer surface to ambient (W/m^2K)
h_i	Heat transfer coefficient from glazing inside surface to inside test cell (W/m^2K)
h_{tg}	Conductive heat transfer coefficient glazing panes (W/m^2K)

$I_{h,g}$	Horizontal global solar radiation (W/m^2)
$I_{h,d}$	Horizontal diffuse solar radiation (W/m^2)
$I_{h,b}$	Horizontal beam solar radiation (W/m^2)
I_{extra}	Extraterrestrial solar radiation (W/m^2)
I_v	Vertical plane global solar radiation (W/m^2)
I_{pv}	Photovoltaic current (A)
I_{sc}	Solar constant (W/m^2)
I_{01}	Diode saturation current of 1^{st} diode (A)
I_{02}	Diode saturation current of 2^{nd} diode (A)
I_{D1}	Diode current of 1^{st} diode (A)
I_{D2}	Diode current of 2^{nd} diode (A)
k_{gl}	Luminous efficacy
k_T	Hourly clearness index
K_d	Diffuse factor
k_t	Thermal conductivity of glazing (W/mK)
k_{pl}	Thermal conductivity of polystyrene (W/mK)
k_{wd}	Thermal conductivity of wood (W/mK)
L_{adp}	Adaptation luminance of the surroundings
L_{ext}	Exterior luminance of the outdoor source
L_i	Test cell interior horizontal luminance (cd/m^2)
L_o	Test cell exterior horizontal luminance (cd/m^2)
L_{win}	SPD glazing luminance (cd/m^2)
L_{pl}	Thickness of polystyrene (m)

L_{wd}	Thickness of wood (m)
LPSP	Loss of power supply probability
M_{tc}	Mass of air inside test cell (kg)
$\dot{m}_g$	Mass flow rate (kg/s)
Q_g	Heat through the glazing due to incident solar radiation (W)
Q_{in}	Total energy incident on the glazing (W)
Q_{tc}	Total energy available inside the test cell (W)
$Q_{loss,wall}$	Heat loss through the surfaces of test cell
R	Thermal resistance of combined wood and polystyrene (m^2K/W)
R_{pl}	Thermal resistance of polystyrene (m^2K/W)
R_{wd}	Thermal resistance of wood (m^2K/W)
$R_{airinside}$	Thermal resistance of test cell internal ambient (m^2K/W)
$R_{airoutside}$	Thermal resistance of test cell external ambient (m^2K/W)
$T_{out,tc}$	Test cell outside temperature (^0C)
$T_{in,tc}$	Test cell inside temperature (^0C)
U-value	Overall heat transfer coefficient (W/m^2K)
V_T	Thermal voltage (V)

Greek symbols

α	Absorptivity
τ_v	Vertical global transmittance

τ_{dir}	Direct transmittance
τ_{diff}	Diffuse transmittance
τ_{g}	Reflected transmittance
θ	Incident angle
τ	Glazing transmittance
$\tau(\lambda)$	Spectral transmittance of the SPD glazing
θ_1	The solid angle from visible sky patch to the viewers
ω_N	Apparent solid angle
Ω_{pN}	Solid angle subtended by source

Subscripts

in,tc	Inside test cell
out,tc	Outside test cell

Chapter 1. Introduction

1.1. Background

Buildings play an important role in energy consumption of all over the world. Energy consumption by both residential and commercial buildings in developed countries account for 20%–40% of total energy used (Lombard et al. 2008). The building sector consumes 41% of energy in US, 41% energy in the EU and 25% in China (Nejat et.al. 2015). As of 2011, households accounted for about 14.2% of the total energy consumption in Japan, which has more than doubled since the 1970s (Hara et.al. 2015). It has been estimated that buildings worldwide account for about one-third of global greenhouse gas emissions (GHG) (Levermore 2008). Buildings are responsible for 32% of the GHG emissions in Europe, 48% in USA and 33% in Australia (Ma et.al. 2012; Daly et.al. 2014; Wang et.al. 2011). In Australia commercial building emissions is projected to increase GHG emissions by 154% from 2005 to 2050 (Ma et.al. 2012; Wang et.al. 2010). It was reported in 2003 that the CO_2 emissions in the residential sector of Japan was 50.5 million tonnes of carbon which increased by 43.5% in comparison with that of 1990 (Ashina and Nakata 2008; Ren et.al. 2009). These figures make buildings an important target for GHG emissions reduction.

Space heating, cooling and lighting are the main use of energy in residential and commercial buildings (Lee et.al. 2013). Building energy performance improvement is an important part of European Union (EU) 2020 and 2030 energy targets (EC, 2014). The improved energy efficiency of the building stock is expected to play a key role in meeting EU commitments to the Kyoto Protocol with respect to the

reduction of CO_2 emissions. Hence Ireland as an EU member state, must implement the EU 2020 targets, which include the following:

- 30% reduction of GHG emissions by 2020;
- 20% energy generation from renewable energy sources.

In order to meet the EU energy targets, Ireland has defined its own targets for 2020 that are (SEAI, 2013)

- 16% final energy consumption from renewable sources;
- 40% gross electricity consumption from renewable energy sources;
- 12% renewable contribution to heating and cooling.

This informs the roadmap for moving towards a competitive low carbon economy in 2050 (EC, 2011).

Energy-efficiency and renewable energy utilization in buildings can be a solution for reduced building energy consumption. This can be performed by developing new net zero energy buildings (NZEB) and retrofitting of older buildings. In a NZEB, energy comes from renewable sources and not from fossil fuel (Jian and Zhao 2014; Maurizio et.al. 2015; Kolokotsa et.al. 2011). These renewable energy resources are placed near to the consumption site (Wang et.al. 2009) to reduce power transmission losses. The US Department of Energy (2012) has a strategy to have zero energy-building concepts in place by 2020 and to commercialise these by 2025. By achieving the objective of net zero energy, energy and environmental problems in a building will be addressed holistically. In zero energy buildings, windows will play a vital role by reducing the cooling, heating and lighting load (Xing et.al. 2011; Gratia and Herde 2003).

For old buildings, the average energy use is significantly higher than in new buildings (and obviously from a NZEB). Energy retrofitting of building stock can

achieve savings of energy. Such measures include retrofit windows, mechanical ventilation and inside insulation (Morelli 2012; Klainsek et.al. 1996; Martins and Carlos 2014). Insulation placed on the interior of walls can provide for 20% of energy savings. Internal insulation and retrofitting window together can save 47% annual energy of a building (Harrestrup and Svendsen 2015). Windows are responsible for 20–40% of wasted energy in a building. For existing building, retrofitting of building envelope especially windows has potential to reduce the energy consumption for heating and cooling (Takashi et.al. 2013; Yildiz and Arshan 2011; Rodriguez 2013).

1.2. Research justification

In 2007, the residential sector accounted 22% of total final energy consumption while 96.5% of that energy was derived from fossil fuels (Howley and Gallachoir 2008). In northern Europe, Ireland's housing stock has been identified as being amongst the least energy efficient (Brophy et.al. 1999; Lapillonne et. al. 2012; Ahern et.al. 2013). Per capita emissions in the residential sector accounted for 27% of total emissions in 2011 in Ireland and were the second largest after transport with 33.2% (SEAI 2013). The residential sector was responsible for 27% (10.5 million tonnes) of energy related CO_2 emissions in 2011 (SEAI 2013). In 2008, CO_2 emission from the EU building sector was 431.9 $MtCO_2$, which accounted for 10.7% of the total CO_2 emissions within the EU (IEA 2010).

In Ireland, windows are required to have less than 1.6 W/m^2K overall heat transfer coefficient (*U*-value) according to building regulations. Replacement of poor quality single glazing or double-glazing with upgraded low *U*-value glazing is easier than replacing other building components.

The primary functions of a window are -

a) to maintain visibility from inside a room to the outside;

b) to daylight an interior;

c) to be a physical barrier that separates internal conditions from those outside.

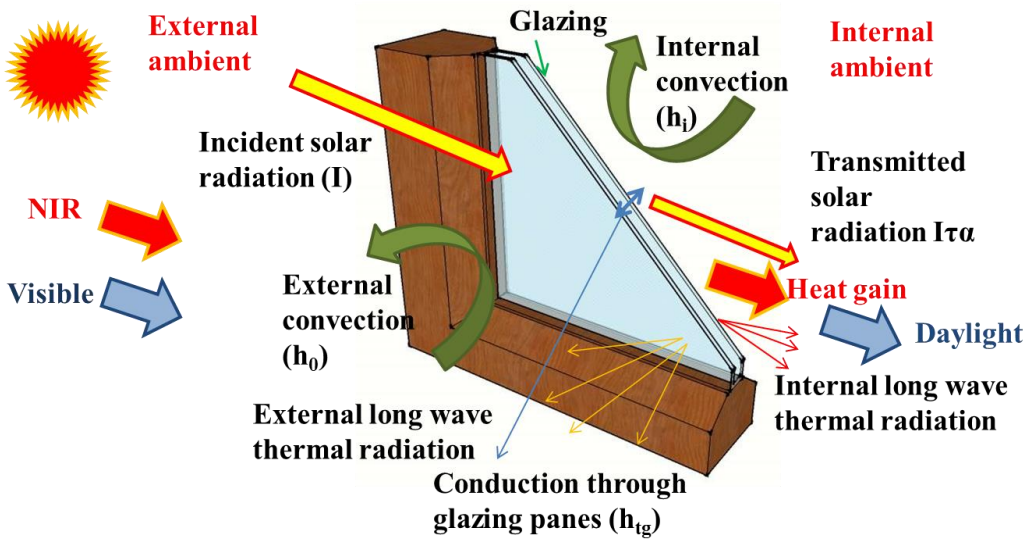

Figure 1-1: Schematic diagram of a window showing heat loss, heat gain and daylighting.

Daylight, glare, heat gain and heat loss are the four phenomena that are involved with windows of a building as shown in Figure 1-1. Incoming solar radiation spectrum through a window is electromagnetic waves shown in Figure 1-2. The entire solar spectrum from ultraviolet (UV) to radio wave, solar radiation at the earth surface (air mass = 1.5) is within the wavelength range of 380-2500 nm. The ultraviolet (UV) solar radiation ranges between 100-380 nm, the visible light is at 380-780 nm and the near infrared (NIR) solar radiation is at 780-2500 nm.

A glazing must control NIR to avoid overheating, have low heat loss to avoid excessive energy cost and allow sufficient daylight penetration to reduce artificial lighting during the day.

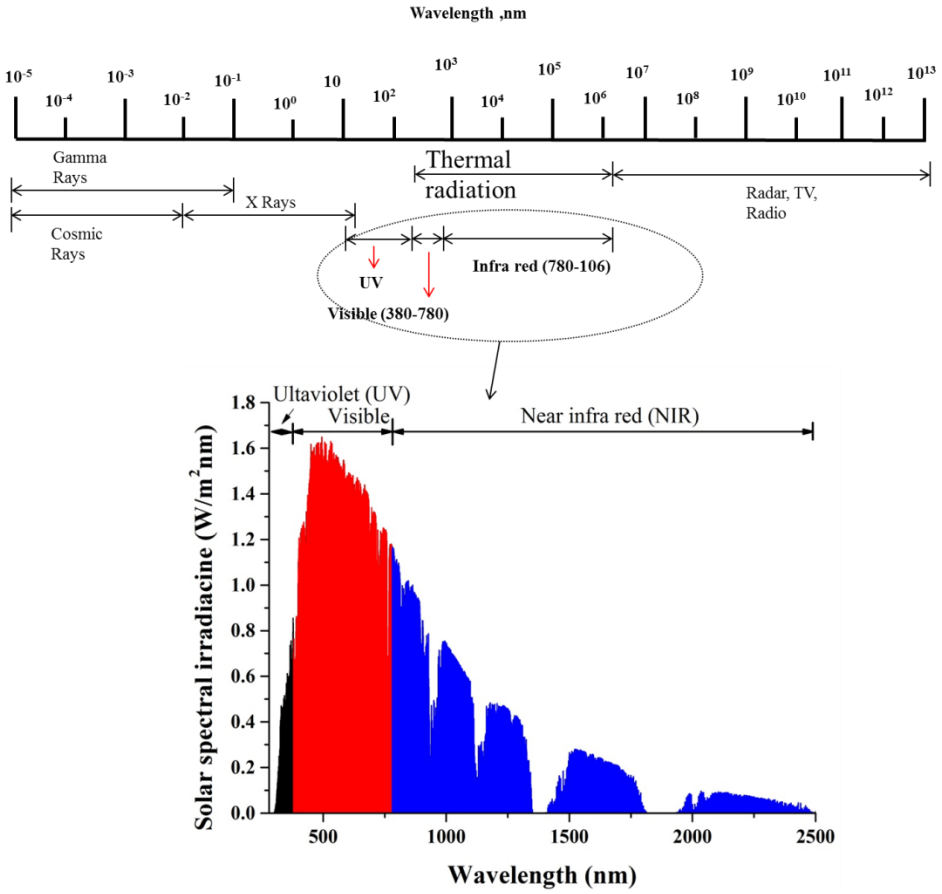

Figure 1-2: Spectrum of electromagnetic radiation.

In Figure 1-3 available glazings are classified into three categories; low heat loss control, solar heat gain control and daylight and glare control glazings. Furthermore, electrically-actuated glazings are categorised as electrochromic (EC), liquid crystal (LC) and suspended particle device (SPD).

In this project, electrically actuated SPD switchable glazing was investigated. To obtain low heat loss, a vacuum glazing was combined with an SPD glazing. To achieve autonomous (self-powered) glazing, the combined SPD and vacuum was powered by a PV device. The latter is shown in Figure 1-4.

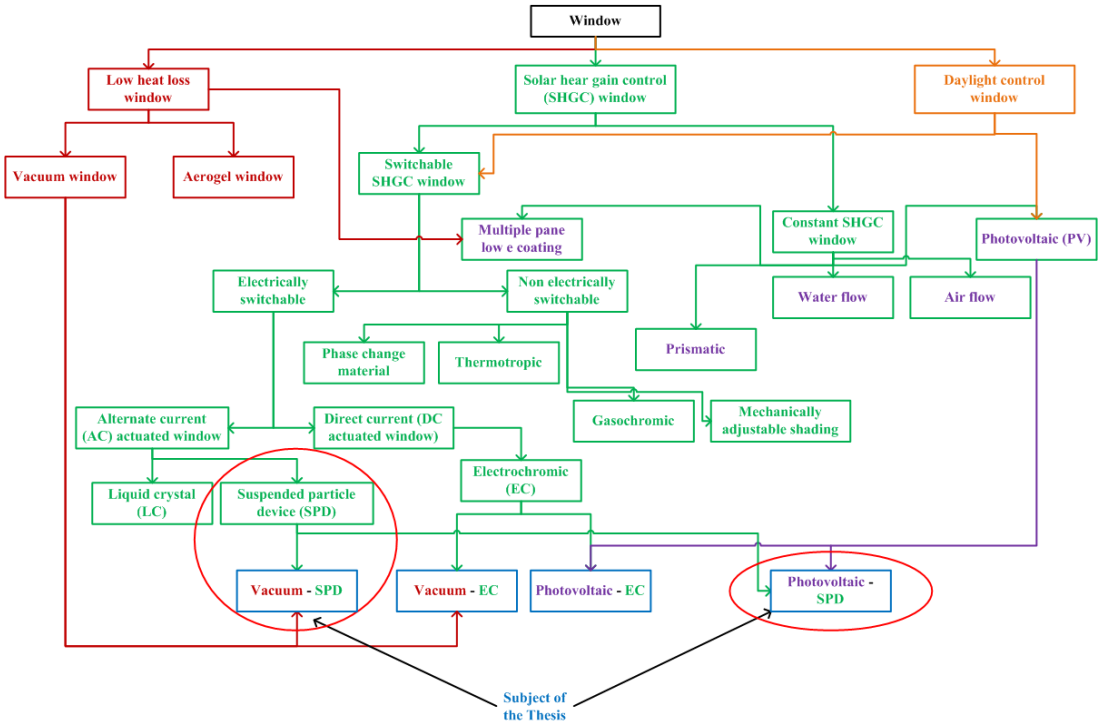

Figure 1-3: Taxonomy of different windows.

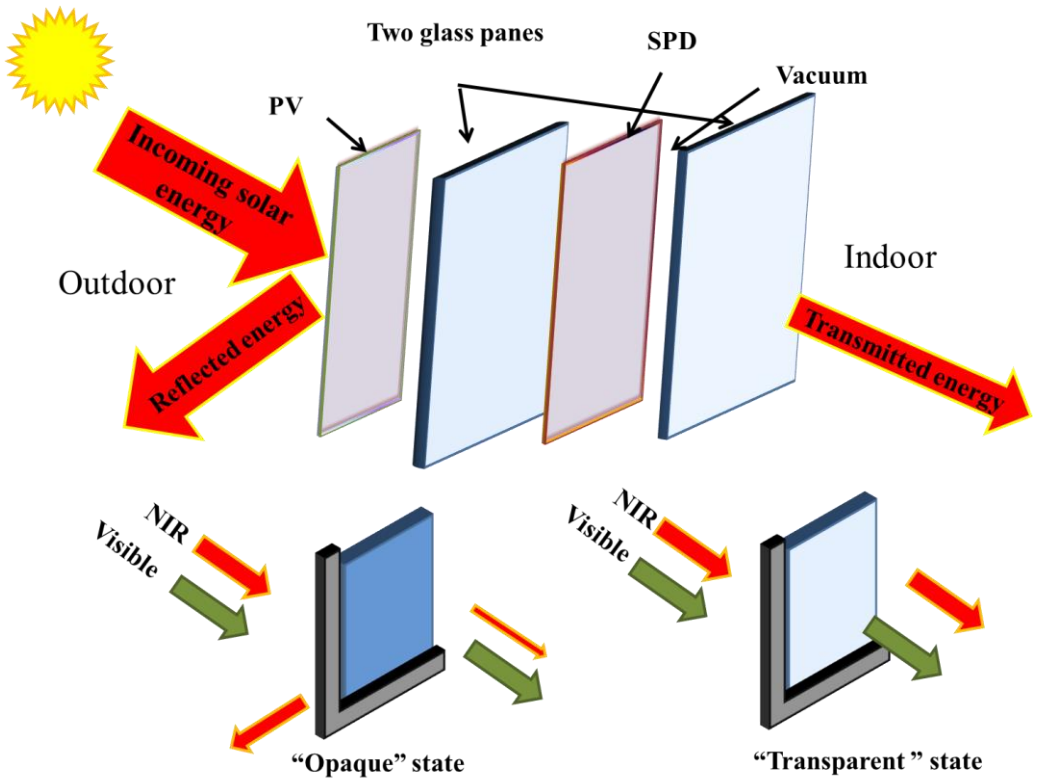

Figure 1-4: Schematic illustration of self-powered low heat loss suspended particle device glazing "transparent" and "opaque" state and different possible layer position of that glazing.

The following set out the reasons for the scope of the research

- Electrically actuated glazings (EC, LC and SPD) have the advantage of being operated based on occupant choice.
- Though EC glazing is the most explored electrically-actuated glazing technology due to its capability to control the NIR spectrum, surface temperature increases are a heat source for the interior.
- EC glazing is not durable (Nagai et.al. 1999), after 4000–20,000 cycles at elevated temperature and irradiance, degradation of EC glazing occurs (Tracy 1999).
- Direct connection with a mains power supply is not possible as EC requires a DC supply.
- LC glazing is AC-powered glazing but it has no intermediate state between its opaque and transparent states (Papaefthimiou et.al. 2006).
- SPD glazing requires more research. To date only three peer reviewed articles have been reported on the use of SPD glazing in which electro-optical behaviour of a commercial SPD has been analysed with the angular transmittance of total and diffuse transmittance (Vergaz et.al. 2008; Barrios et.al. 2013; Barrios et.al. 2015).
- No previous research work has been reported with combined SPD – vacuum glazing and PV powered SPD glazing. Reported results of EC – vacuum (Papaefthimiou et.al. 2006) and PV powered EC (Deb 1969) were not satisfactory due to poor EC glazing performance.
- Vacuum glazing was selected as low heat loss glazing over use of an aerogel as it has higher transparency and it is available. Silica aerogel material scatters visible light particularly if the aerogel glazing is exposed to direct

sunlight. This strong haze caused by diffusion of the light makes the glazing almost impossible to see through (Schultz and Jensen 2008).

1.3. Research aims and objectives

The aims of this research were to investigate;

- thermal, daylighting and electrical behaviour of a suspended particle device (SPD) switchable glazing;
- self-powering of SPD glazing using a PV device;
- low heat loss glazing from a combined SPD and vacuum glazing.

This aims were accomplished via the;

- design and fabrication of a test cell to perform the outdoor characterisation;
- characterisation of a suspended particle device (SPD) switchable glazing using a test cell under real outdoor weather conditions;
- analysis of the thermal behaviour of SPD-type switchable glazing;
- daylight and glare analysis of SPD switchable glazing;
- analysis of using PV to power SPD switchable glazing;
- analysis of the thermal behaviour of combined SPD and vacuum glazing.

1.4. Research methodology

1. A review of existing literature including technology identification.
2. The design and set up of test cell and data collecting :
    - Fabrication and installation of test cells;
    - Collection of on-site weather data for ambient temperature, solar radiation (direct, diffuse), illuminance and PV power output.

3. Using semi empirical thermal and daylighting model, *U*-value, SHGC, glare and DF were calculated.
4. For PV powered SPD work, first field data was collected and is presented in Chapter 6. PV powered SPD modelling was used to calculated loss of power supply probability (LPSP).

A flow diagram is presented for research methodology as shown in Figure 1-5.

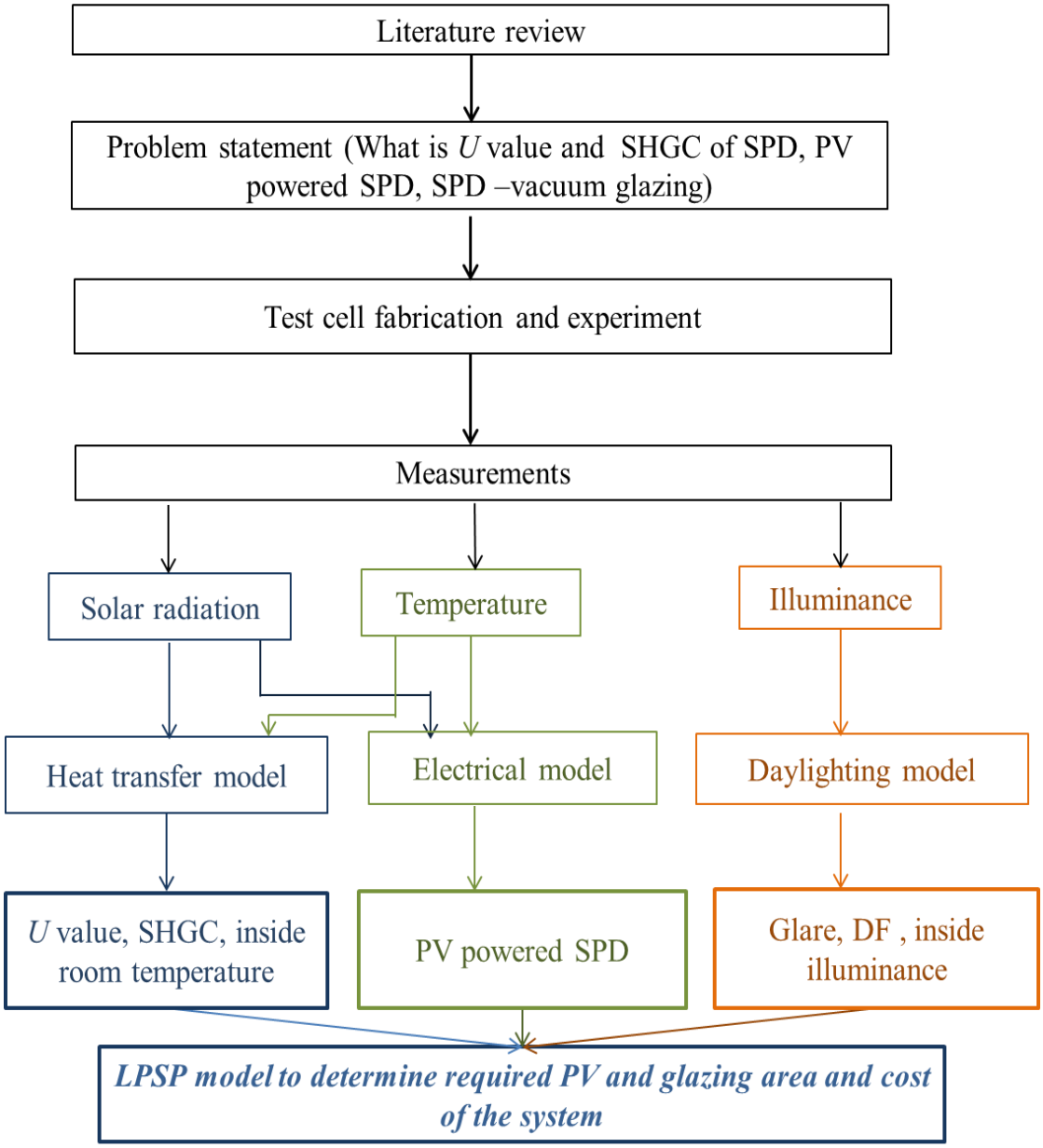

Figure 1-5: Flow diagram of research methodology.

1.5. Thesis overview

Chapter 1 describes the background of the thesis followed by the motivation of the research and establishes the problem statement. It presents the main aim of the research, specific objectives and the methodology used to carry out the research.

Chapter 2 presents an extensive literature review that identifies the state-of the- art for currently available glazing systems.

Chapter 3 illustrates the overall research methodology. Fabrication and design of a test cell to investigate required input parameters for semi empirical model is described.

Chapter 4 discusses the measured and calculated solar radiation. Clearness index and luminous efficacy have been calculated from the measured data. Correlation between clearness index and glazing transmittance is presented.

Chapter 5 presents the daylighting, glare and daylight factor calculations and results from the measured data of SPD glazing in each of its two states.

Chapter 6 presents the successful powering of SPD glazing using a photovoltaic panel.

Chapter 7 introduces the thermal performance of SPD glazing. Overall heat transfer coefficient for SPD glazing and solar heat gain coefficient for this type of glazing for its two states were evaluated.

Chapter 8 presents the thermal and daylight performance of a low heat loss vacuum glazing.

Chapter 9 presents the thermal behaviour of combined low heat loss vacuum glazing and switchable solar heat gain control SPD glazing.

Chapter 10 discuss the cost of a combined switchable low heat loss glazing system.

Chapter 11 presents overall conclusions and recommendation for future work.

1.6. Contribution to knowledge

The contributions of this work to knowledge in the area of smart glazing behaviour are:

- Provision of new outdoor performance data for the glazing systems unique for climates similar to Dublin
- Overall heat transfer coefficients (*U*-values) and solar heat gain coefficients (SHGC) of SPD switchable glazing, double-glazing, SPD double-glazing, vacuum glazing and SPD vacuum glazing under Dublin weather condition have been determined.
- SPD – vacuum combination has been found to offer lowest overall heat transfer coefficient together with variable transparency.
- Inside illuminance, daylight factor, daylight glare index for SPD switchable glazing was evaluated for its “transparent” and “opaque” states.
- A PV powered SPD glazing with and without battery storage was evaluated.

Chapter 2. Review of glazing systems

2.1. Introduction

The different types of available glazing systems are divided mainly into three categories, constant transparency, switchable transparency and combined glazing. Three parameters; solar heat gain coefficient, overall heat transfer coefficient and daylight glare decide the suitability of glazing for different weather conditions, building use and occupancy conditions.

2.1.1. Solar heat gain coefficient

Solar heat gain coefficient (SHGC) is the fraction of the incident solar radiation that enters a room after passing through the window. A solar heat gain coefficient 0.4 indicates that 40% of the incident radiation enters the room in the forms of transmitted radiation and secondary heat gain due to long wave radiation emitted by the internal surface of the glazing. These solar gains passively heat the room, which is usually desired during the heating season but often unwanted in summer (Kuhn 2014, Norton 2014).

2.1.2. Overall heat transfer coefficient

Overall heat transfer coefficient (*U*-value) of glazing is specified by the internal and external heat transfer coefficient and thermal conductance of glazing. Heat loss through glazing occurs when indoor temperature is warmer than outdoor.

The *U*-value of a glazing unit with panes of the same area can be represented by equation (2-1) (Bülow-Hübe, 2001) where h_{ig} is the convection heat losses from glazing internal surface, h_{0g} is the convection heat losses from the glazing external surface and h_{tg} is the conductive heat transfer coefficient of glazing panes as shown in Figure 1-1 in Chapter 1.

$$\frac{1}{U} = \frac{1}{h_i} + \frac{1}{h_0} + \frac{1}{h_{tg}} \qquad (2\text{-}1)$$

where

$h_i = 2.0 + 3V_{wind}$, $h_0 = 5.7 + 8.8V_{wind}$, and $h_{tg} = \frac{k_t}{d_g}$

k_t is the thermal conductivity of glazing and d_g represents the area of glazing.

When a glazing is installed in a building, external surface of the glazing facing outdoor environment interact directly with the outside real time condition. This offers variation of convective heat loss from the outside surface. This influences to vary the *U*-value of glazing.

2.1.3. Daylight

Daylight is considered as the best source of light for good colour rendering as it most closely matches human visual response. Comfortable daylight through building's window leads to occupant satisfaction, performance and productivity.

Excess light availability creates glare (Littlefair 1987; Littlefair 1988; Littlefair 1990) whilst insufficient light inside a room also generates discomfort for occupants (Joshi et. al. 2007; Muneer 2004; Rea 2000; McHugh et.al. 2004). Appropriate daylighting design can reduce

- artificial lighting energy consumption;
- the cooling load due to heat dissipation from electric lighting (Hunt 1979) and
- the emission of greenhouse gases from fossil fuel power plants (Lam and Li 1999; Smith 2004; Chel et.al. 2009).

Use of daylight-illumination schemes in apartments (Balaras et.al. 2000), offices (Bodart and Herde 2002), hotels (Santamouris et.al. 1996), large atrium spaces

(Littlefair 2002; Atif and Galasiu 2003) and corridors (Lam and Li 1999) has been shown to reduce building lighting energy costs. Different daylight levels are summarised in Table 2-1.

Table 2-1: Different level of daylight

	Illuminance level (lux)
Bright sun	50,000 - 100,000
Hazy day	25,000 - 50,000
Cloudy bright	10,000 - 25,000
Cloudy dull	2,000 - 10,000
Very dull	100 - 2,000
Sunset	1 – 100
Good street lighting	≈20
Poor street lighting	≈0.1
Full moon	0.01 - 0.1
Starlight	0.001 - 0.001
Overcast night	0.00001 - 0.000

2.1.4. Glare

Discomfort glare caused by direct sunlight and/or bright skylight, is a sensation of pain caused by receiving higher luminance than the limit of eye adaptation (IESNA, 2000). Glare is a direct function of both the size of a window and the brightness of the sky seen through it. Glare can be reduced by decreasing the brightness of the visible patch of sky by reducing the size of window (Hopkinson 1972). Different methods to measure glare includes visual comfort probability (VCP) method (IES, 1996; IESNA 2000), British glare index (BRS) (Hopkinson 1957), unified glare rating (UGR), The CIE glare index (CGI) (Einhorn 1969, 1979) and the unified glare rating (UGR) system (CIE), daylight glare index (DGI) (Hopkinson 1970). In the presence of discomfort glare, an occupant may not feel any disturbance on their performance of work directly but the glare will create some physiological symptoms such as headache that will affect the work indirectly (Osterhaus 2005). In general, for artificial light glare is caused by use of wide sources (Iwata et.al. 1991).

2.2. Constant transparency glazings

2.2.1. Double glazing

Windows made by gas-filled double-glazing is the most widely used fenestration technology. Due to its low cost, air is often employed between the two glass panes in a double glazing even though the thermal conductivity of air at room temperature and atmospheric pressure is 0.026 W/mK, which is higher than alternative gases such as Argon (0.018 W/mK), Krypton (0.0095 W/mK) and Xenon (0.0055 W/mK). Argon filled glazing is likely to increasingly dominate the double glazing sector due to its low cost compared with that of Krypton and Xenon (Jelle et.al. 2012). Difluoromethane (HFC-32) and sulfur hexafluoride (SF6) (Eriksson et.al. 1987) infrared absorbing gas filled double-glazings are also more thermally insulating than current double glazing units (Ismail et.al. 2009).

The spacing between the two glass panes in a double glazing influences the overall heat transfer coefficient but has no influence on the solar heat gain coefficient (Aydin 2000; Aydin 2006; Ismail and Henríquez 2005; Arici and Karabay 2010). Double glazing possess constant transparency which are not suitable for building application as a building experiences diurnal solar heat gain and daylight. These variation increases the cooling load demand of buildings.

2.2.2. Low emittance coated glazing

Low long wave emittance coatings (low-e coating) are metals or metallic oxides that allow visible light in the solar spectrum to be transmitted while blocking other wavelengths responsible for undesired solar heat gain (Chiba et.al. 2005; Leftheriotis and Yianoulis 1999) as shown in Figure 2-1. Low-e coatings on the outside surface of the glazing are capable of reducing heat gain through windows up to 48%.

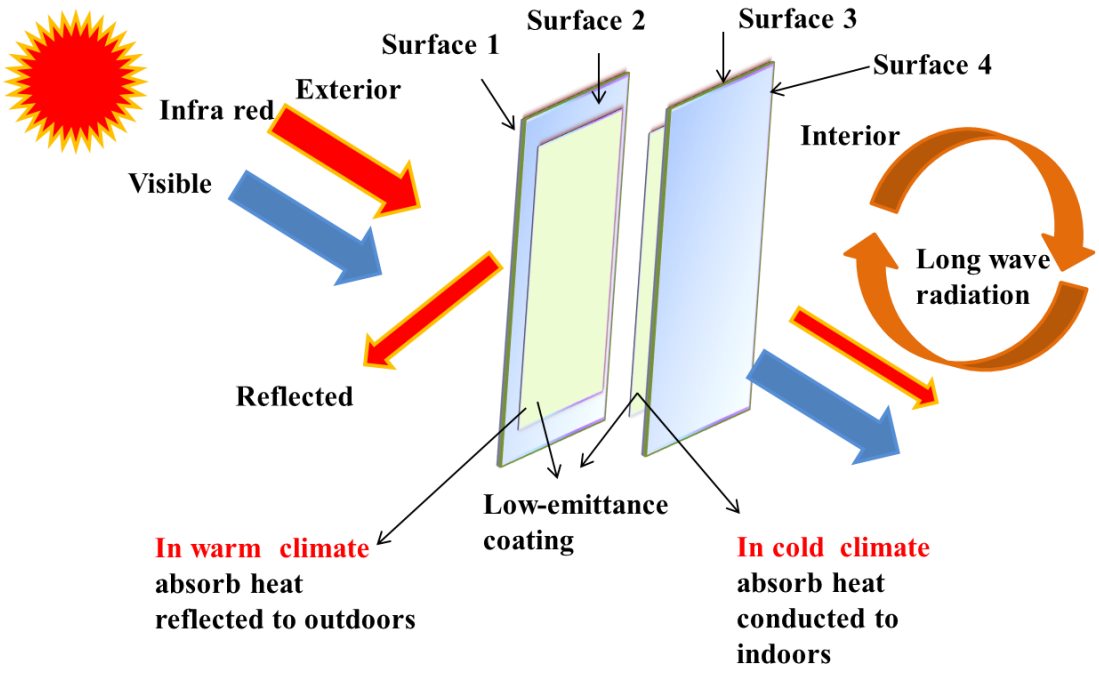

Figure 2-1: Schematic diagram of low emittance coating glazing.

A low-e coating inside a glazing prevents heat from the interior being transmitted outside thus giving a low glazing *U*-value (Han et.al. 2010). "Hard" and "soft" are the two types of low-e coatings. Soft low-e coatings are more transparent than hard low-e coating but due to low durability, extra protective layers are used to enhance the durability. Soft low-e coatings have higher infrared reflection than the hard low-e coatings (Chiba et.al. 2005; Reidinger et.al. 2009; Hammarberg and Roos 2003; Del Re et.al. 2004). At present, all window coatings with emissivity values below 0.1 are based on thin silver films. The most challenging point of existing low-e coatings is the reduction in light transmittance, which makes the indoor environment darker (Bullow 1995). Another disadvantage is their current high cost of production.

2.2.3. Prismatic glazing

A prismatic glazing unit consist of outer and inner prismatic panes to provide solar control, daylighting and energy conservation (Lorenz 2001; Andersen et.al. 2003). The upper faces of the inner prismatic pane are coated with a diffusely reflecting

layer and the lower faces of the outer prismatic pane are coated with a specularly reflecting layer. The prismatic glazing unit can be used for common window tilt angles and for window directions with significant solar irradiation at sites with a temperate climate. During the summer and the transitional seasons, it provides improved protection against solar irradiation and distinctly reduced irradiated heat fluxes. The reflecting surfaces of the prismatic ribs prevent glare (Lorenz 2001; Shehabi et. al. 2013). No commercial device is available.

2.2.4. Water flow glazing

A window made by water-flow glazing carries a water circuit between two glass panes that allows a stream of clean water to flow upward or downward within the entire space between two glass panes shown in Figure 2-2. Water passage in this way lowers the inner glass pane temperature; reduces room heat gain and therefore, air-conditioning electricity consumption. This type of window can enhance thermal and visual comfort (Chow et.al. 2010; Chow and Li 2013; Chow et.al. 2011a). Compared to conventional double and single pane windows a water flow window reduces annual room heat gain by 32% and 52% respectively, which saves 111 kWh and 140 kWh electricity per unit window surface area (Chow et.al. 2011b). Water flow inside the double-glazing can control heat gain more effectively than airflow inside double-glazing (Lopez et.al. 2013).

Disadvantages of this type of systems are the requirement of auxiliary water collector, which may not be feasible for retrofitting window application or even in new zero energy building. Pumping systems are required to generate the water flow from lower header to upper header. This system is not commercially available.

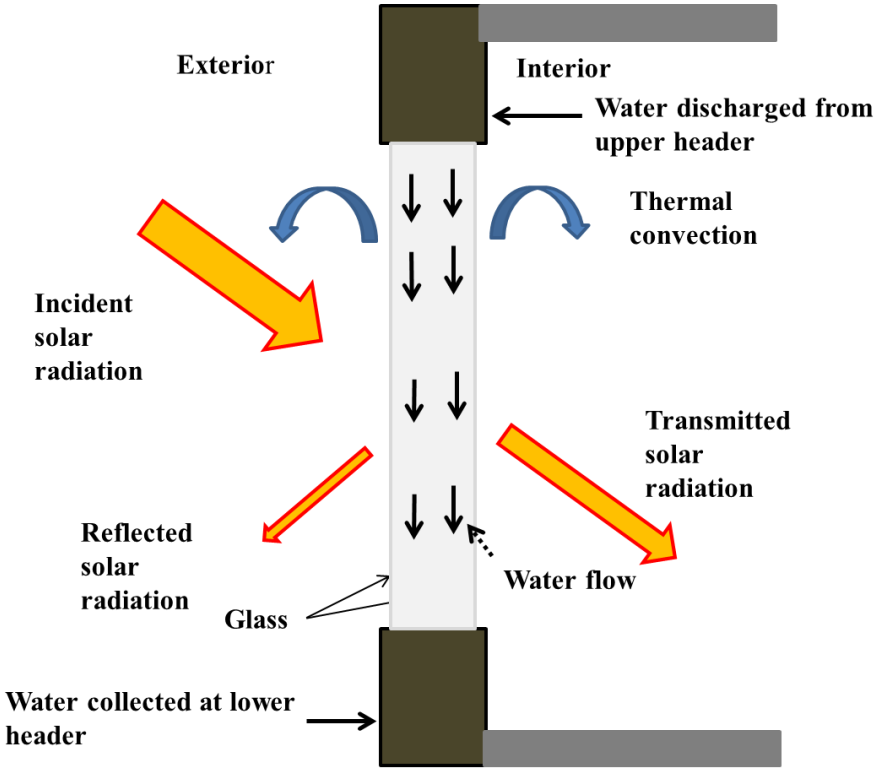

Figure 2-2: Energy flow path at water flow double pane window (Chow et.al. 2010).

2.2.5. Air flow glazing

The airflow window has been the subject of experiment for several years most notably in Canada and Finland in the 1970s and 1980s (Yuill 1987; Wright 1986). In an airflow window, space between inner and outer glazing surface is an airflow path shown in Figure 2-3. Air is pulled in from outside or from the building either buoyancy or mechanical extraction process and is heated through conduction, convection and radiation in the cavity and is brought into the room at the top of the window (Baker and McEvoy 2000; McEvoy et.al. 2003; Southall and McEvoy 2006). In this way, the heat absorbed in the cavity is partially reclaimed. The reclaimed heat leads to a reduced heating load on heating, ventilation and air conditioning (HVAC) equipment during the cold seasons and improved indoor air quality.

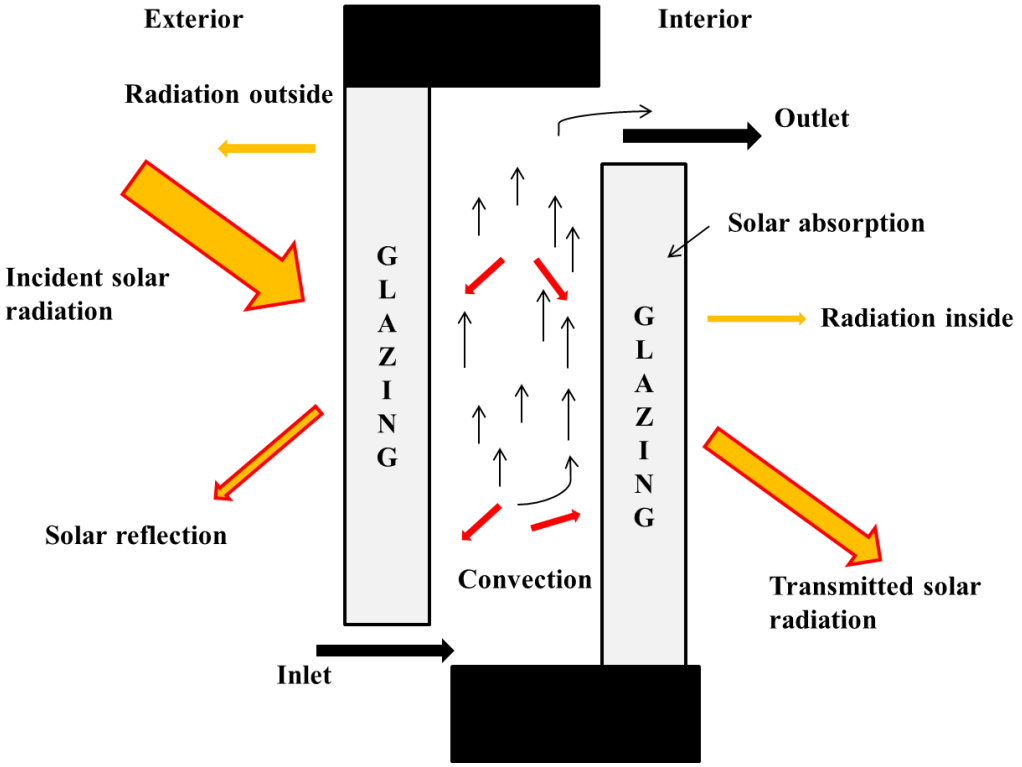

Figure 2-3: Schematic diagram of an airflow window (McEvoy et.al. 2003).

Airflow glazings also need the air collector and pumps to collect and flow the air between the glazing panes. This auxiliary system requirement makes it less suitable for building application. Air chamber needs maintenance as presence of dust in the air can create scatter and reduce the visibility through the glazing.

2.2.6. Evacuated (Vacuum) glazing

Highly insulating vacuum glazing consists of a vacuum between two glass panes separated by small pillars to withstand atmospheric pressure (Robinson and Collins 1989; Collins and Robinson 1991; Collins et.al. 1992; Collins et.al. 1993; Collins et.al. 1995; Fischer-Cripps et.al. 1995; Lenzen and Collins 1997; Collins and Simko 1998; Wilson et.al. 1998; Simko et.al. 1998; Griffiths et.al. 1998; Hyde et.al. 2000; Fang et.al. 2000; Ng et.al. 2005; Ng et.al. 2006; Ng et.al. 2007; Fang et.al. 2005; Fang et.al. 2006; Griffiths et.al. 2006; Zhao et.al. 2007; So et.al. 2007; Wang et.al. 2007; Eames 2008; Fang et.al. 2009a; Fang et.al. 2009b; Wullschleger et.al. 2009;

Koebel et.al. 2010; Zhao et.al. 2013; Miao et.al. 2015). Heat flow through the pillars is independent and parallel to the radiative heat flow between the glasses (Hyde et.al. 2000; Fang et.al. 2000; Ng et.al. 2005). Vacuum glazing has a hermetic (leak free) edge sealing around the periphery of two glass sheets and a stable pressure (<0.1 Pa) between two glass sheets (Fang et.al. 2005; Fang et.al. 2006; Griffiths et.al. 2006). Vacuum glazing was patented in 1924 (Zoller 1924). Figure 2-4 indicates the different view of vacuum glazing and one commercial sample from NSG SPACIA. In 1989 at the University of Sydney (Robinson and Collins 1989), a vacuum glazing system was manufactured and tested (Collins and Robinson 1991; Wilson et.al. 1998). The first successful vacuum glazing fabrication process was achieved using solder glass edge sealing at above 450 ^{0}C (Robinson and Collins 1989; Collins and Robinson 1991). A powdered form of solder glass was mixed with water and applied in the mating face of the two glasses enhanced the edge sealing by overcoming the difficulties of glass to metal sealing, corrosion and fatigue issues for long term applications. A 1 m × 1 m vacuum glazing was developed which offered lower *U*-value of 0.90 W/m^{2}K. This value was lower than *U*–value of double-glazing (1.3 W/m^{2}K) (Collins et.al. 1995). The addition of transparent low-e coatings reduces radiative heat transfer between panes (Collins and Simko 1998); thermal resistance increases while the solar heat gain decreases (Hollands et.al. 2001). High temperature vacuum glazing fabrication can cause performance degradation of soft low-e coating. High temperature vacuum glazing fabrication was found successful with hard low-e coating. To enable lower emittance, soft coating can be used to lower overall heat loss. Low temperature edge seal fabrication (less than 200 ^{0}C) method using indium alloy was developed (Griffiths et.al. 1998; Hyde et.al. 2000) for vacuum glazing with (Fang et.al. 2005 Fang et.al. 2006; Fang et.al. 2000, 2006)

U-value less than 1 W/m^{2}K for the centre-of-glass area at University of Ulster. *U*-value of vacuum glazing increased by 0.28 W/m^{2}K due to glass panes thickness increased from 3 mm to 6 mm. It was also observed while edge seal increased from 2 mm to 12 mm, *U*-value increased by 0.36 W/m^{2}K due to the change of glass thickness (Fang et.al. 2007). It was evident that edge seal was less effective to increase the rate of heat transfer compare to glass pane thickness. Use of two low-e coatings does not reduce the overall heat transfer rate over a single low-e coating layer. One layer of low-e coating also reduces the overall system cost, as low-e coatings are costly (Fang et.al. 2007).

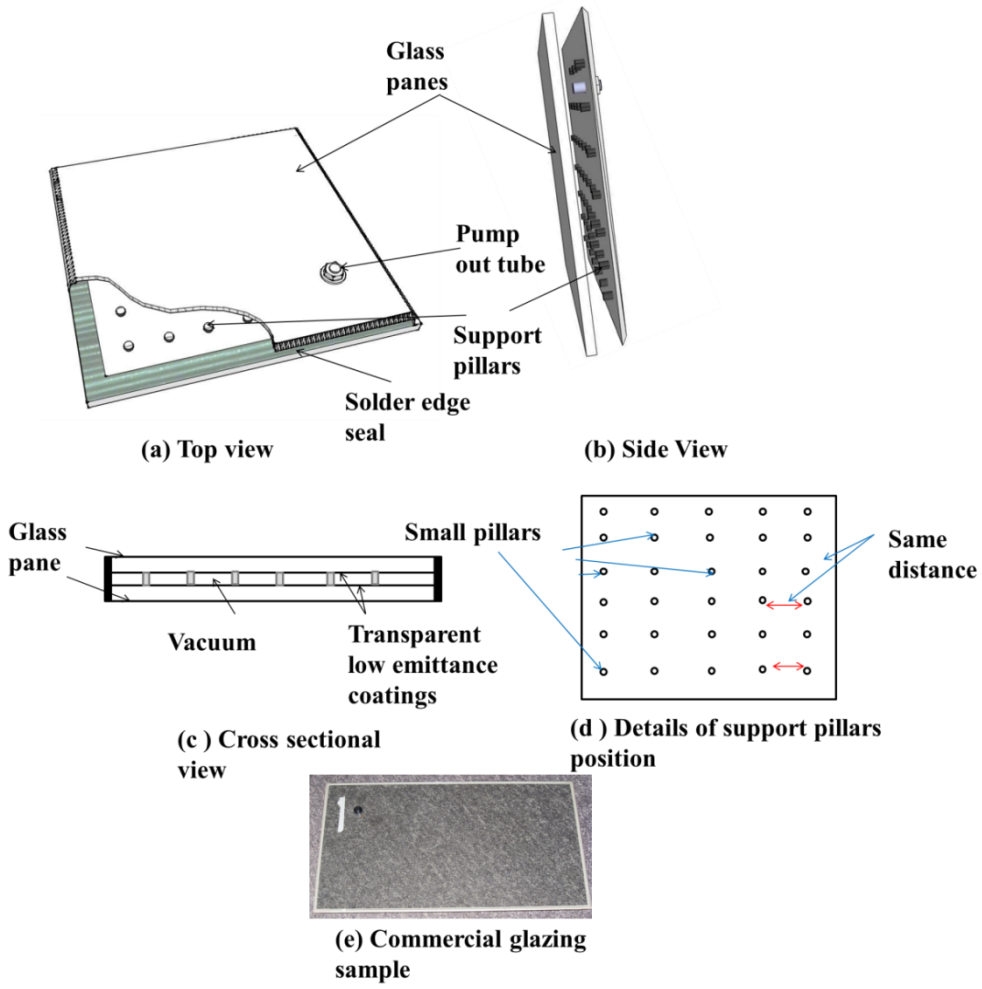

Figure 2-4: Schematic diagram of different view of vacuum glazing and photograph of NSG SPACIA vacuum glazing.

2.2.7. Aerogel glazing

Aerogel is a translucent solid gel that exhibits high thermal insulation (thermal conductivity 0.01-0.03 W/mK) and a suitable candidate for low heat loss windows. In addition, it has also low refractive index (<1.1) and very low density (3-350 kg/m^3). This material is very fragile and needs protection from water. In the presence of water, surface tension of the aerogel pores breaks the aerogel structure. Pure silica does not absorb visible light. Under the form of a fine dispersion of particles with colloidal dimensions (nanoparticles) in a transparent medium like air, silica aerogels do scatter visible light and exhibit a faint bluish colour in the best of the cases. Viewing through aerogel is shown in Figure 2-5.

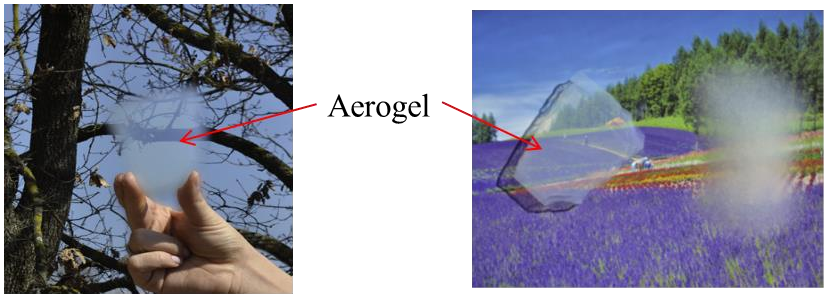

Figure 2-5: (a) Viewing through an aerogel sample, (b) monolithic and granular aerogel (Buratti et.al. 2012).

To date several aerogel glazings have been manufactured and tested. The results are summarised in Table 2-2.

Silica aerogel scatters the transmitted light, which is a major barrier to produce transparent aerogel window. Thus, aerogel glazings are not suitable for window applications, but applicable for building wall insulation and spandrel components in a façade (Ihara et.al. 2015a; Ihara et.al. 2015 b). Presently available commercial aerogels are opaque in nature (ASPEN aerogel).

Table 2-2: Thermal and optical properties of Aerogel glazing.

Type	Dimension (m × m)	Overall heat transfer coefficient (*U*-value) (W/m^2K)	Transmittance	Thickness of glazing	Reference
Monolithic silica aerogel	0.55 × 0.55	0.72	73-75%	15±1% mm	Jensen et.al. 2004
Monolithic silica aerogel	0.58 × 0.58	0.66	76-80%	15 mm	Schultz and Jensen 2008
Monolithic Silica aerogel	0.55 × 0.55	0.7	76%	15 mm	Schultz et.al.2005
Silica aerogel	0.075 × 0.25	0.2	90%	10 mm	Kim et.al. 2003
Monolithic Silica aerogel	a) 0.5 × 0.5 b) 1.0 × 1.0 c) 1.5 × 1.5	0.40			Duer and Svendsen 1998
Granular silica aerogels		0.4	35%	20 mm	Reim et.al. 2002

2.2.8. Photovoltaic (PV) glazing

In photovoltaic (PV) glazing, PV cells are placed between the two glass panes or on the top of the glass panes where PV cells can be inorganic or organic type. Inorganic crystalline silicon (c-Si) type PV cells encapsulated between highly transparent glasses panes are shown in Figure 2-6 (Park et.al. 2010) and amorphous type PV cell glazing is shown in Figure 2-7. Organic PV (OPV) cells encapsulated between double-glazed windows, can be coated on the inner surface of the glass are shown in Figure 2-7.

When replacing traditional window systems, they act as UV and NIR radiation blocking layers, reducing heating and cooling loads of the building. Apart from energy savings, a PV window converts undesired radiation into valuable electricity.

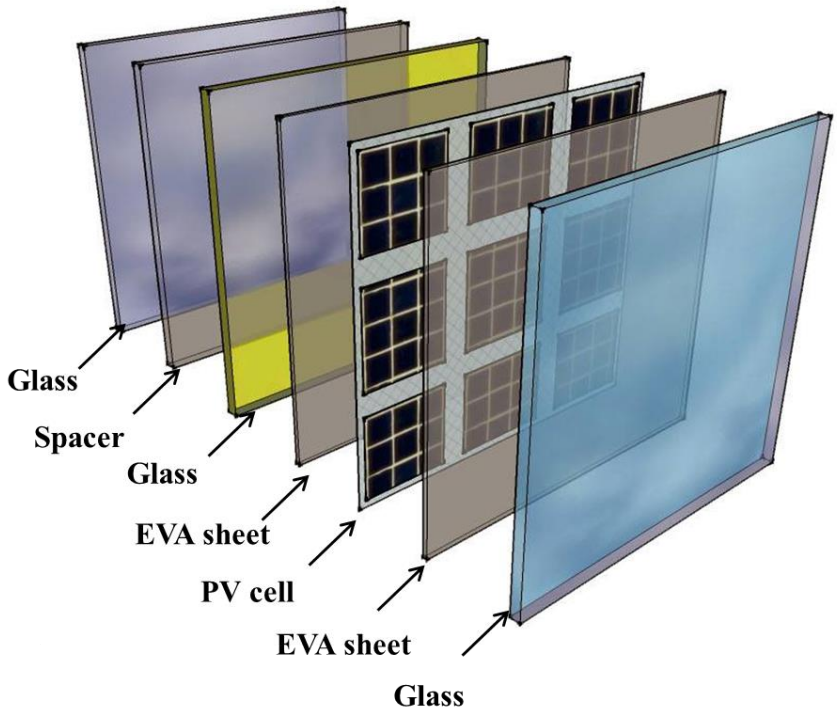

Figure 2-6: Schematic diagram of a c-Si PV window (Park et.al. 2010).

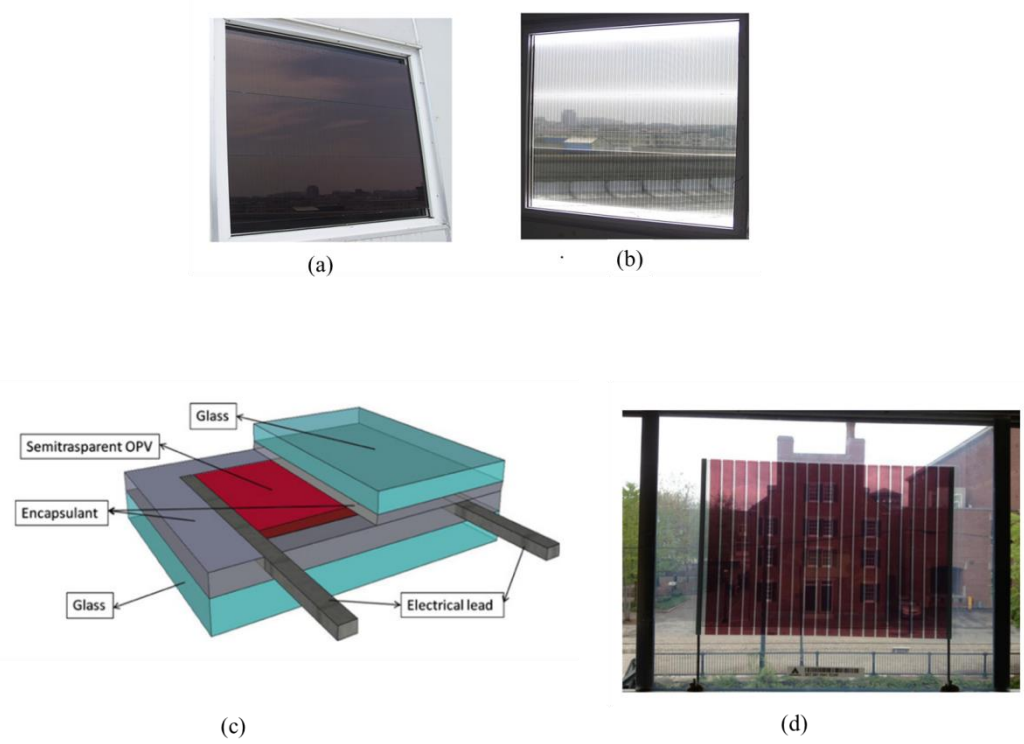

Figure 2-7: (a) Double glazing (b) Single glazing PV (semi-transparent amorphous silicon) window (He et.al. 2011), (c, d) Illustration of organic solar cells for window applications: glass laminated organic photovoltaic module (Yan et.al. 2013).

The main purposes of PV glazing are to

- reduce the solar heat gain coefficient (SHGC), which reduces the cooling load;
- introduce daylighting control.

Another advantage of this type of glazing is that due to the presence of PV, small-scale electricity generation is possible (Ng and Mithraratne 2014). This type of glazing system can save energy by reducing the air conditioning cooling load in subtropical climatic conditions and simultaneously provide visual comfort in the indoor environment (Han et.al. 2009). Presence of a low-e coating reduces the heat transfer through radiation (Han et.al. 2010). Building-integrated photovoltaic (BIPV) technology is becoming widely used as a part of the façades of modern buildings (Taleb and Pitts 2009). Thus, PV glazing system can form part of a BIPV system (Park 2010; Peng 2011; Norton et.al. 2011).

Transparency is an issue with PV glazing as widely available PV devices are mainly crystalline silicon type due to their high durability. This type of PV device (c- Si) has 90.5% absorption (Santbergen and Zolingen 2008) which is suitable for opaque facades (Quesada et.al. 2012). The surface temperature of PV modules are affected by solar radiation, ambient temperature, wind speed, wind direction, building material properties and the installation method of modules (Tonui and Tripanagnostopoulos 2007). This reduces electrical production and introduces the possibility of thermal cracking due to overheating of PV modules under high solar radiation.

Reduction of PV material cost is possible by using solar concentrator, which are made by inexpensive materials. A concentrating PV device generates low cost power compare to a non-concentrator counterpart. Concentration can be high with a

concentration ratio >100, medium concentration ratio between 10-100 and low concentrator concentration ratio <10 (Chemisana 2011). Low concentrator provides less additional heating of PV material and is suitable for BIPV and glazing applications. Several different types of low concentration devices have been investigated for BIPV application such as compound parabolic types and dielectric material type (Sarmah and Mallick 2015; Baig et.al. 2015; Sellami and Mallick 2013; Mallick et.al. 2006; Mallick et.al. 2004; Zacharopoulos et.al. 2000).

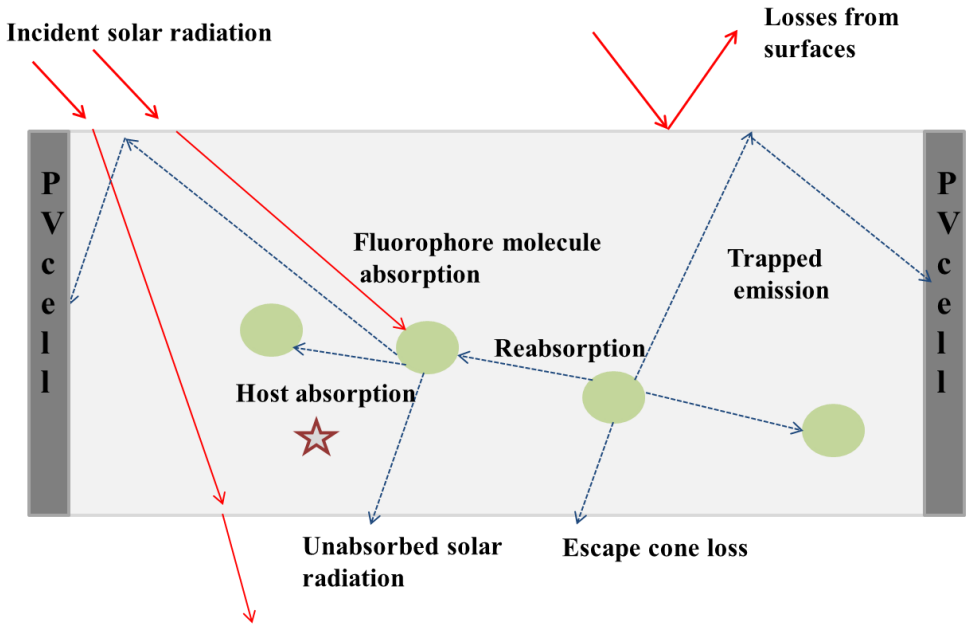

Figure 2-8: Schematic diagram of luminescent solar concentrator.

These systems are not usually transparent which make them unsuitable for PV window applications. For PV glazing applications, luminescent solar concentrators (LSC) are a good candidate as the PV cells are placed on the edge of this type of concentrator and not on the surface (Olson et. al. 1981; Goetzberger et. al. 1979; Norton et.al. 2011). The LSC technology was introduced in late 1970s (Goetzberger and Greubel 1977, Trupke et. al. 2002, Weber and Lambe 1976, Rapp and Boling 1978). Basic working principles of LSCs plate connected with PV cells at its edges are shown in Figure 2-8. A LSC can concentrate both direct and diffuse radiation (Smestad et. al. 1990) and are well suited for building integrated photovoltaic

(BIPV) applications due to their static nature. The narrow emission band of luminescent species can be matched to the spectral response of PV cells.

2.3. Switchable transparency glazings

2.3.1. Suspended particle device (SPD) glazing

Suspended particle device (SPD) technology was first invented in 1930 and patented by Dr Edwin Land in 1934 (Marks 1969). SPD device works on same principle as of light valve. The light valve was defined as a cell formed of two transparent sheets of insulating material spaced apart a small distance and containing a suspension of small particles in a liquid medium (Land 1934). Particles can be dihydrocinchonidine bisulfite polyiodide or heraphathite. Shape of the particle can be needle-shaped, rod-shaped, or lath-shaped types. In the absence of an applied electrical field, the particles in the liquid suspension moves randomly due to Brownian movement (Saxe 1981). Hence, a beam of light passing into the cell is rejected, transmitted or absorbed depending upon the cell structure, the nature of particles, concentration of the particles and the energy content of the light. The light valve is thus relatively dark in the OFF state. However, when an electric field is applied through the liquid light valve, the particles become aligned and most of the light can pass through the cell. The light valve is thus relatively transparent in the ON state (Saxe 1979). This technology has been known for more than seventy years for the application of modulation of light in the field of alphanumeric displays, television displays, and filters for lamps, cameras, optical fibers. For window applications, plastic films are preferred than a liquid suspension. Plastic film eliminates the possibility of bulging effect during high column of suspension due to hydrostatic pressure and leakage possibility from the device. Another advantage of using a plastic film is that, the

particles are generally presents only within very small droplets in a plastic film and do not noticeably agglomerate when the film is repeatedly activated with a voltage. SPD light valve was proposed by Chakrapani et.al. 2002 where film was made by a cross-linked polymer matrix and having droplets of a liquid light valve suspension distributed in the matrix of 1.4 refractive index. A clear unit of shatter-resistant laminated suspended particle device (SPD) was proposed by Slovak et.al. 2005. For architectural and windshield glass applications, the lamination process generally involves bonding a plastic interlayer in between two sheets of flat or curved glass, with the goal of producing a shatter-resistant glass. Research Frontiers Inc (RFI) is the major developer of commercial SPD devices for goggles, eyeglasses and windows. Light transmission of SPD can be from 0.1 to 60%, with switching speed of 100 to 200 ms.

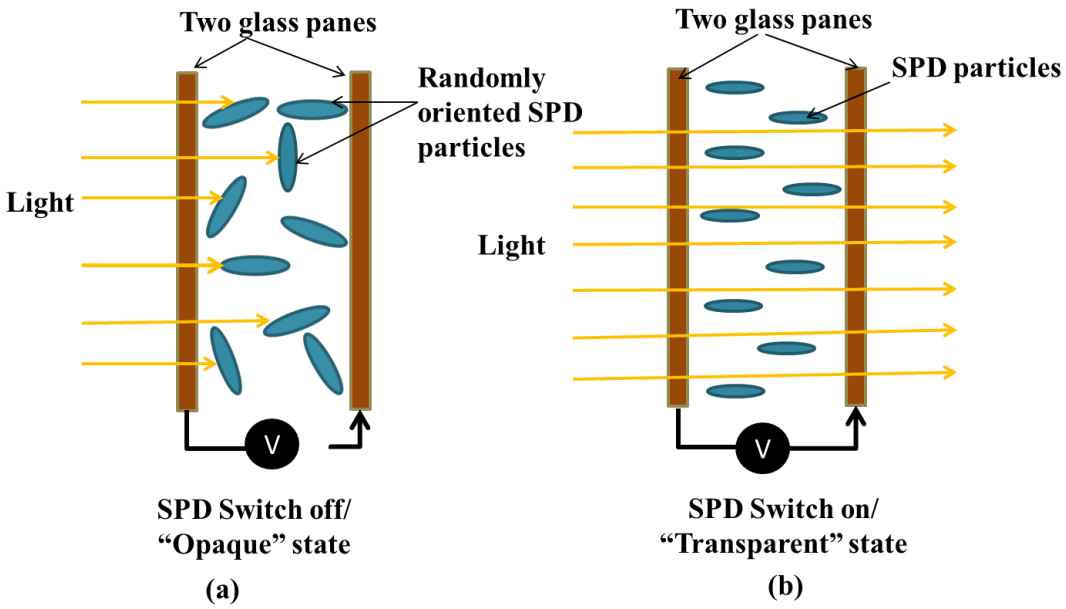

Figure 2-9: The working principle of SPD in (a) switching off (opaque) and (b) switching on (transparent) state.

The voltage required for the device which depends on thickness, ranges from 0-20 V to above 150 VAC. Without an applied voltage, particles suspended randomly block all light passing through. The application of an AC voltage aligns particles

perpendicularly to the charged plates so that nearly all light passes as seen in Figure 2-9 (Lampert 1998).

A group of 50 RF 0.01 m × 0.01 m windows were installed as a demonstration in the Japan Steel Works Building in Fuchua, Japan. Gloverbel, S.A. is developing SPD automotive mirrors and visors in Brussells, Belgium. Others commercial groups working on this technology include Hankuk Glass Industries (Korea), St. Gobain in Paris, France for architectural glass and Sanyo Electric in Japan for flat display panels (Lampert 1998).

Modelling and electro optical test of a commercial SPD manufactured by Cricursa found switching times were sufficient for smart glazing applications, which usually need only a few changes of state per day (Vergaz et.al. 2008). An optical modulation test of a commercial SPD from Cristales Curvados S.A., Barcelona, Spain showed that the modulation was high for visible light while almost nil for near infrared; however haze in diffuse light was observed, which can be an obstacle for windows applications (Barrios et.al. 2013).

The main challenges of SPD glazing is the absence of memory effect. Without constant power supply, it cannot maintain its continuous “transparent” state (Barrios et.al. 2013). High voltage requirement to operate this material is also a barrier of using this widely. Power requirement of this glazing also increases with area of the glazing (Vergaz et.al. 2008). A number of technological problems including long-term stability, cyclic durability, particle settling, agglomeration and spacing control for larger glazing (Lampert 1998) has slowed down the development of suspended particle glazing. Due to the patents on the technology, only little information has been found on recent developments of suspended particle devices.

SPD can be a good solution to control the solar heat gain, introducing daylight and controlling glare for hot climatic country. During the daytime, no need of power as SPD glazing remains "opaque" without power supply. It can save huge amount of energy to operate this in a large-scale application. Responses of SPD material are instant and irrespective of the size of the material, the transparent and opaque process is uniform, making it potentially attractive for glazing application. Suspended particle device glazings are commercially available.

2.3.2. Liquid crystal (LC) glazing

In a Liquid Crystal (LC) Glazing, liquid crystal is sandwiched between two glass panes (Lampert 1993). In the presence of constant AC power supply the glazing offers "transparent" view. With no supply, it becomes "opaque" due to random orientation of the particles as shown in Figure 2-10. The LC phase was first observed by Friedrick Reinitzer in 1888 during his work with cholesteryl benzoate (Chandrasekhar 1992; De-Gennes and Prost 1995).

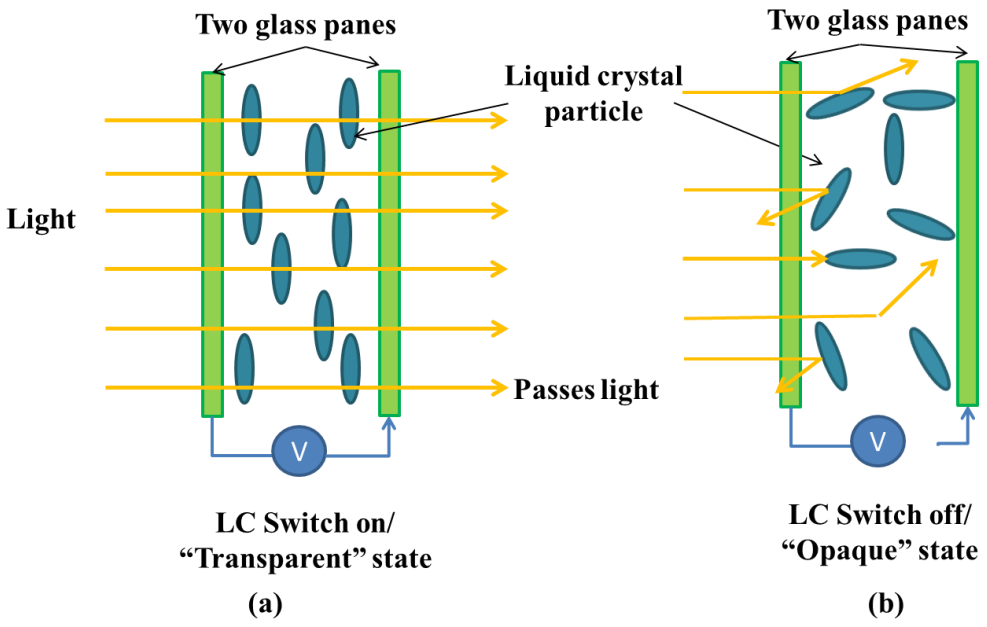

Figure 2-10: (a) LC glazing in switch "on" condition ("transparent" state), (b) LC glazing switch "off" condition ("opaque" state).

A semectic LC glazing achieved “opaque” state for 66 volt at 100 Hz (rms) supply and 36 volt at 1 kHz produced “transparent” state with a response time strongly dependent on voltage (Gardiner et. al. 2009). Transmittance of a 12.5 cm × 12.5 cm and 6 μm thick LC window can vary from 30% to 55% (Anjaneyulu et.al. 1986). Another form of LC, which can be used as window application is Polymer Dispersed Liquid Crystal (PDLC) films composed of liquid crystal microdroplets dispersed in a polymer matrix (Cupelli et.al. 2009). This electro-optical system behaves similar like LC as electric field causes the “transparent” state and absences of field makes it “opaque”. The refractive indices of the polymer matrix and liquid crystal must match to achieve both “transparent” state and “opaque” state (Cupelli et.al. 2009). The apparent optical state depends on the temperature and the angle of incident light. PDLC films on glass block 98% of UV, modulates the NIR band in the range 12–38%, and exhibits good temperature stability from 0 °C to 60 °C (Park and Hong 2009). The PDLC film has been found to exhibit excellent durability to electrical switching up to 3 million times at 100 VAC at 60 Hz when the switching interval was 1sec (Zhang et.al. 2003). Less thick LC material requires less switching time. Electro – optical switching effect of a 50 μm thick film polymer dispersed liquid crystal offered a 190 μs rising time to be “transparent” and a 2 ms decay time when an external electric field was applied (Petti et.al. 2003).

2.3.3. Electrochromic glazing

The electrochromic (EC) behaviour of tungsten oxide due to application of electric voltage was first observed by Deb in 1969 (Deb 1969), previously electrochromism was only associated with organic materials. The main purpose of EC glazing is to control the solar heat gain (Granqvist 2000; Granqvist et.al. 2003; Granqvist 2005; Klems 2001). Electrochromic (EC) (Marcelli 1998) includes (i) transition metal

oxides for example tungsten, iridium, rhodium, ruthenium, manganese and cobalt possesses (Lampert 1984; Goldner et.al. 1986) (ii) organic material such as prussian blue, viologens, buckminsterfullerene, polypyrrole and polyaniline (Lampert et.al. 1999; Mortimer et.al. 2006). An EC glazing is shown in Figure 2-11.

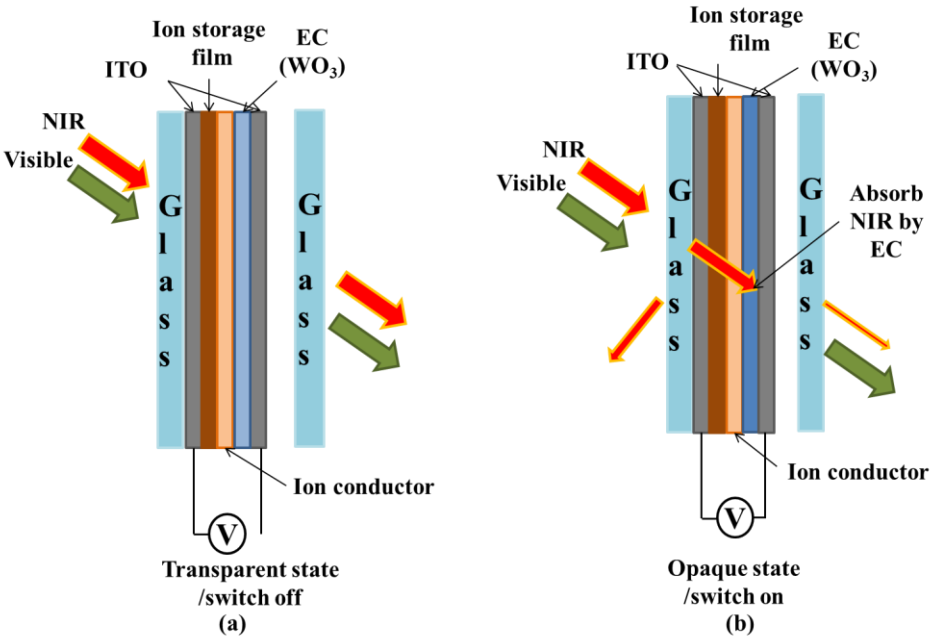

Figure 2-11: Schematic diagram of electrochromic glazing in its "transparent" and "opaque" state.

An EC material changes from "transparent" to "opaque" by redox reaction in the presence of applied D.C. voltage typically from 0 to 5 V (Fasano et.al. 2002; Rosseinsky et.al. 2001) and is reversible by inversion of electrical supply (Lee et.al. 2004; Granqvist et.al. 2012). The speed of this colour change process is lower at higher environment temperatures. Transition time from "transparent" to "opaque" state is higher than "opaque" to "transparent" state. EC material has potential to control transmissivity, absorptivity, reflectivity and emissivity of a glazing (Granqvist et.al. 2003; Granqvist 2005). In a typical EC device an EC layer, ion storage layer and ion conducting layer are sandwiched between two transparent

conducting oxides (Nagai et.al. 1999; Deb et.al. 2001; Papaefthimiou et.al. 2009). EC glazing can be considered as battery like in structure (Heckner and Kraft 2002; Kraft et.al. 2006; Granqvist et.al. 2010). Among all the materials, tungsten tri oxide (WO_3) material is suitable for EC glazing.

EC glazing controls solar heat gain by changing its transparency from "transparent" to "opaque" (Goldner and Rauh 1984; Pennisi et.al. 1999; Granqvist 2000). It has potential to control the NIR (780 nm-2300 nm) which makes it more viable in smart glazing application. In its "opaque" state crystalline type WO_3 blocks the near infrared (NIR) or reflect it (Schuster et.al.1986). By controlling NIR, an EC glazing can provide heating and cooling energy savings range from 5 to 15 kWh/m^2 yr for commercial and residential building, in comparison with high performance non switching glazing (DeForest et.al. 2013). Solar heat gain coefficients were found to be 0.39 to 0.05 for an EC material having 63% transparent state and 1.2% transparent state respectively (Georg et.al. 2009). An EC system using tungsten oxide and vanadium pentoxide showed solar transmittance modulation between 58% and 9% and visible transmittance modulation between 65% and 13% in the "transparent" and "opaque" states, respectively. Over 2000 colouration-bleaching cycles were achieved with such systems (Ashrit et.al. 1996). Another research work has reported 72.6% transparency during "transparent" state and 17.6% during "opaque" state of an EC device (Nagai et.al. 1999). 45% energy saving was found using an EC glazing for an office building in hot climate of Arizona or the very cold climate of Minnesota (Sbar et.al. 2012). A simulation study showed that 18% retrofit using near infrared switching electrochromic (NEC) of a building window stock could save 50% energy and 39% retrofit could save 75% of buildings total energy saving (DeForest 2015). EC materials have poor durability due to sensitivity to the

UV radiation (Tracy 1999; Lampert 2003; Lampert 2004). EC materials can only be used nearly 2000 cycles (transparent to opaque; opaque to transparent). Frequent ion insertion during colouring and bleaching process also reduces the durability of an EC material (Masetti et.al. 1995). As switching process of EC materials are not uniform, they are not generally suitable for large area application. Switching below 0 °C may cause device degradation due to ice formation in WO_3 pores (Lampert et.al. 1999).

2.3.4. Thermochromic glazing

Thermochromic glazing can control the infrared radiation transmission (IR) by changing their crystal structure in the presence of environmental temperature variations (Ye et.al. 2012; Long and Ye 2014; Saeli et.al. 2010). A colour change for thermochromic glazing is shown in Figure 2-12.

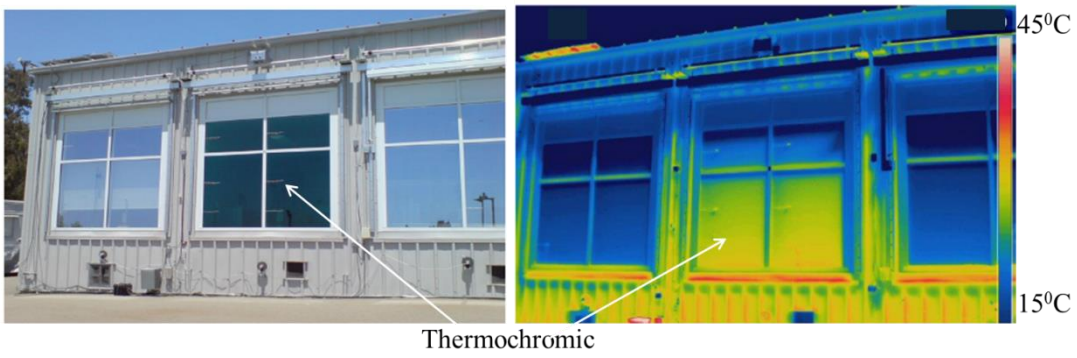

Figure 2-12: Outdoor view of the south-facing thermochromic window (middle room with the dark windows). Below: Corresponding infra-red image showing the surface temperature of the windows (^{0}C) on June 16, 12:02 PM, Berkeley, California at a latitude of 37.91 ^{0}N (Lee et.al. 2013).

Vanadium dioxide (VO_2) is the most popular thermochromic glazing material with a transition temperature (T_C) of 68 ^{0}C (Morin 1959) above which it behaves like metal and reflects infrared and below this it behaves like insulator being infrared transparent. Other thermochromic materials include iron oxide (Fe_3O_4), iron silicide ($FeSi_2$), niobium dioxide (NbO_2), nickel sulphide (NiS), and titanium oxide (Ti_2O_3;

Ti_4O_7; Ti_5O_9). This phase change from metal to insulator occurs within 10-12 sec (Wang et.al. 2013 Huang et.al. 2011; Ye et.al. 2013; Khan et.al. 1998; Khan and Granqvist 1989; Lee et.al. 2013; Lee et.al. 2002).

For large area applications, the expensive method of fabrication is the biggest drawbacks of using VO_2. In addition, high transition temperature (68 ^{0}C) of thermochromic glazing is also proven to be a barrier for many building applications.

2.3.5. Thermotropic glazing

Thermotropic materials at low temperature are "transparent" and above a switching temperature, both transmitted and reflected lights are scattered rendering it "opaque". Figure 2-13 illustrates a thermotropic glazing, at low temperatures; the two transparent main components are mixed homogeneously, thus appearing transparent. Above the threshold switching temperature, the components separate and the layer becomes "opaque". Thermotropic materials can be

- phase separating systems (Hydrogels, polymer blends and lyotropic);
- systems with fixed domain;
- phase change material (Nitz 2005).

A hydrogel type thermotropic is an aqueous polymer gel consisting a long chain of a second polymer. A hydrogel thermotropic glazing has been reported for large area application where the matrix material was water with water-soluble polymer hydrophobic groups, sodium chloride, and an amphipathettic molecule (Watanabe 1998) shown in Figure 2-13. The main components of thermotropic polymer blends are polystyrene-co-HEMA and polypropylene oxide. At low temperature, these two layers having different refractive indices mix to each other. These two polymers become separated at the switching temperature (Raicu et.al. 2002). For lyotropic type thermotropic material a liquid crystal, changes its colour from "transparent" to

"opaque" state (Seeboth et.al. 2000). To date no such glazing is available commercially.

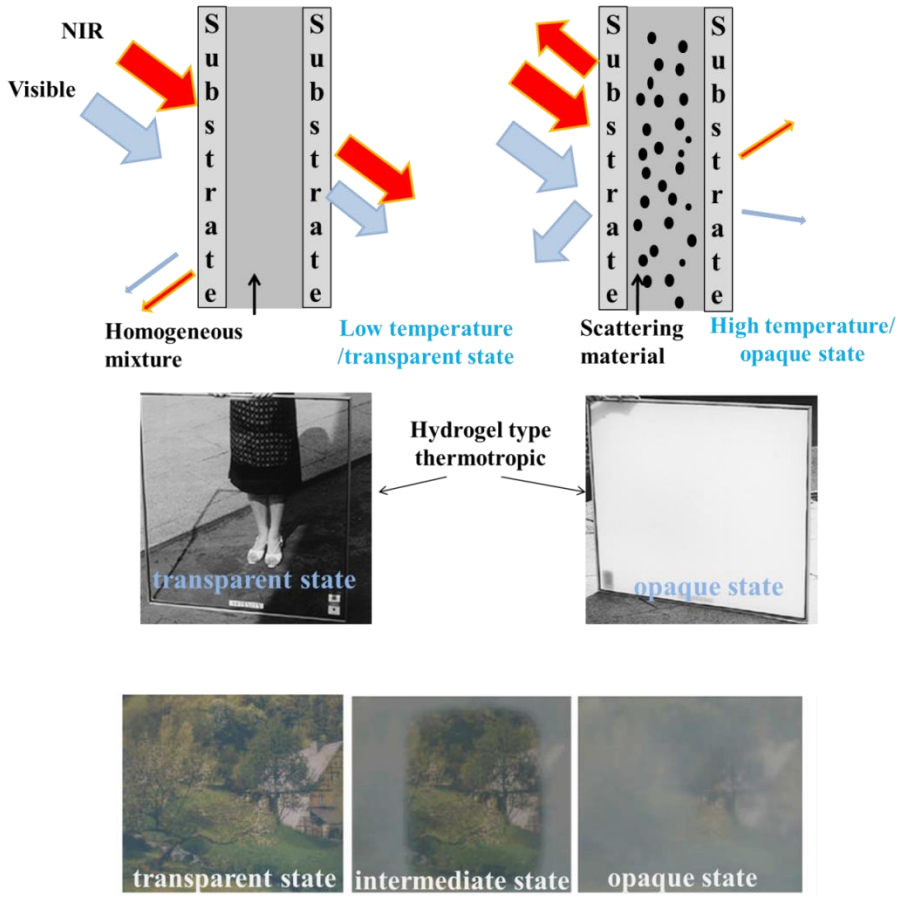

Figure 2-13: From top to below - Thermotropic glazing in "transparent" and "opaque" state (Nitz 2005), Hydrogel thermotropic glazing "opaque" state and "transparent" state (Watanabe 1998), Switching process of a thermotropic resin glazing laminate Okalux GmbH, Germany (Nitz 2005).

Although a number of studies on thermotropic materials have been done, most of them were conducted on chemical materials (Zrinyi et.al. 2001; Resch et.al. 2008; Dimitrov et.al. 2007; Starovoytova and Spevcek 2006; Mitsumata et.al. 2007), which are expensive and require complex technical process, even some of the materials are toxic (Arno and Hans-Rainer 1996). Moreover, many important properties such as energy, indoor thermal environmental and daylighting performance have rarely been investigated which hinders the application of thermotropic windows in reality.

2.3.6. Phase change material glazing

Phase change material (PCM) is a type of thermotropic material, opaque when solid and become transparent when melted shown in Figure 2-14.

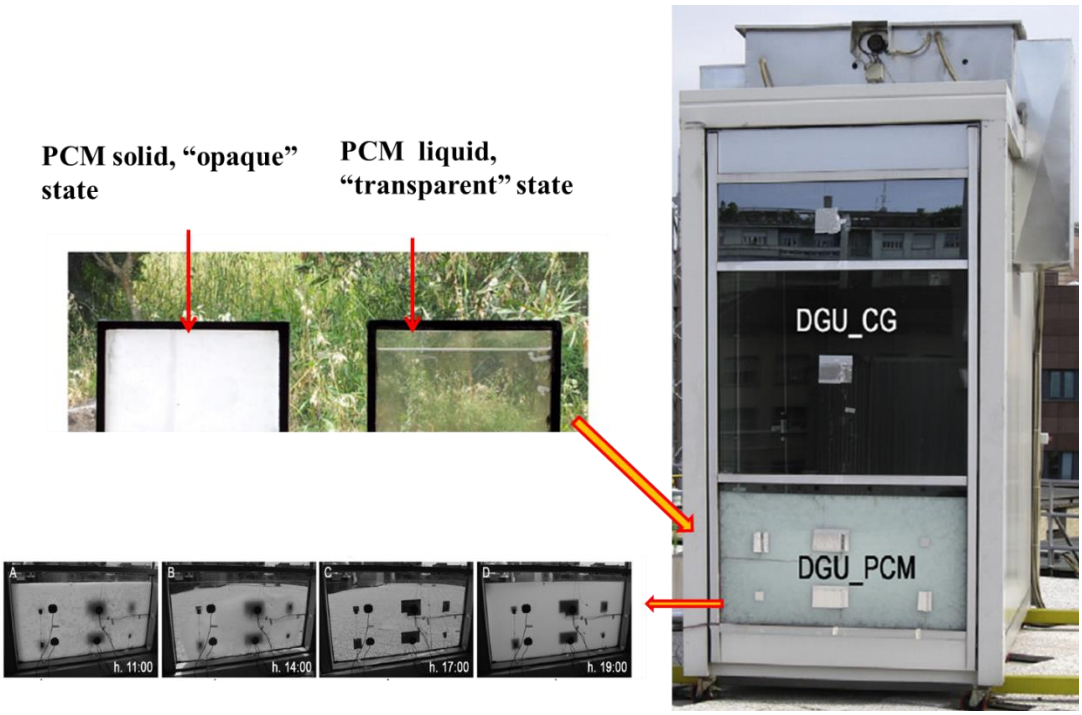

Figure 2-14: Paraffin wax phase change material in double glazing unit (DGU-PCM) in "opaque" and "transparent" state, DGU-PCM glazing unit in a test cell and a dynamics of the melting and re-solidification process of the paraffin layer within DGU-PCM during a sunny summer day (Goia 2012; Goia et.al. 2013; Goia et.al. 2014).

It can store large amounts of energy within their phase transition (Goia et.al. 2013; Goia et.al. 2014; Goia et.al. 2015; Manz et.al. 1997; Zhou et.al. 2012; Jin et.al. 2013; Ismail and Henriquez 2002; Ismail et.al. 2008). The temperature of the PCM is nearly constant during the melting and solidification process. Some PCMs are highly transparent for the visible part of solar radiation whereas the infrared part is absorbed within the PCM. Because of the latent heat storage effect of the PCM, they can equalise energy balances over the course of day. Especially on winter evenings, facade panels with PCM have been shown to improve thermal comfort considerably (Weinlader et.al. 2005). At high temperature PCM become clear and transparent

which makes it not suitable for solar heat gain control and daylight application, as it cannot provide low visibility at high temperature.

2.3.7. Gasochromic glazing

Gasochromic glazing changes its colour due to alternate addition of hydrogen and oxygen (Georg et.al. 2000; Georg et.al. 2001; Yoshimura et.al. 2009; Chan et.al. 2010; Witter et.al. 2004). This glazing consists of a porous, less than 1 μm thick columnar film of WO_3, which is coated with a thin film of platinum (Pt) (Granqvist 1995). On exposure of low concentration of hydrogen (below the combustion limit of 3%) gas, the glazing colours blue and when expose to oxygen, it bleaches to the original transparent state (Georg et.al. 2000). This switching process takes less than 10 s. Gasochromic material sandwiched between double-glazing have potential to offer up to 75% solar transmittance.

2.4. Combined glazing systems

Research has been done to combine low heat loss and heat gain reduction using EC-vacuum. EC glazing needs an external supply that can be reduced by combining PV and EC. Descriptions of these combinations are provided in this section.

2.4.1. EC-vacuum glazing systems (low heat loss switchable glazing)

Vacuum glazing and EC glazing have been combined to achieve low heat loss, control, daylight and solar heat gain together as shown in Figure 2-15 (Papaefthimiou et.al. 2006).

This device used 3 glass panes where two glass panes were separated with a vacuum and the other glass panes having a small layer of EC are sealed with the vacuum glazing. 1st Vacuum – EC device was fabricated by Papaefthimiou et.al. (Papaefthimiou et.al. 2006).

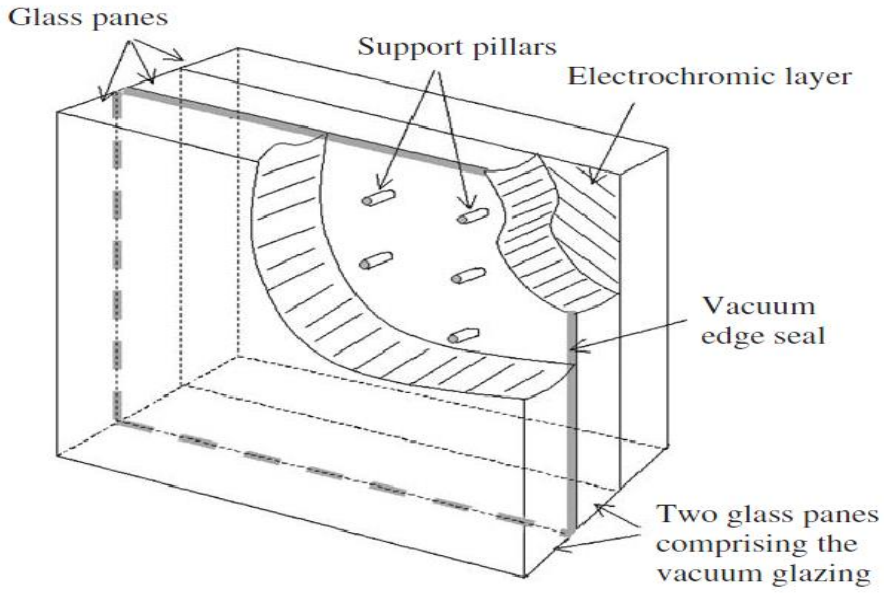

Figure 2-15: Schematic diagram of EC-vacuum glazing (Papaefthimiou et.al. 2006).

This prototype (40 cm × 40 cm) was able to achieve transparency from 63 % (bleached state) to 2 % (coloured state) with a mid-pane *U*-value of 0.86 W/m^{2}K. Fang and Eames study showed that, to avoid intolerable over heating an EC layer between vacuum glazing, a third glass pane should always face the outside environment (Fang and Eames 2006). During opaque condition of EC layer, the absorbed solar radiations works as a heat source and transmit heat to the inside of the room. Addition of low emittance layer with the vacuum gap on the glass panes also works as a heat source with EC and it was found that using two low-e coating is not effective compare to one low-e coating (Fang and Eames 2006; Fang et.al. 2008; Fang et.al. 2010).

2.4.2. Photovoltaic-Electrochromic (PV-EC) glazing systems (Self-powered switchable glazing)

Electrochomic (EC) device needs external supply to change the colour from bleaching state to colour state. Inclusion of PV with EC will eliminate the need for external supply and make it a self-sustainable device. The idea of combining a

photoconductive and EC device (PV-EC) was first explored for an electrophotographic application (Deb 1969).

Combined PV-EC device has shown numerous advantages

- PV device generates DC power, which matches the use of DC for enabling direct coupling of PV and EC.
- At high temperature PV device efficiency drops which enhance the reduction of maximum power output (Krauter et.al. 1999; Raziemska 2003; Browne et.al. 2015). For crystalline PV above 25 ^{0}C its power drops with a coefficient between 0.4%/K (Weakliem and Redfield 1979) to 0.65%/K (Raziemska 2003). At higher temperatures due to higher ion mobility, switching responses of EC devices are faster which reduce the amount of required voltage (Skryabin et.al. 1999; Matthews et.al. 1999; Matthews et.al. 2001). These two properties also enhance the coupling of PV-EC device.

To date, different types of PV power EC devices have been investigated. Figure 2-16 illustrates the different types of PV and EC and combined structure of these types of PV-EC. In a PV-EC device, PV material can be four types and EC are two types. These six different types create three possible types of structure.

Dye sensitized solar cell (DSSC) based PV-EC device (DeBerry and Viehbeck 1983; O'Regan and Gratzel 1991; Bechinger et.al. 1996; Hauch et.al. 2001; Nokki et.al. 2007; Ahn et.al. 2007; Hsu et.al. 2008; Wu et.al. 2009) are potentially low-cost devices with a good match to typical diffuse solar spectra. However, they can have low stability due to photochemical degradation (Nogueria et.al. 2006; Macht et.al. 2002).

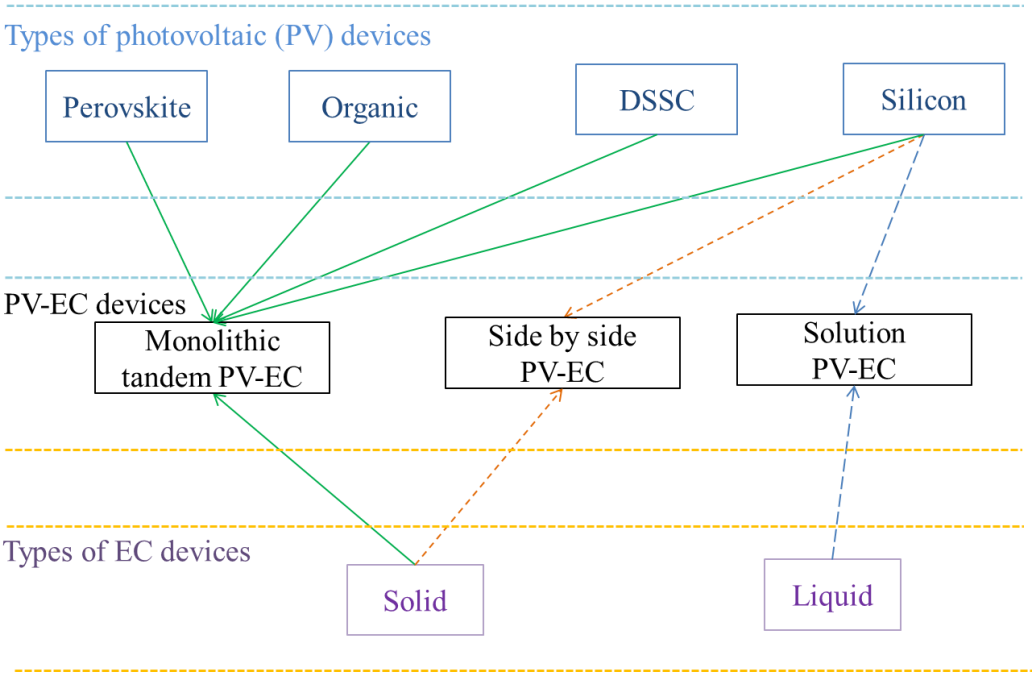

Figure 2-16: Classification of PV - EC devices.

A silicon based PV-EC device is shown in Figure 2-17 where the upper half is the EC and the lower half is the PV.

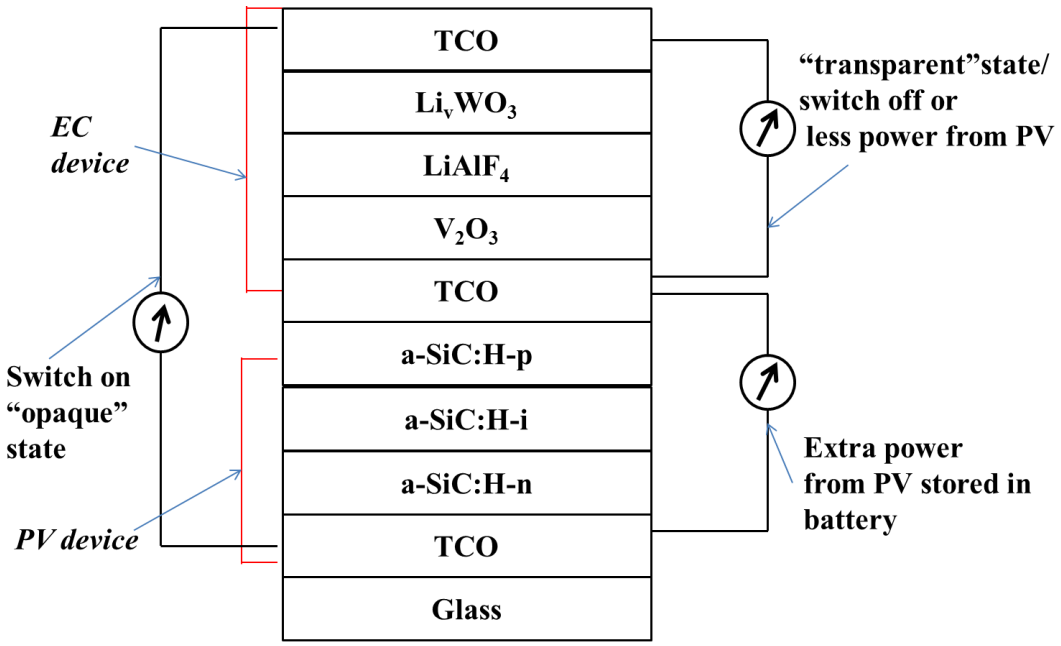

Figure 2-17: Schematic diagram of PV–EC device (Deb et.al. 2001).

The middle contact permits battery and user control. The critical issue in silicon based PV-EC device (Branz et.al. 1994; Benson and Branz 1995; Bullock et.al. 1996; Gao et.al. 1999; Gao et.al. 2000; Deb et.al. 2001) development lies in its low optical contrast in between opaque and transparent state. The transparency of the PV-EC device can be improved by the incorporation of wide band gap semi-transparent amorphous silicon carbon alloy. However, as the semi-transparent PV thin films become very thin, electrical short circuit occurs easily that renders the PV-EC stacks inoperable (Deb et. al. 2001; Ahn et. al. 2007).

Semi-transparent perovskite PV and solid-state EC cells enables solid-state photovoltachromic devices with 26% average visible transmittance and 3.7% maximum light power conversion efficiency has been reported for a new PV-EC device as shown in Figure 2-18. Activating self-tinting, the average visible transmittance drops to 8.4% (Cannavale et.al. 2015).

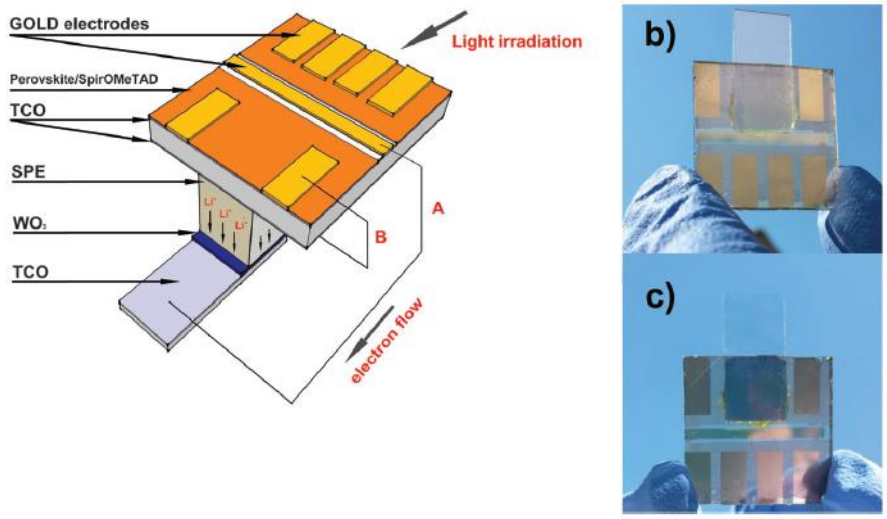

Figure 2-18: Axonometric view of the photovoltachromic device. Two external circuits connect the photoanode to the electrochromic electrode (a) and the gold cathode to the secondary electrode of the electrochromic device. (b) Pictures of the device under bleached (c) and coloured conditions (Cannavale et.al. 2015).

Using two-inverted transparent organic PV, a solution-processed polymer vertically integrated PV-EC window has been reported (Dyer et.al. 2014). The achievement of low intensity of 250 W/m^2 with a switching time of 3–6 s had demonstrated the feasibility of the PV-EC in window applications under oblique illumination of the Sun.

All the four types of PV can be integrated with solid type EC materials. Solution type PV-EC material has been reported (Huang et.al. 2012a) where electrochromic solution is located between the transparent non-conductive substrate and the silicon-thin film solar cell (Si-TFSC) substrate and shown in Figure 2-19. This system has advantages as electrodes in the PV-EC device is planarly distributed in the semi-transparent Si-TFSC substrate, which can create a uniform electric field. This makes large area PV-EC module application feasible. Thickness of thin film PV cell can be made thinner due to low power requirement of PV-EC and overall system will have higher transparency (Huang et.al. 2012a; Huang et.al. 2012b).

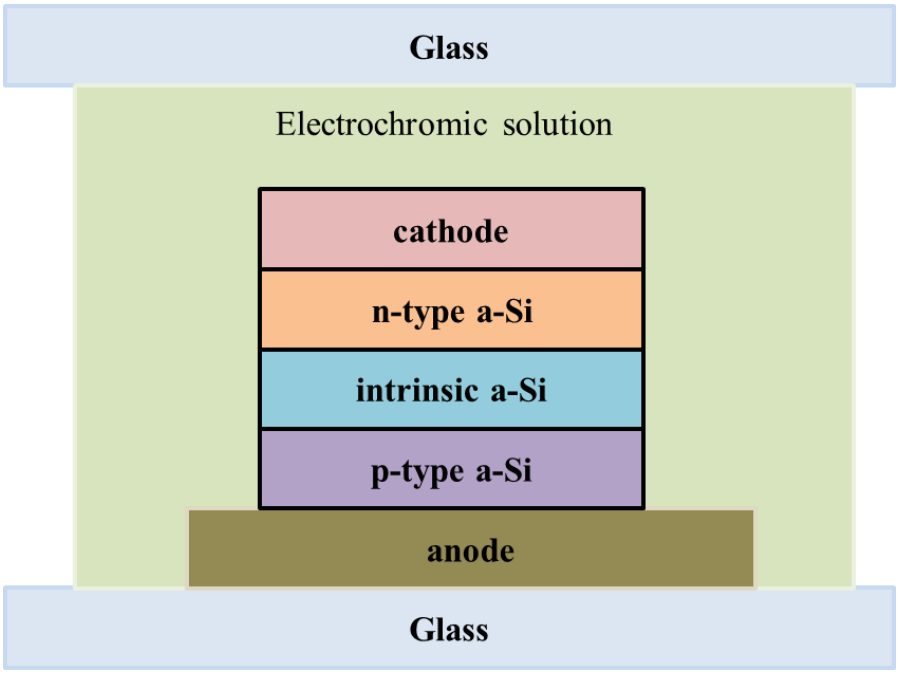

Figure 2-19: Solution type PV – EC device.

From Figure 2-16, four different types of PV and two different types of EC produce three different PV-EC structures, which are side-by-side, tandem types and solution types.

Tandem structure- DSSC (Ahn et.al. 2007; Nokki et.al. 2007) and hydrogenated amorphous silicon-carbon (a-SiC:H) photovoltaic-powered monolithic tandem EC devices were reported (Gao et.al. 1999). Monolithic and monolithic tandem both reduce the overall transmittance of the system as sunlight passes through both the PV and the EC (Bechinger et.al. 1996; Bullock et.al. 1996; Gao et.al. 1999). Fabrication process of this tandem structure is also challenging (Deb et.al. 2001). To obtain higher transparency, semi-transparent PV is recommended which eventually reduces the overall cell efficiency (Ahn et.al. 2007). However, no external wiring makes this type of device advantageous. For a side by-side PV–EC device, PV can be placed on the window frame (Benson and Branz 1995) or PV can be building integrated photovoltaic (BIPV) types (Ma and Chen 2012). High efficiency opaque PV can be used as no blocking of insolation occurs from the PV device.

Solution EC and PV type structures solve the short circuit problems encountered in the tandem PV-EC structures (Deb et.al. 2001; Gao et.al. 1999).

Advantages and disadvantages of constant and switchable transparent glazings have been listed in Table 2-3 and Table 2-4 respectively.

Table 2- 3: Advantages of constant and switchable transparent glazings

Double glazing	Easily accessible, low cost, matured technology, potential *U*-value control compare to single pane
Low-e coated glazing	It has potential to control *U*-value and solar heat gain
Water flow glazing	Potential candidate to control solar heat gain without losing the transparency
Air flow glazing	Mostly used for solar heat gain control
Aerogel glazing	Good candidate for controlling overall heat transfer coefficient
Evacuated glazing	Mature technology for controlling overall heat transfer coefficient, commercially available from Nippon sheet glass
PV glazing	Good candidate for solar heat gain control and can be applied for small-scale renewable energy generator
Gasochromic glazing	Due to switchable transparency two different types of solar heat gain is possible , control near infra-red solar radiation
Thermochromic glazing	It has potential to reflect infrared solar radiation.
Thermotropic glazing	Can control solar heat gain by reflecting near infra-red solar radiation
Phase change material glazing	Low cost material and available. Control solar heat gain by absorbing infrared solar radiation
Electrochromic glazing	It has potential to control near infra-red solar radiation, switchable, low voltage and power requirement to switch
Liquid crystal glazing	Fast switching process and work with AC power supply, which enhance the powering from mains
Suspended particle device glazing	Fast switching, intermediate transparency and work with AC power supply

Table 2- 4: Disadvantages of constant and switchable transparent glazings

Double glazing	Due to constant transparency no control of glare, and excessive incoming daylight and solar heat gain, extra shading device is required.
Low-e coating glazing	Cost and durability is a major issue. For daylighting and glare control this is not suitable
Water flow glazing	Changing the water flow the solar heat gain can be controlled but no control on transparency, which can offer high glare
Air flow glazing	Changing the water flow the solar heat gain can be controlled but no control on transparency, which can offer high glare.
Evacuated glazing	No control on transparency, which can offer high glare and solar heat gain
Aerogel glazing	Due to opaque in nature for glazing application is not suitable
PV glazing	Durability of PV is an issue and PV device can get warmer at high temperature
Gasochromic glazing	Using hydrogen chamber can be dangerous for everyday use in office or domestic application
Thermochromic glazing	Requires high temperature (68^0C) to change the colour
Thermotropic glazing	Most of thermotropic materials are expensive and require complex technical process, even some of the materials are toxic
Phase change material glazing	During daytime when it needs to be opaque to control glare become transparent. No control of overall heat loss
Electrochromic glazing	Durability and power requirement for both states and slow switching process is major drawbacks
Liquid crystal glazing	No intermediate state and scattering light make it hazy to see through
Suspended particle device glazing	High voltage requirement, constant power requirement to obtain transparent state

2.5. Summary

Available constant transparency glazing such as double pane glazing, low-e coated glazing, water flow and PV glazing offer control of solar heat gain. Constant transparency makes them less attractive as they are only suitable for particular situation and after installation transparency changes is not possible based on dynamic solar radiation.

Non-electrically actuated switchable glazing such as thermochromic, thermoctropic, gasochromic, phase change material glazing are not controllable as they change their states depending on some external specified condition which reduces the potential selection of these type of glazing.

Electrically actuated switchable transparency glazing such as EC, LC and SPD change their transparency in a controllable manner which enhance the usability of this type of glazing.

SPD glazing has the following advantage over LC glazing

(i) in "transparent" state, there is no haze like LC (Papaefthimiou et.al. 2006);

(ii) it has intermediate transmission variations between "opaque" and "transparent" state (Barrios et.al. 2013).

SPD glazing has the following advantages over EC glazing:

(i) it can be directly connected to the main power supply whereas EC glazing requires an inverter to convert an AC main supply to DC;

(ii) to maintain the "opaque" state no power is required;

(iii) switching process of an EC material is not uniform;

(iv) EC materials can only be used nearly 2000 cycles (transparent to opaque, opaque to transparent);

(v) slow switching time of EC glazing is a major drawback of EC. Sky condition changes from 20 to 40 klux within 1-2 s whereas EC glazing changes its colour between 1 to 30 minutes, depends on the size. Switching speed decreases with increased glazing area (Ho 1999; Lee and DiBartolomeo 2002; Lee et.al. 2006);

(vi) EC layer rejects heat by absorption, rather than reflection, and so can get quite hot when irradiated. For some EC devices, switching is not possible if the maximum design temperature is exceeded (Lee 2002).

So far, no experimental work has been performed to investigate the solar heat gain, heat loss and daylighting and glare control potential of SPD glazing.

As SPD needs power to switch on, PV powered SPD can make it an autonomous glazing. There is no reported work on PV powered SPD glazing.

To achieve lower heat loss this glazing can be added with one vacuum glazing as vacuum-EC was not successful. In vacuum-EC glazing, it was recommended to place the EC device facing outside as inside facing could increase the surface temperature at 129.5 ^{0}C for an incident insolation of 600 W/m^{2}. Until now, no SPD-vacuum combined work has been reported.

Chapter 3. Research methodology and design of experimental set up

3.1. Introduction

This chapter introduces the overall methodology to find out the four parameters of SPD glazing and experimental characterisation details. Reviews of available test cell experiments for thermal and daylighting characterisations are presented. The design and fabrication of test cell, glazing specification and experimental set up are also described in this chapter.

3.2. Glazing selection

The requirement for electrical actuating and fast switching from on to off state determined the selection of SPD glazing for this research. To achieve combined low heat loss switchable glazing SPD-vacuum glazing system were considered. A PV panel through an inverter powered this SPD glazing to achieve a self-powered low heat loss switchable SPD (PV SPD/vacuum) glazing system. Details of SPD glazing, SPD double-glazing, vacuum glazing and SPD vacuum glazing systems are described in section 3.6 of this Chapter.

3.3. Overall methodology

This proposed research includes the experiments and modelling parts as shown in Figure 3-1. Thermal, daylighting and electrical characterisation of SPD glazing was performed to determine overall heat transfer coefficient (*U*-value), solar heat gain coefficient, daylight and daylight glare index using semi empirical method.

A semi-empirical model consists of a series of equations, where critical parameters are determined according to real performance data. To measure this critical parameters test cell experiment was employed.

Major variable parameters such as solar radiation and external illuminance were measured to use them in daylighting, electrical and thermal semi empirical method. From measured solar radiation and using extra-terrestrial solar radiation, clearness index was calculated. Solar radiation and using illuminance luminous efficacy was calculated as described in Chapter 4. Correlation between clearness index and glazing transmittance was evaluated.

In the semi empirical daylighting method, external and test cell internal illuminance were measured. Internal illuminance parameters were then employed to find out daylight glare index and daylight factor due to SPD glazing as described in Chapter 5.

In electrical characterisation, first PV powered SPD glazing was performed as described in Chapter 6. Measured field data was then used to find out the optimized PV and glazing area and cost of the system using loss of power supply probability (LPSP) method. Detailed methods of LPSP are explained in Chapter 10.

Semi-empirical models are often applied to describe the thermal behaviour of glazing due to the complex internal and external heat transport mechanisms. In a thermal semi-empirical method solar radiation and temperatures were measured to be used as an input variable to find out the *U*-value and solar heat gain coefficient of SPD glazing, vacuum glazing and SPD-vacuum glazing as described in Chapter 7, 8, 9.

Details of test cell approach and experimental design and instruments are described in the following sections.

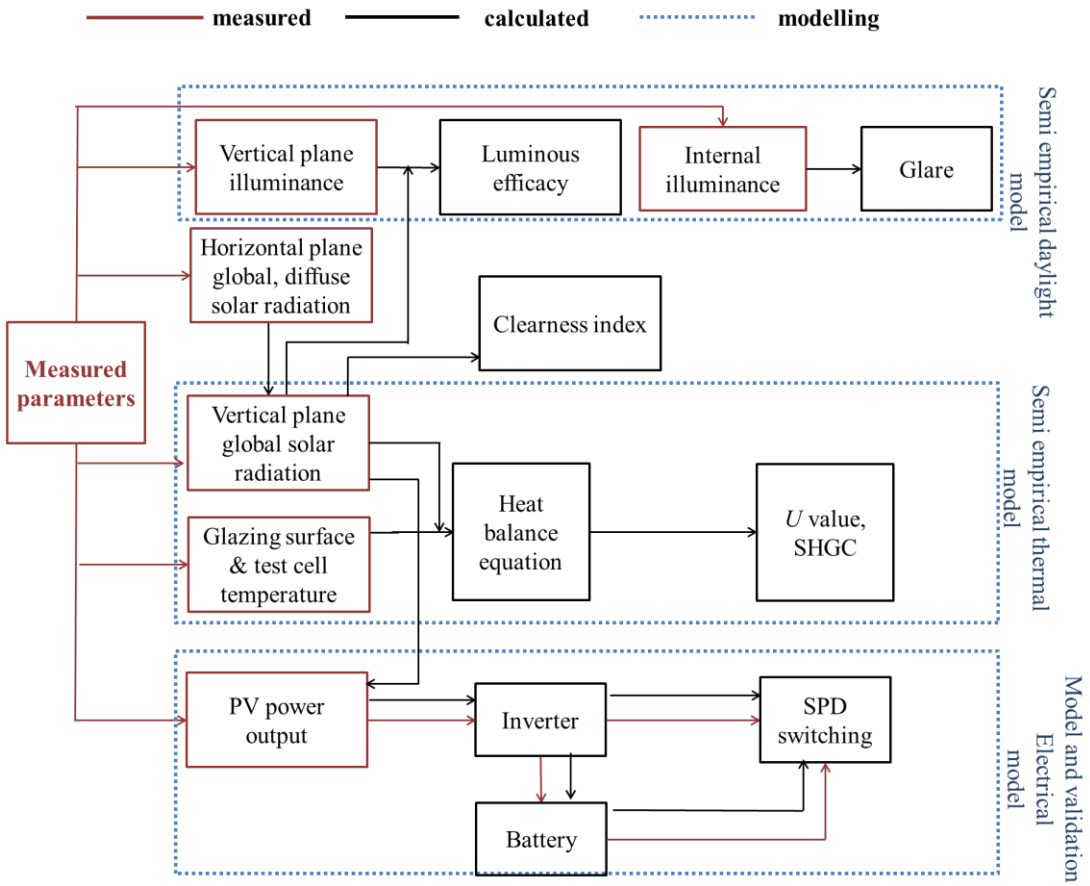

Figure 3-1: Schematic diagram of overall methodology.

3.4. Review of test cell research methodology

Thermal properties of glazing systems can be evaluated by using indoor or outdoor experiment.

Indoor experimental process of glazing systems involves hotbox method. Each hotbox configuration consists of two-closed chambers where one is cold chamber and other one is hot. The two chambers are divided by the glazing that allow to heat-flow from hot chamber to cold one. The heat-flow between the two chambers produces the glazing's thermal properties (Kuhn et.al. 2000; Harrison and Dubrous 1992; Harrison and van Wonderen 1994). The measurement method for the thermal properties in the lab has become relatively mature and many standards, such as ISO (ISO 1991; ISO 1991b; ISO 1992; ISO 2010) and ASTM (ASTM 2000; ASTM

2004) have been formulated since 1991. At present, the heat flow meter method (HFM), the guard hot box method (GHB) and the calibrated hot box method (CHB) are commonly used in the indoor laboratory conditions (Jones and Jones 1999). The common characteristic of above three methods is that the environmental temperature on two sides of the measured object is carefully controlled to ensure the measurement accuracy. To obtain efficient results from HFM, the indoor and outdoor air temperature difference needs to be sufficiently high. Therefore, the HFM is only used in heated buildings in winter or air-conditioned buildings in summer, demonstrating that the HFM has a great dependence on seasons and heating & air-conditioning equipments (Cesaratto and Carli, 2013). The GHB is not limited by indoor and outdoor air temperature, but it needs large area of the metering box and the guard boxes. Small devices (less than 1 m^2) are not suitable for this experiment. The CHB is used to measure wall thermal transmittance in the lab; it needs to utilize a standard wall to calibrate the boundary heat loss of the hot box under the certain environment. In the hotbox method, indoor sun simulator is often used for heat source. Ideally, the sun simulator radiation should resemble the standard sun radiation condition used in the glazing or fenestration performance rating method (NFRC 200-2010; NFRC 300-2010). Sun simulators are often suffers from their spectrum mismatch, spatial non-uniformity and temporal instability. Sun simulator spectrum-shows the normalized solar spectrum in the wavelength range of 300–1678 nm, in comparison with the standard AM1.5 direct normal irradiance spectrum (Chen et.al. 2012). Characterisation made in indoor laboratory give the chance to accurately control on ambient temperature, relative humidity and air velocity but never fully offer the complex interactions of pure stochastic processes typical of real climate. Also, lack of appropriate sun simulator, which does not match with sun

spectrum, limits the use of indoor facility for thermal characterisation of glazing systems.

The *U*-value and solar heat gain coefficient of a glazing is not constant parameter but varies with the temperatures of the internal and external environments (Robinson and Littler 1993) of a building and solar radiation. Standard American Society of Heating, Refrigeration and Air-conditioning Engineers (ASHRAE) U-value calculations and laboratory-based measurements, such as those carried out in guarded and calibrated hot boxes are inadequate to assess fully the thermal performance of glazing leading to significant errors when such results are used in building energy performance models (Robinson and Littler 1993). Outdoor characterisation using test cell (Tait 2006a, Tait 2006b) offers to investigate the influence of real time external driving forces, such as external temperature, wind speed and direction, solar direct radiation, diffused radiation from the sky and the ground, external humidity on the glazing sample. Test cells fill the gap between laboratories and full-scale buildings, by allowing all the necessary controlled indoor conditions and varying outdoor conditions in the real environment. Glazing system characterisation under dynamic, real climatic conditions and in an indoor environment that is rather similar to an actual office space in terms of visual, acoustic, and thermo-physical properties and airflow patterns, test cell set up is the best (Robinson and Littler 1993; Alvarez et.al. 2000; Aleo et.al. 2001; Loutzenhiser et.al. 2008; Krüger et.al. 2009; Olivieri et.al. 2014). In addition, test cell experiments can be used to assess the representativeness of laboratory results and to empirically validate modules of building energy simulation tools. Results obtained through test cell experiments can be beneficial to designers and manufacturers to optimise the design and realisation of their products, researchers to analyse and model the heat

transfer phenomena and other physical phenomena occurring under measured boundary conditions and end-users. Table 3-1 illustrates the comparison between indoor hotbox method and outdoor test cell method.

Table 3- 1: Comparison between indoor hotbox and outdoor test cell experimental characterization.

		Indoor hot box	Outdoor test cell
Properties	Location	Indoor set up	Outdoor set up
	Source of heat	Indoor sun simulator (limited solar spectrum is available)	Sun is the main source (full solar spectrum is available)
	Control on parameter	Ambient temperature, air velocity, simulator intensity can be controlled	Controlling parameters are not possible
	Experiment period	Testing period does not required longer compared to test cell. Within few hours, targets can be achieved	longer testing periods compared to steady-state laboratory tests, although test cell experiments provide more information on the dynamic performance of the test sample
	Results from the experiment	Due to measure in control environment, data used in simulation will have less chance to produce in appropriate results	Measured results can be used in building dynamic simulation
	Uncertainty of the experiment	Standard procedures are available which reduce the test conditions uncertainty	Lack of standardized procedures (CEN, ISO or national) still hinders the wide penetration of this kind of tests in the building market

3.4.1. Test cell for thermal analysis

A test cell experiment is the most suitable apparatus for glazing thermal performance measurement (Alvarez et.al. 2000; Aleo et.al. 2001) leading to evaluation of *U*-value and solar heat gain calculation. A test cell allows passive solar components such as

window to be characterised under real environment condition (Grimmer et.al. 1979; Wouters et.al. 1993; Manz et.al. 2006).

An insulated test cell can be considered as a representation of an insulated small-scale room (Baker and McEvoy 2000) for the thermal and daylighting experiment of passive solar components (Wouters et.al. 1993) and should have a large enough south facing glazing which can admit solar radiation, offer high thermal insulation and large thermal capacity within the insulated envelope. Three major test cells are particularly noteworthy

- The Mobile Window Thermal Test facility (MoWiTT) was designed mainly to measure the dynamic net energy of window system at the Windows and Daylighting Group at Lawrence Berkeley Laboratories (Klems et.al. 1982; Klems 1987; Klems 1984). It had capabilities of full scale testing of window and skylight units of various size and types.
- The Room Calorimeters at the National Bureau of Standards in Washington;
- Passive Solar Systems and Component Testing (PASSYS) test cells in the European Community Programme (Hahne and Pfluger 1996; Vandijk and Vander 1993; Wouters et.al. 1993; Strachan 1993; Aleo et.al. 2001; Wouters and Vandaele 1994) was designed for characterising of building products. 35 identical outdoor test cells were set up in 10 countries of the European Union. Investigations of various advanced building facades were carried out and the thermal properties were determined by outdoor tests at various locations in Europe.

To date different low internal volume (< 8 m^3) test cell has been investigated for glazing thermal characterisation. Piccolo 2010 employed a small cubic test cell (interior edge of 43 cm) to study the thermal and optical properties of a small-size

electrochromic glazing. The thermal transmittances of the front-wall and of a sidewall of the test cell were estimated to be respectively 2.4 and 1.2 $W/m^2 K^{-1}$. The experimental testing facility at Hong Kong Polytechnic University was composed of two identical test cells, each with the dimensions of 1.22 m × 0.82 m × 0.99 m. The cells were used to study the fluid flow in the air cavity and thermal performance of a double sided façade with transparent thin-film or a-Si solar cells (Han et.al. 2013). Lopez et al. 2013 reported of a test cell with circulating water chamber. The stratigraphy of the test cell from the inside to the outside was: 0.012 m thick plywood with anti-damp treatment, 0.16 m thick extruded polystyrene and 0.004 m thick reflective insulation comprising a 8×10^{-6} m pure aluminium sheet and a 0.004 m layer of polyethylene bubbles. The overall thermal transmittance was estimated about 0.18 W/m^2 K. Olivieri et.al. 2014 reported of a test cell in Madrid which was made of 0.16 m thick extruded polystyrene (XPS) board with phenolic plywood in both sides and a protective plastic film as outer layer. The overall thermal transmittance was about 0.2 W/ m^2 K. The facility was used to test the thermal, daylighting and electrical performance of semi-transparent photovoltaic modules and compare it with a code-compliant conventional glass. Different other test cells are mentioned elsewhere (Mara et.al. 2000; Roche and Milne 2004; Cheng et.al. 2005; Qahtan et.al. 2011; Revel et. al. 2014; Roche and Umberto 2014; Silva et. al. 2015a, 2015b).

To maintain the inside temperature of a test cell, water flow or airflow through a heat exchanger is used (Ghosal et.al. 2004; Prabhakant and Tiwari 1991; Yadav et.al. 1989; Lawrence and Tiwari 1990; Tiwari and Lawrence 1991; Norton and Probert 1982; Norton and Probert 1984). Of all the fluids that can be used inside the heat exchanger, water has the following benefits:

- Low cost, it is easily available (on new construction sites as well as in renovation work); it is highly opaque to infrared radiation and highly transparent.
- The heat capacity of water is about 1000 kcal/m^3K, which is about 3000 times that of air. The figure is even over that of iron, which is about 740 kcal/m^3K. Thus, water has potential to extract higher amount of heat compared to air and even iron (Lee et.al. 2006).
- Water film absorbs the short wave radiation and transmissivity of the glazing is not destroyed as water films work as an antireflection coating (Qahtan et.al. 2014).

Experimental investigations also shown that the test cell with water flow has more potential to control the inside heat than airflow (Lopez and Molina 2013). Heat gains through the test glazing were balanced by the energy extracted by the heat exchanger of the test cell.

3.4.2. Test cell for daylighting and glare calculation

Daylight glare index using an outdoor test cell for switchable glazing was first investigated by Picolo (Picolo et.al. 2009a; Picolo and Simone 2009b) using Nazaals glare index method (Nazaal 2001; 2005). The switchable glazing and test cell ratio was 1:10 (Picolo et.al. 2009a). Evaluation of daylight discomfort glare in test chambers with simulated windows has been investigated (Boubekri and Boyer 1992; Boyce and Beckstead 1991; Chauvel et.al. 1980; Iwata et.al. 1991; Iwata et.al. 1992; Iwata and Tokura 1998). Results from this method do not adequately represent discomfort glare from real daylight, as the light source used is artificial.

3.5. Design and fabrication of test cell

From review, it was evident that to achieve best results a test cell should have south facing opening for glazing, thermally insulated and test cell and glazing ratio between 1:10. Two small-scale test-cells, dimensions of 0.7 m × 0.7 m × 0.7 m were fabricated in the Dublin Energy Lab in DIT. Different stages of the test cell fabrication processes are shown in Figure 3-2. Each cell was made by wood and inside was 0.15 m thick polystyrene insulation material. Full view of test cell is illustrated in Figure 3-3. All the internal walls of the cell (floor and ceiling included) are coloured with matt white paint of reflectance 0.8. The test cells were placed on the DIT Kevin Street building roof to get unobstructed solar radiation and illuminance. The area of glazing and the test cell were 1:8. It was considered representative of the scale model (1:8) of an unfurnished room approximately cubic in shape and is used as test module for lighting measurements. Photographic view of two test cells are shown in Figure 3-4.

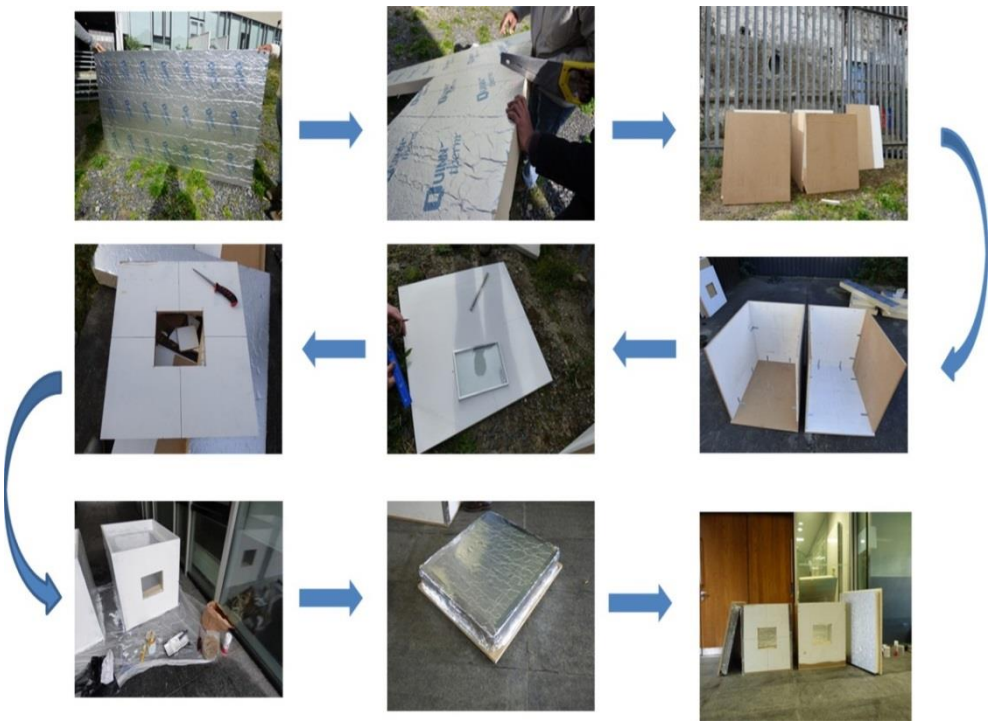

Figure 3-2: Different stages for test cells fabrication process.

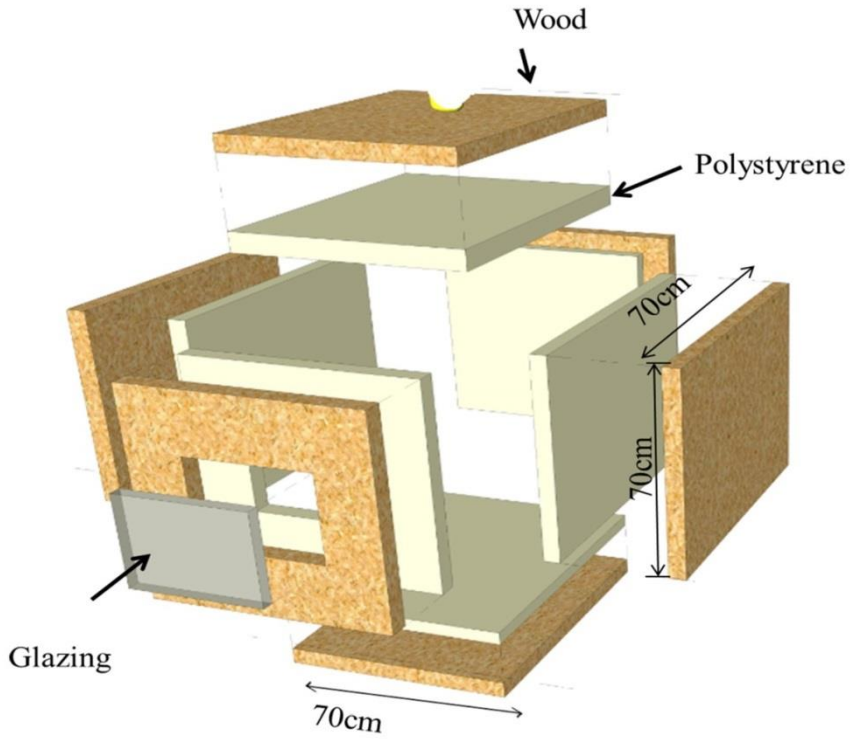

Figure 3-3: Schematic diagram of a test cell.

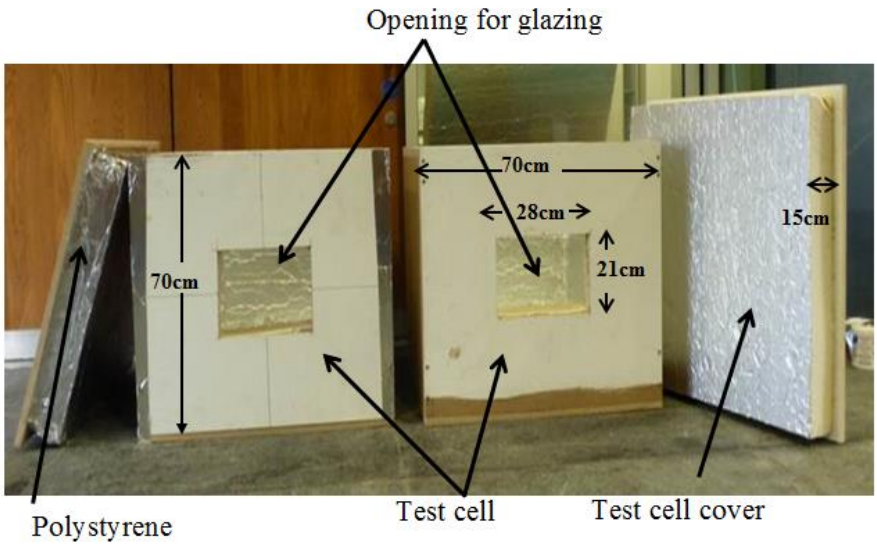

Figure 3-4: Photographic view of the two-test cells.

3.6. Details of Glazing

In this work, the primary glazing was a suspended particle device (SPD) switchable type. It was first investigated under outdoor conditions. In addition, the use of

double-glazing and vacuum glazing was also explored. Details of these types of glazings are shown in Table 3-2.

Table 3-2: Details of glazing used in experiment.

		Dimension (m × m)	Transmittance	Power supply	Supplier
Glazing	Double glazing	0.28 × 0.21	78 %	Not applicable	Pilkington K glass
	Vacuum glazing	0.35 × 0.20	71%	Not required	NSG
	SPD glazing	0.28 × 0.21	55 % (transparent state)	110 V	Smart Glass International
			5% (opaque state)	0 V	

3.6.1. SPD glazing

A photograph and schematic diagram of SPD glazing in its opaque and transparent states are shown in Figure 3-5. Daylighting, electrical and thermal characterisation of SPD glazing is reported in the Chapters 5, 6 and 7.

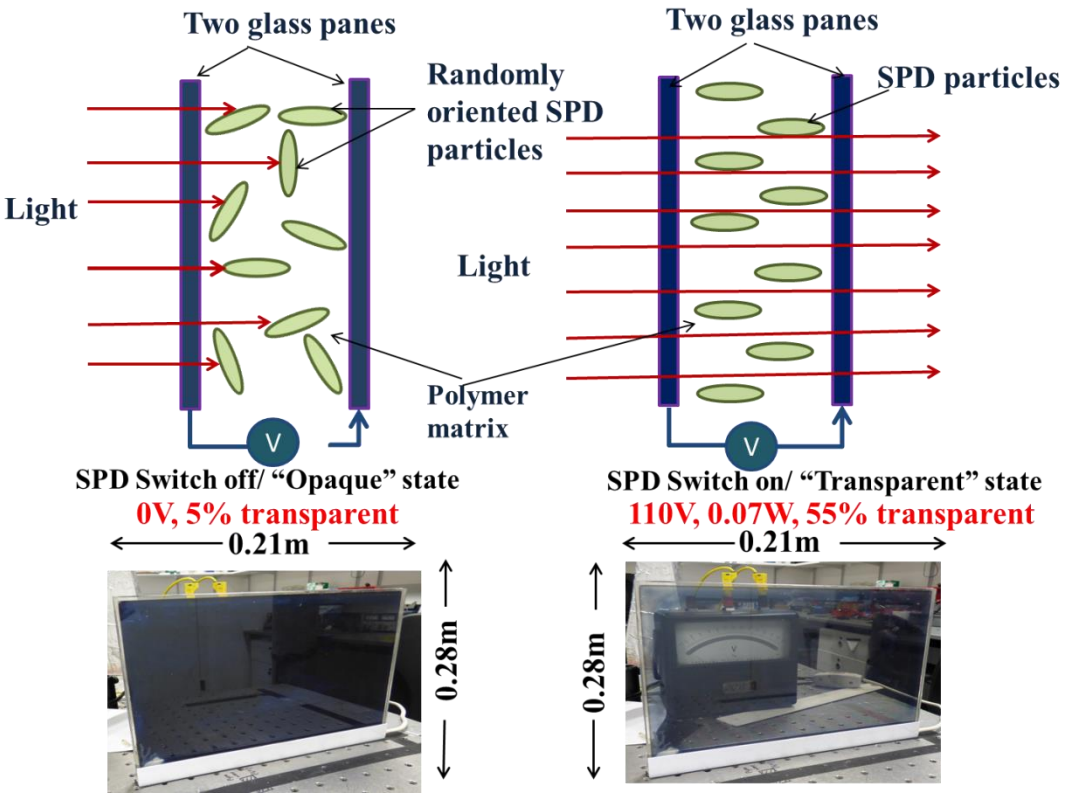

Figure 3-5: Details of suspended particle device opaque and transparent state.

3.6.2. SPD double glazing

SPD single glazing was attached to a double-glazing. This system was similar to a double-glazing having one side attached completely airtight with the SPD glazing. To compare its behaviour experimentally, a single glazing attached to the double-glazing was used as a reference system. The two systems are shown in Figure 3-6. Thermal results of their combinations are reported in section 9.2.1 of Chapter 9.

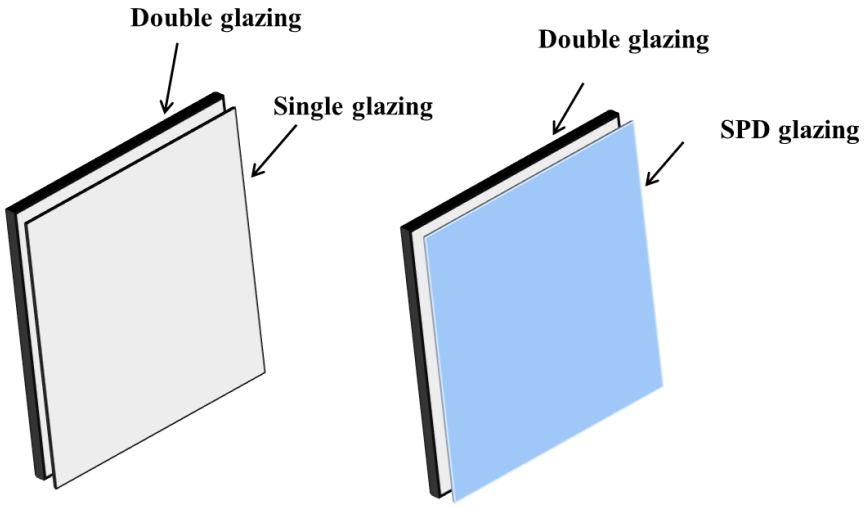

Figure 3-6: Suspended particle device switchable glazing and double glazing attached with another double glazing and single glazing respectively.

3.6.3. Vacuum glazing

Operating principle of a vacuum glazing is shown in Figure 3-7. Thermal and daylighting results of a vacuum glazing are reported in section 8.4 of Chapter 8.

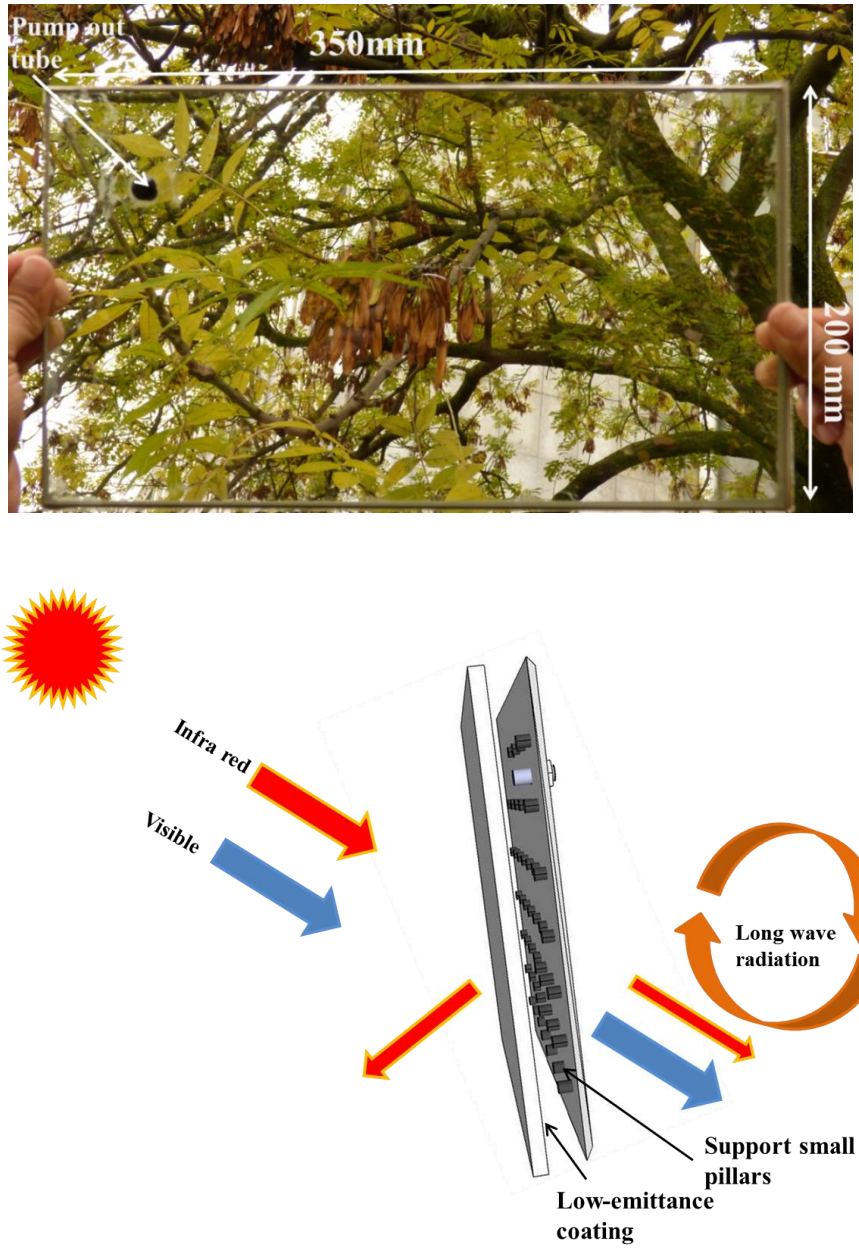

Figure 3-7: Photograph and schematic diagram representing of a vacuum glazing's working principle.

3.6.4. SPD vacuum glazing

SPD and vacuum glazing was attached together to obtain switchable low heat loss, heat gain glazing as shown in Figure 3-8. Thermal behaviour of this glazing is discussed in the section 9.3 of Chapter 9.

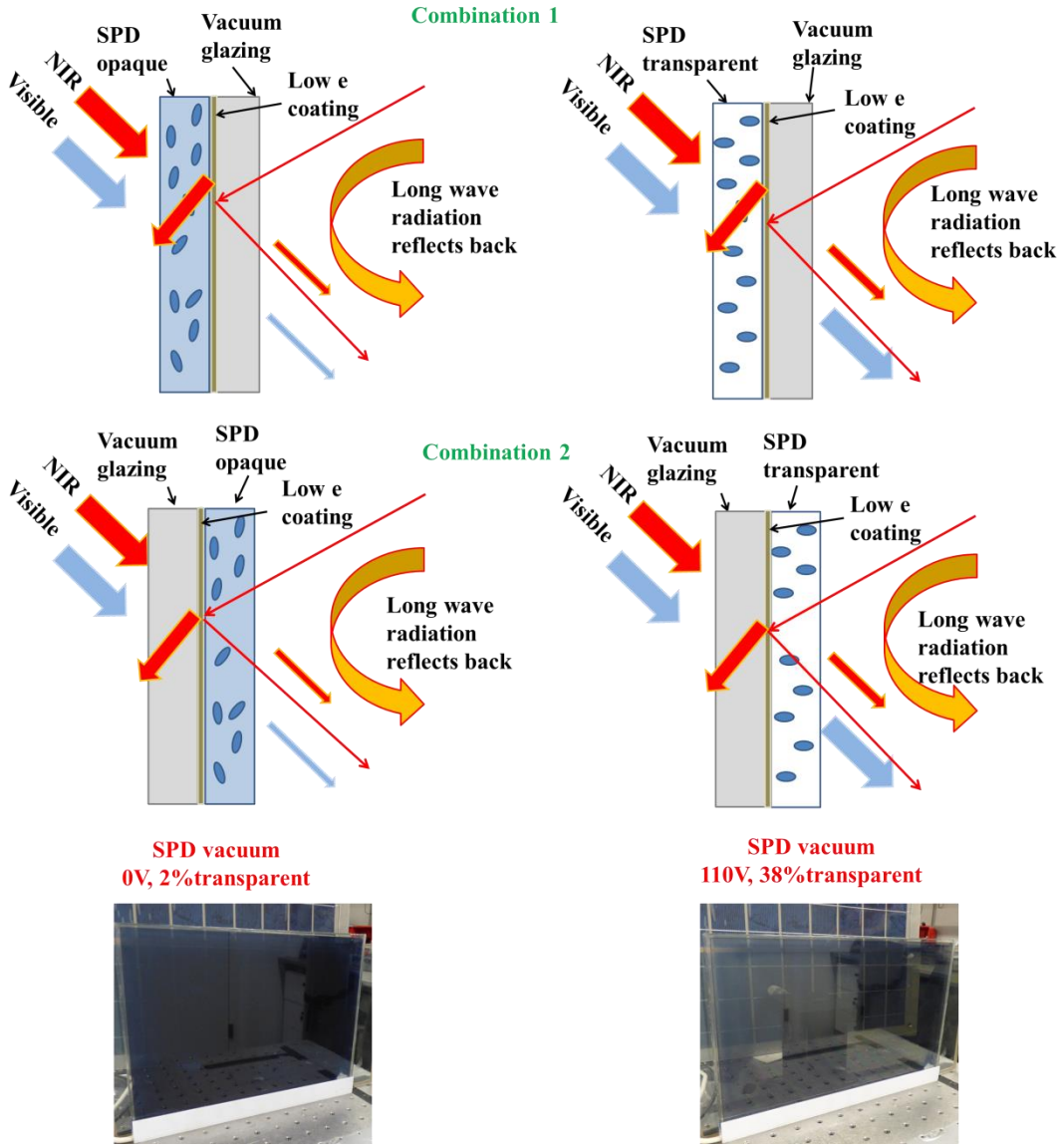

Figure 3-8: Details of a combined SPD vacuum glazing system in its "opaque" and "transparent" states.

3.7. Experimental set up

To perform thermal daylighting and electrical characterisation the instruments employed are listed in Table 3-3.

Table 3-3: Instruments required for this project.

			Characterisation			
		Number	Thermal	Daylight	Electrical	error
Instrument	Thermocouple (T type)	9	Required		Required	$\pm 0.5^0$C
	Pyranometer (Kipp and Zonen)	2	Required	Required	Required	±2%
	Data logger (Delta Type)	1	Required	Required	Required	
	Heat exchanger	1	Required			
	Flow meter	1	Required			±0.2%
	Illuminance sensor	10		Required		
	PV	1			Required	
	Inverter	1			Required	
	Battery	1			Required	
	Charge controller	1			Required	

3.7.1. Calibration of measurement equipments

The accuracies of heat flow meters and T type thermocouples were 5% and 0.5 °C respectively. Heat flow meters were calibrated by ifm and T-thermocouples were calibrated using a constant temperature water bath. Thermocouples and heat flow meters, with errors lower than 0.3 °C and 3% respectively, were selected for measurements. All measurement data were recorded by delta T type datalogger with the data-collection interval of 5 min.

3.7.2. Test cell characterisation

Test cell heat retention property was evaluated by analytically and experimentally.

From Figure 3-3 the thermal resistance across the test cell can be drawn as shown in Figure 3-9. Thermal resistance (R) caused by the wood and polystyrene combination was 4.6 m^2K/W.

$$R = R_{pl} + R_{wd} = \left(\frac{k_{pl}}{d_{pl}} + \frac{k_{wd}}{d_{wd}} \right) = 4.6 \text{m}^2\text{K/W}$$

where K_{pl} was thermal conductivity of polystyrene (0.022 W/mK), d_{pl} was thickness of polystyrene (0.15m), K_{wd} was thermal conductivity of wood (0.09 W/mK), and d_{wd} was thickness of wood (0.02 m).

Considering the average wind speed was 5 m/s for roof of Kevin Street, the thermal resistance for inside and outside heat transfer coefficient were

$$R_{airinside} = 1/h_i = 1/(2.0 + 3V_{wind}) = 0.06 m^2 K/W$$

$$R_{airoutside} = 1/h_0 = 1/(5.7 + 8.8V_{wind}) = 0.02 m^2 K/W$$

It can be seen that the thermal resistance of the combined wood and polystyrene was higher than the internal and external convective heat transfer coefficient. It proves that the test cell was thermally insulated and absolutely no heat flow occurred through the test cell surface.

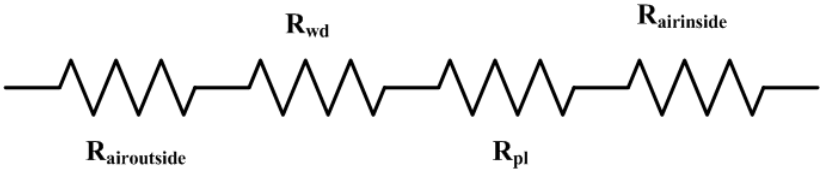

Figure 3- 9: Thermal resistance across the test cell

Experimental investigation was performed to evaluate the thermal insulation of the test cell. Test cell had one side open to place the glazing (as shown in Figure 3-3) was replaced by polystyrene block and experiment was performed for two days. Experiment was started from 7 am. At the beginning, the test cell temperature was similar to the ambient as shown in Figure 3-10 but due to the presence of solar radiation ambient temperature increased. Temperature did not increase for the test cell. For two days, the test cell temperature was nearly 11^0C.

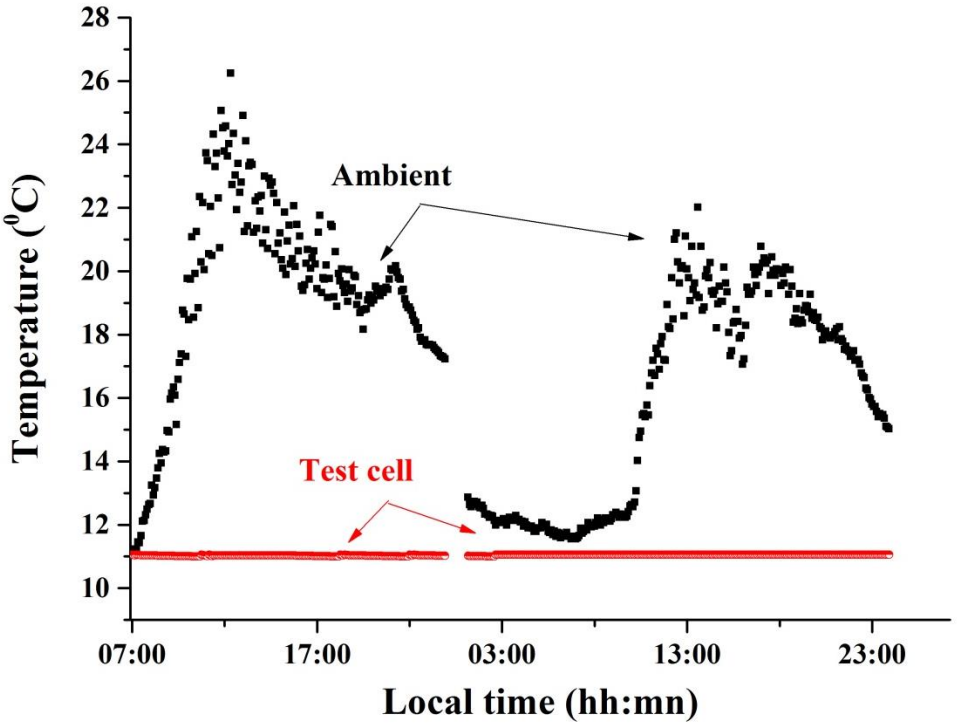

Figure 3- 10: Test cell temperature and ambient temperature for two different days.

3.7.3. Thermal characterisation

Thermal characterisation of SPD glazing was performed in two stages. Measured parameteres were solar radiation, ambient temperature and glazing surface temperatures.

3.7.3.1. Experiment set up without heat exchanger-

Global solar radiation on the horizontal and vertical surface of the test cell was measured using two pyranometers. Ambient and glazing surface temperatures were measured using T type thermocouples, five of which were placed on each glazing surface. Test cell internal temperature was measured using four thermocouples, two of them connected to the top and two to the bottom surfaces. All thermocouples were connected to a DL2 data logger which stored data collected on the interval of five

minutes. Data logger was connected directly to a computer from which the stored data was retrieved. Figure 3-11 indicates the front view of the experimental set up.

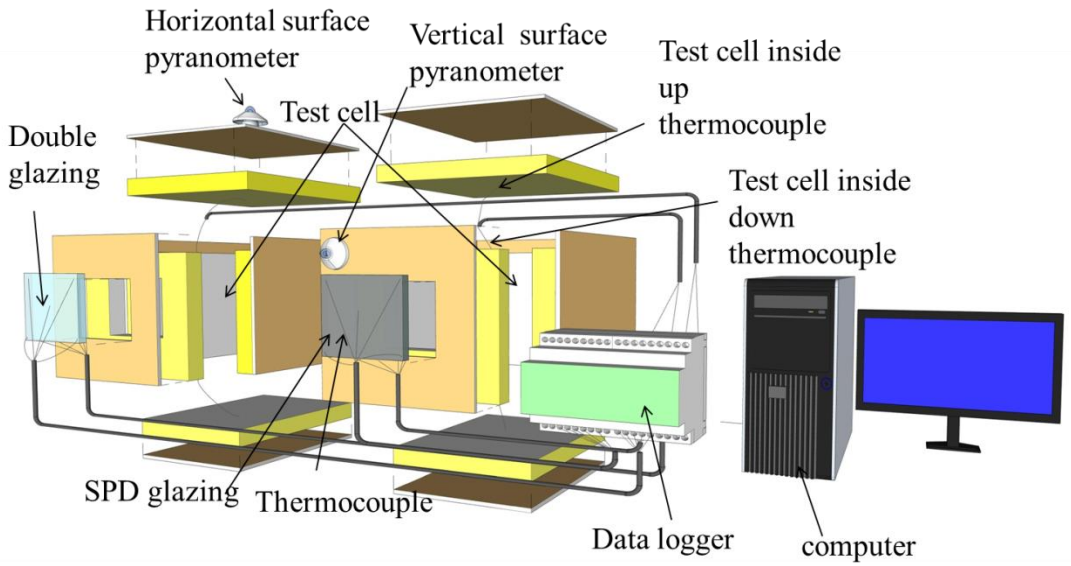

Figure 3-11: Schematic diagram of experimental set up without heat exchanger.

3.7.3.2. Experiment set up with heat exchanger

In the 2nd experiment using same test cell, heat exchanger was employed to keep the test cell temperature constant. Copper coil heat exchangers were placed for both test cells. Length of the heat exchanger pipe was 45 cm and diameter 0.5 cm. Water flow was controlled using ultrasonic flow meter from ifm electronics. Flow meter was powered with 24 V DC supply to provide continuous supply. Front view of experimental set up is shown in Figure 3-12 and rear view is shown in Figure 3-13. The inside temperature was controlled by maintaining the inlet temperature of the circulating water through the heat exchanger at a constant level of 0.016 kg/s. The temperature rise and the flow rate of the fluid across the heat exchanger were measured enabling the amount of energy lost by the heat exchanger to be calculated.

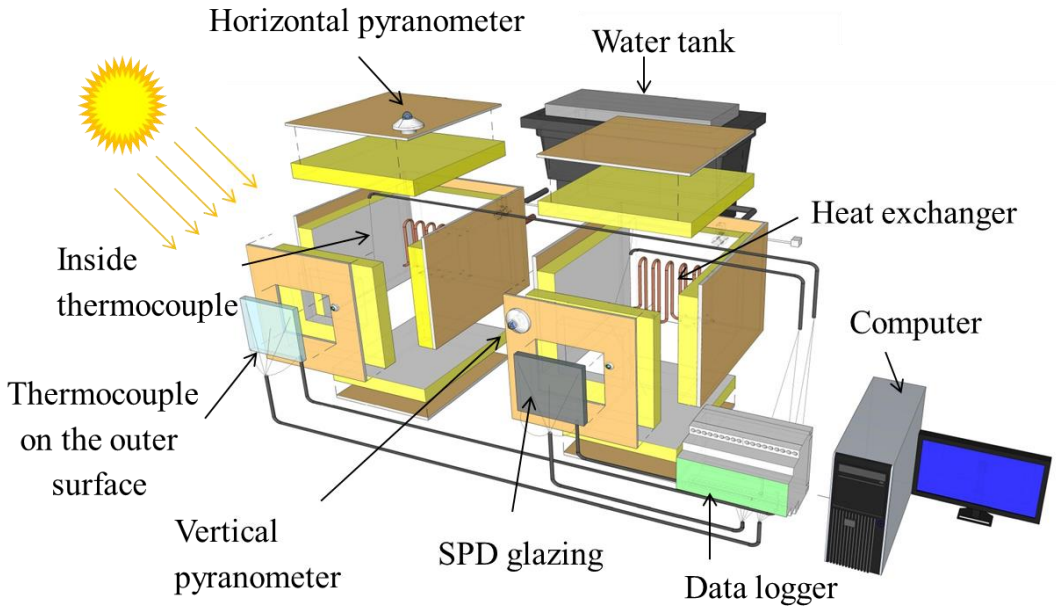

Figure 3-12: Schematic diagram of experimental set up with heat exchanger.

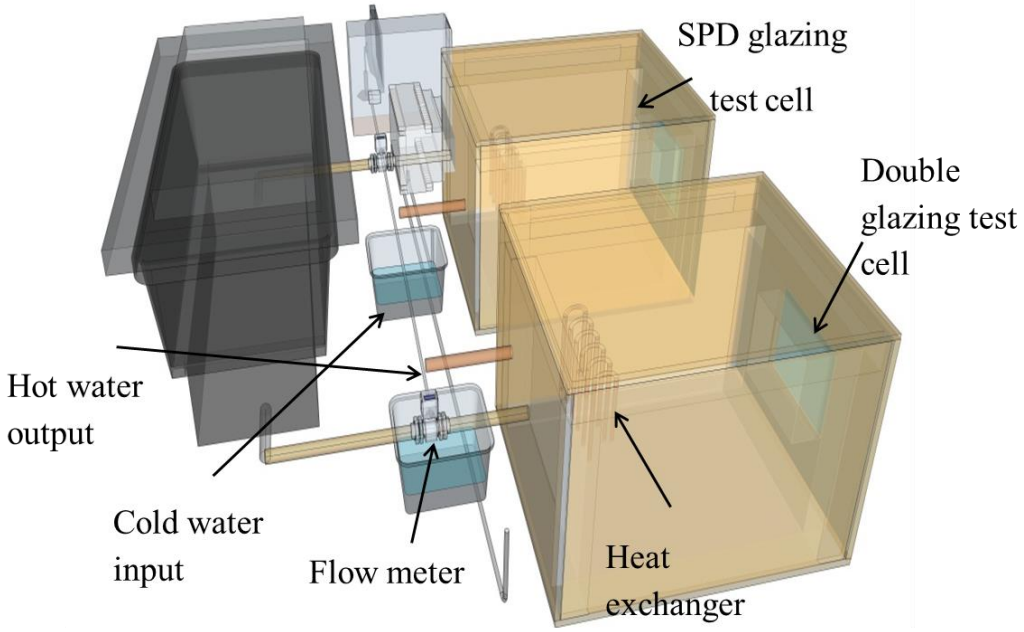

Figure 3-13: Rear view of experimental set up.

3.7.4. Daylighting characterisation

In this experiment, the measured variable was illuminance. The test cell was equipped with ten illuminance sensors that monitored illuminance levels both

outside and inside the cell in different locations. One was on the vertical surface of the outside surface of the test cell and four were inside the test cell. All illuminance sensors had a 350 – 820 nm sensitivity spectral range and a spectral response curve adapted to human eye sensitivity. In this experiment, data was collected using a delta T type data logger. The ten illuminance sensor (lux meter), five for each test cell was connected to the data logger and 5 min interval data was recorded. Data logger was then connected with a computer to save and read the data.

3.7.5. Electrical characterisation

To characterise vertical PV powered SPD glazing, a PV, an inverter, one battery, and one charge controller were employed. SPD glazing was installed in a south facing test cell. This can be considered building integrated photovoltaic (BIPV) powered SPD. The test cell is an insulated small room as shown in Figure 3-3 and Figure 3-4. Details of PV devices are listed below in Table 3-4.

Table 3-4: Details of PV devices.

		Types of PV	
		Polycrystalline PV module	Monocrystalline PV module
Properties	Maximum Power (P_m)	40 W	245 W
	Open circuit voltage (V_{oc})	21.6 V	37.5 V
	Short circuit current (I_{sc})	2.51 A	8.7 A
	Maximum voltage (V_m)	17.8 V	30.5 V
	Maximum current (I_m)	2.25 A	8.04 A
	Efficiency (η)	16-16.5%	14.9%
	Area (A)	0.52 m × 0.66 m	Total active area1.469 m^2

Charge controllers link the PV modules, battery and SPD glazing and protect the battery from overcharge or excessive discharge (Woodworth et.al. 1994). The lead-acid battery is the most mature technology for electrical energy storage in distributed

generation application. Deep-cycle lead-acid batteries are ideal for small-cycle renewable energy integration applications. These batteries can be discharged repeatedly by as much as 80% of their capacity. Low investment cost, low maintenance, low self-discharge makes lead acid battery a popular choice (Farret and Simoes 2006). The 12 V 12 AH lead acid batteries were used in this experiment. An inverter is a crucial component for this type of application. It was found that higher rated inverter is cheaper compare to a low rated inverter. The inverter's main functions are transformation of DC electricity into AC, wave shaping of the output AC electricity and regulation of the effective value of the output voltage. The details of inverter are listed in Table 3-5.

Table 3-5: Details of Inverter.

		Inverter 1 connected with 40 W PV (sizing ratio 4.8)	Inverter 2 connected with 245 W PV (sizing ratio 1.12)
Properties	Max input voltage	12 V	54 V
	Max input current	16 A	8.9 A
	Rated output voltage	230 V	240 V
	Max output current	0.89 A	1.12 A

SPD glazing powered by PV was connected by two ways

- PV inverter and SPD glazing, without storage device is shown in Figure 3-14.
- PV was connected to SPD glazing via a charge controller to an inverter and to a battery as shown in Figure 3-15.

Solar radiation on the vertical plane was measured using pyranometer. Four T type thermocouples measured PV module temperatures.

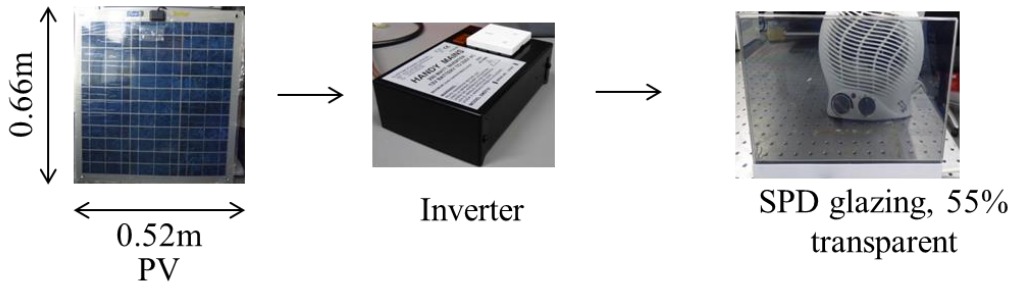

Figure 3-14: PV is connected to the glazing by inverter.

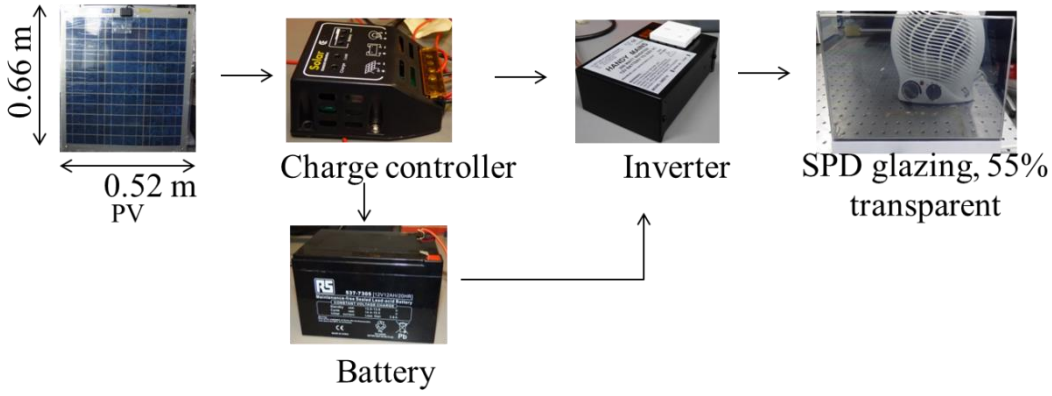

Figure 3-15: PV powered SPD glazing connection with a charge controller, an inverter and a battery.

3.7.6. Experimental data repeatability

Experiments were performed from 1st February 2014 to 1st October 2014 and from 1st Feb 2015 to 1st SEP 2015. Due to dynamic weather condition, obtaining exact data were not possible, however the nature of the curve for typical clear sunny day, intermittent cloudy day and overcast days were similar. Representative data for 4 clear sunny days, 4 intermittent cloudy days and 4 overcast cloudy days for SPD glazing transparent, SPD glazing opaque, vacuum glazing, SPD transparent-vacuum and SPD opaque- vacuum were presented in this thesis.

3.8. Summary

Two test cells were fabricated to characterise the SPD glazing thermal, daylighting and electrical properties. Each test cell can be considered as a scale model of an

unfurnished room. Test cells were manufactured with wood and 15 cm thick polystyrene foam, which made it completely insulated. Pyranometers to measure solar radiation, thermocouples to measure temperature, illuminance sensors to measure illuminance level were employed in this project. A PV device and an inverter were employed to power this SPD glazing. To collect continuous measured data, all the sensors were connected to one delta T type data logger.

Chapter 4. Global transmissivity and glazing transmittance

4.1. Introduction

For any particular location, alongside the global solar radiation, the high quality and reliable knowledge of its direct and diffuse solar radiation is an essential for glare and thermal comfort analysis and particularly for PV powered SPD glazing as PV power output depends on the solar radiation. Glazing applications involve vertical solar planes, it is therefore necessary to transform the horizontal global, direct and diffuse solar radiation to that for vertical planes.

Horizontal plane global and diffuse solar radiation, vertical global solar radiation, vertical plane global illuminance were measured. Vertical plane diffuse solar radiation was evaluated from horizontal plane diffuse solar radiation. Vertical plane global solar radiation was calculated from horizontal plane global and diffuse solar radiation and was compared with measured vertical global solar radiation.

Using clearness index and diffuse factor correlation, diffuse solar radiation can be calculated. To obtain clearness index only measured global solar radiation data was required. Relations between clearness index and luminous efficacy reduce necessity of the global illuminance measurement.

Glazing transmittance is not constant but changes with the diurnal variation of solar radiation. Correlations between glazing transmission and global transmission are presented in this chapter.

4.2. Calculation of vertical plane solar radiation

Total solar radiance on a vertical plane can be divided into three components:

- the beam component from direct radiation of the vertical plane;
- the diffuse component as shown in Figure 4-1 (isotropic diffuse component which is uniform irradiance from the sky dome, horizon brightening

component is concentrated in a band near the horizon and most pronounced in clear skies; circumsolar diffuse component resulting from the forward scattering of solar radiation and concentrated in an area close to the sun);

- reflected component quantifies the ground reflected radiation (albedo) to the tilted surface.

Klucher (1979) found that the isotropic model offered promising results for overcast skies but underestimates radiance under clear and partly overcast conditions. The first modifying factor in the sky diffuse component was taken into account horizon brightening and the second was the effect of circumsolar radiation. The anisotropy index (A_i) was introduced by Hay and Davies (1980). Perez model represents detailed analyses of the isotropic diffuse, circumsolar and horizon-brightening radiation by using empirically derived coefficients. Table 4-1 presents selected vertical plane solar radiation model.

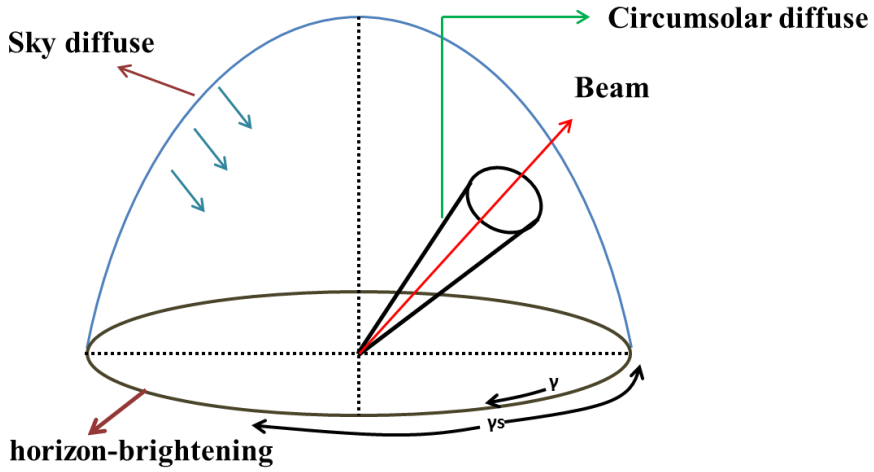

Figure 4- 1: Schematic of the distribution of diffuse solar radiation over the sky dome, showing the circumsolar, and horizon brightening components added to the isotropic components.

Table 4-1: Selected vertical plane global solar radiation model.

$I_v = I_{h,b}R_b + I_{h,d}\left(\frac{1+\cos\beta}{2}\right)\left[1+k_T\sin^3\left(\frac{\beta}{2}\right)\right]\times\left[1+k_T\cos^2\theta\sin^3\theta_z\right]$ $+I_{h,g}\rho\left(\frac{1-\cos\beta}{2}\right)$	Klucher 1979
$I_v = \left(I_{h,b}+I_{h,d}A_i\right)R_b + I_{h,d}\left(1-A_i\right)\left(\frac{1+\cos\beta}{2}\right)+I_{h,g}\rho\left(\frac{1-\cos\beta}{2}\right)$ $A_i = \frac{I_{h,b}}{I_{extra}}$	Hay and Davies 1980
$I_v = I_{h,b}R_b + I_{h,d}\left[\left(1-F_1\right)\left(\frac{1+\cos\beta}{2}\right)+F_1\frac{a}{b}+F_2\sin\beta\right]+I_{h,g}\rho\left(\frac{1-\cos\beta}{2}\right)$ F_1= Circumsolar brightening coefficient F_2= Horizon brightening coefficient $F_1 = F_{11}+F_{12}\Delta+F_{13}Z$ $F_2 = F_{21}+F_{22}\Delta+F_{23}Z$ $a = \max\left(0,\cos\theta\right)$ $b = \max\left(0.087,\cos Z\right)$	Perez et.al. 1990

4.3. Calculation of clearness index

Global transmissivity of atmosphere (Carroll 1985), is often referred to by the clearness index (k_T) or the cloudiness index, is the ratio of the actual global radiation ($I_{h,g}$) to the extraterrestrial radiation incident on a horizontal plane (I_{extra}) as shown by equation 4-1. This parameter is an important one from which various parameters can be found such as prediction of solar radiation using previous clearness index data of a location (Perez et.al. 1990; Hove et.al. 2014; Ayodele and Ogunjuyigbe 2015), diffuse solar radiation on the horizontal plane (Gopinathan 1988; Coppolino 1990; Ahwide et.al. 2013), outdoor illuminance (Perez et.al. 1993) and solar heat gain factor (Li and Lam 2001).

$$k_T = \frac{I_{h,g}}{I_{extra}} \tag{4-1}$$

where

$$I_{extra} = I_{sc}\left(1+0.033\cos\frac{360n}{365}\right)\left(\cos\phi\cos\delta\cos\omega+\sin\phi\sin\delta\right) \tag{4-2}$$

I_{sc} is the solar constant (1367 W/m^2) n is the day of year , ϕ latitude angle, δ declination angle ω hour angle

4.3.1. Diffuse fraction from clearness index

k_d defined as the diffuse factor which is the ratio of horizontal diffuse radiation and horizontal global radiation, shown in equation 4-3.

$$k_d = \frac{I_{h,d}}{I_{h,g}} \tag{4-3}$$

Different correlation method between diffuse factor and clearness index are presented in Table 4-2.

Table 4-2: Diffuse fraction and clearness index correlation.

Correlation	Location	Reference
$k_d = 1.02 - 0.258k_T$ For $k_T \le 0.3$ $k_d = 1.45 - 1.67k_T$ For $0.3 < k_T < 0.78$ $k_d = 0.147$ For $k_T \ge 0.78$	Horizontal surface registered at 5 locations in the USA and Europe (28–60 ^{0}N latitude).	Reindl et.al. 1992
$k_d = 1.0 - 0.09k_T$ For $k_T \le 0.22$ $k_d = 0.9511 - 0.160k_T + 4.388{k_T}^2 - 16.638{k_T}^3 + 12.336{k_T}^4$ For $0.2 < k_T \le 0.80$ $k_d = 0.165$ For $k_T > 0.80$	5 stations in the USA with latitudes between 31 ^{0}N and 42 ^{0}N latitude. The data were of short duration, ranging from 1 to 4 years.	Erbs et.al. 1982
$k_d = 0.98$ For $k_T \le 0.20$ $k_d = 0.61092 + 3.6259k_T - 10.171{k_T}^2 + 6.338{k_T}^3$ For $0.2 < k_T \le 0.7$ $k_d = 0.672 - 0.474k_T$ For $k_T > 0.7$	Belfast (Northern Ireland) 54.59 ^{0}N	Mondol et.al. 2008
$k_d = 0.99$ For $k_T \le 0.17$ $k_d = 1.188 - 2.272k_T + 9.473{k_T}^2 - 21.865{k_T}^3 + 14.648{k_T}^4$ For $0.17 < k_T < 0.75$ $k_d = -0.54k_T + 0.632$ For $0.75 < k_T < 0.80$ $k_D = 0.2$ For $k_T \ge 0.80$	Albuquerque, New Mexico, 35.05 ^{0}N ,1961-64 Fort Hood, Texas, 31.08 ^{0}N, 1974-76 Livermore, California , 37.7 ^{0}N, 1974-75 Maynard, Massachusetts, 42.42 ^{0}N, 1975-76 Raleigh, North Carolina, 35.87 ^{0}N, 1975-76	Collares-Pereira and Rabl 1979
$k_d = 1 - 0.249k_T$ For $k_T < 0.35$ $k_d = 1.577 - 1.84k_T$ For $0.35 \le k_T \le 0.75$ $k_d = 0.177$ For $k_T > 0.75$	Toronto (Canada, 42.8 ^{0}N) in the years 1967–1971	Orgill and Hollands 1977

4.3.2. Luminous efficacy from clearness index

Luminous efficacy (k_{gl}) is defined as the ratio of the illuminance (in lux or lm/m^2) produced by solar radiation (W/m^2) to the radiation itself (Littlefair 1988).

$$k_{gl} = \frac{E_v}{I_v} \tag{4-4}$$

Often outdoor illuminance data is not available for any place. Outdoor illuminance values (in lux or lm/m^2) can be simulated from the measured solar irradiance (W/m^2) and luminous efficacy (lm/W).

Polynomial model of global luminous efficacy and diffuse luminous efficacy for all sky types in which the clearness index (k_T) is the only independent variable is given by equation (Muneer and Kinghorn 1997; Muneer and Kinghorn 1998) 4-5 and 4-6.

$$k_{gl} = 136.6 - 74.54k_T + 57.3421{k_T}^2 \tag{4-5}$$

$$k_{dl} = 130.2 - 39.828k_T + 49.979{k_T}^2 \tag{4-6}$$

Luminous efficacy varies with atmospheric parameters such as solar elevation and atmospheric composition including water vapour, aerosols and clouds. Thus, the luminance efficacy also varies significantly from region to region. List of different luminous efficacy for different location are summarized in Table 4-3.

Table 4-3: List of different luminous efficacy for different location.

Location	Luminous efficacy (lm/W)	Reference
37.24 ^{0}N 107.07 ^{0}E Yongin, South Korea	114.81	Kong and Kim 2013
36.65 ^{0}N 139.53 ^{0}E Tokyo Japan	104.9	Inanuma and Takeda 2002
37.97 ^{0}N, 23.72 ^{0}E Athens Greece	92.40	Tsikaloudaki 2005
60.11 ^{0}N 24.50 ^{0}E Helsinki, Finlad	109.40	Vartiainen 2000
22.3 ^{0}N 114.2 ^{0}E Hong Kong	118±15	Chung 1992

Maximum luminous efficacy was found 180 lm/W in Norway and minimum was 98 lm/W in Japan. In the tropics, the sky is highly luminous and the daylight is abundant throughout the year.

4.4. Experimental procedure

To find out the clearness index and luminous efficacy solar radiation and illuminance data were essential. Details of pyranometer and illuminance sensors set up are described in Chapter 3. Measurements were carried out from 1st February 2014 to 1st SEP 2014 in Dublin.

4.5. Results of weather characterisation of Dublin

4.5.1. Results of solar radiation & clearness index

Figure 4-2 shows the measured horizontal plane global and diffuse solar radiation and vertical plane global solar radiation for typical clear sunny, intermittent cloudy and overcast cloudy day in Dublin.

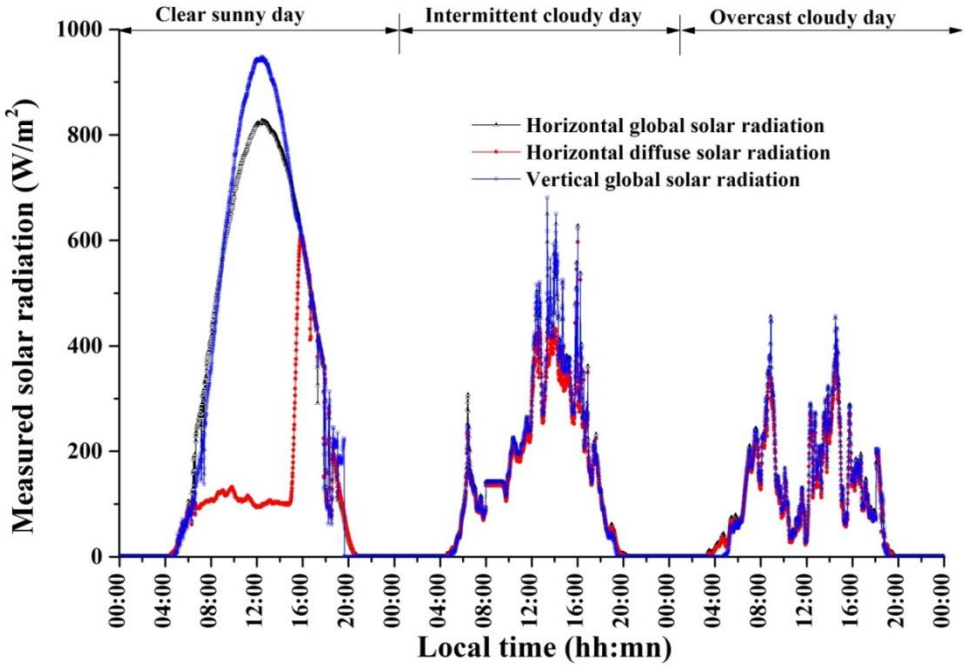

Figure 4-2: Measured horizontal plane global and diffuse solar radiation and vertical plane global solar radiation for typical clear sunny (1st July 2014), intermittent cloudy (3rd April 2014) and overcast cloudy (31st August 2014) day in Dublin.

For clear sunny day till 16:00 hh diffuse solar radiation was lower than 200 W/m^2. From afternoon, contribution of diffuse solar radiation was higher than 600 W/m^2.

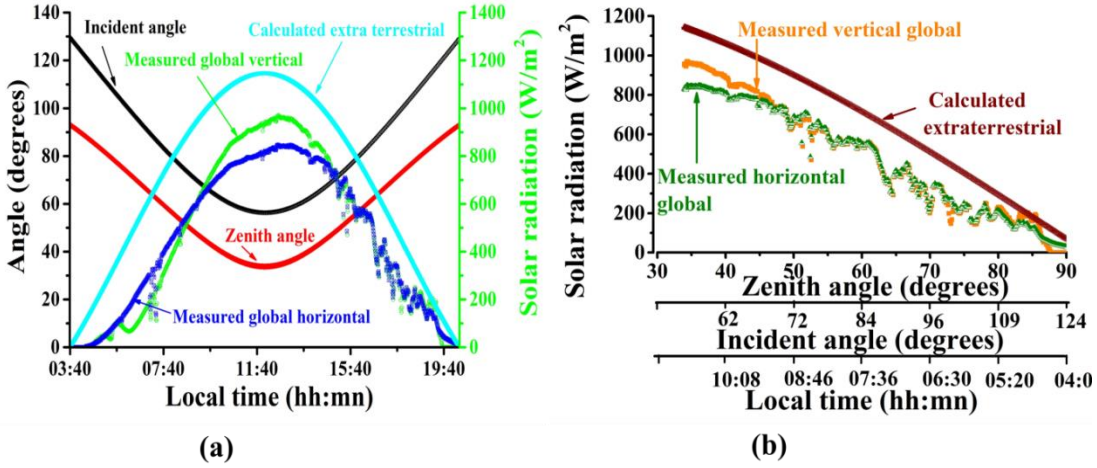

Figure 4-3: (a) Variation of vertical and horizontal global solar radiation and extraterrestrial solar radiation for different zenith and incident angle and (b) diurnal variation of zenith angle, incident angle, calculated extraterrestrial solar radiation, measured horizontal and global solar radiation.

Figure 4-3 illustrates the diurnal variation of vertical global solar radiation, horizontal solar radiation and calculated extraterrestrial solar radiation with incident angle and zenith angle. Solar radiation between extraterrestrial and earth surface was different. The transmission of solar radiation through the atmosphere is mainly dependent on the scattering by the molecules (Rayleigh scattering), the scattering and absorption by solid and liquid particles, and the selective absorption by gaseous constituents aerosol attenuation (Bird and Hulstrom 1983).

Figure 4-4 (b) presents calculated vertical plane diffuse solar radiation from (a) measured horizontal plane diffuse solar radiation. Perez, Klucher and Hay & Davice models were used to calculate vertical plane diffuse solar radiation. Figure 4-4 (c) indicates the calculated global vertical plane solar radiation from horizontal plane global and diffuse solar radiation using equation described in Table 4-1. Klucher and Hay & Davice model offered lower value of vertical diffuse solar radiation. As sky is

anisotropic in nature, Perez model gave best result counting isotropic diffuse, circumsolar and horizon-brightening diffuse solar radiation.

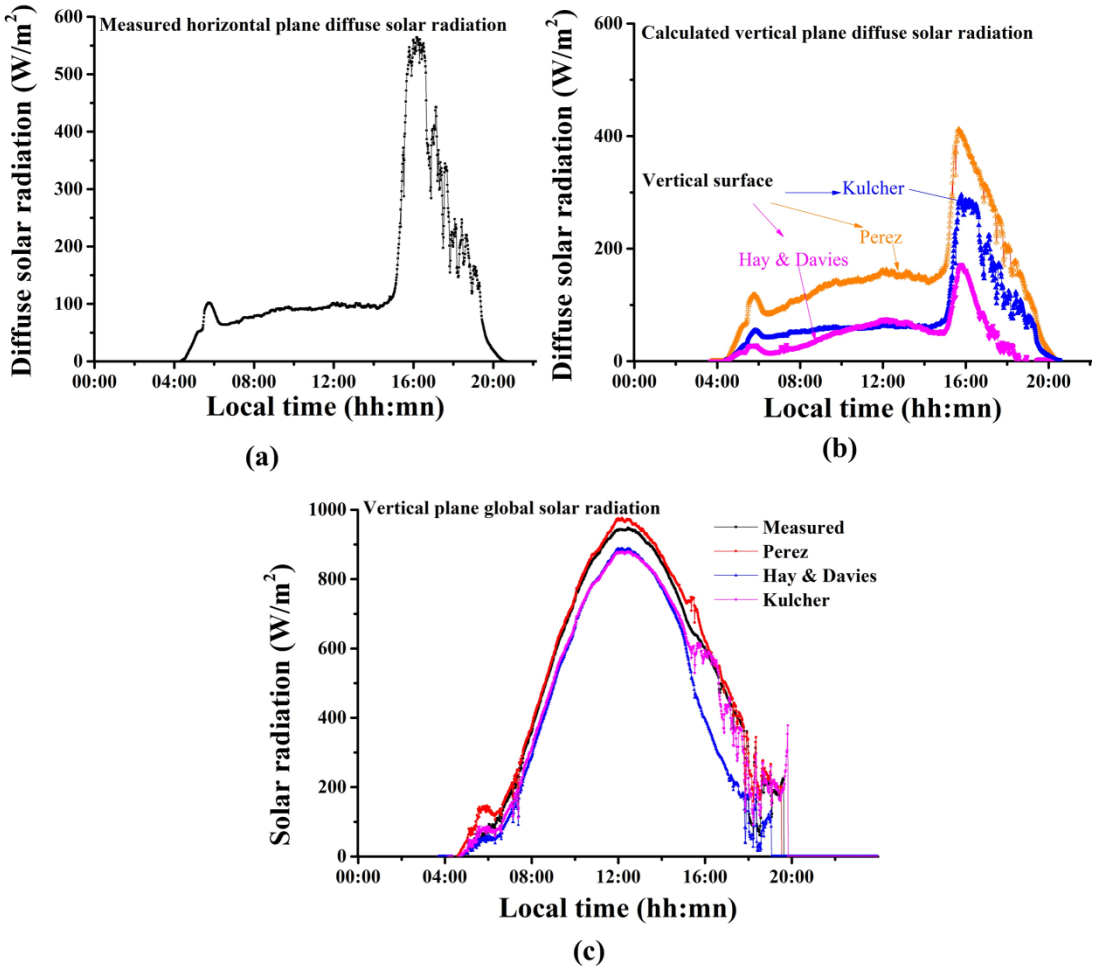

Figure 4-4: Measured horizontal diffuse solar radiation and calculated vertical diffuse solar radiation using four different equations for clear sunny day. Measured and calculated vertical plane global solar radiation for clear sunny day in Dublin.

Figure 4-5 illustrates the calculated extra-terrestrial solar radiation, vertical surface global solar radiation, clearness index, density and cumulative density of clearness index for clear sunny, intermittent and cloudy overcast day. For a clear sunny day clearness index was maximum 0.8 at mid-day period.

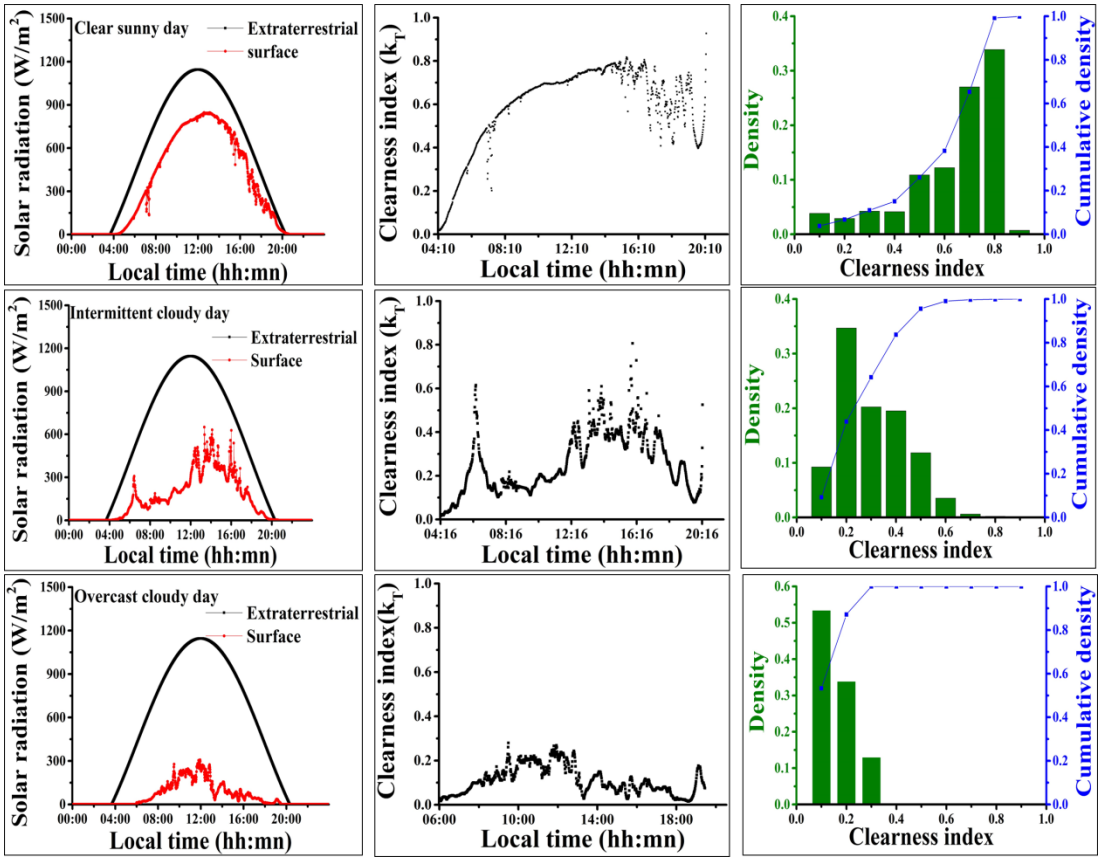

Figure 4-5: Calculated extra-terrestrial solar radiation, vertical surface global solar radiation, clearness index, density and cumulative density of clearness index for clear sunny, intermittent cloudy and overcast cloudy day.

Figure 4-6 illustrates the calculated diurnal variation of the diffuse factor, clearness index and anisotropic index using equation 4-1, 4-3 and Table 4-1 respectively, for a clear sunny day, intermittent cloudy day and overcast cloudy day. Clearness index was achieved maximum 0.8 at mid-day period for a clear sunny day.

Anisotropy index (A_i) represents the transmittance of the atmosphere for the direct solar radiation whereas cleanness index indicates the global solar radiation transmission. For a clear sunny day, higher values of anisotropic index and higher values of clearness index during mid-day period indicated that the global solar radiation was mostly direct solar radiation. At this time diffuse factor values were low nearly 0.3. This indicates the diffuse radiation at this time was lower compare to

direct solar radiation. For intermittent and overcast day, lower clearness index and lower anisotropic index were achieved where as higher values of diffuse factor were obtained.

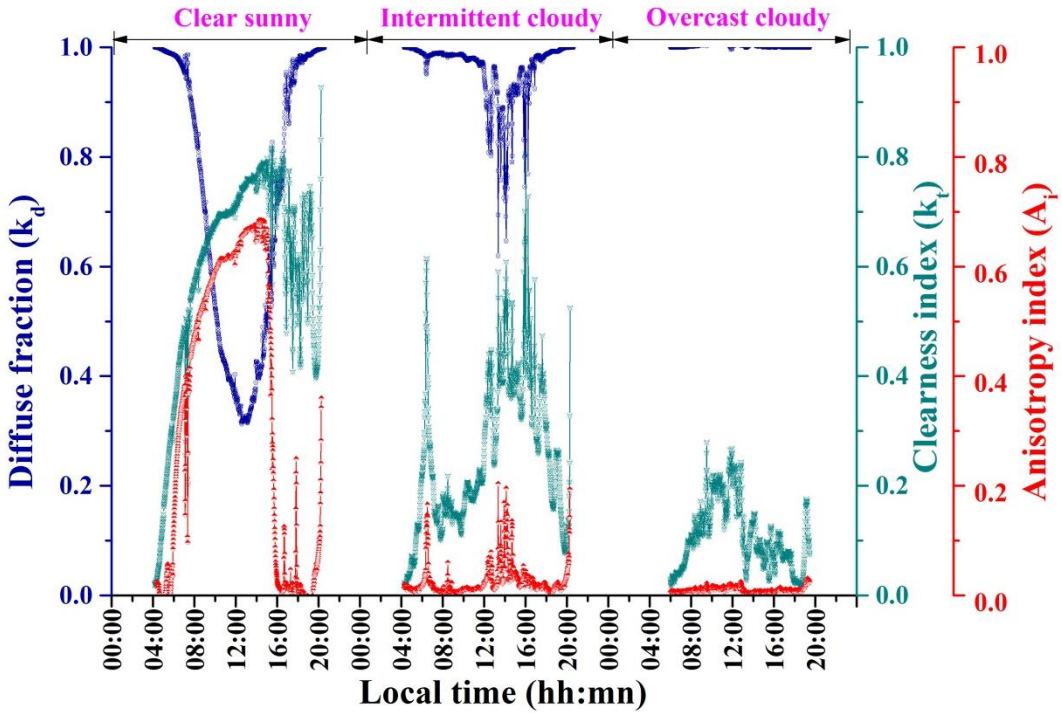

Figure 4-6: Diurnal variation of diffuse fraction, clearness index and anisotropy index for a clear sunny day, intermittent cloudy day and overcast cloudy day.

4.5.2. Results of illuminance

Measured vertical plane global illuminance for typical clear sunny day, intermittent cloudy day and overcast cloudy day is illustrated in Figure 4-7.

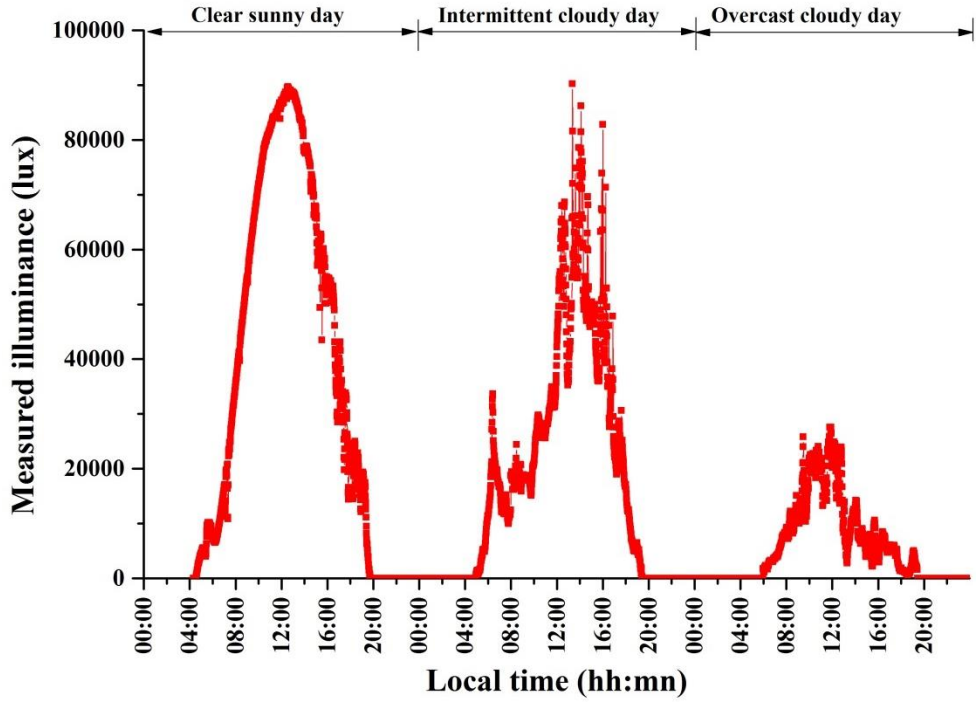

Figure 4-7: Diurnal variation of vertical surface global illuminance, for clear sunny, intermittent cloudy and overcast cloudy day.

Figure 4-8 illustrates the luminous efficacy for typical clear sunny, intermittent cloudy and overcast cloudy day for Dublin. Luminous efficacy was calculated by using equation 4-4.

A typical clear sunny day in Dublin, global luminous efficacy varies from 95 to 115 lm/W. For an intermittent day, luminous efficacy varies between 130 to 169 lm/W. For an overcast day, this values changes from 85 to 140 lm/W. For overcast and intermittent sky condition, higher luminous efficacy values occurred due to increase of water vapour absorption (Perez et.al. 1990). It can be conclude that in Dublin the luminous efficacy varies between 85 lm/W to 169 lm/W.

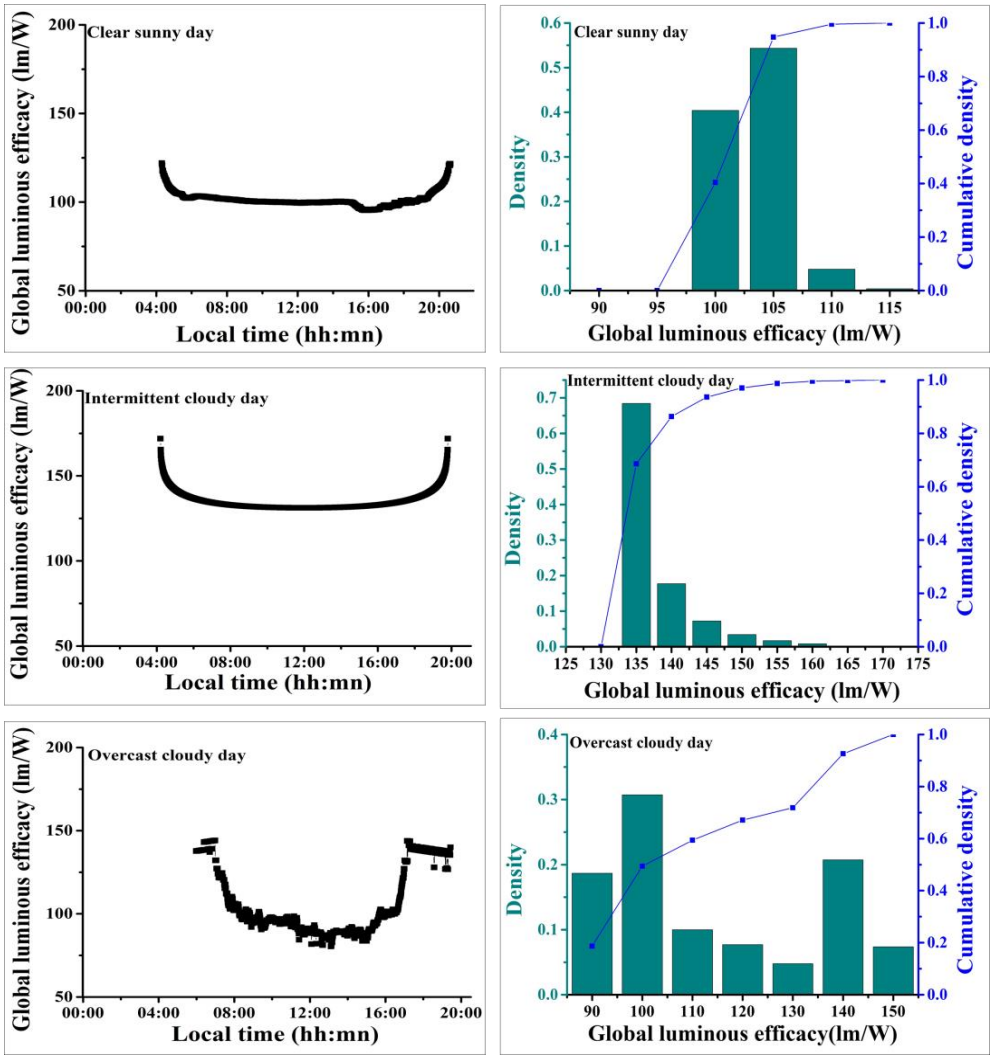

Figure 4- 8: Global luminous efficacy, its density and cumulative density for clear sunny day, intermittent cloudy day and overcast cloudy day.

4.5.3. Results of different correlations

Figure 4-9 indicates correlation between hourly clearness index (k_T) and hourly diffuse fraction (k_d). The diffuse fraction indicates the portion of the diffuse component received for a vertical surface. k_T is an indicator of the relative clearness of the atmosphere (Waide and Norton 2003). In general, when the atmosphere is clear, a small fraction of the radiation is scattered, resulting in direct radiation being predominant with a large k_T value. Low k_T values indicates the sun rising and sun set period or overcast cloudy day. High k_d values represents the majority of the global radiation is of diffuse nature, associated with cloudy sky conditions. Low k_d values

indicate that the majority of the global radiation is the direct component, which predominates in clear sky.

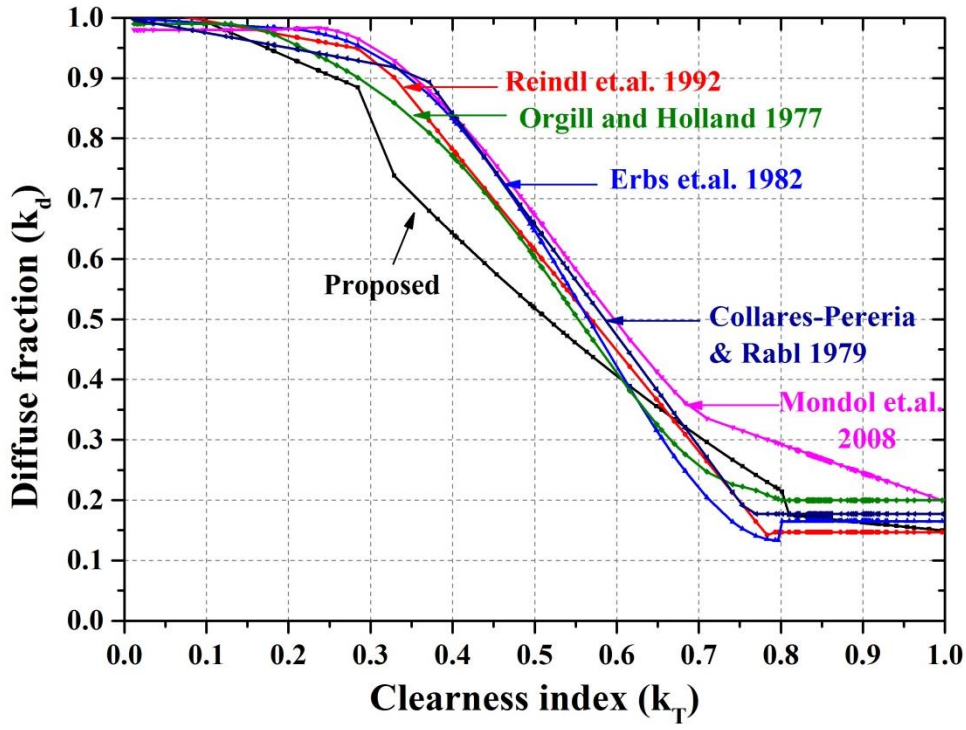

Figure 4-9: Correlation of hourly clearness index and hourly diffuse fraction for sunny, intermittent and overcast day.

Figure 4-10 illustrates the correlation between clearness index and luminous efficacy, of global luminous efficacy for three types of days. Luminous efficacy variation with clearness index trend for three types of days are shown to be very similar for the US and Swiss location reported by Perez et.al. (Perez et.al. 1990).

Figure 4-11 shows the luminous efficacy and clearness index correlation using Muneer equations 4-5 and 4-6. It can be seen that diffuse luminous efficacy is higher after clearness index 0.2. It is due to increase contribution of molecular (Rayleigh) scattering (Perez et.al. 1990). The same threshold was found for Scotland data where after 0.25 clearness index diffuse luminous efficacy became higher than global (Muneer 1997).

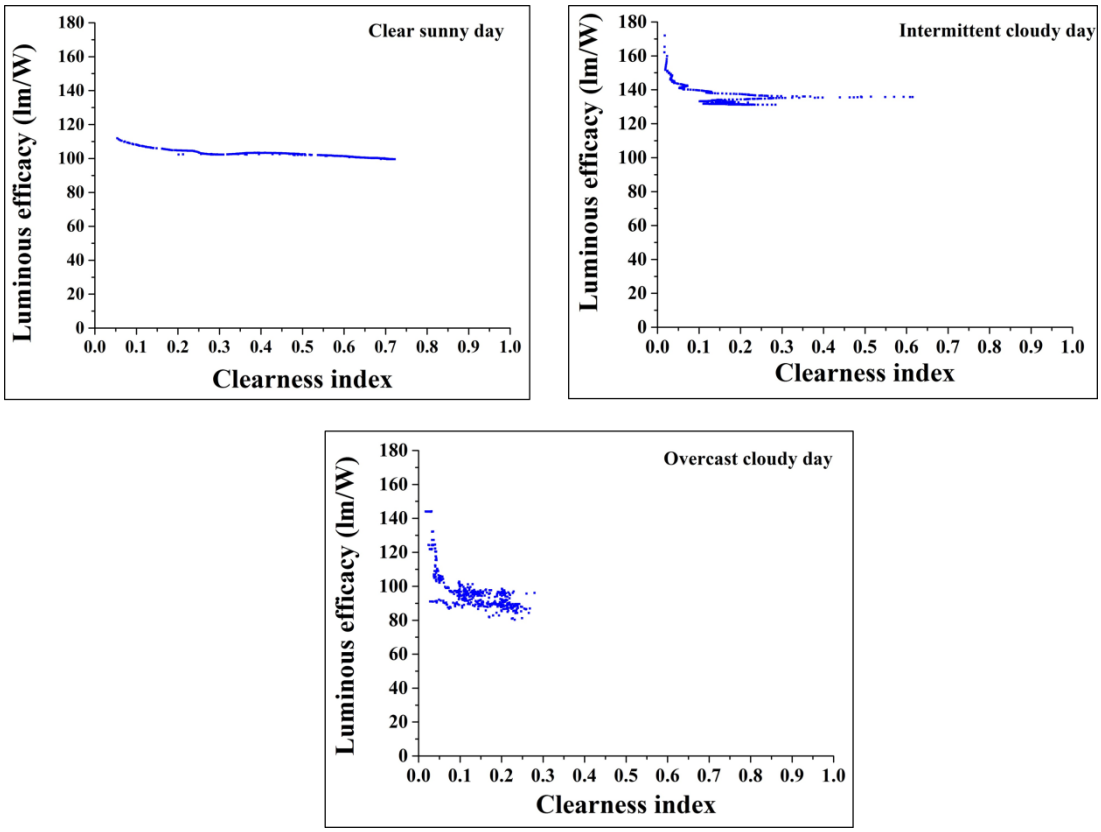

Figure 4-10: Correlation of luminous efficacy and clearness index calculated from measured data for clear sunny, intermittent cloudy and overcast cloudy day.

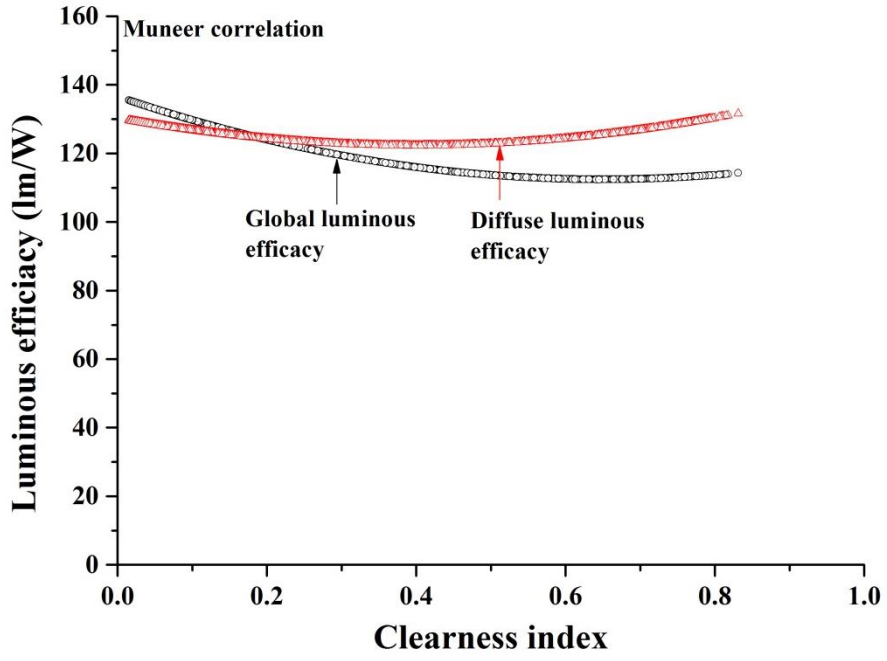

Figure 4-11: Muneer correlation with luminous efficacy and clearness index for Dublin.

4.6. Spectrometric glazing transmission measurement

Transmission of SPD glazing, vacuum glazing and combined SPD glazing for it's on and off state was measured using an AvaSpec-ULS2048L Star Line Versatile Fiber-optic spectrometer as shown in Figure 4-12. To obtain variable transmission for variable applied voltage, SPD glazing was connected with one variac (range 0-200 V). One indoor sun simulator was employed as a source as shown in Figure 4-12. It was found that SPD glazing had variable transmission between 5% (switch off) to 55% (switch on) for variable applied voltage between 0 to 110 V. 55% transmission remained constant above 110 V applied voltage. Complete view of experiment is illustrated in Figure 4-12.

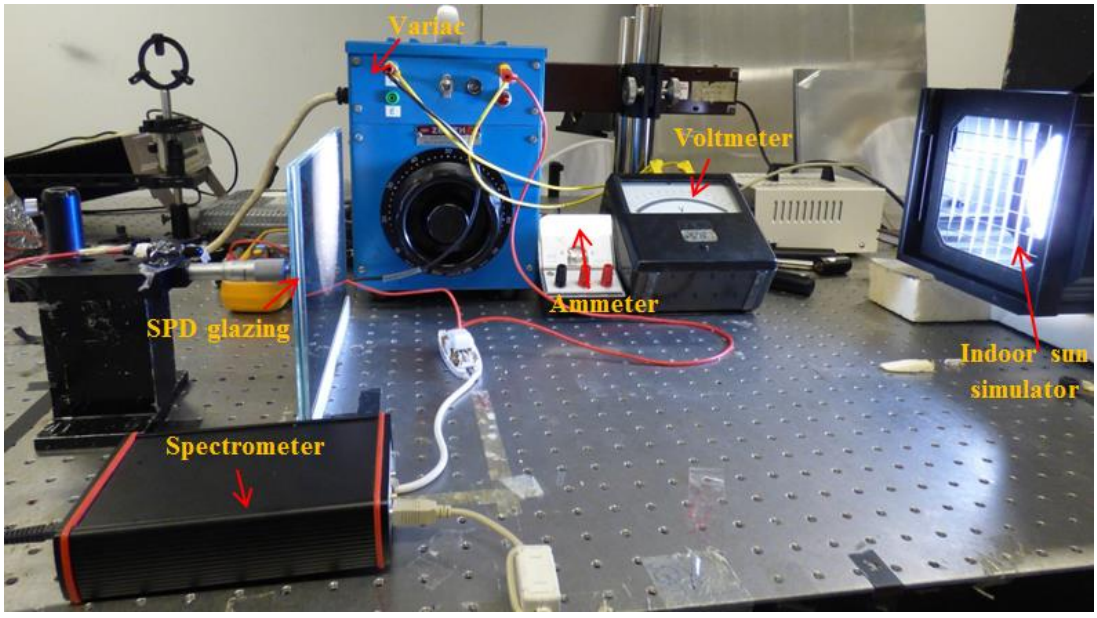

Figure 4-12: Indoor Experiment of SPD glazing.

Figure 4-13 illustrates the voltage dependent transmission of SPD glazing and solar spectral irradiance. A higher change of transmission was observed under applied voltage between 20 V to 70 V. Between this ranges transmissions changed rapidly. Voltage between 70 V to 110 V, the change of transmission range was less at all wavelengths.

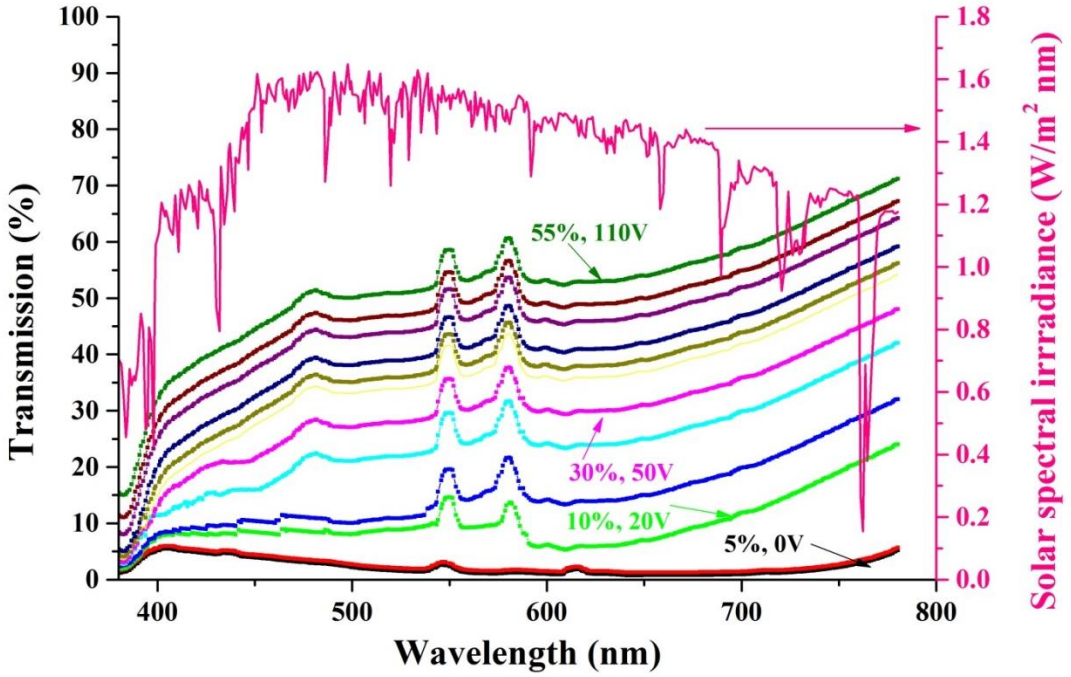

Figure 4-13: Luminous transmittance of SPD glazing for its different voltage level. SPD is in "opaque" state for 0 V and "transparent" state while 110 V supply is applied.

Figure 4-14 illustrates the transmission spectra of vacuum glazing and SPD glazing and combined SPD and vacuum for its opaque and transparent state.

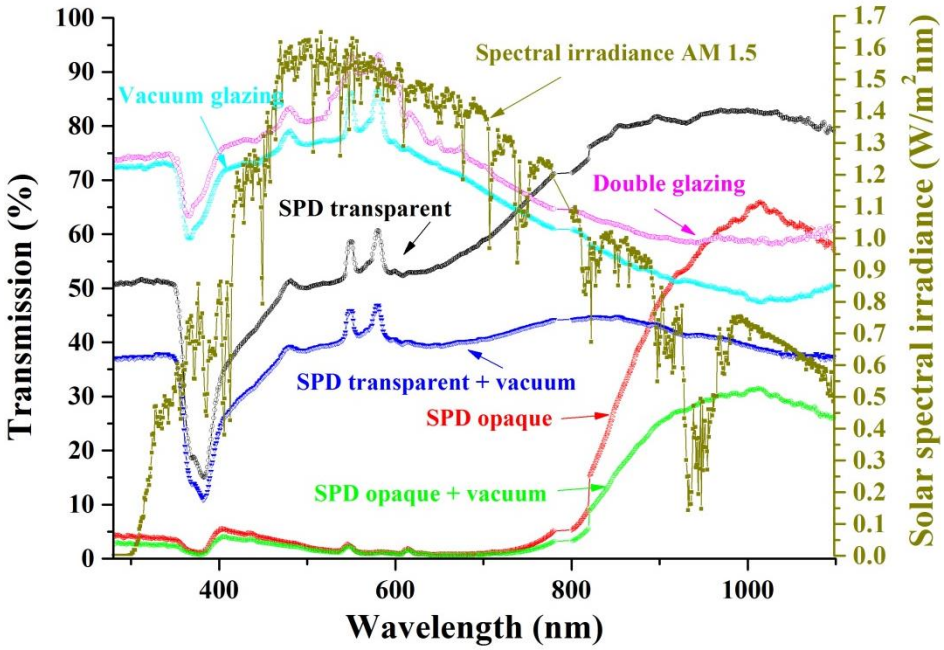

Figure 4-14: Transmission spectra of SPD glazing "opaque" and "transparent" condition, vacuum glazing, SPD transparent vacuum and SPD opaque vacuum glazing.

Transmission spectrum was measured using the experimental set up of Figure 4-12. This transmission spectrum was compared with standard solar spectra at AM 1.5. Table 4-4 summarise the average solar transmission of different glazings.

Using Fresnel equation (Band 2010) the reflection from the SPD glazing system can be possible by using 4-7.

$$R = \frac{n_g - n_{air}}{n_g + n_{air}} \tag{4-7}$$

Where the refractive index of SPD glazing (n_g), double glazing, vacuum glazing and air (n_{air}) are 1.6, 1.4, 1.4 and 1.0 respectively. Absorption for different combinations are described in Table 4-4.

Table 4-4: Transmittance of different glazings.

		Average solar transmittance in visible wavelength	Absorption
Glazings	SPD opaque	5%	90%
	SPD transparent	55%	40%
	Vacuum	72%	21%
	Double	78%	17%
	SPD-vacuum transparent	38%	57%
	SPD-vacuum opaque	2%	93%

4.6.1. Angular transmittance of glazing

For vertical surface glazing as shown in Figure 4-15, direct solar radiation is not usually at normal incidence to the glazing surface but mostly at oblique incidence angles at which the transmittance is different from the near-normal values.

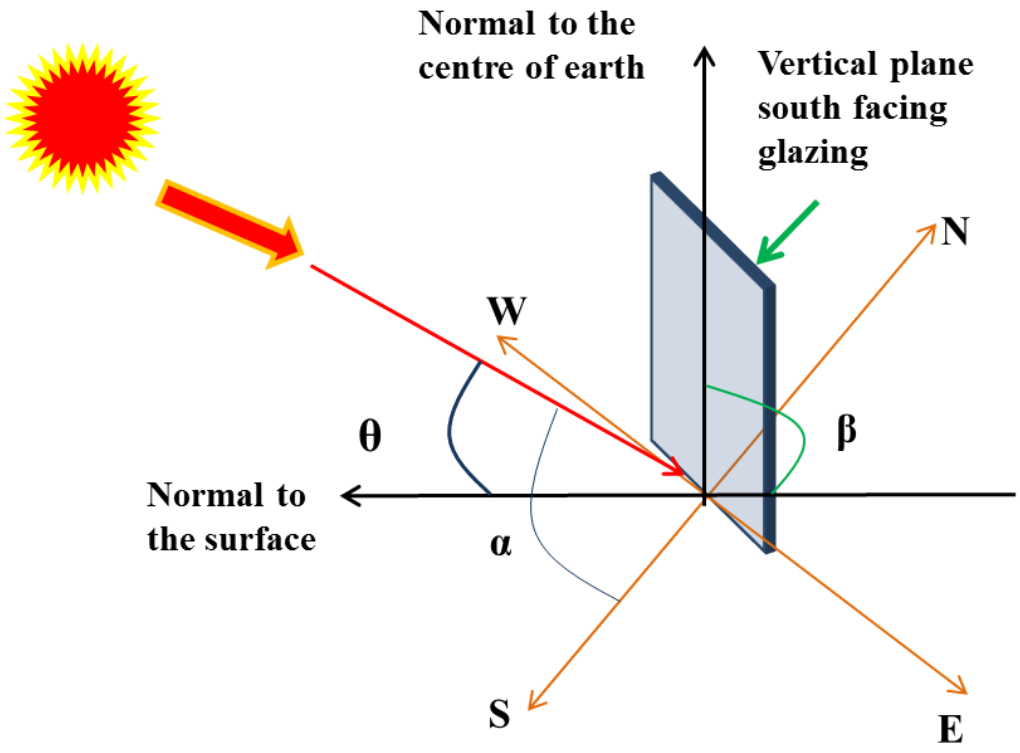

Figure 4- 15: Schematic diagram of a south facing vertical plane glazing with incident angle and solar elevation angle.

Incident angle (θ) of a south facing vertical surface glazing can be found from equation 4-8.

$$\cos\theta = -\sin\delta\cos\phi\cos\gamma + \cos\delta\sin\phi\cos\gamma\cos\omega + \cos\delta\sin\gamma\sin\omega \quad (4\text{-}8)$$

Where δ is the declination angle, ϕ is latitude, γ is surface azimuthal angle and ω is hour angle.

Solar elevation angle to calculate the sun path diagram can be calculated from equation 4-9.

$$\sin\alpha = \sin(90 - \theta_z) = \cos\theta_z = \cos\phi\cos\delta\cos\omega + \sin\phi\sin\delta \quad (4\text{-}9)$$

Knowledge of the glazing angular transmission (τ_v) allows accurate calculations of daylighting and energy performance of buildings considering direct sunlight and can be calculated (Waide and Norton 2003).

$$\tau_v = \left[k_d \left\{ k_T R_b \left(1-k_d\right) + \left(1-\cos\beta\right)\left(1-k_T\left(1-k_d\right)\right)\right\} + R_b\left(1-k_d\right) + R_g \frac{1-\cos\beta}{2} \right] \times$$
$$\tau_{dir} R_b \left(1-k_d\right)\left(1+k_d k_T\right) + \frac{\tau_{dif} k_d}{2}\left(1+\cos\beta\right)\left(1-k_T\left(1-k_d\right)\right) + \frac{\tau_g R_g \left(1-\cos\beta\right)}{2} \quad (4\text{-}10)$$

$$\tau = \frac{1}{2}\left[\frac{1-\left\{\frac{\sin\left(\theta-n\right)}{\sin\left(\theta+n\right)}\right\}^2}{1+\left(2n_g-1\right)\left\{\frac{\sin\left(\theta-n\right)}{\sin\left(\theta+n\right)}\right\}} + \frac{1-\left\{\frac{\tan\left(\theta-n\right)}{\tan\left(\theta+n\right)}\right\}^2}{1+\left(2n_g-1\right)\left[\frac{\tan\left(\theta-n\right)}{\tan\left(\theta+n\right)}\right]^2} \right] \times \exp\left(\frac{-k_g n_g t_g}{\cos\theta}\right)$$

Where

$\tau = \tau_{direct}$ when $\theta = \theta_{direct}$

$\tau = \tau_{dif}$ when $\theta = \theta_{dif} = 59.68 - 0.1388\beta + 0.001497\beta^2$ (Brandemuehl and Beckman 1980)

$\tau = \tau_g$ when $\theta = \theta_g = 90 - 0.5788\beta + 0.002693\beta^2$ (Brandemuehl and Beckman 1980)

4.7. Results

4.7.1. Glazing angular transmittance

Figure 4-16 indicates sun path and variation of solar elevation for 1st January and 1st July in Dublin. Position of sun is also shown in Figure 4-16 b, and c. Due to change of sun position, incident angle varied. In Dublin for vertical plane south facing glazing, incident angle varied from 53^0 to 13^0 on 1st of January from 7 am to 12 pm. In the month of July this incident angle varied from 82^0 to 59^0 from 7 am to 12 pm. Figure 4-17 shows the variation of SPD glazing transmission of these two different days for different incident angles. Low transmission variation was observed in wintertime.

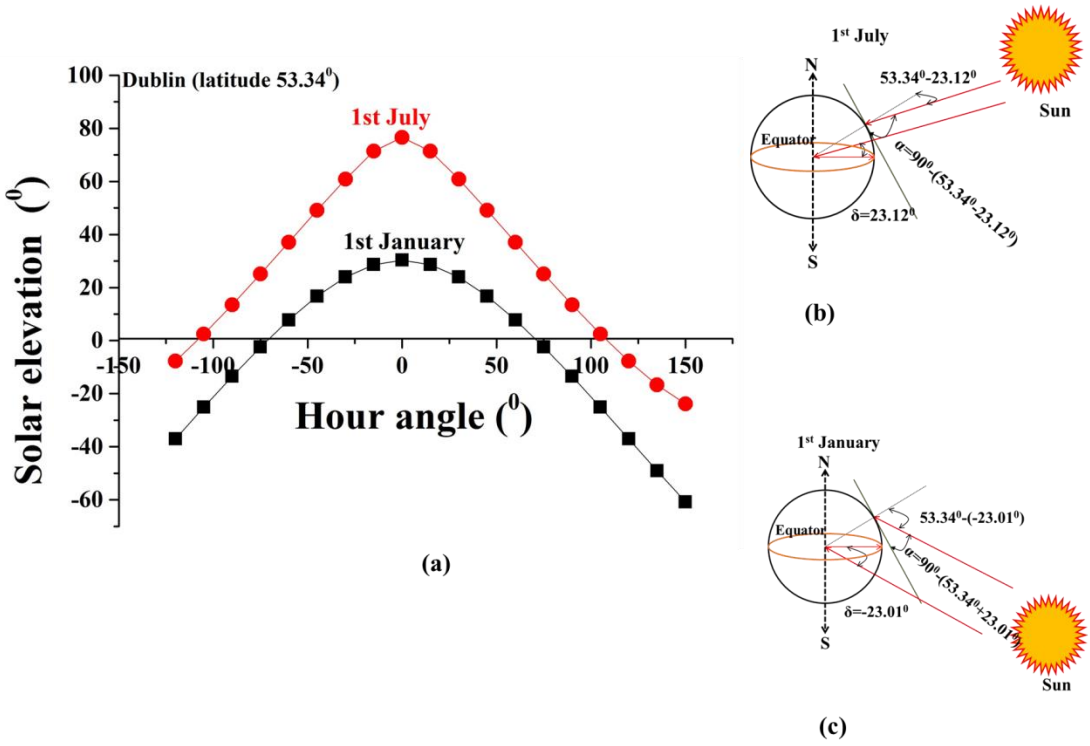

Figure 4- 16: (a) the sun path diagram in Dublin for 1st of July and 1st of January, (b) the sun ray strike the ground on at an angle 59.78⁰, (c) the sun rays strike the ground at an angle of 13.65⁰

Figure 4-18 the shows the angular transmittance behaviour throughout the year for the SPD glazing “opaque” and “transparent” state and double-glazing using equation 4-8. At lower incident angle window has higher transmittance. South facing oriented vertical plane glazing transmitted higher illuminance near mid-day period. Due to higher incident angle, transmitted illuminance was less during sunrise and sunset time.

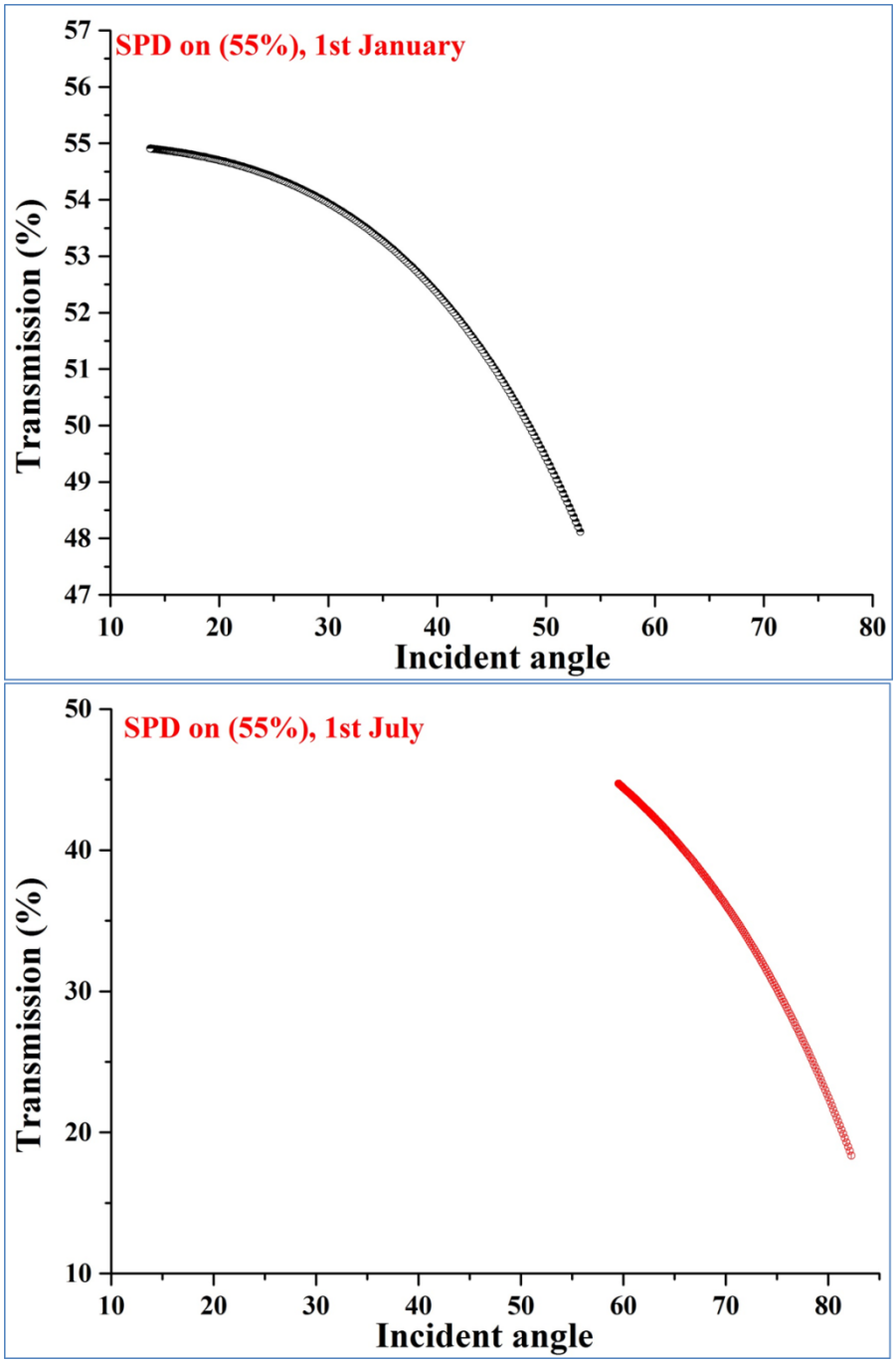

Figure 4- 17: Variation of SPD glazing (55% transparent) transmission for different incident angle in 1st of July and 1st of January.

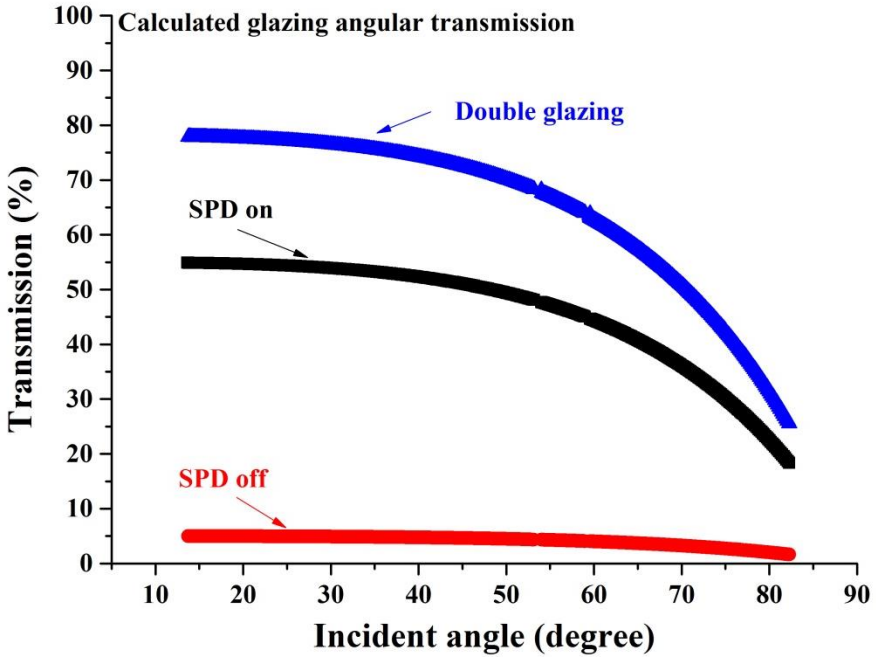

Figure 4-18: Change of transmissivity of south facing SPD "transparent", SPD "opaque" and double-glazing in Dublin.

4.7.2. Correlation of clearness index and glazing angular transmittance

Figure 4-19 shows the correlation of glazing transmission with clearness index. It is evident that higher transmission occurred at higher clearness values. Figure 4-20 shows the combined effect of transmission due to clearness index and incident angle for a south facing SPD glazing in its "transparent" state. During mid-day period, low incident angle and high clearness index were found. At higher clearness index, transparency of glazing was high. Maximum transmissions occurred between the incident angles 55 to 60. A critical value was found for the clearness index above which transmittance increases with clearness index. This indicates the solar radiation becoming decreasingly direct so the influence diminishes on overall transmittance of the isotropic incident angles associated with their diffuse components.

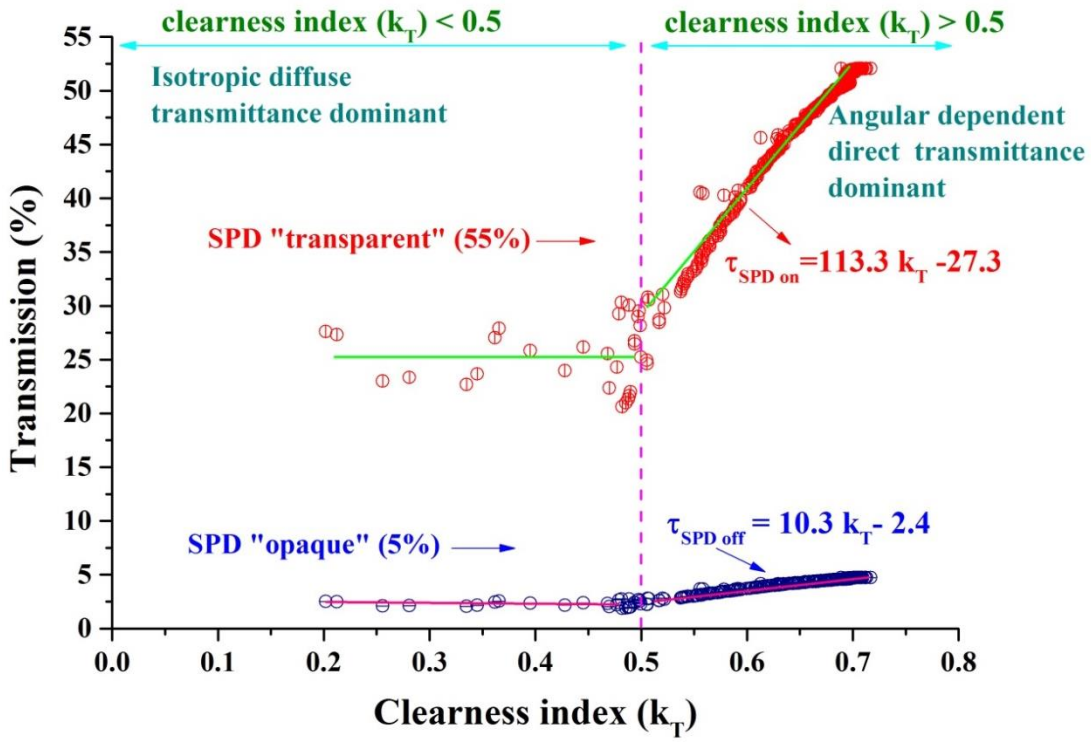

Figure 4-19: Correlation of glazing transmission with clearness index.

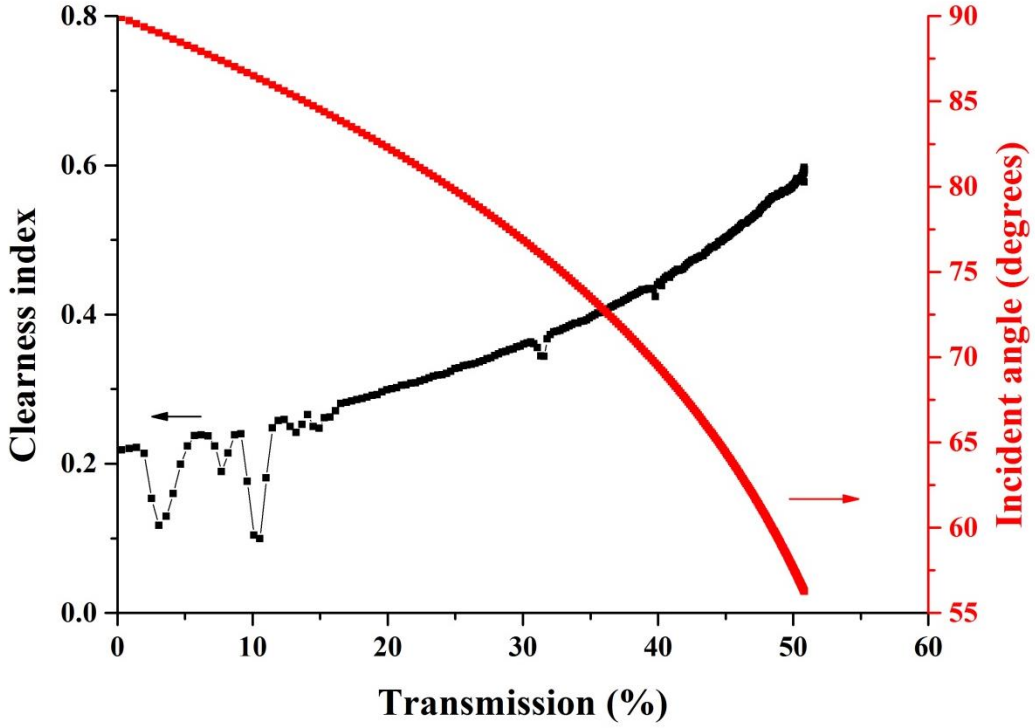

Figure 4-20: Change of SPD glazing 55% transmission due to clearness index and incidence angle.

4.8. Summary

This chapter introduces the solar radiation and illuminance in Dublin, which is an essential input parameter to characterise the SPD glazing for the project. In Dublin, three types of days are common, clear sunny day, intermittent cloudy day and overcast cloudy day. From measured vertical plane global solar radiation, clearness index was calculated. Clearness index is an important parameter, which reduces the necessity for diffuse radiation and illuminance measurement. SPD glazing has high transmittance from 700 nm to 1100 nm for both opaque and transparent state. Glazing angular transmittance indicates that during mid-day when the incident angle is low, high transmittance occurs through the glazing. Correlation between the clearness index and glazing transmittance suggests that at higher clearness indices the highest glazing transmittance occurs.

Chapter 5. Daylight performance analysis of a SPD switchable glazing

5.1. Introduction

The aim of this chapter is to evaluate the daylight performance for the suspended particle device (SPD) type glazing system under real weather condition in Dublin.

Comfortable daylight between 100-2000 lux has been named useful daylight illuminance (UDI) (Nabil and Mardaljevic 2006). Available horizontal illuminances on a work plane inside the test cell due to south facing SPD glazing opaque and transparent state was discussed in this work for three different types of day using UDI level. Daylight glare index (DGI) was evaluated for a typical sunny day. Daylight factor (DF) was also calculated.

5.2. Calculation of glare and daylight factor

5.2.1. Daylight and glare

Comfortable daylight is a variable parameter as it depends on the individual occupant. Daylight illuminances typically diminish rapidly with increasing distance from windows and daylight illuminances varies at a point greatly from one moment to the next due to changing sun position and/or sky conditions. There are varieties of different acceptable range, which has been shown in Figure 5-1. This shows that acceptable illuminance range for work and study inside a room can vary between 100-2000 lux (Nabil and Mardaljevic 2006). Illuminance between 100-2000 lux has been named useful daylight illuminance (UDI) (Nabil and Mardaljevic 2006). Below 100 lux illuminance are insufficient and requires other form of light source such as artificial light and above 2000 lux creates discomfort (Nabil and Mardaljevic 2006).

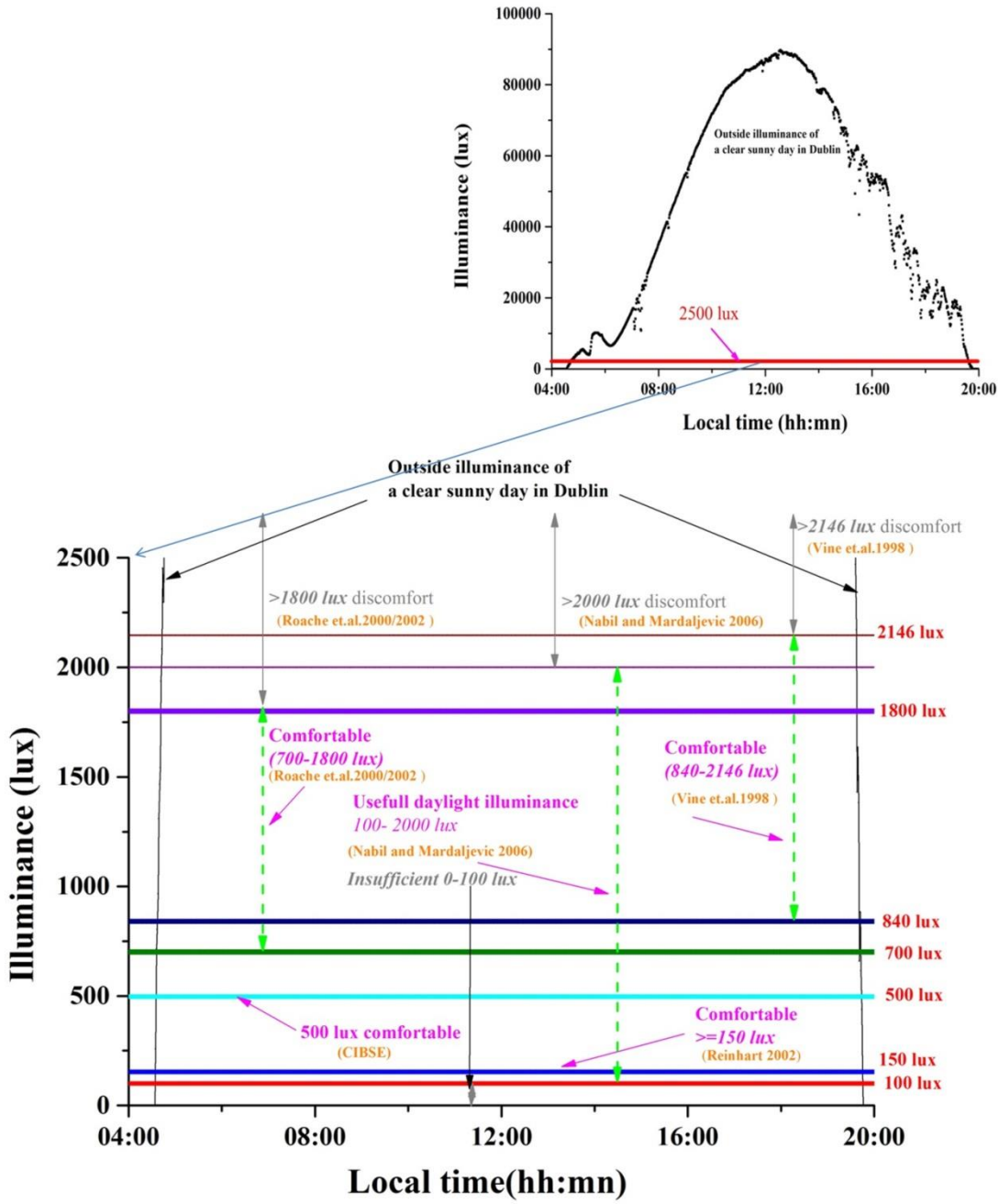

Figure 5-1: Suggested acceptabilities of illumination levels.

Discomfort glare can be evaluated by different methodologies such as visual comfort probability (VCP) method [IESNA] (IES, 1996; IESNA 2000) , CIE glare index (CGI) method (Einhorn 1969; Einhorn 1979) , unified glare index method (UGR), British glare index (BGI) (Petherbridge and Hopkinson 1950), daylight glare probability (DGP), and daylight glare index (DGI) (Hopkinson 1972; Chauvel et.al. 1982). Table 5-1 illustrates the different glare evaluation methods.

Table 5-1: List of different glare evaluation methods.

		Equations
VCP	Visual Comfort Probability (VCP) (Guth 1996)	$VCP = 279 - 110\left[\log_{10}\sum_{i=1}^{n}\left(\frac{0.5L_s\left(20.4\omega_s + 1.52\omega_s^{0.2} - 0.075\right)^{n^{-0.0914}}}{P \times E_{av}^{0}.44}\right)\right]$
UGR	Unified glare rating (UGR) (CIE 1995)	$UGR = 8\log_{10}\frac{0.25}{L_b}\sum_{i=1}^{n}\frac{L_s{}^2\omega_s}{P^2}$
Glare index	CIE glare index (CGI) (Einhorn 1969; Einhorn 1979)	$CGI = 8\log_{10}\frac{2\left[1+E_d 500\right]}{E_d + E_i}\sum_{i=1}^{n}\frac{L_s{}^2\omega_s}{P^2}$
	British glare index (Petherbridge and Hopkinson 1950)	$BGI = 10\log_{10} 0.478\sum_{i=1}^{n}\frac{L_s^{1.6}\omega_s^{0.8}}{L_b P^{1.6}}$
	The Cornell glare equation (Hopkinson 1957; Hopkinson and Bradley 1960; Hopkinson 1972)	$GI = 10\log_{10} 0.478\sum_{i=1}^{n}\frac{L_s^{1.6}\Omega^{0.8}}{L_b + 0.07\omega^{0.5}L_s}$
	The parameters in the modified version by (Chauvel et al. ;1982)	$GI = 10\log_{10} 0.478\Sigma\sum_{i=1}^{n}\frac{L_s^{1.6}\Omega^{0.8}}{L_b + 0.07\omega^{0.5}L_w}$
	Nazzal's and termed as New Daylight Glare Index (DGI_N) (Nazzal, 2001) (equation 5-6),	$DGI_N = 10\log_{10} 0.478\sum_{i=1}^{n}\frac{L_{ext}^{1.6}\Omega_{pN}^{0.8}}{L_{adp} + 0.07\omega_N^{0.5}L_{win}}$

- VCP, CGI, UGR methods are mostly applicable for artificial lights or uniform light sources and are not appropriate to large glare sources such as light coming through windows (Chauvel et. al. 1980; Chauvel and Perraudeau 1995; Hopkinson 1957; Hopkinson and Bradley 1960; Iwata et. al. 1991). None of them predicts discomfort glare from daylight or particularly from direct sunlight. British glare index (BGI) (Petherbridge and Hopkinson 1950) is limited to small sources with solid angles inferior to 0.027 sr (Osterhaus 1996). The monitoring protocol to measure the needed parameters has not been presented either in the publications of Chauvel or Hopkinson (Nazzal 2001).
- Most of them react only to the horizontal illuminance, which however, is not sufficient for user comfort. DGP (Wienold and Christoffersen 2006; Wienold 2009) method was developed to calculate glare in a simplified way that can correlate only the vertical illuminance to the levels of glare. Standard daylight glare probability is mentioned in Table 5-2.

Table 5-2: Glare level for DGP, DGI and GI (Wienold 2009; Iwata et.al. 1991).

		DGP	DGI	GI
Level of light	Imperceptible	0.33		
	Just perceptible		16	10
	Perceptible	0.38	18	13
	Just acceptable		20	16
	Acceptable	0.39	22	18.5
	Just uncomfortable		24	22
	Uncomfortable	0.42	26	25
	Just intolerable		28	28
	Intolerable	0.53		

Modified form of new daylight glare index was evaluated by Nazzal's and termed as New Daylight Glare Index (DGI_N) (Nazzal 2001; Nazzal 2005) (equation 5-1). This evaluation method specifically was formulated for daylight applications.

$$DGI_N = 10\log_{10} 0.478 \sum_{i=1}^{n} \frac{L_{ext}^{1.6} \Omega_{pN}^{0.8}}{L_{adp} + 0.07 \omega_N^{0.5} L_{win}} \quad (5\text{-}1)$$

Where L_{ext} is the exterior luminance of the outdoor source including direct sunlight, diffuse skylight and reflected light from the ground and other external surfaces (cd/m^2), L_{win} is window luminance (cd/m^2) and L_{adp} is adaptation luminance of the surroundings including reflections from internal surface (cd/m^2), ω_N solid angle subtended by the window, Ω_{pN} solid angle subtended by the glare source. In the new DGI_N method, the apparent solid angle ω_N subtended by the window, and the solid angle Ω_N subtended of the source are modified to include the effect of the observation position (the position of the measuring equipment) and configuration factor. It also replaces the background luminance with the adaptation luminance L_{adp}. This second entails including the contribution of the immediate surrounding luminance of the source (and the source itself) which is recognized to play a very important role on eye's adaptation level. In comparison to other methodologies (Hopkinson and Bradley 1960; Chauvel et. al. 1982; Tokura et. al. 1996; Wienold and Christoffersen 2006), this DGI_N index allows to measure the defining physical and geometrical parameters through simplified procedures.

5.2.2. Daylight factor

Daylight factor is the ratio of inside horizontal illuminance (L_i) and the outside horizontal illuminance (L_0) level, represent by equation 5-2 (CIBSE).

$$DF = \left(\frac{L_i}{L_0} \right) \times 100 = DF = \frac{\tau A_w \theta_1 M}{A_{wall} \left(1 - R^2\right)} \quad (5\text{-}2)$$

Where τ is glazing transmission, A_w is area of window, θ is the solid angle from visible sky patch to the viewers, M is maintenance factor for cleaning dirt, A_{wall} is the total area of interior surface, R is the internal reflectance. A detail of DF is shown in Figure 5-2.

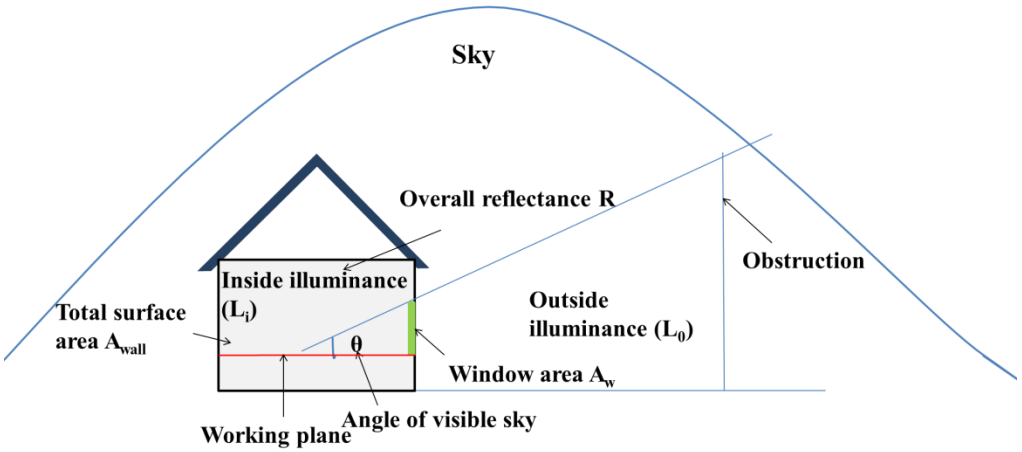

Figure 5-2: Parameters for DF calculation.

5.3. Experimental procedure

The complete experiment set up together with the unobstructed view from the test cell is shown in Figure 5-3 and 5-4 respectively. Details of set up are described in section 3.5.2 of Chapter 3.

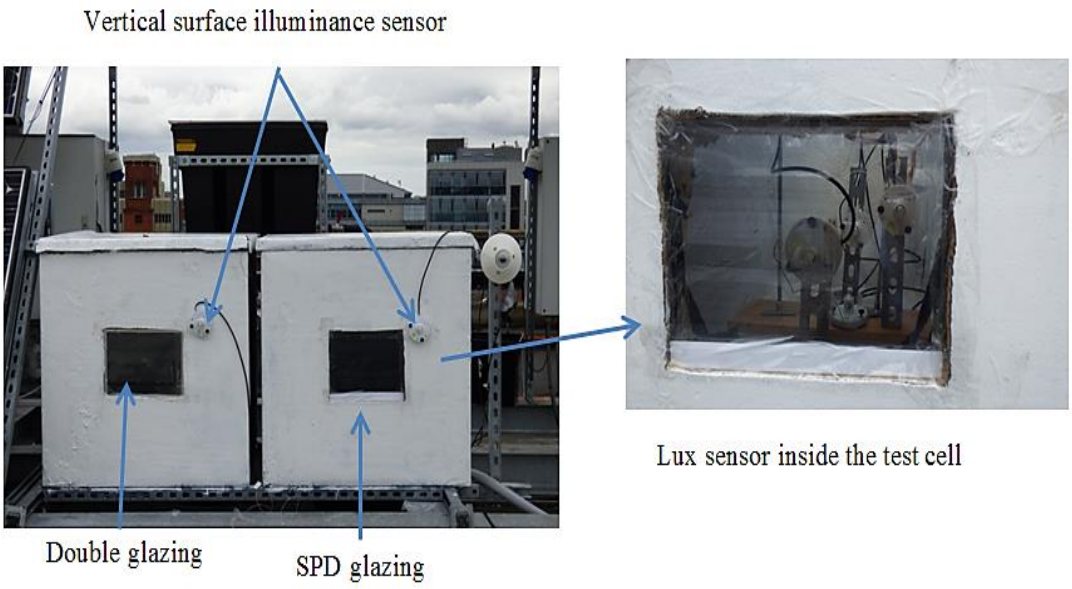

Figure 5-3: Photograph of SPD and double-glazing placed on the test cell and illuminance sensor placing inside the test cell.

Figure 5-4: Photograph of the front side ‘‘viewed’’ from the test-cell when oriented towards the south direction.

To obtain the measurements to calculate the DGI_N, the experimental set up used was similar to that by Picolo et.al. 2009a as shown in the Figure 5-5. Four light sensors were employed inside each test cell. Three light sensors were employed for glare effect assessment purposes. Their arrangement follows the criteria in Nazzal (2001) (Section 3.3). To measure vertical illuminance near the glazing $E^{in}_{v,neag}$ illuminance sensor was employed just 1 cm away from the glazing. Window illuminance was

measured using $E^{in}_{V,win}$ illuminance sensor. This sensor looks at the window centre with a 20 restricted field of view imposed by a pyramid shaped black cone; in this way it is shielded from light contributions coming from multiple wall reflections. To measure the adaptation illuminance $E^{in}_{V,adp}$ sensor, this was placed just below the pyramid cone. The horizontal illuminance was measured using E^{in}_{H} illuminance sensor at a distance of 25 cm from the front-wall and at a height of 20 cm from the floor.

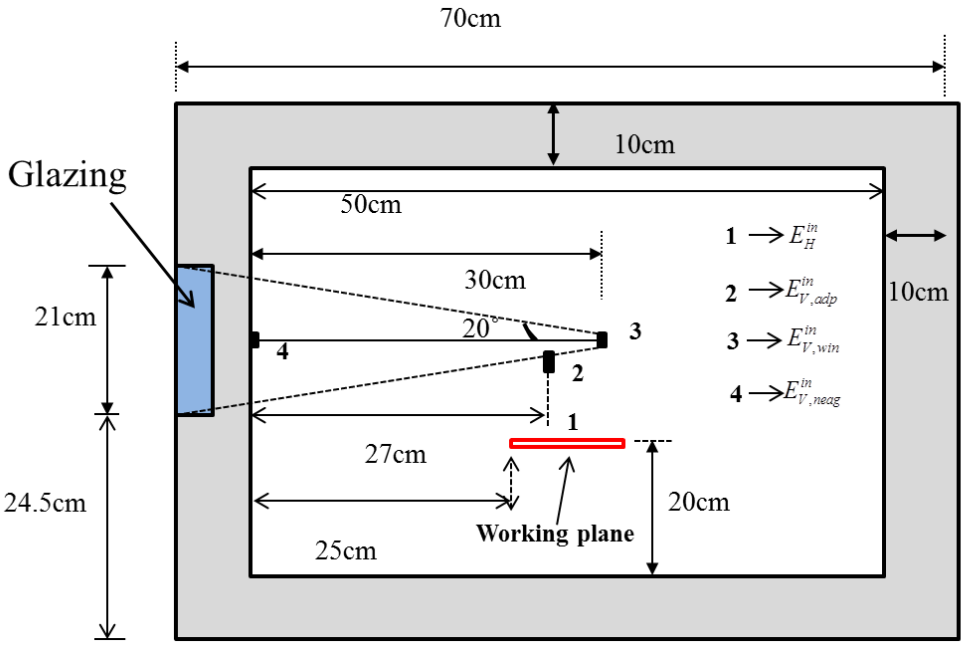

Figure 5-5: Schematic diagram of the experimental set up to obtain data for the calculation of DGI_N.

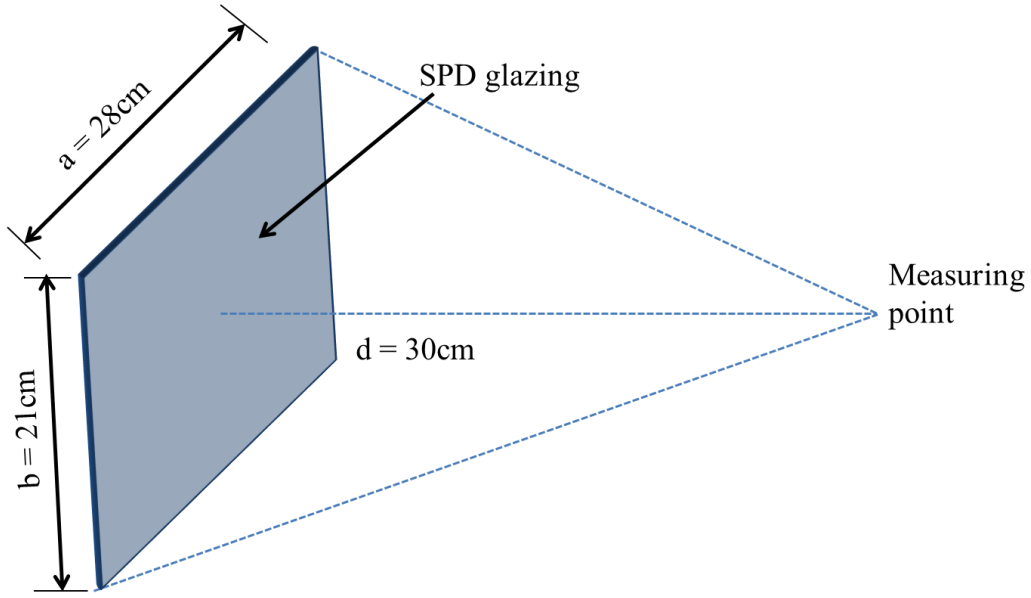

Figure 5- 6: Schematic diagram for the configuration factor calculation.

Configuration factor ϕ was calculated from the equation 5-3 using Figure 5-6 (Howell et.al. 2011)

$$\phi = \frac{\left(A\tan^{-1}B + C\tan^{-1}D\right)}{\pi} \tag{5-3}$$

Where

$$A = \frac{X}{\left[\sqrt{\left(1+X^2\right)}\right]},\ B = \frac{Y}{\left[\sqrt{\left(1+X^2\right)}\right]},\ C = \frac{Y}{\left[\sqrt{\left(1+Y^2\right)}\right]},\ D = \frac{X}{\left[\sqrt{\left(1+Y^2\right)}\right]}$$

X and Y can be calculated from equation 5-4 and 5-5.

$$X = \frac{a}{2d} \tag{5-4}$$

$$Y = \frac{b}{2d} \tag{5-5}$$

Where

a= width of SPD glazing

b= Height of SPD glazing

d= perpendicular distance from the observation place of the centre of glazing.

The configuration factor (ϕ) of the window from the observation point was 0.0835, while solid angles subtended by the glare source (Ω_N) and solid angles angle subtended by the window (ω_N) are calculated (Nazzal 2001) from equation 5-6 and 5-7 and their value were found 0.5 sr and 0.55 sr, respectively.

$$\omega_N = \frac{\left[ab\cos\left(\tan^{-1} X\right)\cos\left(\tan^{-1} Y\right)\right]}{d^2} \tag{5-6}$$

$$\Omega_N = 2\pi\phi \tag{5-7}$$

Luminance level of glazing, adaptation and exterior can be evaluated by equation 5-8, 5-9, 5-10.

$$L_{win} = \frac{E_{V,win}^{in}}{2\pi\phi} \tag{5-8}$$

$$L_{adp} = \frac{E_{V,adpt}^{in}}{\pi} \tag{5-9}$$

$$L_{neag} = \frac{E_{V,neag}^{in}}{2\left(\pi - 1\right)} \tag{5-10}$$

Here

$L_{ext} = L_{neag}$

$$DGI_N = 10\log_{10} 0.478\sum_{i=1}^{n} \frac{L_{ext}^{1.6}\Omega_{pN}^{0.8}}{L_{adp} + 0.07\omega_N^{0.5}L_{win}} \tag{5-11}$$

5.4. Results

5.4.1. Internal illuminance and switching property of SPD

Figures 5-7 represents the internal horizontal illuminance of a double-glazing and SPD "opaque" and "transparent" states for a clear sunny day in Dublin. Horizontal measuring point was 27 cm away from the glazing inner surface as shown in Figure 5-5. Maximum illuminance through double-glazing was 10000 lux whereas SPD "transparent" and "opaque" were 7400 lux and 640 lux during mid-day period. SPD glazing "opaque" condition has a potential to limit the light coming through window

and average illuminance levels were less than 600 lux. SPD “transparent” state after 8:20 am needed to be “opaque” state to maintain the UDI level. During the afternoon after 03:15 pm, the SPD glazing could be switch to make it “transparent”.

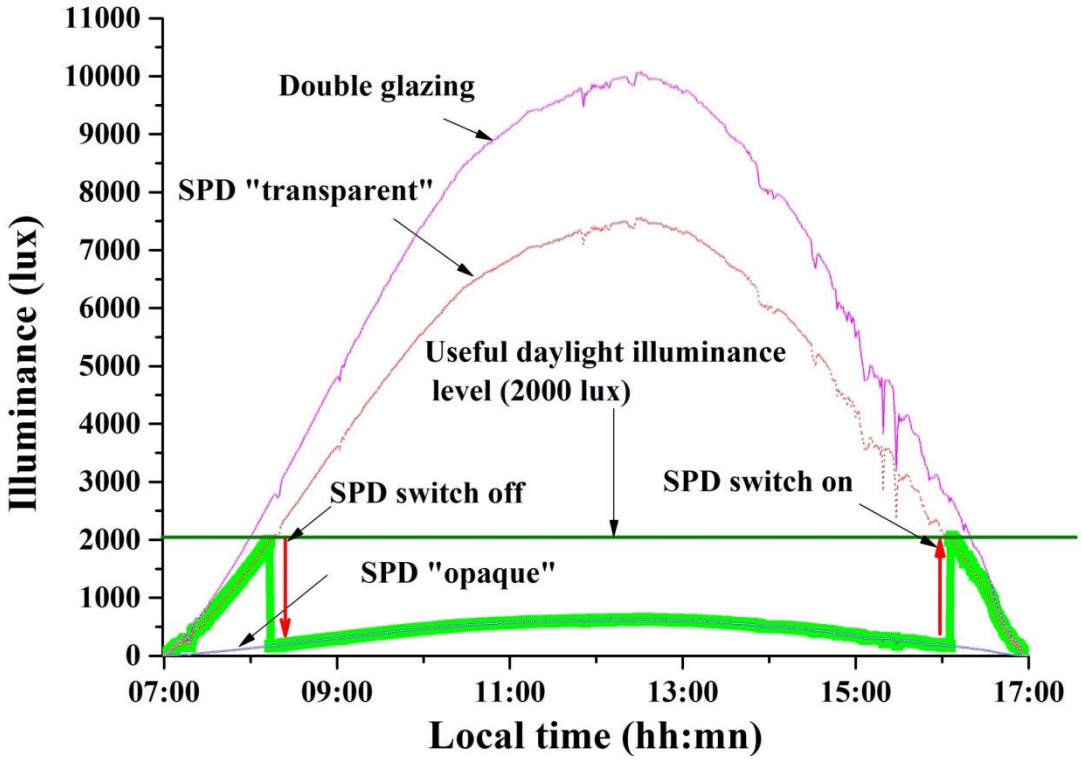

Figure 5-7: Inside illuminance of double-glazing and SPD “transparent” and “opaque” state and the switching of suspended particle device to maintain useful daylight illuminance level for a typical sunny day.

Inside horizontal illuminance on the working plane for double-glazing and SPD glazing “opaque” and “transparent” states are shown in Figure 5-8 for an intermittent cloudy sky condition. Inside illuminance levels for double, SPD “transparent” and SPD “opaque” were 7430 lux, 5600 lux and 490 lux during mid-day period. SPD glazing requires switching to being opaque at 11:10 am, which was much later than for a clear sunny sky.

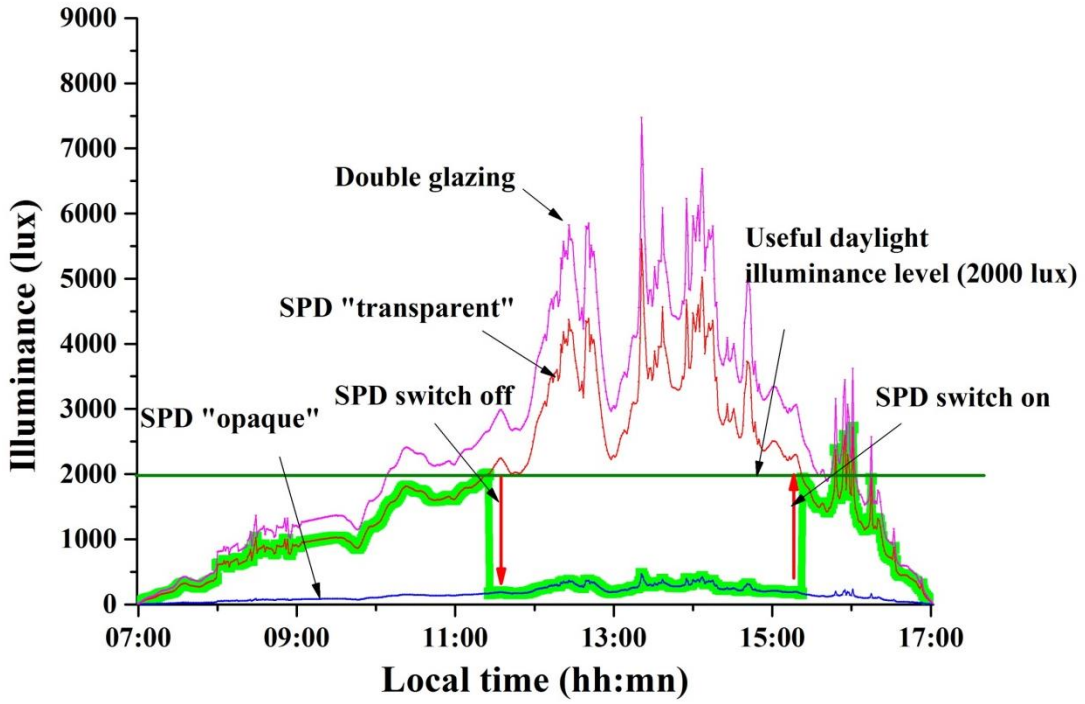

Figure 5-8: Inside illuminance of double-glazing and SPD "transparent" and "opaque" state and the switching of suspended particle device to maintain useful daylight illuminance level for a typical intermittent cloudy day.

Inside horizontal illuminance on a working plane for double-glazing, SPD "transparent" and "opaque" states for an overcast cloudy day are illustrated in Figure 5-9. Light level for SPD "opaque" state was most of the time below 200 lux. SPD "transparent" state light level was nearly 1500 lux. For an overcast day, the SPD glazing remains transparent allowing 55% transmission to maintain the inside illuminance of the test cell.

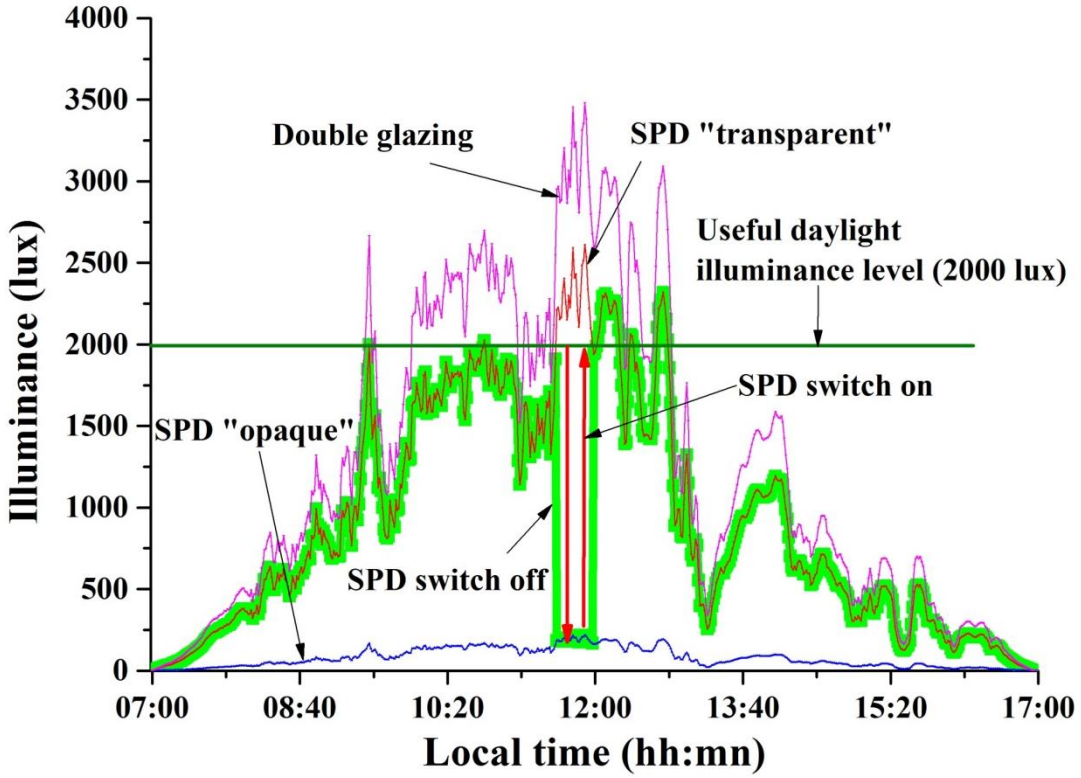

Figure 5-9: Inside illuminance of double-glazing, SPD "transparent" and SPD "opaque" condition and the switching of suspended particle device to maintain useful daylight illuminance level for overcast sky condition.

5.4.2. Daylight glare index

Daylight glare index of SPD glazing "transparent" and "opaque" states were calculated for sunny, intermittent and overcast day using the method mentioned in section 5.3.

Figure 10 (a) and (c) illustrate the measured illuminance for three different positioned illuminance sensor as described in section 3.3 for SPD glazing "transparent" and "opaque" states in a sunny day. Figure 10 (b) and (d) illustrate the luminance calculated from the equation 5-8, 5-9 and 5-10 using the measured values shown in Figure 10 (a) and (c) for SPD "transparent" and "opaque" states respectively.

Daylight glare index was calculated using equation 5-11. Calculated values of daylight glare index for SPD “opaque” and “transparent” states are shown in Figure 10 (e). SPD in a transparent state was unable to control the glare 9 am to 03:30 pm., as it was clear sunny day and direct sunlight penetrated through the SPD glazing. SPD “transparent” state was able to control glare before 9 am and after 03:30 pm.

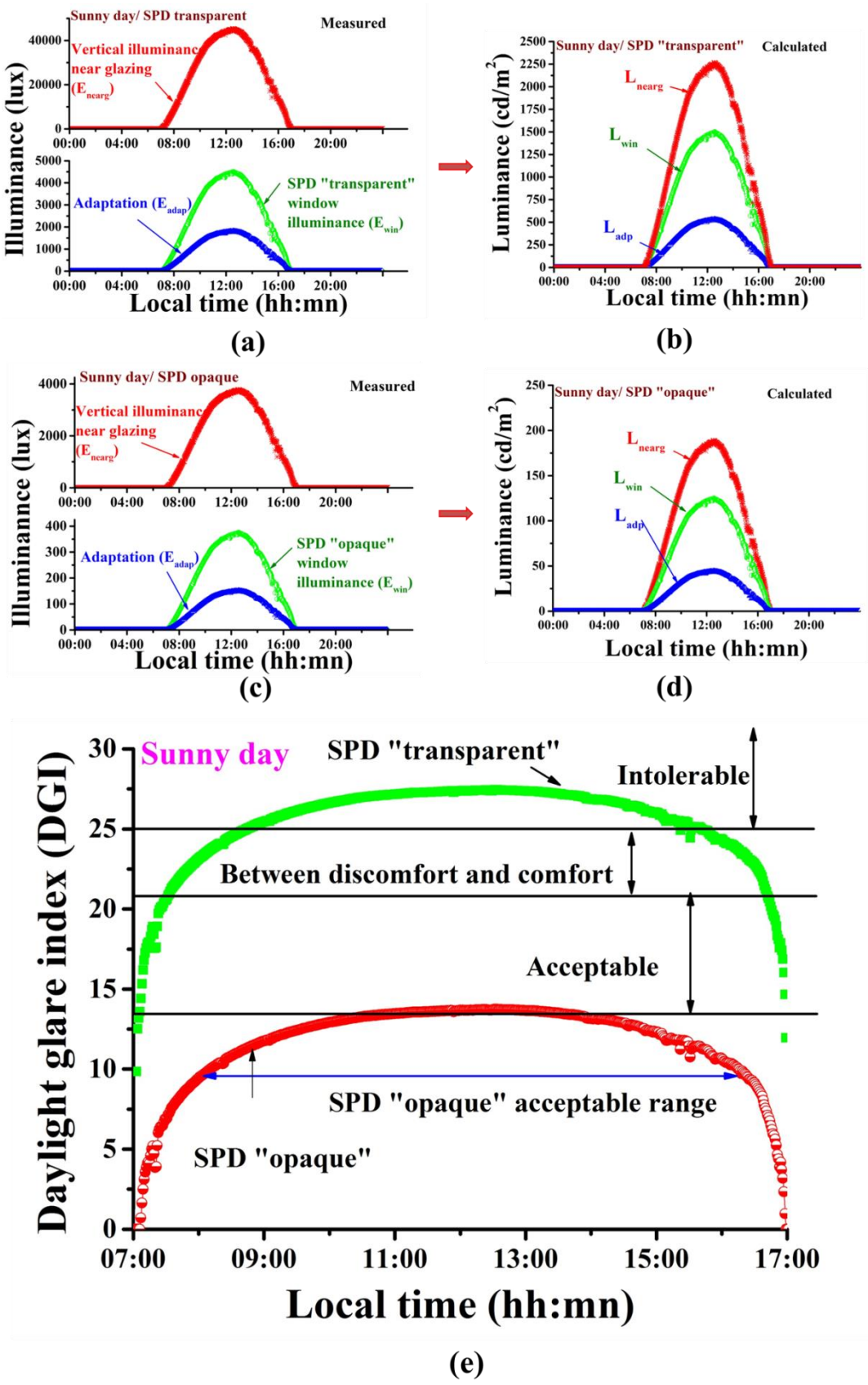

Figure 5- 10: (a) and (c) measured illuminance level for near to glazing, window illuminance and adaptation level and (b) and (d) calculated luminance using equation 5-8, 5-9, 5-10 for SPD " transparent" and "opaque" states, (e) DGI of SPD "transparent" and "opaque" states for a sunny day in Dublin.

Figure 11 (a) and (c) show the measured illuminance level for near to glazing, window illuminance and adaptation level and Figure 11 (b) and (d) show the calculated luminance using equation 5-8, 5-9, 5-10 for SPD “transparent” and “opaque” states. Figure 11 (e) illustrates DGI of SPD “transparent” and “opaque” state for an intermittent day in Dublin. In that day SPD glazing “transparent” state was able to control the glare till 12:00 am. It was unable to control the glare for short duration. It can be estimate that that day SPD can be kept “transparent” state during most of the sunshine period.

Figure 12 (a), (b), (c), (d) and (e) show the measured illuminance level for SPD “transparent” and “opaque” state, calculated luminance for SPD “transparent” and “opaque” state and DGI respectively for an overcast day. For an overcast day SPD “transparent” state never reached the intolerable limit.

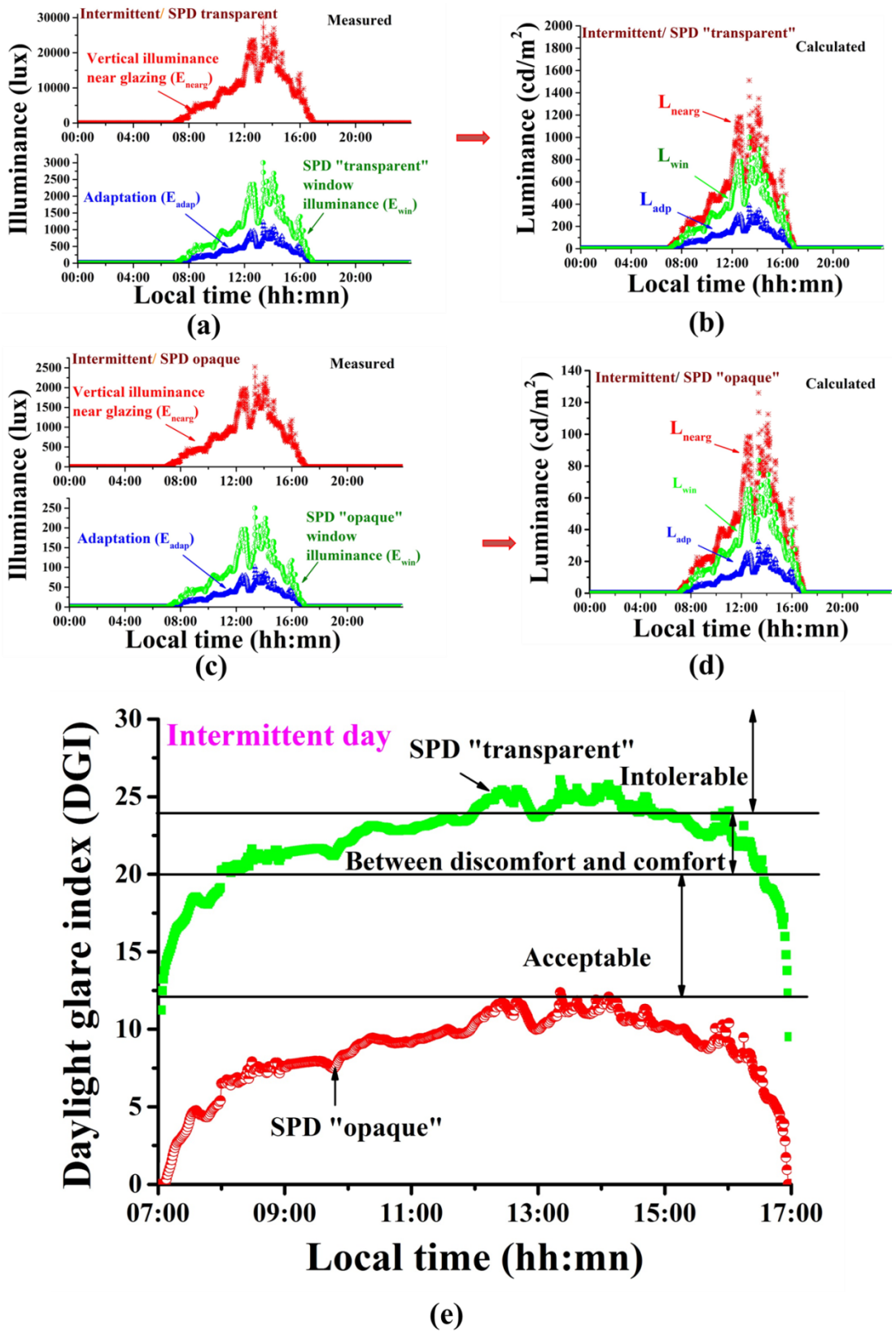

Figure 5- 11: (a) and (c) measured illuminance level for near to glazing, window illuminance and adaptation level, (b) and (d) calculated luminance using equation 5-8, 5-9, 5-10 for SPD " transparent" and "opaque" states, (e) DGI of SPD "transparent" and "opaque" states for an intermittent day in Dublin.

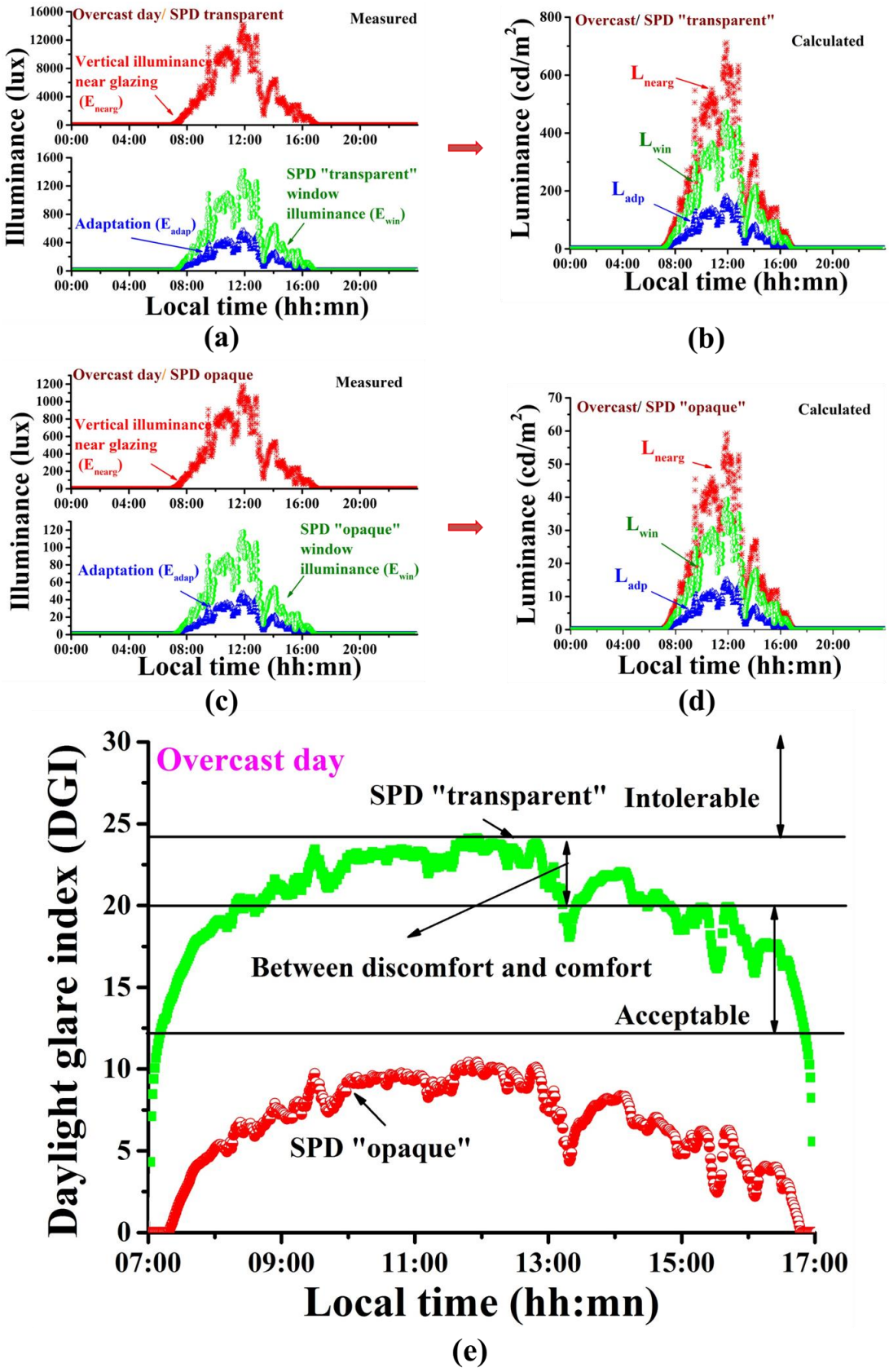

Figure 5- 12: (a) and (c) measured illuminance level for near to glazing, window illuminance and adaptation level, (b) and (d) calculated luminance using equation 5-8, 5-9, 5-10 for SPD " transparent" and "opaque" states, (e) DGI of SPD "transparent" and "opaque" states for an overcast day in Dublin.

5.4.3. Daylight factor

Figure 5-13 indicates the Daylight factor (DF) for double-glazing, SPD “transparent” and SPD “opaque” state for any type of condition. As it is the ratio of inside and outside-unobstructed horizontal illuminance, it is equal for three different types of days.

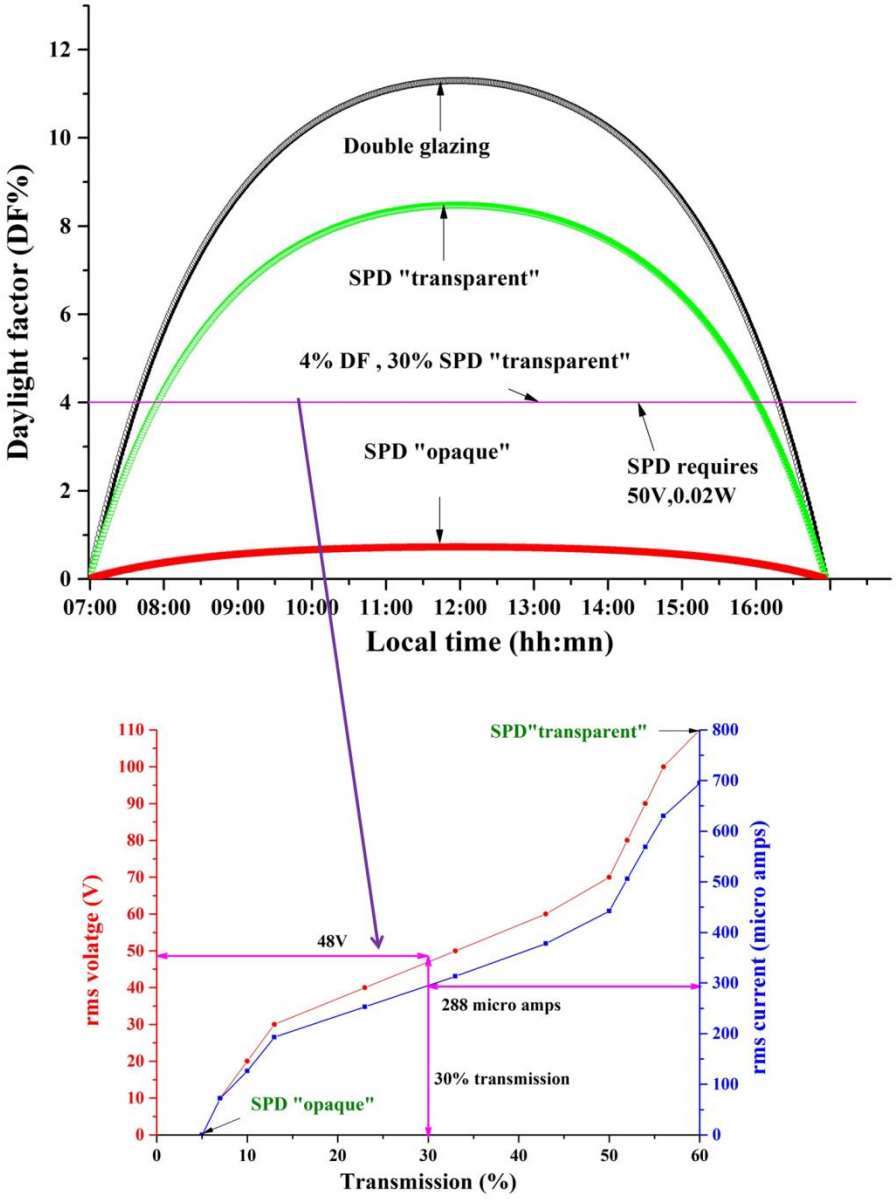

Figure 5- 13: Percentage DF of a working plane 27 cm away and 20 cm above from the ground for double-glazing, SPD “transparent” and “opaque” state.

5.4.4. Advantages of using SPD glazing

In this experiment, the 0.05 m^2 SPD device took 0.07 W to become completely clear. To achieve 4% DF that is allowable for any type of room, SPD needs to 30% transparent (using DF equation), which is possible using 48 V with the power required being 0.0138 W. If it is assumed that this 20 SPD windows of 1 m^2 size then it will consume 0.4 W to generate 4% DF. Transmission of SPD for different power consumption is shown in Figure 5-14.

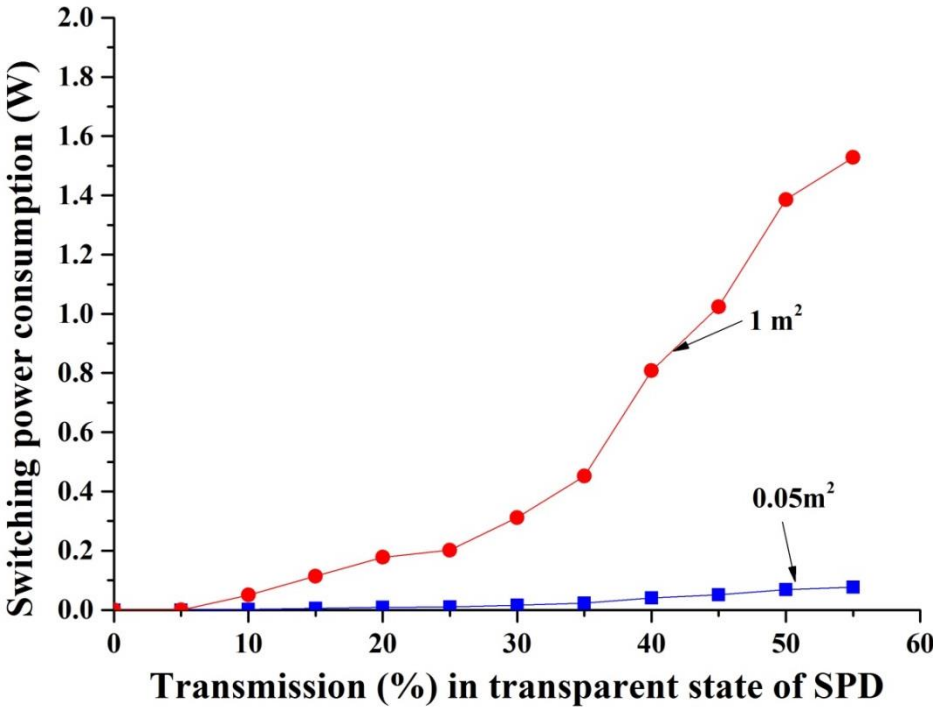

Figure 5- 14: Power requirements to achieve different transmissions for transparent state SPD.

If it is considered that a room having no daylighting option, requires an artificial light (assume 60 W light bulb) to maintain 4% DF then the energy consumption will be 0.7 kWh for 12 hours.

If one opaque south-facing wall of this same room is now replaced with 1 m2 of 30% transparent SPD glazing to allow moderate 4% DF for this same 12 hours period, the power requirement will be only 0.0048 kWh.

Saving of energy = (0.7 - 0048) kWh = 0.69 kWh

If this condition is considered for 356 days, then the saving total will be = 255.5 kWh

The mitigation of CO_2 emission from the actual amount of lighting energy saving potential due to SPD glazing can be determined using the relation reported by Watt et.al. 1998

Mitigation of CO_2 emissions = Energy saving (kWh/year) × (kg of CO_2 generated /kWh electricity generation)

Table 5-3 and Figure 5-15 illustrate the potential CO_2 emissions reduction from the reference single room using a $1m^2$ SPD glazing for different countries.

Table 5-3: CO_2 emission for 1 kWh electricity generation of different countries.

		CO_2 emission /kWh electricity	Reference
Country	Ireland	0.469 kg	SEAI 2013; Clancy et.al. 2015
	India	1.568 kg	Ahmad and Tiwari 2010, Chel and Tiwari 2010
	USA	0.317 kg (only from Bituminous coal)	EIA 2011; Yi 2015
	Australia	0.75 kg	AEMO 2014
	New Zealand	1 kg	Walmsley et.al. 2014

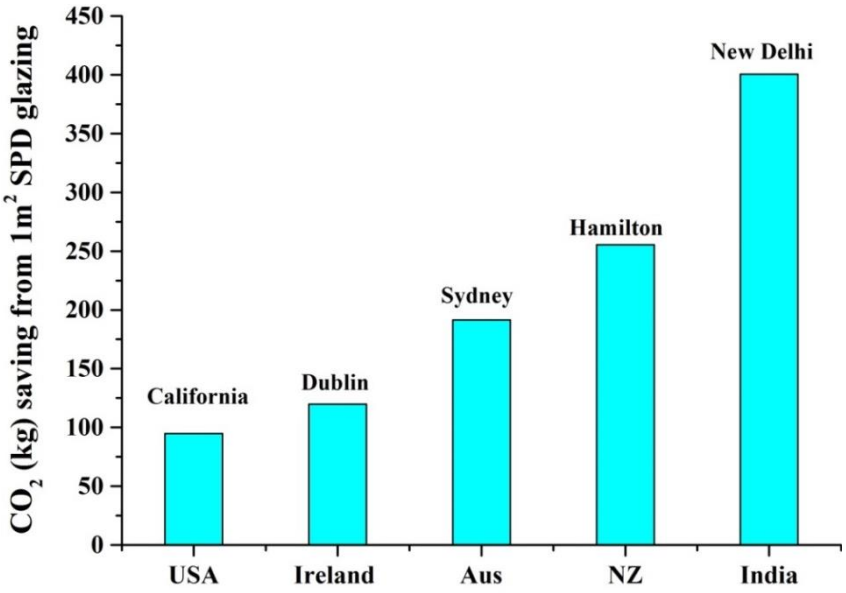

Figure 5- 15: Saving of CO_2 emissions for $1m^2$ SPD glazing in different country.

5.5. Summary

Suspended particle device glazing can be a good solution for daylight and glare control windows. It has advantages over EC glazing as it can be connected directly to AC supply and over LC glazing that it has intermediate states between transparent and opaque. Variable applied voltage between 0 to 110V, offered a variety of different level of SPD glazing transmission between 5% to 55% respectively.

Useful daylight illuminance (UDI) of a SPD switchable glazing in transparent and opaque states has been measured using the test cell for clear sunny, intermittent cloudy and overcast cloudy skies. It was found that the SPD "opaque" state was achieved the UDI level under clear sunny and intermittent cloudy day while SPD in "transparent" state is required for an overcast cloudy day. DF measurements indicate an acceptable range for SPD in an opaque state. To achieve an acceptable range of UDI, DGI and DF, the use of intermediate transmission levels of the SPD glazing is more appropriate. An advantage of SPD glazing is that the comfort level of light inside a room can maintained possible by changing the transparency.

Chapter 6. Electrical performance analysis of SPD switchable glazing

6.1. Introduction

The goal of this chapter is to evaluate the photovoltaic (PV) powering of a suspended particle type glazing system under real weather condition in Dublin.

Specific objectives are

- Outdoor characterisation of PV powered SPD glazing system.
- Three different days' clear sunny day, intermittent cloudy day and overcast cloudy day were considered in this experiment for south facing test cell.
- SPD was connected in two different ways to PV power. (1) PV directly connected to glazing by inverter, (2) PV connected to glazing and battery by inverter and charge controller.

6.2. Experimental procedure

PV powered SPD glazing experiment was carried out in Dublin, Ireland (53.34 ^{0}N, 6.25 ^{0}W) from 1st of May to 1st July 2014. Photograph of full experimental set up is illustrated in Figure 6-1. Details of this experimental set up are mentioned in section 3.5.3. of Chapter 3.

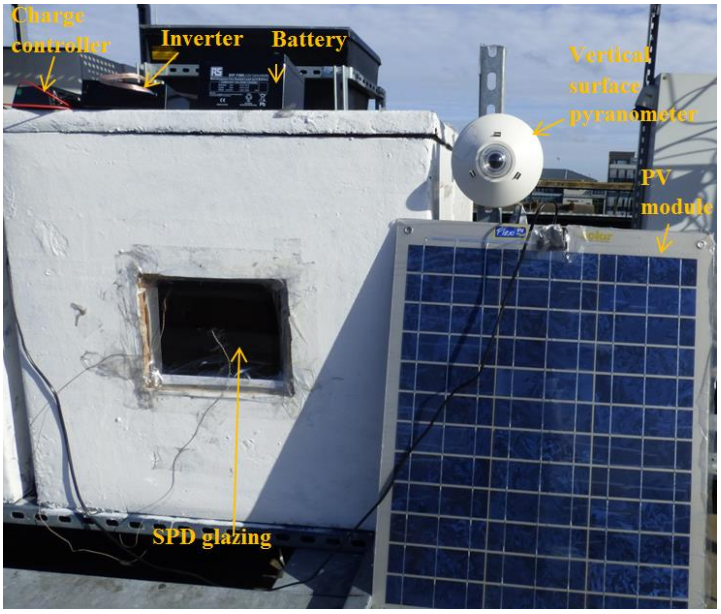

Figure 6-1: Full view of experimental set up of PV powered SPD glazing.

6.3. Experimental results

6.3.1. Results from outdoor characterisation

The diurnal variation PV module DC power output due to the solar radiation from 1st to 10th May 2014, is presented in Figure 6-2. Change of PV module temperature with solar radiation and ambient temperature are also depicted in this figure. In a sunny day, the PV device achieved maximum power nearly 33 W, which was less than its rated power 40 W. Reduction of power, occurred due to higher increased temperature of PV module. During mid-day period, 50 ^{0}C cell temperature was nearly achieved. PV device power reduced at higher temperature as silicon has negative temperature coefficient and approximately 0.5% of generation efficiency decreases when the surface temperature increases by 1 ^{0}C. Negative temperature coefficient of this module varied between 0.2-0.3/K.

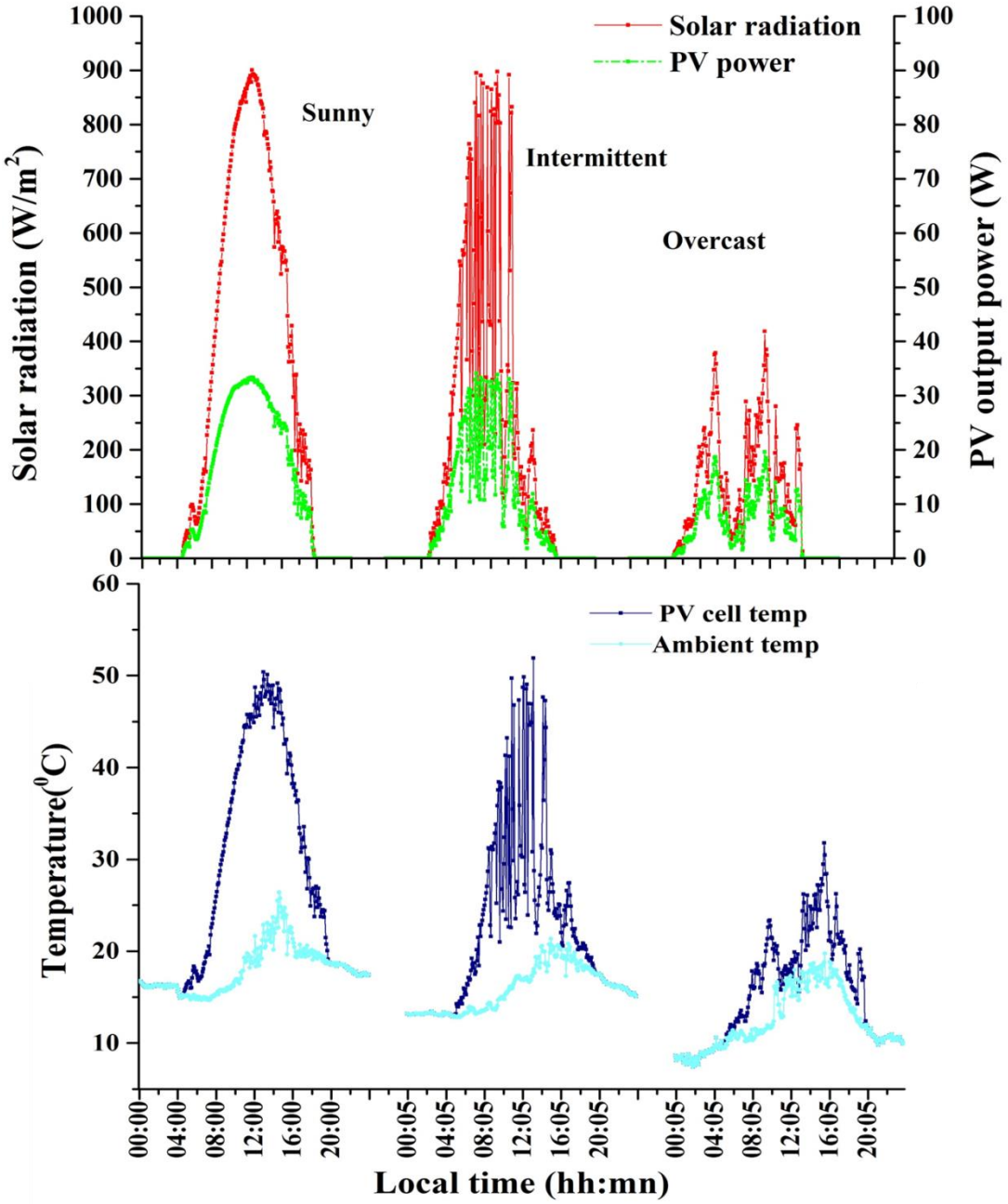

Figure 6-2: Diurnal variation of solar radiation, power output from 40W_p PV, PV module temperature and ambient temperature for sunny, intermittent cloudy and overcast day.

Figure 6-3 illustrates the correlation of PV power output, PV module temperature, and PV module efficiency with clearness index. These graphs clearly show that efficiency decreases as clearness index increases. The decrease is rapid for low clearness indices but less for high clearness indices.

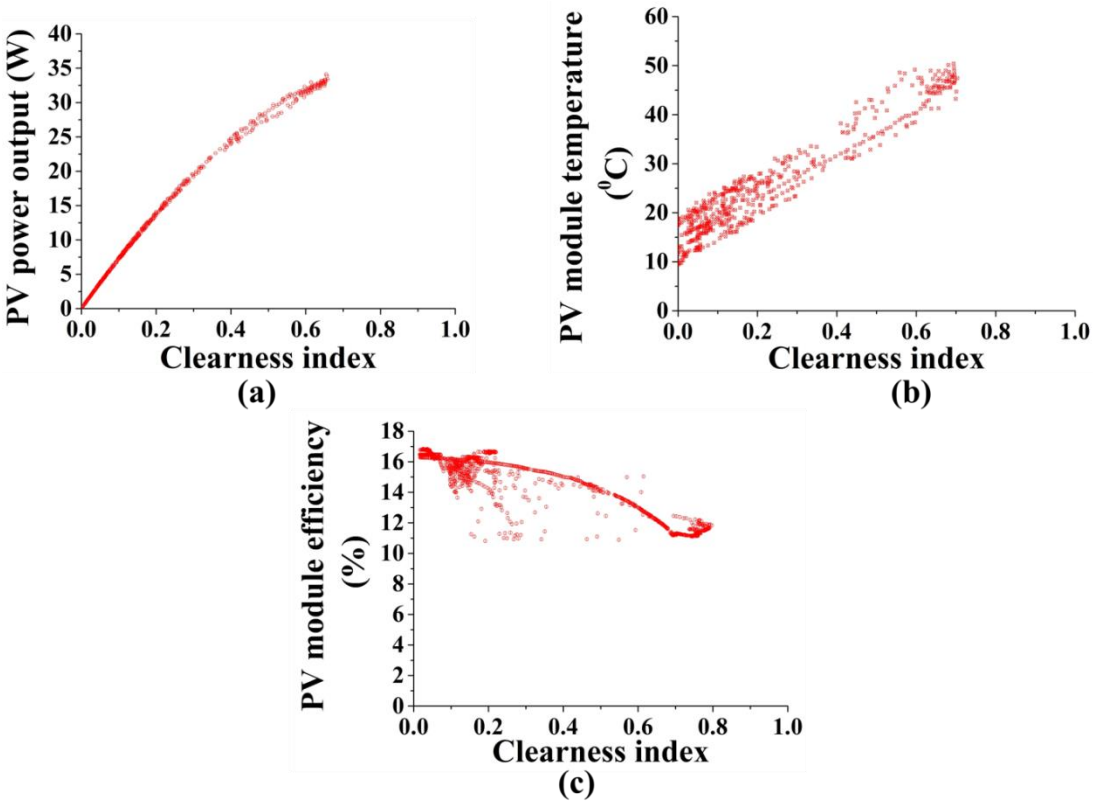

Figure 6- 3: Correlation between (a) clearness index and PV module power, (b) clearness index and PV module temperature and (c) clearness index and PV module efficiency.

6.3.2. Photovoltaic ($40W_p$) powered SPD glazing without battery

Inverter input power (PV output power), output power, SPD glazing power requirement, and inverter efficiency is illustrated in Figure 6-4. This SPD glazing needs 0.07 W power to remain constantly transparent. In case PV directly connected to the inverter PV output will work as inverter input. It was found that SPD glazing was switched off even though PV generated output power from early morning. It was due to the low inverter efficiency as the input power was less than its rated power. Difference between inverter input and output power is present due to the self-consumption losses of the inverter. Inverter output power was high enough compare to required SPD glazing. As there was no battery backup during the midday period,

considerable power produced at that time was unused. This could have been stored in a battery to use later.

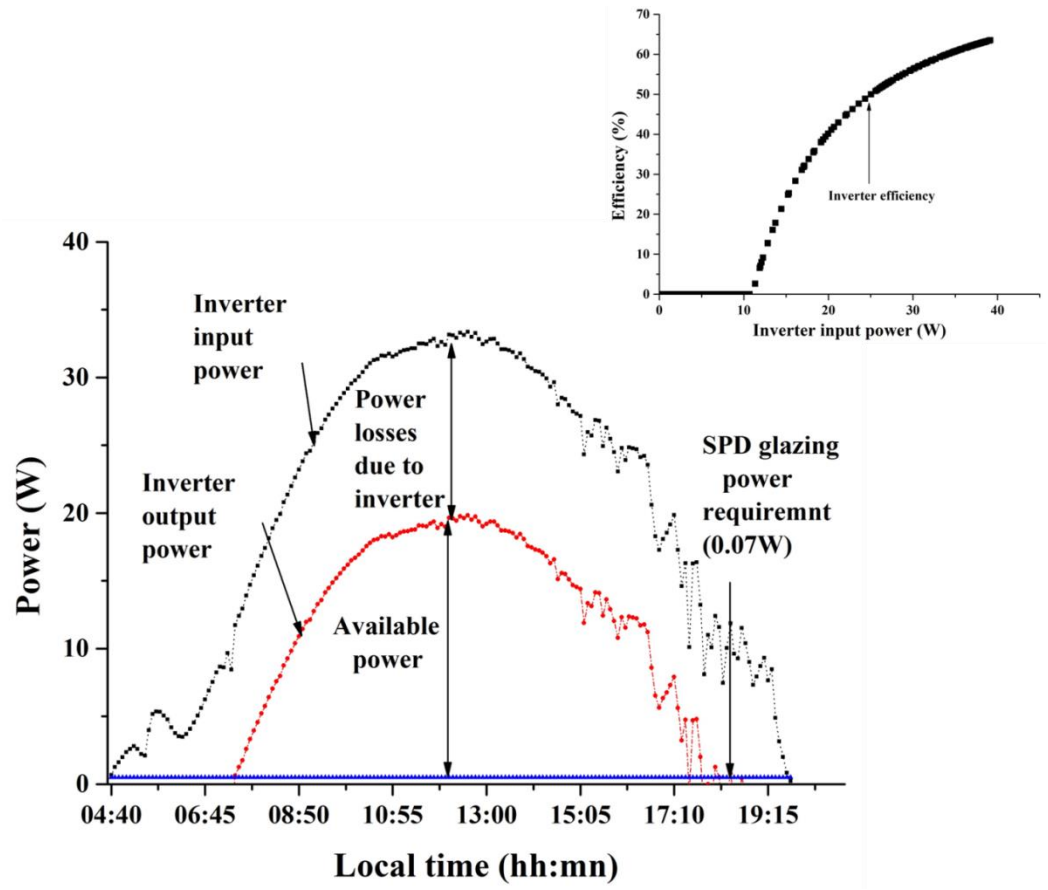

Figure 6-4: **Diurnal variation of inverter input power, output power for clear sunny day while SPD glazing power requirement was constant during sunshine hour.**

Figure 6-5 indicates the behaviour of PV and inverter during an intermittent cloud cover day. Inverter input power dropped due to cloud cover solar radiation that also reduced the inverter output power. There was certain time when 40 W_p PV was not able enough to supply a continuous power to a 0.07 W SPD glazing. Battery storage is required to power the SPD glazing for these types of days.

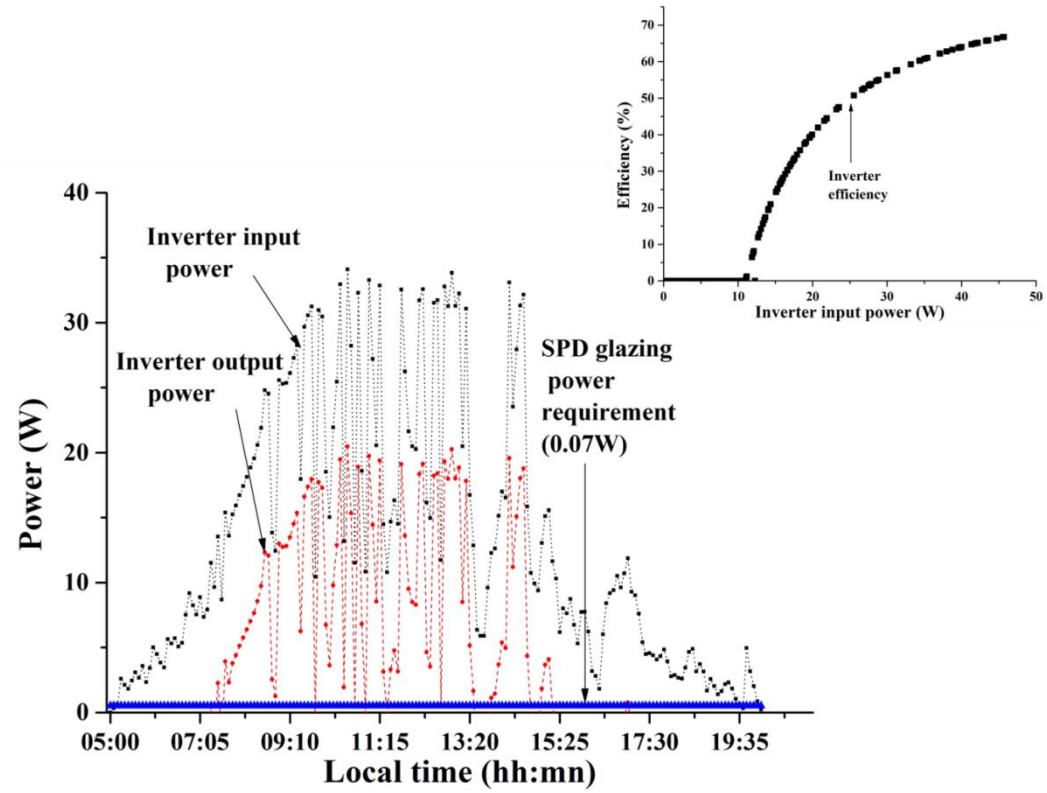

Figure 6-5: Diurnal variation of inverter input power, output power for an intermittent cloudy day and constant SPD glazing power requirement.

PV inverter behaviour for an overcast day is illustrated in Figure 6-6. It is evident from the figure that overcast day SPD glazing was in opaque state (switched off) most of the time due to availability of low solar radiation level. This low-level radiation could not generate sufficient PV power, thus the power from inverter was also very low and most of the time it was absent. For these types of days, a battery storage device is essential to supply uninterrupted power to SPD glazing.

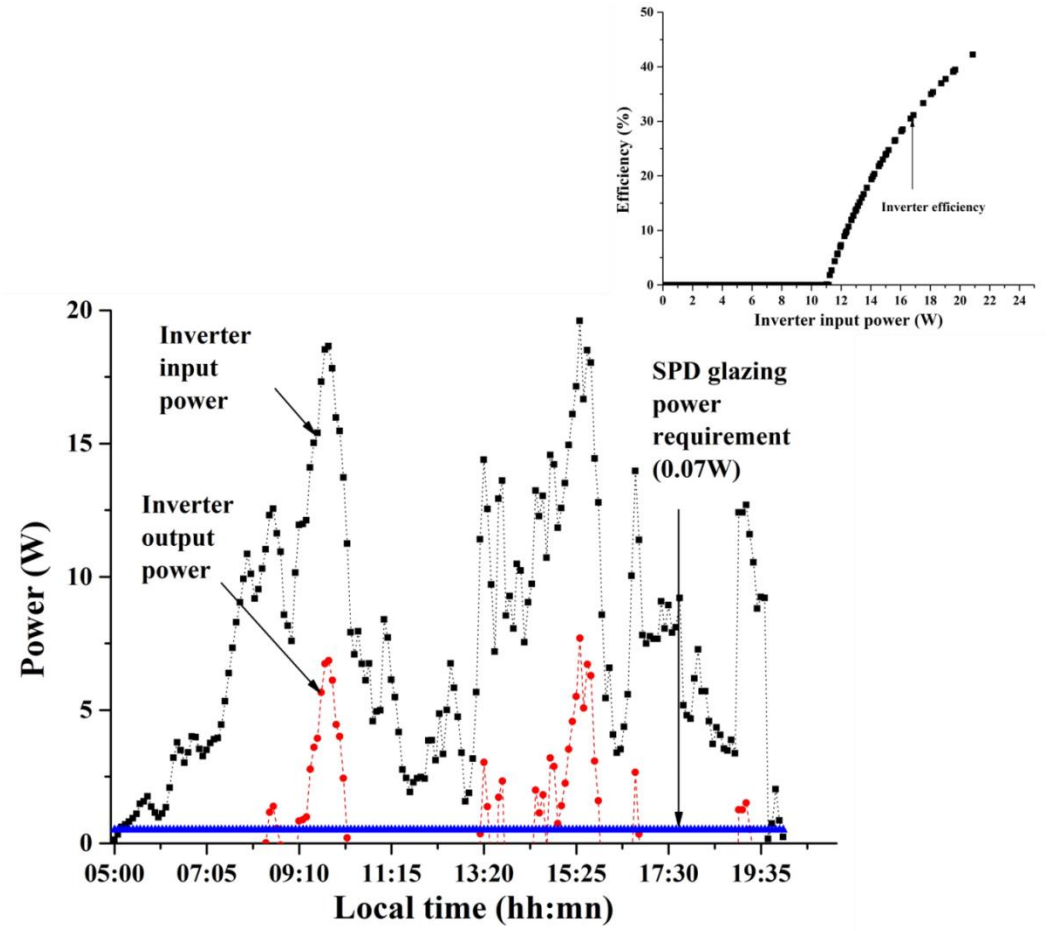

Figure 6-6: Diurnal variation of inverter input power, output power for an overcast cloudy day and constant SPD glazing power requirement.

6.3.3. Photovoltaic ($40W_p$) powered battery

The battery capacity in ampere-hour (Ah) is equal to the charge needed to increase the state of charge (SOC) from a fully discharged state to a fully charged state as shown in Figure 6-7. Lead acid battery has slow self-discharge rate. A fully charged battery reduces its capacity 91% only after 3 months and 65% after 12 month at 25 ^{0}C condition. In this experiment, battery was disconnected after charged fully and negligible losses were found for 12 hours which indicating a constant SOC after it was fully charged.

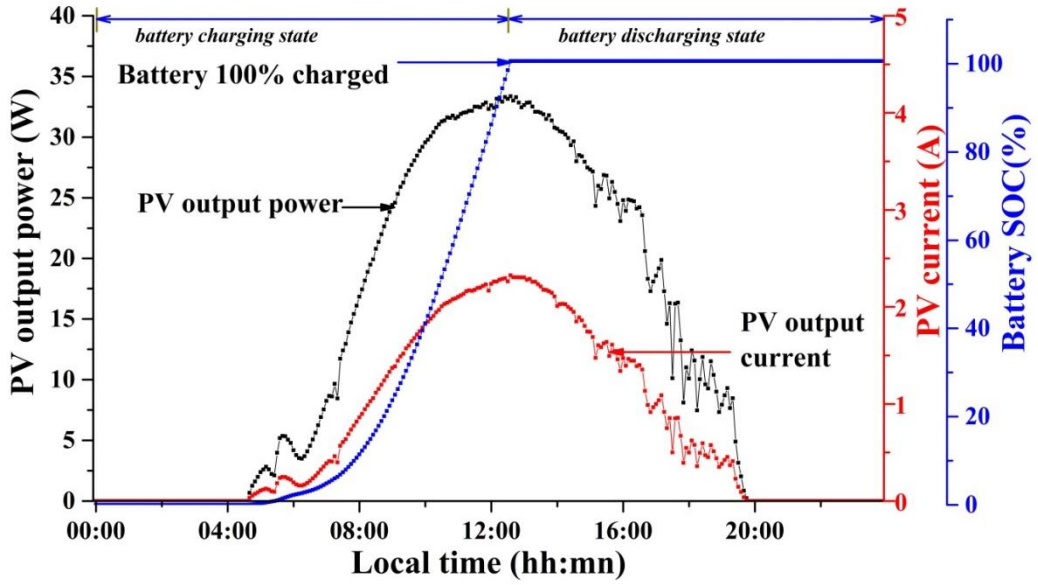

Figure 6-7: State of charge of a 12V, 12 AH battery powered by 40W_p PV device.

6.3.4. Photovoltaic (40 Wp) powered battery and SPD glazing

Dynamic behaviour of PV, charge controller, battery, inverter and SPD glazing was monitored for a sunny day shown in Figure 6-8. PV powered to a SPD glazing and charged a battery from complete zero charge to 100% charged condition. PV powered to the SPD glazing, when battery charged fully. While PV only supplied to battery the battery charging time was from 5 am to 12.30 pm (in Figure 6-7). In Figure 6-10 it was found that battery charging time was higher and around at 2:10 pm battery charged fully. This was due to the power division between inverter and battery. After full charge power coming from PV fully supplied to the inverter and glazing. There is a lag between power coming from PV and input power of inverter. It was due to the charge controller. There are some losses of power due to charge controller though the amount was not significant.

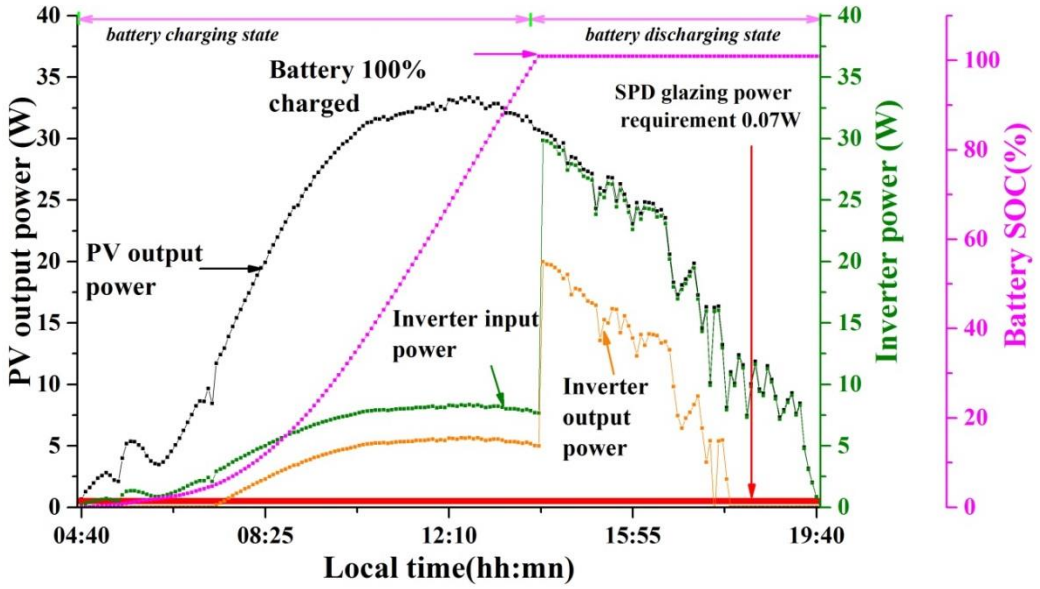

Figure 6-8: Dynamic variation of PV output power, state of charge of a 12V, 12 AH battery, inverter input and output power.

6.3.5. Photovoltaic (245 Wp) powered SPD without battery using low sizing ratio inverter

Figure 6-9 illustrates the incoming power to the SPD glazing from PV and inverter. Ratio between PV power rating and inverter rating was comparatively less than the first case (Figure 6-4). This low sizing ratio system (PV-inverter) reduced the power loss due to inverter.

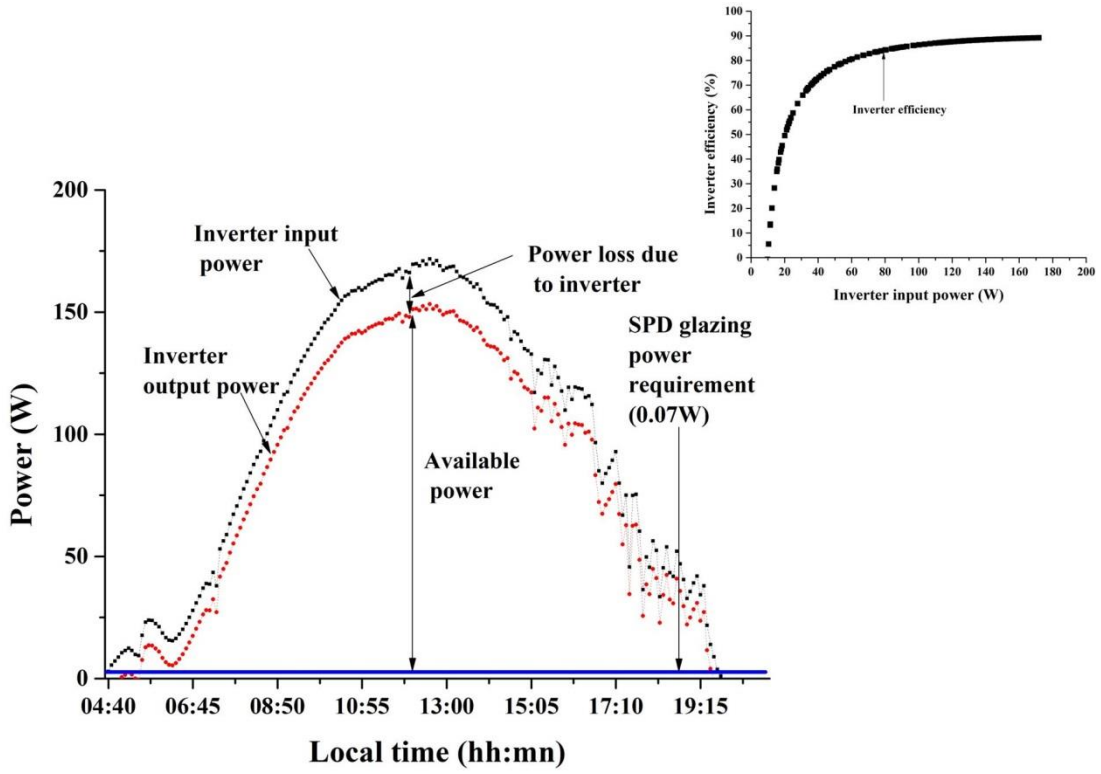

Figure 6-9: Diurnal variation of inverter input power, output power for clear sunny day while SPD glazing power requirement was constant during sunshine hour for low sizing ratio PV-inverter.

6.4. Advantages of PV powered SPD glazing

This 0.0588 m^2 SPD requires 0.07 W power to maintain transparent state. If the glazing remain transparent for 24 hour and 365 days total electricity requirement would be 0.6132 kWh. For a 1 m^2 of SPD this equates to 10.42 kWh

$$\left[\frac{(0.07\times 24\times 365)}{0.0588}=10.42\right]$$

This consumption is the maximum possible for a 1 m^2 SPD glazing. The actual requirement will be less but will also depend on the orientation of glazing. This low power requirement makes this glazing more advantageous for PV powered.

In Ireland 1 kWh of electricity generation, produces 469 g CO_2 (SEAI). For 10.42 kWh electricity generation produces 4.8 kg CO_2 /year, which could be, eliminated by using this PV - SPD device.

6.5. Summary

SPD glazing is a promising electrically actuated switchable solar heat gain control glazing. The dynamic behaviour of the 0.0588 m^2 SPD glazing powered by the 0.3432 m^2 vertical PV was investigated. As SPD glazing works with an AC supply, direct coupling of PV and SPD is not possible. DC generated from PV needs to be converted to AC using an inverter before supplying the SPD. Thus, this investigation was performed using a side-by-side rather than a monolithic tandem structure. The SPD device offered a transparency change from 5% to 55% in the presence of 1.19 W/m^2 power density. To maintain its transparent state, it required continuous power.

Commercially available higher rating inverter influences to use higher rating PV which may not be necessary for the SPD glazing. This 0.058 m^2 SPD requires very less power 0.07 W, which could be powered by 1 W PV. However, 1.1 W rating inverter is not available commercially. For small-scale self-AC powered switchable SPD glazing requires low rated power electronics equipment.

Reduction of power losses could be possible using a 1.12 sizing ratio between PV and inverter rather than the 4.8 used here. In this case, available extra power could be stored in battery. Reduced PV device power output was identified when the PV cell temperature was high. An advantage of PV powered SPD glazing is the inverse relation between PV power generation and SPD glazing power requirement. For a sunny day, SPD glazing requires no power to control the solar heat gain and keep the

room temperature at a normal level. Thus, the power generation from the PV for sunny days can be stored fully to use at night or an intermittent cloudy days. Low solar radiations on overcast and intermittent days are unable to power the SPD glazing continuously using 40 W_p PV. Thus battery storage is recommended for PV powered SPD glazing.

Chapter 6. Thermal performance analysis of SPD switchable glazing

7.1. Introduction

The goal of this chapter is to investigate the thermal analysis of suspended particle device switchable type glazing.

Specific objectives are

- Analysing thermal behaviour of SPD glazing using test cell ;
- Calculation of overall heat transfer coefficient (*U*-value) and solar heat gain coefficient (SHGC) of the SPD glazing.

Thermal analysis of SPD glazing had been carried out using a test cell. This experiment process has two fold.

- First one is the test cell without heat exchanger to monitor the behaviour of SPD glazing. It involves determining the solar energy transmitted through the glazing, SHGC and *U*-value of the SPD glazing and comparison with same area of double-glazing.
- In the second phase, heat exchanger has been equipped with the test cell to investigate the cooling load reduction from SPD transparent to opaque state. *U*-value of the SPD glazing and double-glazing while water circulating inside the test cell was also investigated.

7.2. Calculation of thermal properties

Solar heat gain and thermal transmission are the two primary modes of heat flow through windows (Chen et.al. 2012). Solar heat gain in a building occurs due to long wave (700 nm-1 mm) solar radiation passing through window glazing and warming

the buildings' interior. Thermal transmission through a window is caused by a temperature difference between the external and internal surfaces resulting in thermal conduction and internal heating or cooling. Building controls attempt to maintain a constant internal temperature, while the external temperature of glazing is affected by a variety of factors including the external ambient temperature and solar gains on the glazing exterior. Two coefficients measure the glazing system thermal behaviour:

- the *U*-value ($Wm^{-2}K^{-1}$) is the overall heat transfer coefficient which measures how well the element conducts heat; and
- the SHGC measures the fraction of solar radiation which is admitted through the glazing and heats the interior.

7.2.1. Overall heat transfer coefficient without heat removal from test cell

To calculate the Overall heat transfer coefficient (*U*-value) following assumptions were made that

- measurements were made while the vacuum glazing is in thermal steady state;
- one-dimensional heat transfer from the interior to the exterior through the glazing was considered to be dominant;
- ground reflected solar radiation was assumed to be zero;
- the test cell was made of homogeneous highly insulating materials;
- there were no ventilation/infiltration losses from the test cell.

The heat transfer through glazing Q_g can then be written as equation 7-1 (Fang et.al. 2006).

$$Q_g = Q_{in} - Q_{tc} - Q_{loss,wall} \tag{7-1}$$

Where:

$$Q_{in} = I_v(t) A_w \tau_v(\theta) \alpha \tag{7-2}$$

Where I(t) is the incident solar radiation, A_w is the area of glazing, absorptivity α. Transmission of glazing τ_v varies with the incident angle and can be written from equation 4-8 of Chapter 4

The total heat inside the test cell is given by

$$Q_{tc} = M_{tc} C_{tc} \frac{dT_{in,tc}}{dt} \tag{7-3}$$

Where $M_{tc} = \rho_{air} v_{air}$

The heat losses through the test cell wall can be represented by equation 7-4

$$Q_{loss} = (UA)_{wall} (T_{in,tc} - T_{out,tc}) \tag{7-4}$$

Where the overall heat transfer coefficients is given by equation 7-5

$$(UA)_{wall} = \left[\frac{1}{h_0} + \frac{L_{pl}}{k_{pl}} + \frac{L_{wd}}{k_{wd}} + \frac{1}{h_i} \right]^{-1} \times A_{wall} \tag{7-5}$$

The convective heat transfer coefficient (Duffie and Beckman 2013) between ambient air and outer glazing surface is calculated with the local wind speed V_{wind}

$$h_i = 2.0 + 3\mathrm{V}_{\mathrm{wind}} \tag{7-6}$$

$$h_0 = 5.7 + 8.8\mathrm{V}_{\mathrm{wind}} \tag{7-7}$$

The overall heat transfer coefficient of the glazing U is given by,

$$U = \frac{Q_g}{A_w (T_{in,tc} - T_{out,tc})} \tag{7-8}$$

Where

$$Q_g = I(t)A\tau(\theta)\alpha - M_{tc}C_{tc}\frac{dT_{in,tc}}{dt} - (UA)_{wall}(T_{in.tc} - T_{out,tc}) \quad (7\text{-}9)$$

Table 7-1 represents the physical parameters that were used for the calculation of *U*-value.

7.2.2. Overall heat transfer coefficient after heat removal from test cell

Heat transfer through glazing Q_g can then be written as equation 7-10 (Smyth et.al. 2005).

$$Q_g = Q_{in} - Q_{heatexchanger} - Q_{loss,wall} \quad (7\text{-}10)$$

Q_{in} same as equation 7-2

U_g is the *U*-value of glazing which vary due to diurnal variation on solar radiation, test cell temperature and ambient temperature

$$Q_{hexchanger} = \dot{m}_g\, c_g (T_{wo} - T_{wi}) \quad (7\text{-}11)$$

$$m_g = \rho_g \nu_g$$

$$\nu_g = \pi r_h^2 l_h$$

$$\Delta T = (T_{outw} - T_{inw})$$

Losses Q_{loss} through the test cell wall can be represents by equation 7-4

Overall heat transfer coefficient for glazing can be

$$U_g = \frac{Q_{in} - Q_{hexchanger} - Q_{loss}}{A_w(T_{in,tc} - T_{out,tc})} \quad (7\text{-}12)$$

Table 7-1: Physical parameters of glazing and others parameters used during the calculation

Table 7-1: List of physical parameter used during calculation.

			Value
Parameter	Fixed	Aperture area of glazing (A_{vacuum})	0.0588 m^2
		Interior wall surface (A_{wall})	0.44m^2
		Internal volume of test cell (v_{air})	0.174 m^3
		Thickness of wood (L_{wd})	0.02 m
		Mass of air inside test cell ($M_{tc} = v_{air} \times \rho_{air}$)	0.2134 kg
		Thickness of Polystyrene (L_{pl})	0.15 m
		Length of heat exchanger pipe (l_h)	0.45 m
		Radius of heat exchanger pipe (r_h)	0.005 m
	Physical	Density of air (ρ_{air})	1.2250 kg/m^3
		Density of water (ρ_{water})	997.8 (kg/m^3)
		Heat capacity of air (C_{air})	1.006 (kJ/kgK)
		Heat capacity of water (C_g)	4.18 (kJ/kgK)
		Thermal conductivity of polystyrene (k_{pl})	0.022 W/mK
		Thermal conductivity of wood (k_{wd})	0.09 W/mK
	Variable	Temperature inside test cell ($T_{in,tc}$)	Measured by T type thermocouple (K)
		Temperature outside test cell ($T_{out,tc}$)	Measured by T type thermocouple (K)
		Vertical surface incident solar radiation ($I_v(t)$)	Measured by pyranometer (W/m^2)

7.2.3. Solar energy transmitted through glazing

Solar energy transmitted through SPD glazing can be written as equation 7-13 (Waide and Norton 2003)

$$SE_{SPD} = \left(I_{h,b} + I_{h,d}A_i\right)\tau_{dir}R_b + I_{h,d}\left(1+A_i\right)\tau_{dif,h}\frac{\left(1+\cos\beta\right)}{2} + I_{h,g}\rho_g\tau_g\frac{\left(1-\cos\beta\right)}{2} \quad (7\text{-}13)$$

Where anisotropic index $A_i = \frac{I_{h,b}}{I_{extra}}$

$$I_{extra} = I_{sc}\left(1+0.033\cos\frac{360n}{365}\right)\left(\cos\phi\cos\delta\cos\omega+\sin\phi\sin\delta\right) \quad (7\text{-}14)$$

I_{sc} is the solar constant , n is the day of year , ϕ latitude angle, δ declination angle ω hour angle

7.2.4. Solar heat gain coefficient (SHGC)

Solar heat gain coefficients was calculated from equation 7-15

$$SHGC = \frac{SE_{SPD}}{I_v} \quad (7\text{-}15)$$

7.3. Experimental procedure

The experiment was performed from 1st February 2014 to 1st July 2014 on the roof of Kevin Street building DIT, Ireland (53.34 ^{0}N, 6.25 ^{0}W). Details of experiment set up and data logging and monitor process are mentioned in section 3.3.1 of Chapter 3. A photographic view of experimental set up is shown in Figure 7-1.

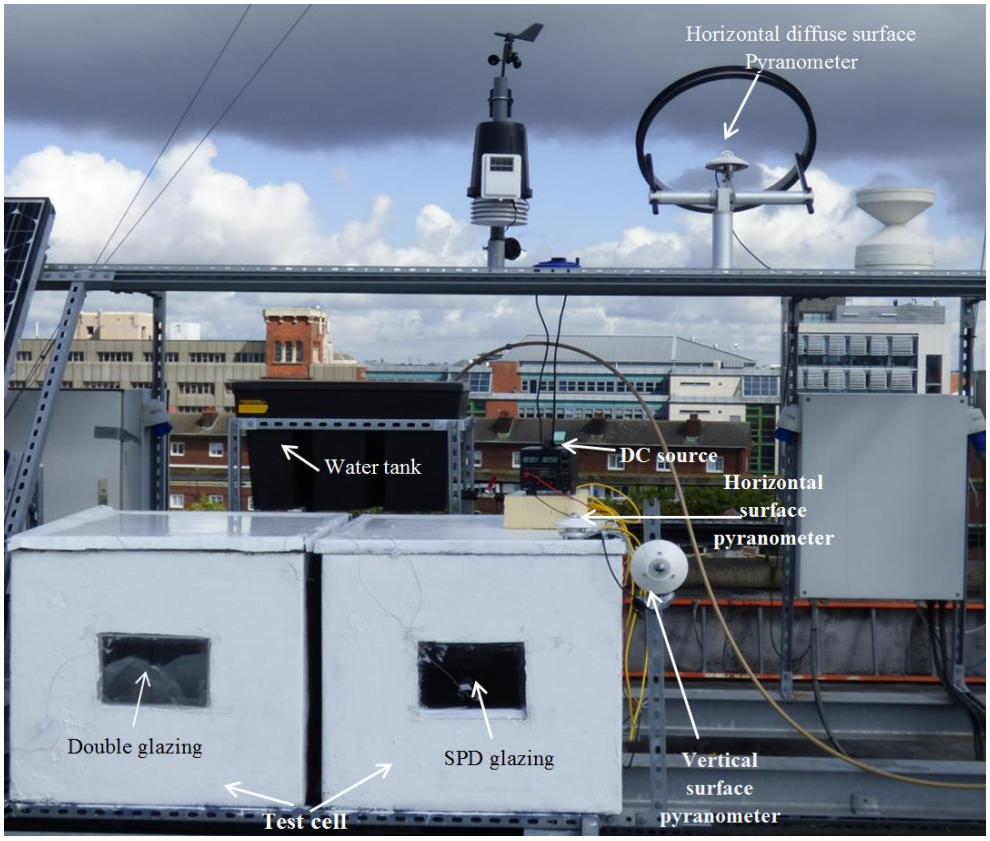

Figure 7-1: Photographic view of experimental set up.

7.4. Results of SPD glazing without heat removal from test cell

7.4.1. Experimental results

Figure 7-2 represents the hourly clearness index and diurnal variation of double-glazing and SPD test cell temperature and ambient temperature. Clearness index has very low values during the hours close to sunrise and sunset. For a clear sunny day due to less cloud cover, the clearness index was nearly 0.65 during mid-day period. During intermittent and overcast day clearness, indexes were below 0.45. On clear sunny day, direct solar radiation through the double and SPD glazing gave maximum test cell temperatures of nearly 45 ^{0}C and 40 ^{0}C respectively. The main purpose of an SPD glazing was to control the heat gain and incoming light by changing its transparency; it was kept opaque only on sunny days. It remained “transparent” state

during overcast and intermittent overcast condition since solar heat gain control was not required in the building in those weather conditions.

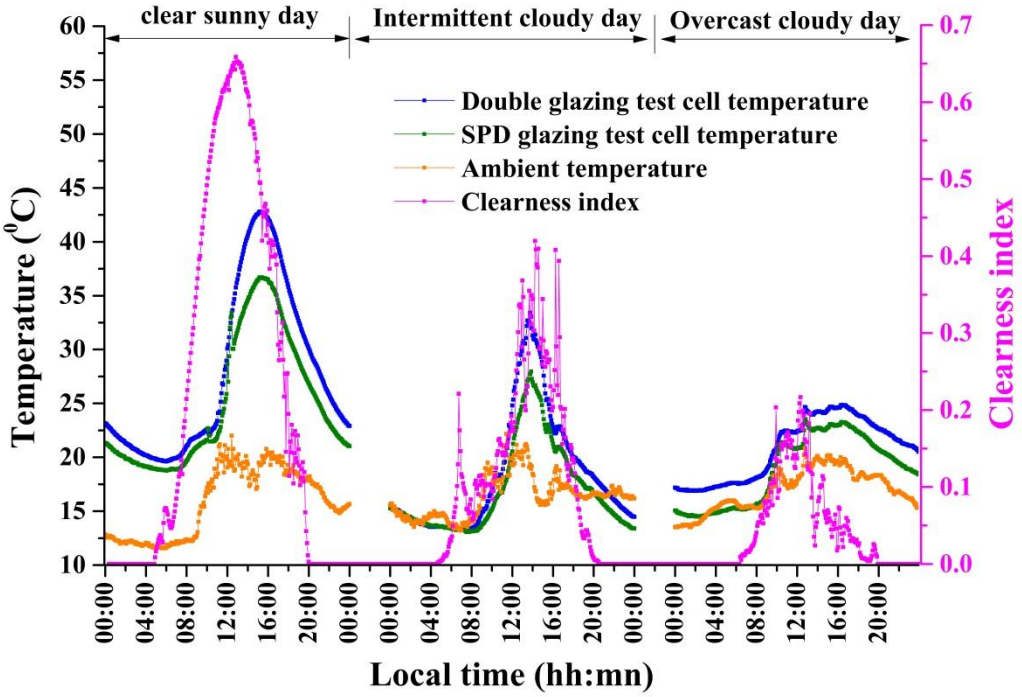

Figure 7-2: Diurnal variation of hourly clearness index, test cell temperature and ambient temperature.

The internal temperatures of SPD glazing test cell for both the "transparent" and "opaque" conditions are compared with double-glazing internal test cell temperatures in Figure 7-3. Under clear sunny day conditions, the SPD glazing "opaque" state limits the rise of test cell inside temperature better than the double-glazing by blocking most of the solar radiation. However, the temperature differences inside test cell temperature for SPD glazing "transparent" and "opaque" conditions are observed close (5 ^{0}C difference) to each other which implies that SPD glazing cannot limit penetration of the full spectrum of solar radiation.

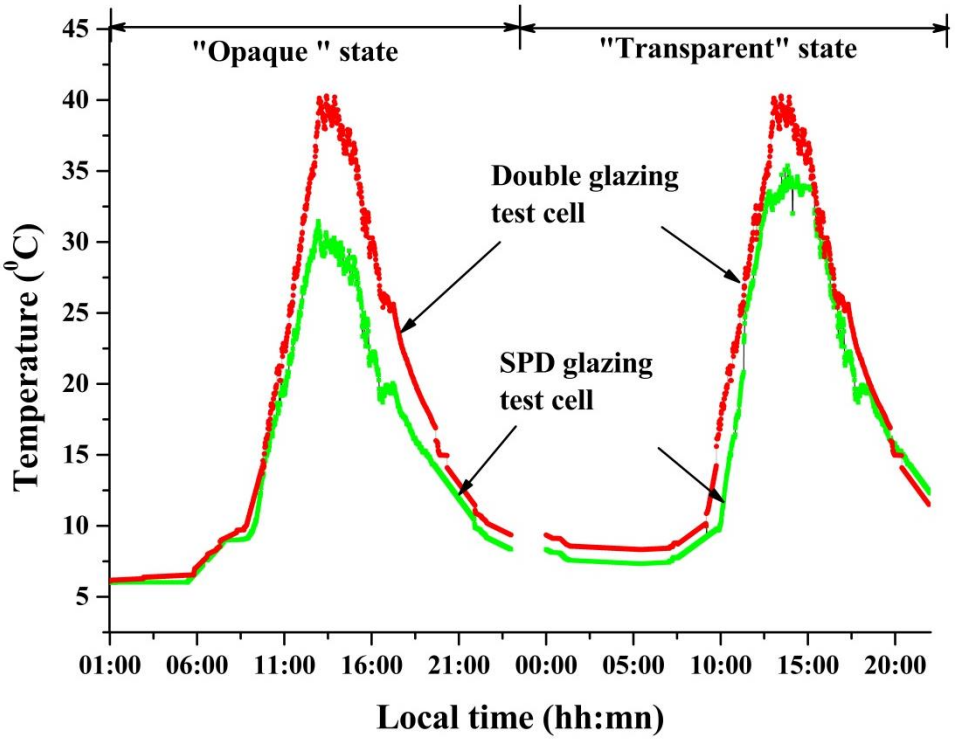

Figure 7-3: SPD glazing test cell and double-glazing test cell temperature during SPD "transparent" and "opaque" states.

Figure 7-4 shows the temperature differences between SPD glazing inside and outside of the surface, SPD test cell inside temperature and outside ambient for clear sunny day condition. SPD glazing inside and outside temperature for "transparent" and "opaque" states were nearly same. In both, the "transparent" and "opaque" states, the total number of particles inside the glazing remains same; the only difference is their alignment. In "opaque" condition the random alignment of particles, blocks the light passing through it. The heat absorbing capacities of SPD particle in both "transparent" and "opaque" conditions were the same. Thus, temperature rises for both "opaque" and "transparent" conditions were identical.

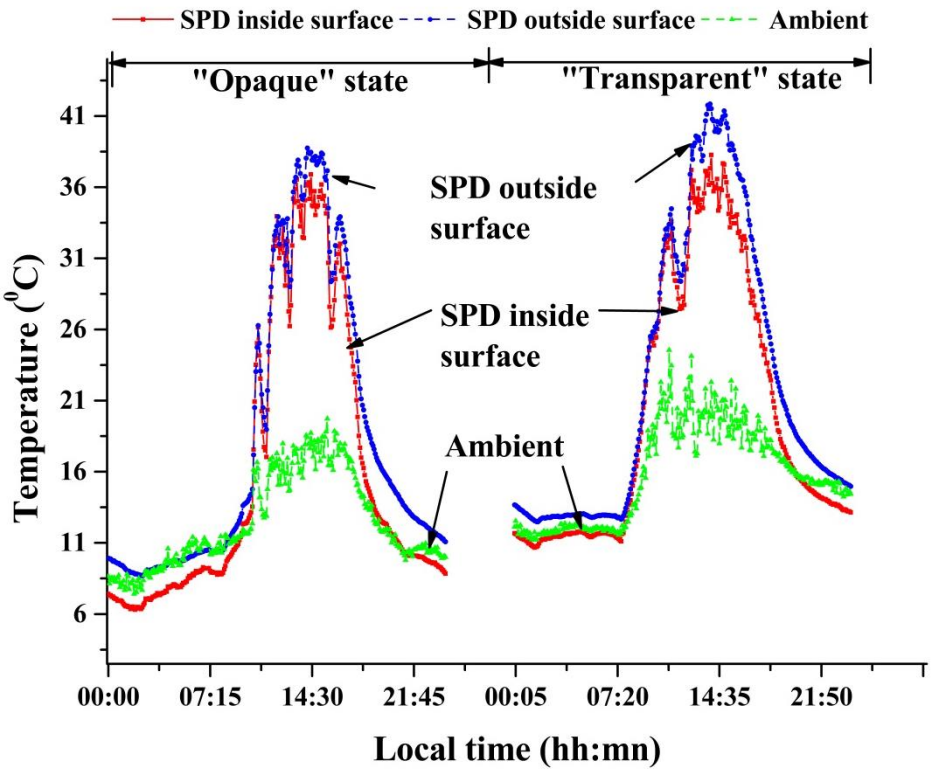

Figure 7-4: SPD glazing inside surface temperature, SPD glazing outside surface temperature, SPD test cell inside temperature and ambient temperature.

Figure 7-5 indicates the test cell internal temperature of SPD glazing transparent and opaque condition and double-glazing, which was recorded for typical Dublin sunny day. Maximum temperature for these three cases was 39 ^{0}C, 37 ^{0}C, and 44 ^{0}C respectively. Ambient temperature was maximum 22 ^{0}C with temperature swing of 11 ^{0}C. This rise of indoor temperature was higher than the standard 20 ^{0}C comfortable room temperature. Maximum temperature rise was 11% and 15% less for SPD transparent and opaque state compared to double-glazing.

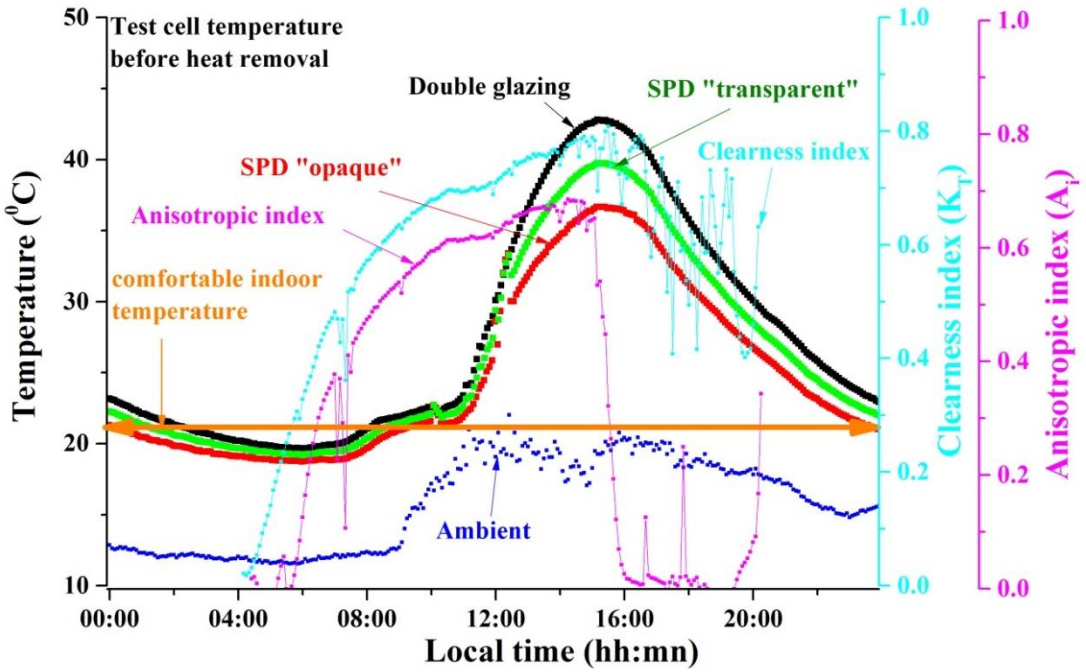

Figure 7-5: Test cell internal temperature of double-glazing, SPD "transparent" and "opaque" condition before using the water flow for typical clear sunny day.

7.4.2. Overall heat transfer coefficient of SPD glazing and double glazing

In this work, transient behaviour of glazing *U*-value was evaluated during the sunshine period. The overall heat transfer coefficient of SPD glazing was calculated with every 5-minute intervals of a sunny day shown in the Figure 7-6. Diurnal variation of *U*-value was found with solar radiation. At mid-day period high losses was found. Total average *U*-value for this condition was nearly 5.9 W/m^2K. In this case, SPD glazing behaves like single glazing. *U*-value of double-glazing is illustrated in Figure 7-7. Total average *U*-value of double-glazing was found 2.98 W/m^2K.

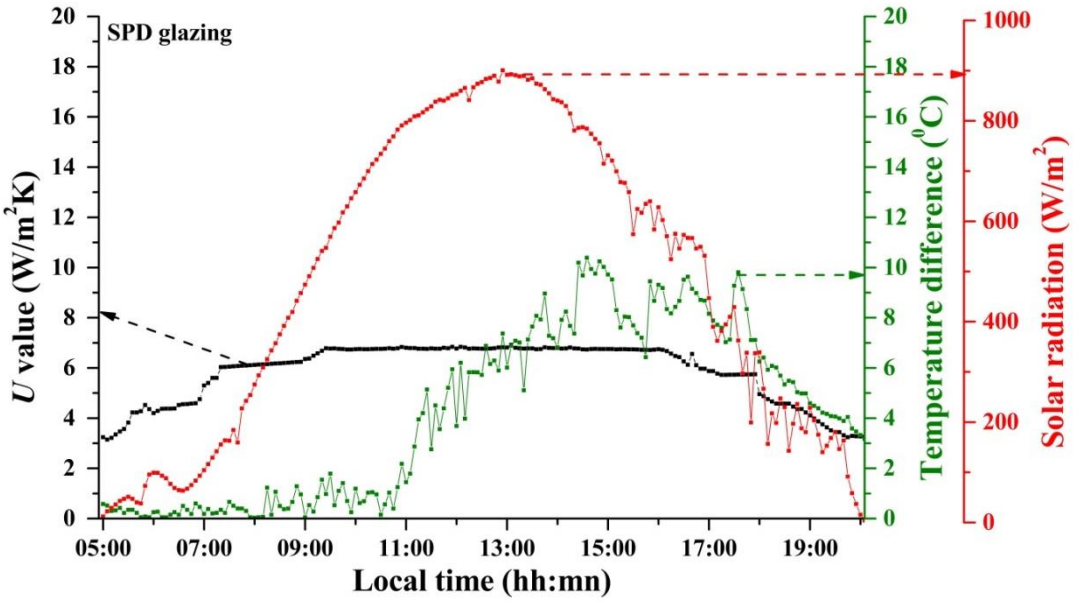

Figure 7-6: Diurnal variation of the overall heat transfer coefficient of SPD glazing, solar radiation and temperature difference between test cell inside and outside ambient temperature.

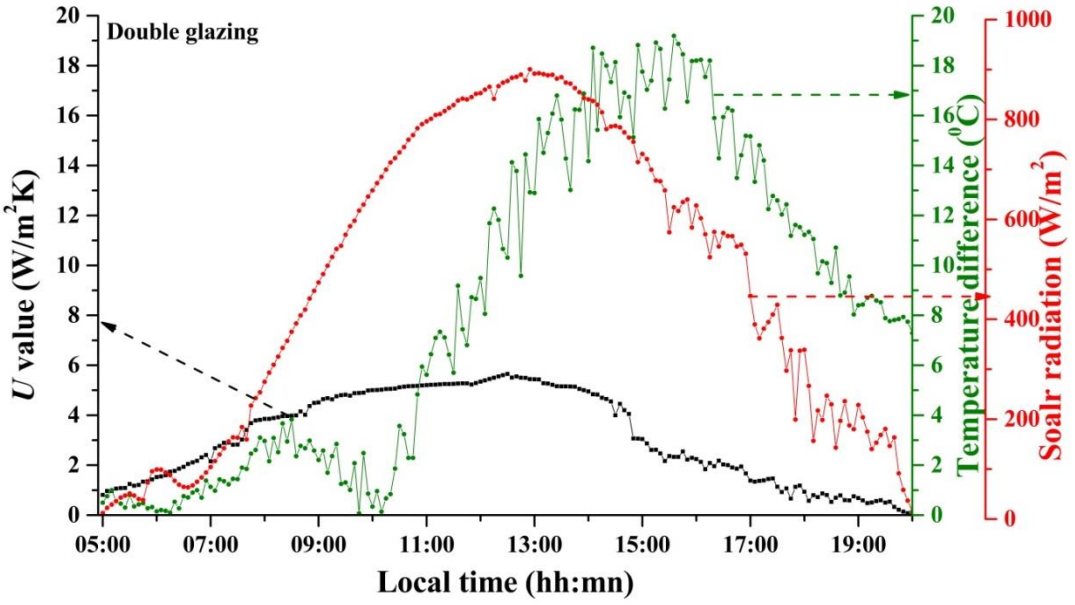

Figure 7-7: Diurnal variation of the overall heat transfer coefficient of double-glazing, solar radiation and temperature difference between test cell inside and outside ambient temperature.

7.4.3. Solar energy transmitted through the glazing

Figure 7-8, 7-9, 7-10 illustrate the angular transmittance and solar energy transmitted through the double-glazing, SPD glazing transparent and opaque state using equation

7-13. Maximum 520 W/m^2 410 W/m^2 and 50 W/m^2 energy transmitted through this double-glazing, SPD glazing transparent and opaque state respectively at 12:00 hh. Maximum transmittance for double, SPD transparent and SPD opaque were 0.75, 0.52, 0.03 at 41^0-incidence angle.

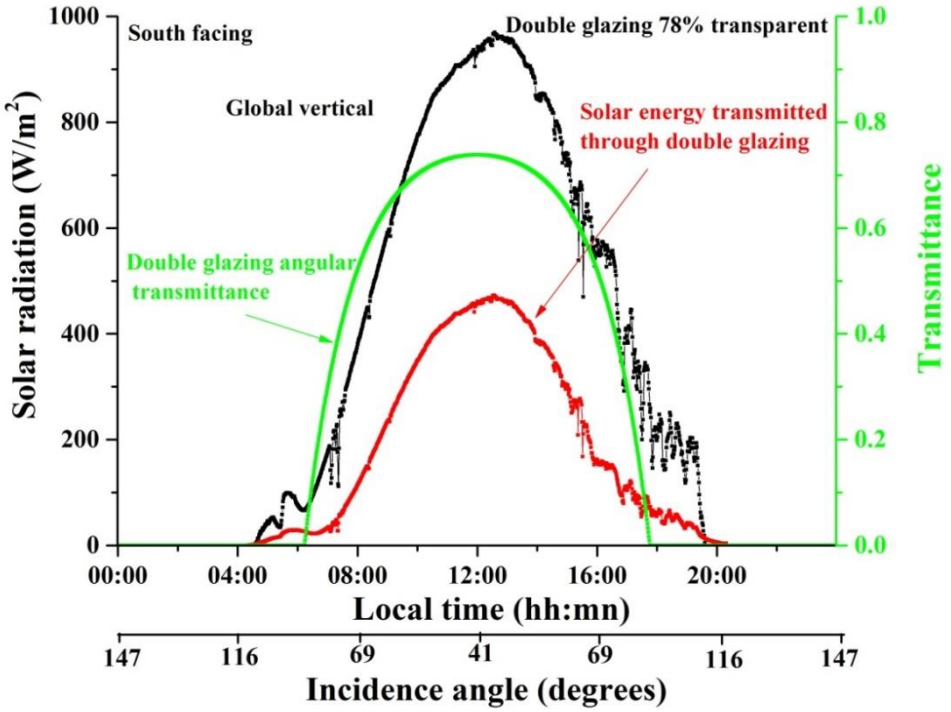

Figure 7-8: Solar energy transmitted through a south facing double-glazing (78% transparent) in a typical sunny day in Dublin.

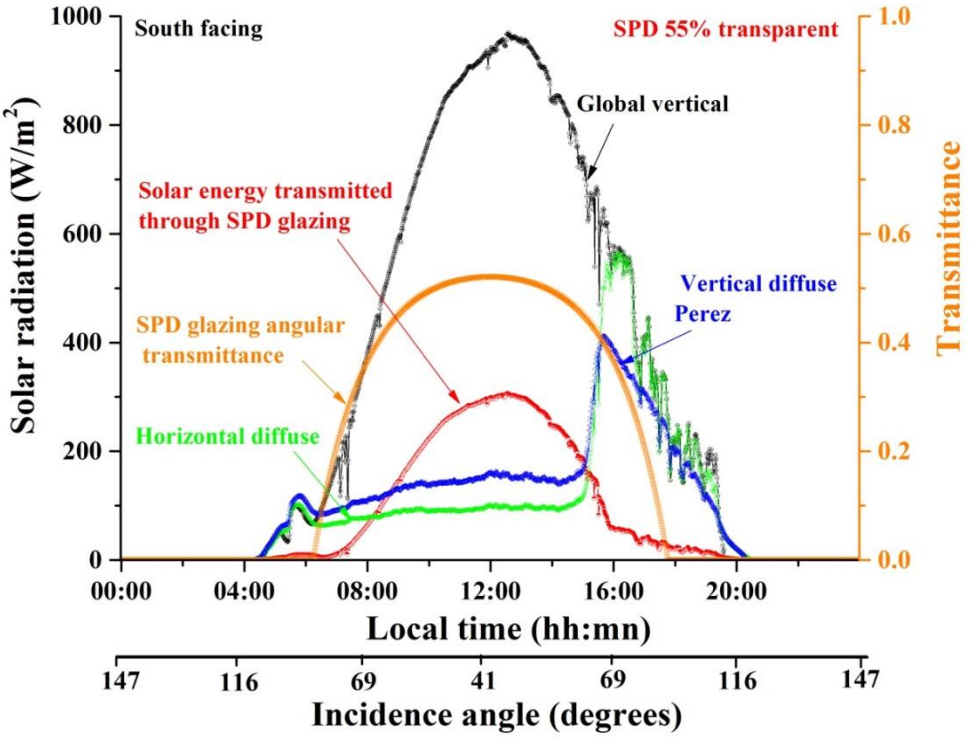

Figure 7-9: Solar energy transmitted through a south facing SPD-glazing (55% transparent) in a typical sunny day in Dublin.

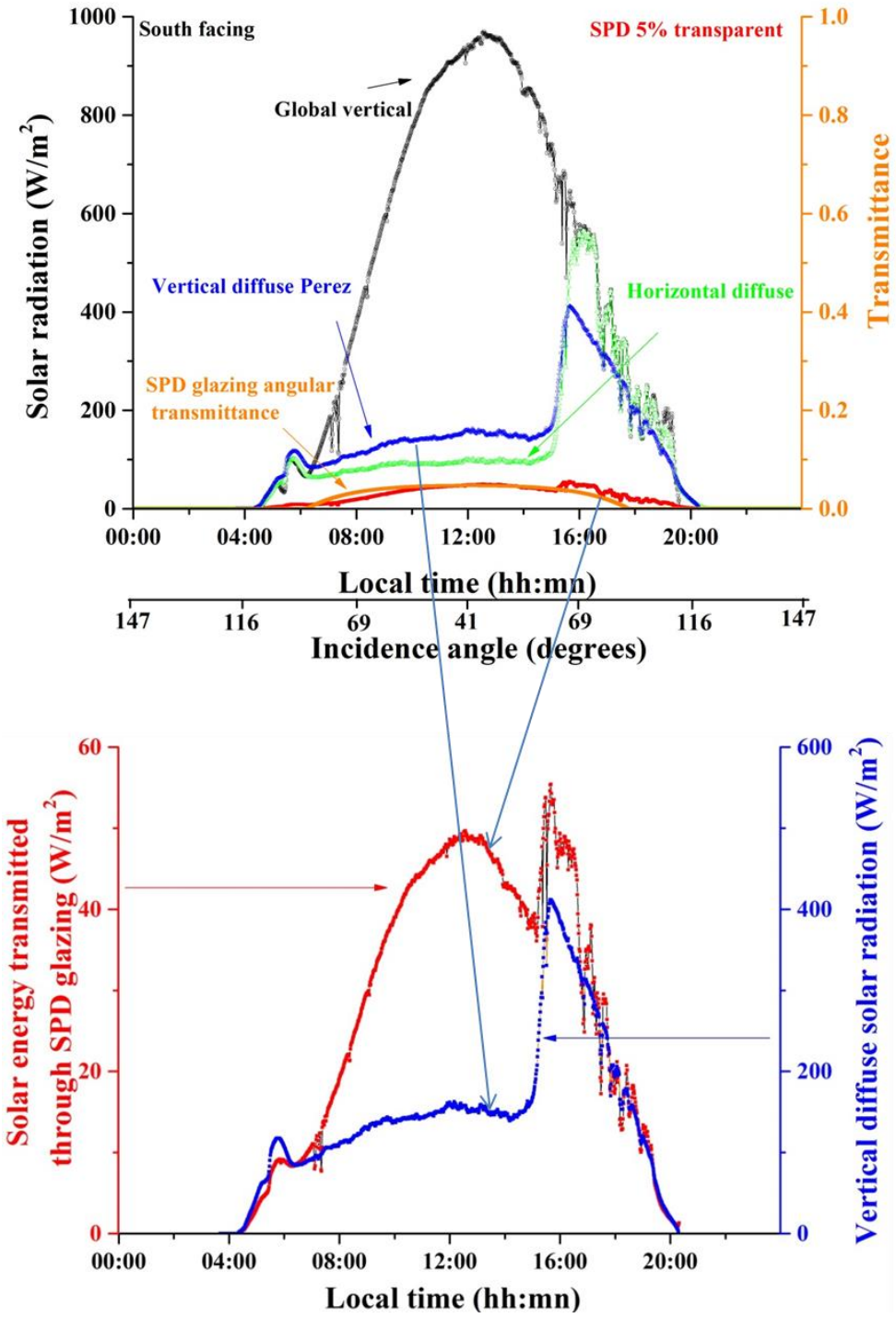

Figure 7-10: Solar energy transmitted through SPD glazing (5% transparent).

7.4.4. Solar heat gain coefficient (SHGC)

SHGC for SPD glazing transparent, opaque and double glazing was calculated using equation 7-15. Maximum SHGC 0.37 was achieved for SPD glazing transparent state at midday period. At evening time, lowest value 0.1 was obtained. SPD opaque state SHGC varied from 0.05 to 0.045. Variation of SHGC was found less at opaque state compared to SPD transparent due to low direct solar radiation transmission through the glazing. However due to transparency (55% to 5%) change, a large direct transmission reduction was possible.

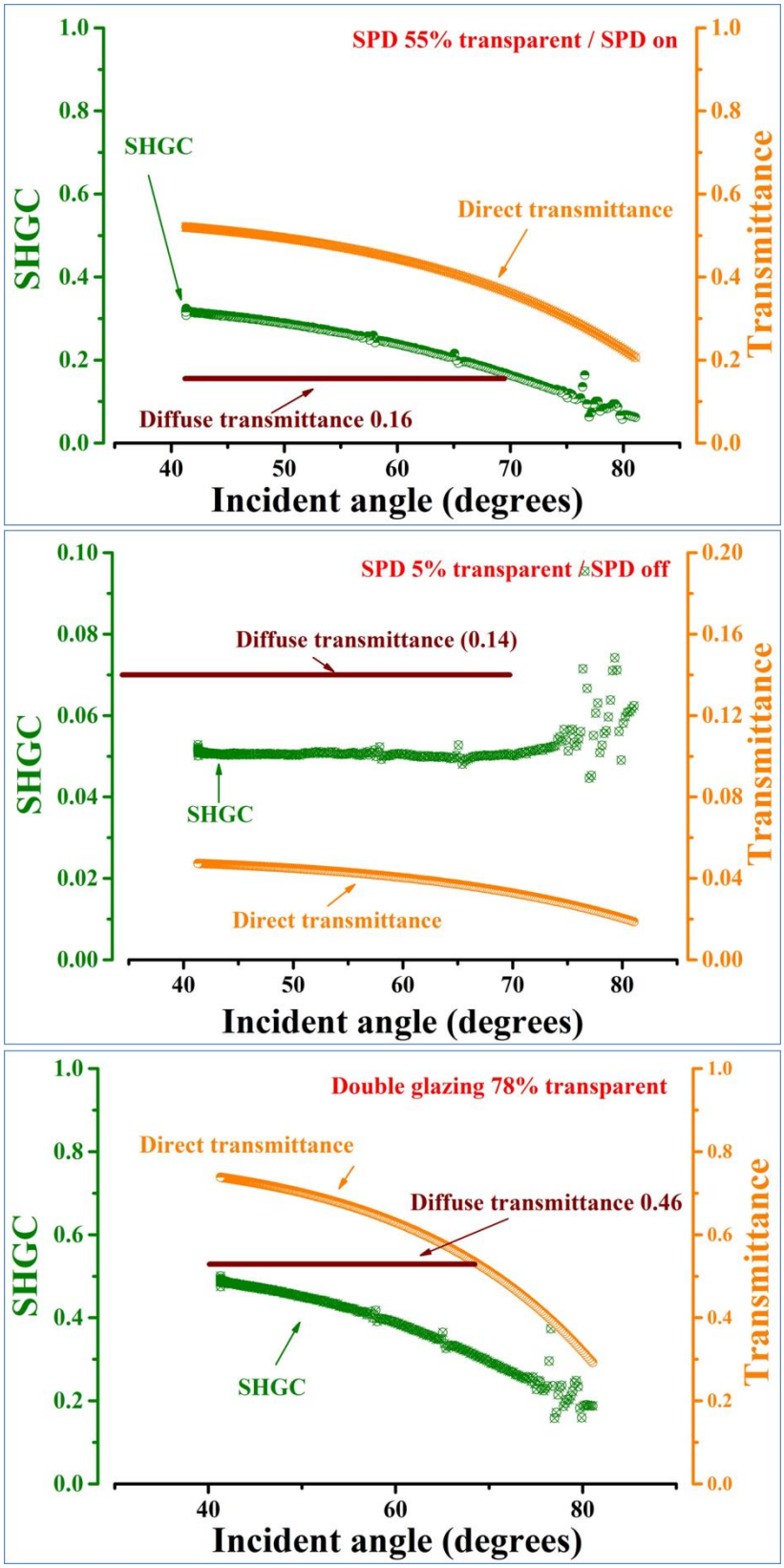

Figure 7-11: Change of SHGC and transmittance of double-glazing (78% transparent), SPD glazing 55% transparent and SPD glazing 5% transparent with incidence angle.

7.5. Results of SPD glazing after heat removal from test cell

7.5.1. Water temperature difference

Figure 7-12 illustrates the temperature difference of water in and out of the test cell for double-glazing, SPD "transparent" and "opaque" states. The mass flow rate was 0.0167 kg/s for all three cases. Temperature difference for double-glazing maximum was achieved at 3 ^{0}C while for SPD "transparent" was 2.4 ^{0}C and "opaque" was 0.8 ^{0}C.

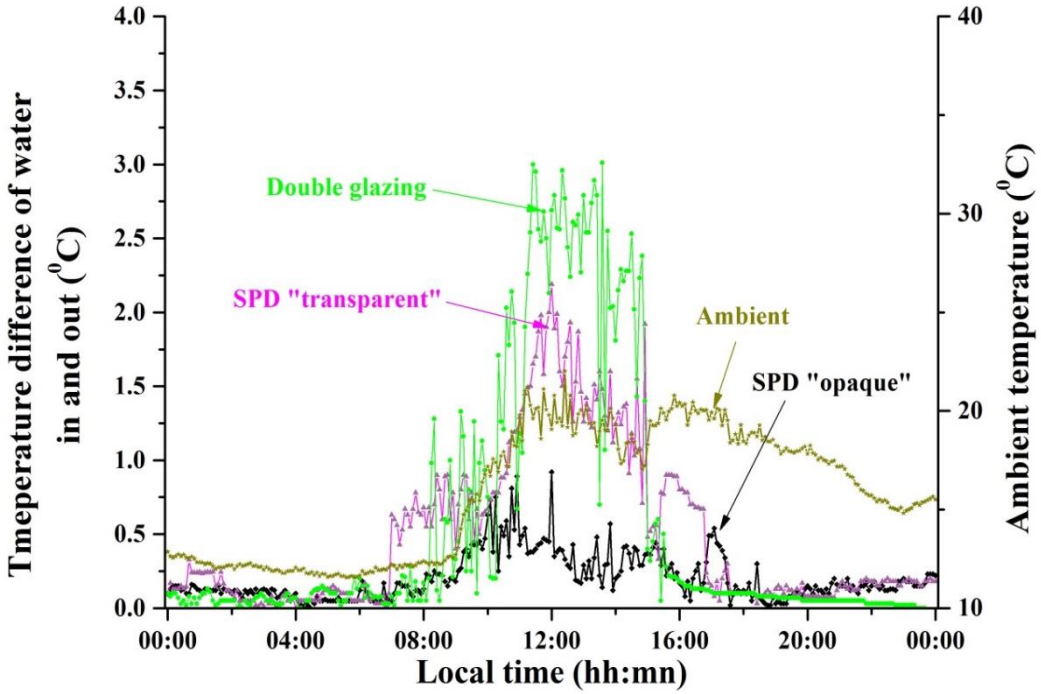

Figure 7-12: Temperature difference of water flowing inside the test cell for double-glazing, SPD transparent and SPD opaque at constant flow rate 0.0167 kg/s.

Total extracted heat from SPD "transparent", double and SPD "opaque" states were 10.38 kWh, 10.64 kWh and 4.02 kWh respectively for a sunny day for 0.016 kg/s mass flow rate as shown in Figure 7-13. It indicates that to keep the room in lower temperature during the summer SPD opaque state is more useful as 62% less heat had to be extracted from test cell and 2% while SPD transparent compared to double-glazing. Compare to SPD transparent state 61% less cooling load is required for SPD

opaque state. The daily energy saving requirement to ensure an indoor temperature close to comfort temperature (21–25 ^{0}C) is 6 kWh for SPD “opaque” and 0.26 kWh for SPD “transparent” compared to double glazing.

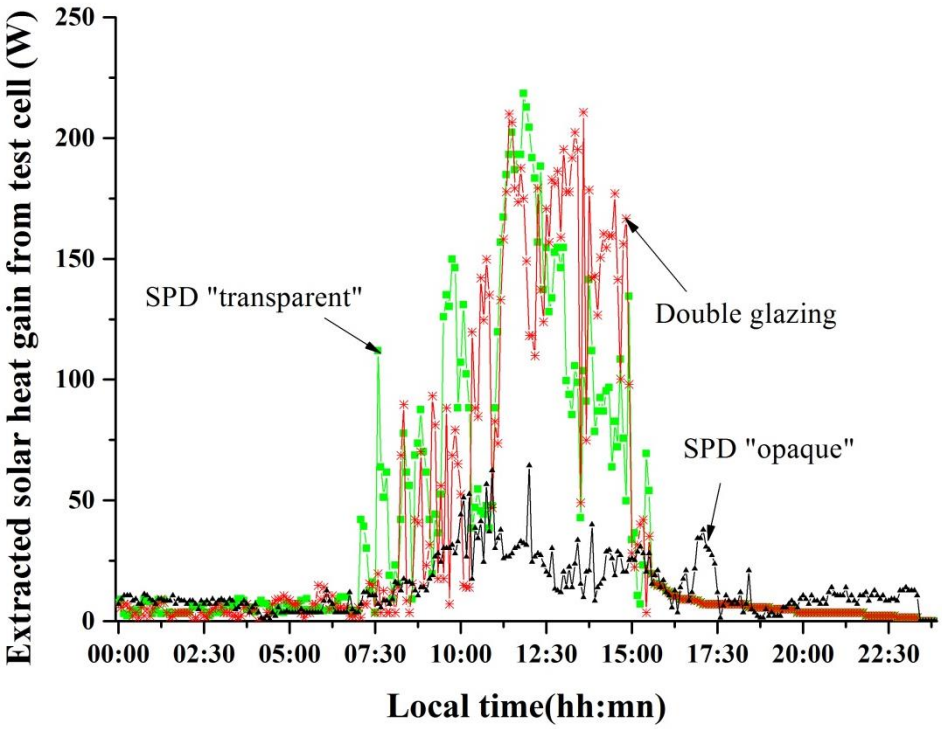

Figure 7-13: Heat extracted from SPD transparent, opaque and double-glazing test cell at constant 0.016 kg/s mass flow rate.

1 kWh electricity generation produce 0.821 kg CO_2 (for fossil fuel)

CO_2 saved for SPD “opaque” condition 6 × 0.821 kg = 4.926 kg for a 0.0588 m^2 glazing in a 1:8 ratio room. Yearly this saving will be 1797.99 kg.

CO_2 saved for SPD “transparent” condition 0.26 × 0.821 kg=0.2136 kg

Figure 7-14 illustrate the correlation between extracted solar heat gain from the test cell and solar radiation.

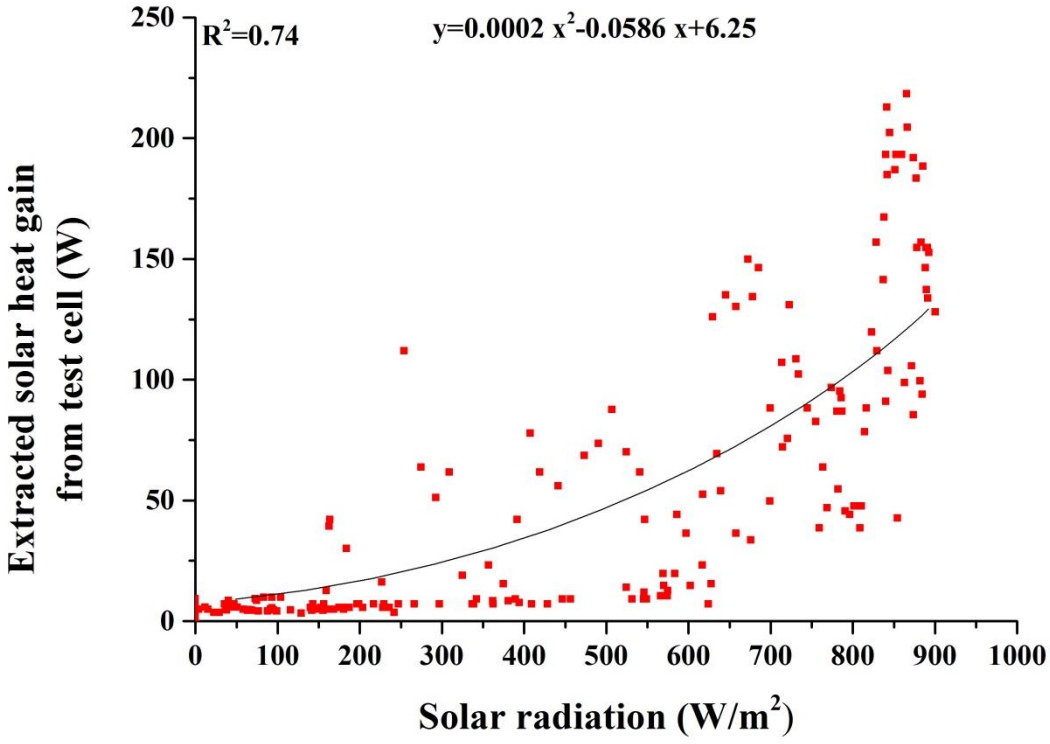

Figure 7-14: Correlation of extracted solar heat gain from test cell and solar radiation.

7.5.2. Test cell temperature

Figure 7-15 shows the test cell internal temperature after water flow through a heat exchanger inside it. Double-glazing maximum temperature reached 29 ^{0}C while SPD "transparent" and "opaque" were 25 ^{0}C and 22 ^{0}C. 32%, 34%, and 37% reduction of test cell internal temperature was achieved for double, SPD "transparent" and SPD "opaque" state respectively compare to no heat removal case (Figure 7-5).

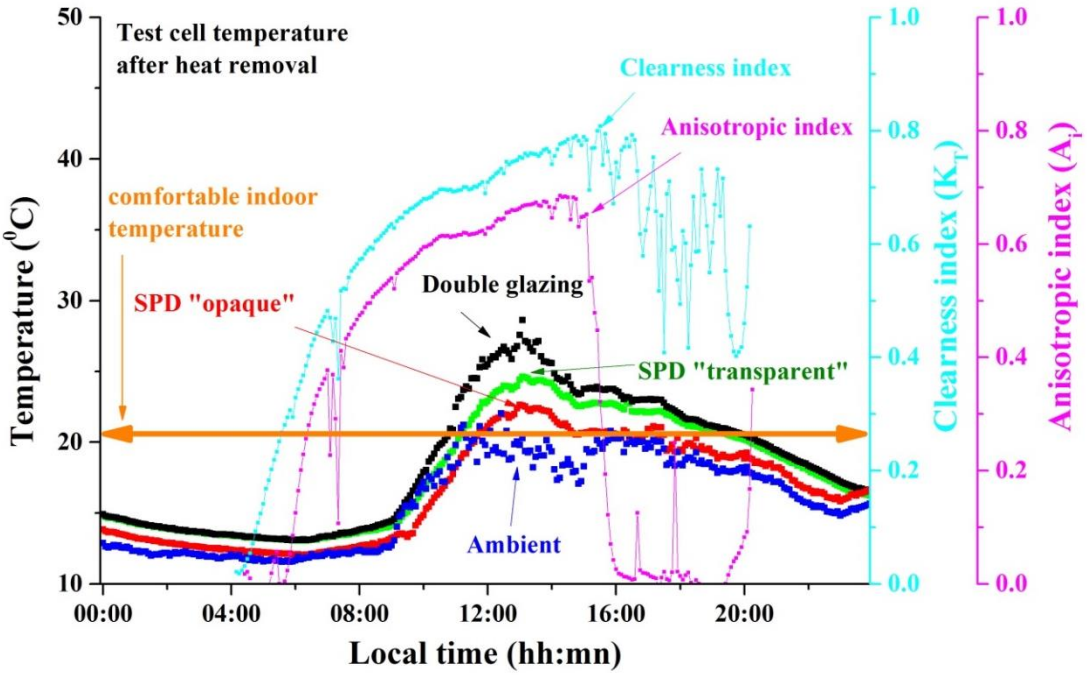

Figure 7-15: Test cell internal temperature of double-glazing, SPD transparent and opaque condition glazing at 0.016 kg/s water flow rate.

7.5.3. Overall heat transfer coefficient

Diurnal variation of *U*-value was calculated for double-glazing, SPD "opaque" and "transparent" states which were 2.3 W/m^2K, 5.0 W/m^2K and 5.32 W/m^2K respectively.

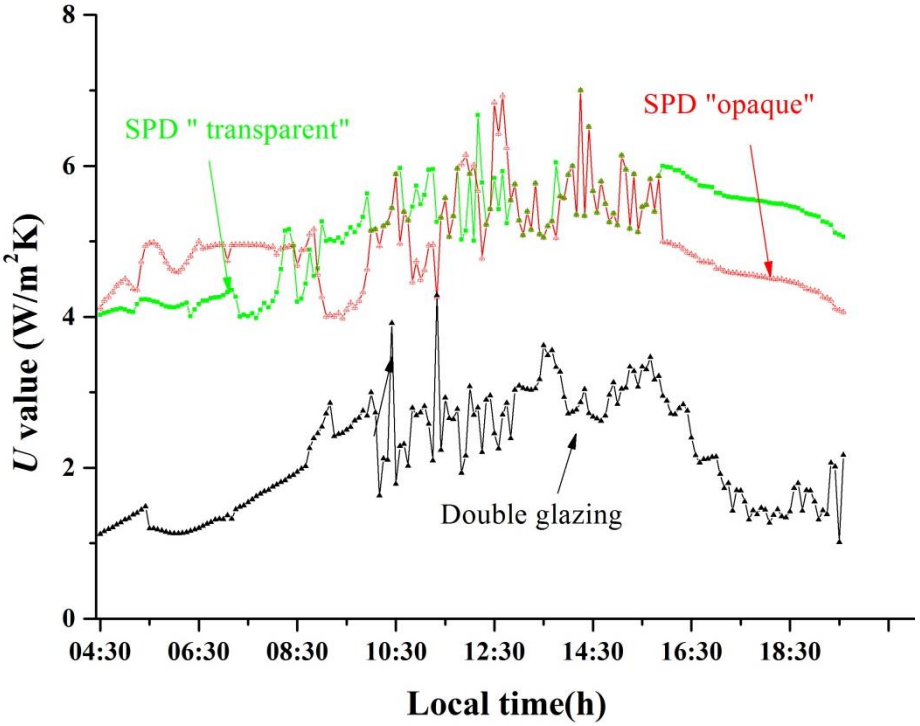

Figure 7-16: Diurnal variation of *U*-value for double-glazing, SPD "opaque" and "transparent" for 0.016 kg/s mass flow rate.

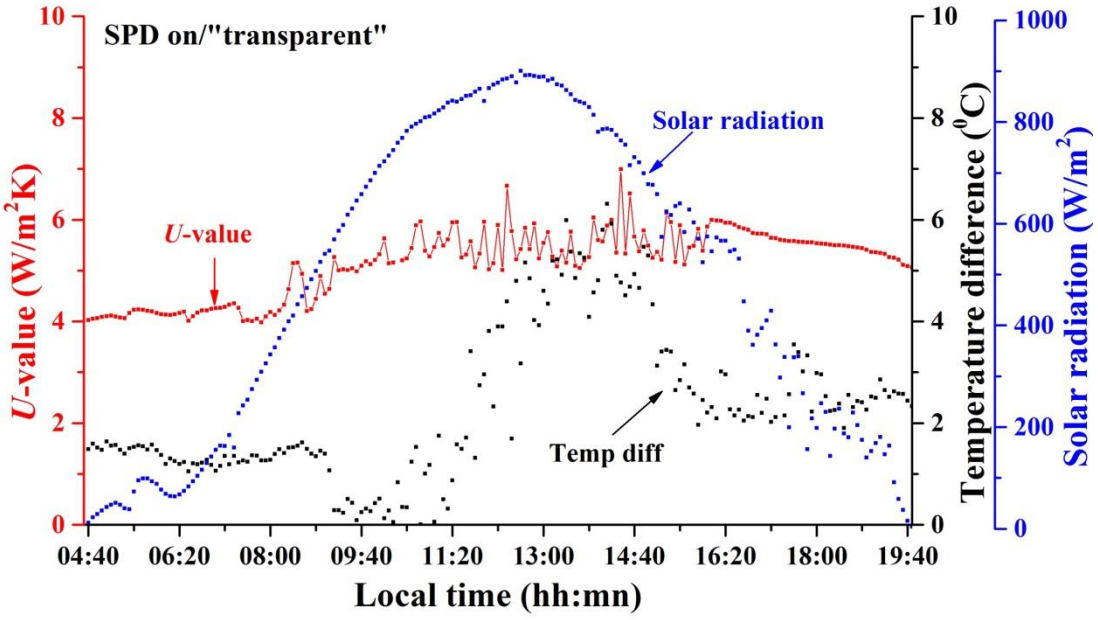

Figure 7-17: Overall heat transfer coefficient (*U*-value) of SPD glazing "transparent" state.

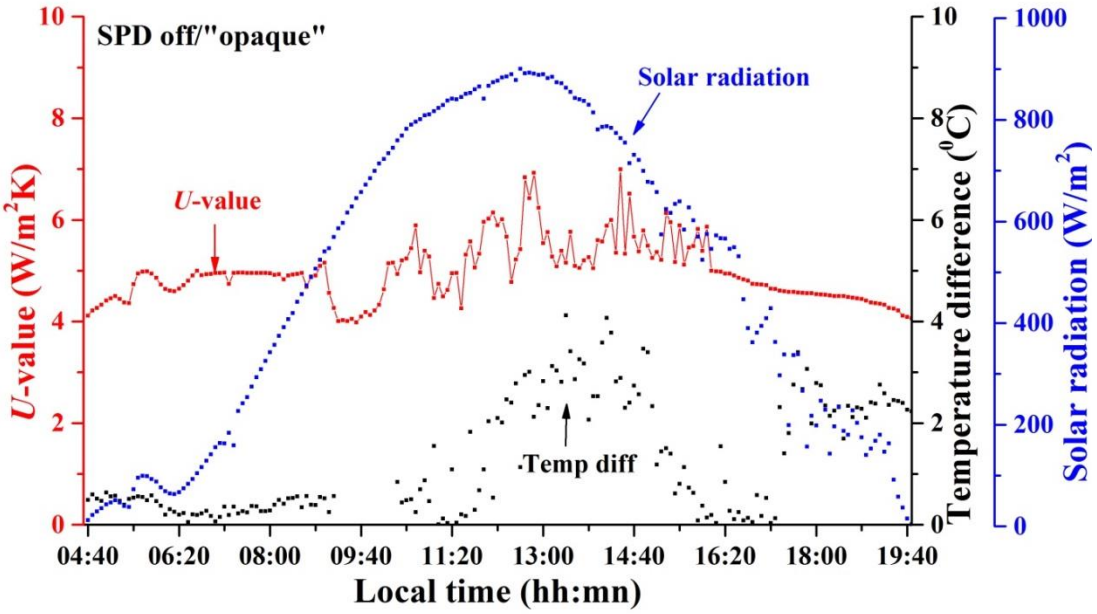

Figure 7-18: Overall heat transfer coefficient (*U*-value) of SPD glazing "opaque" state.

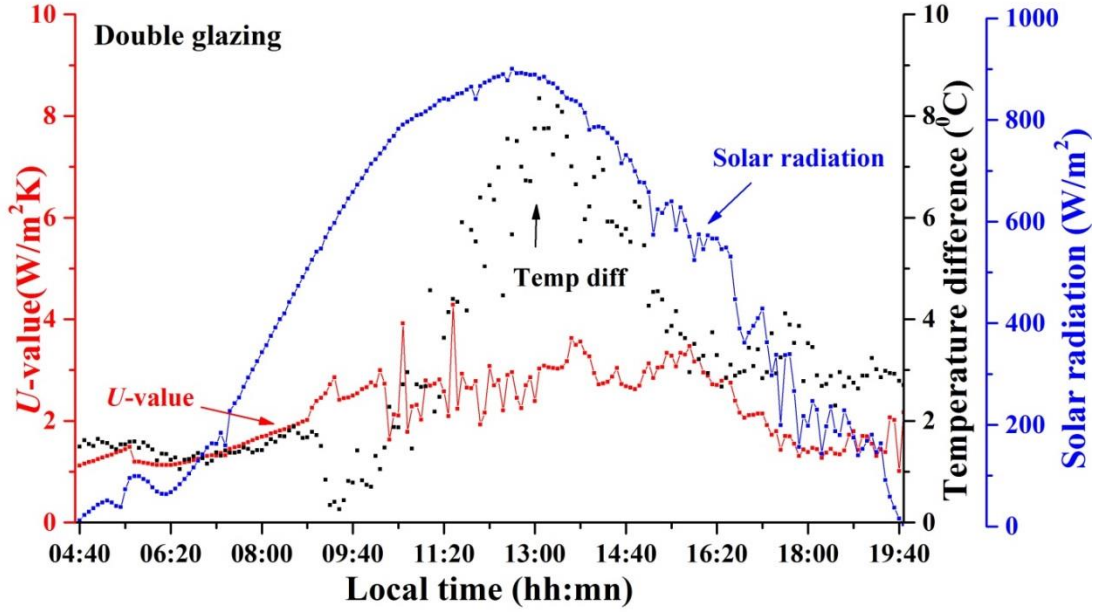

Figure 7-19: Overall heat transfer coefficient (*U*-value) of double-glazing.

7.5.4. Analytical result

Temperature inside the test cell for SPD opaque state was higher than 20 ^{0}C from 11:30 am to 18:30 pm.

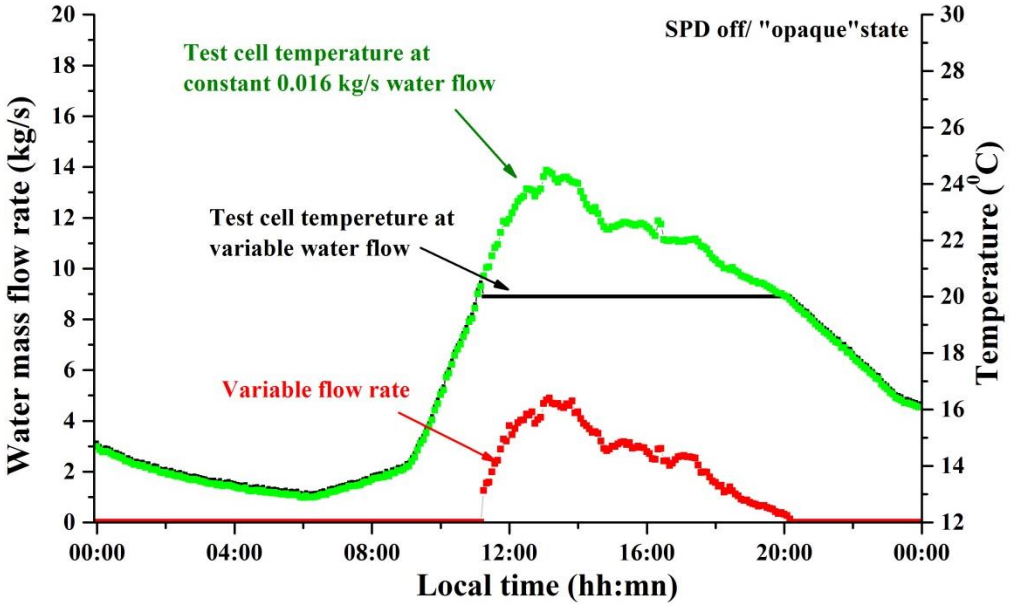

Figure 7-20: Variable flow to keep the test cell temperature 20 ^{0}C for SPD opaque state.

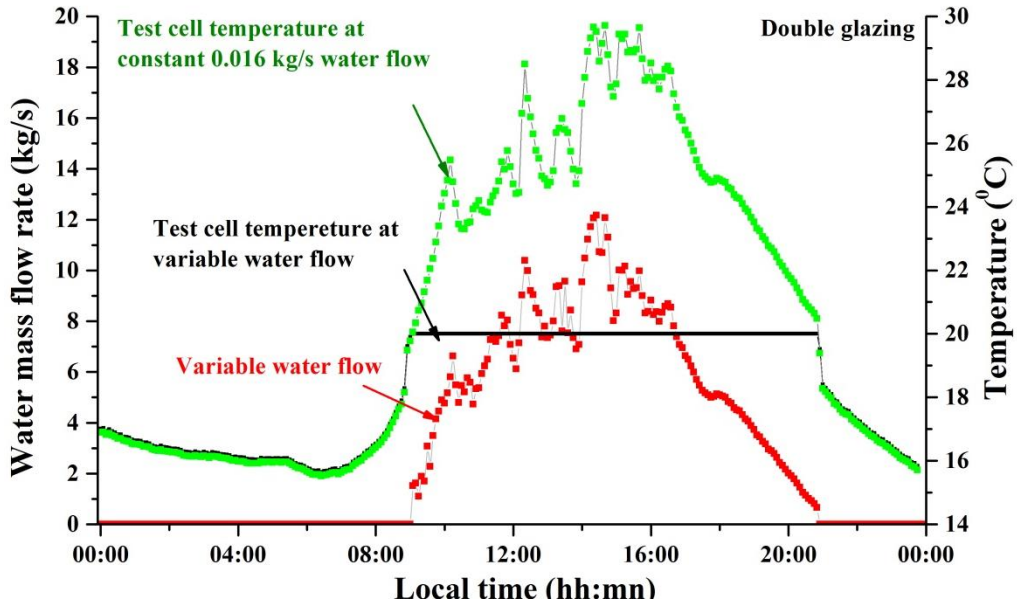

Figure 7-21: Variable flow to keep the test cell temperature 20 ^{0}C for double-glazing.

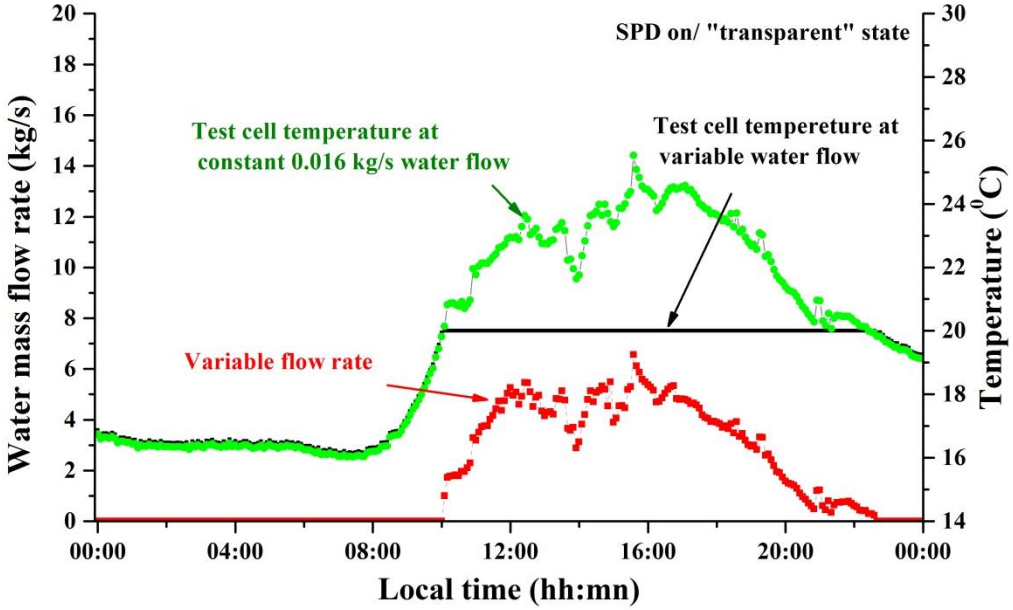

Figure 7-22: Variable flow to keep the test cell temperature 20 ^{0}C for SPD transparent state.

Figure 7-22, 7-23, 7-24 shows the test cell internal temperature on constant water flow and variable water flow. Water flow through heat exchanger was applied to maintain the test cell internal temperature at 20 ^{0}C, which is considered a standard comfortable room temperature. From the experiment, it was found that 0.016 kg/s flow rate was not able to cool down the temperature for any of the three cases. Analytically, variable flow rate was found which could maintain the test cell room temperature at 20 ^{0}C.

7.6. Error analysis

Figure 7-23 and Figure 7-24 show the error bar in the graph of test cell internal temperature and overall heat transfer coefficient of the SPD glazing.

The error bars of the measured temperature profile presented 4% uncertainty.

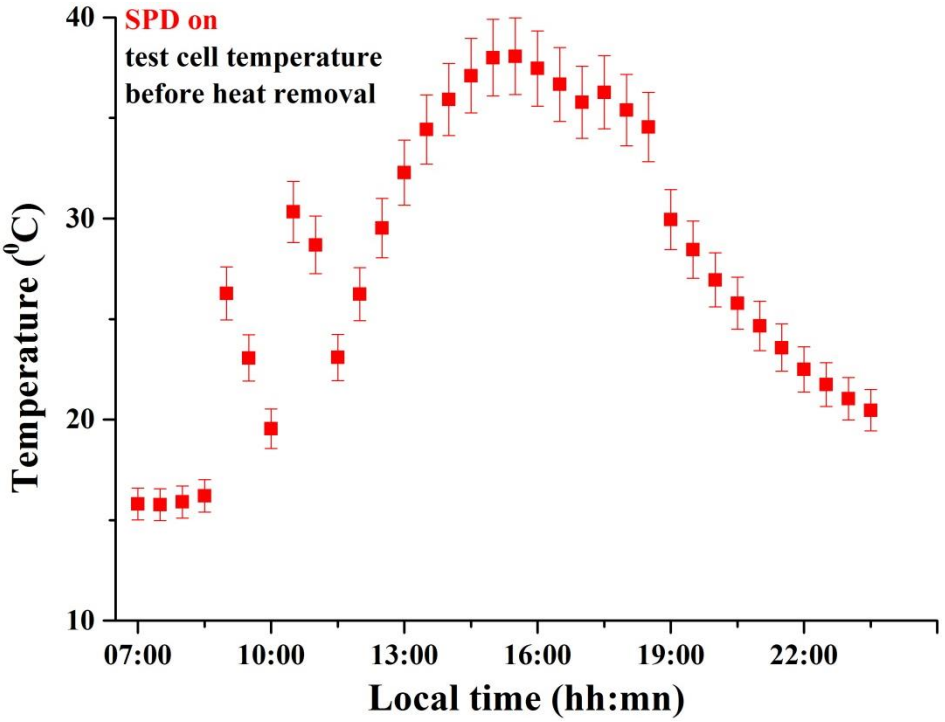

Figure 7- 23: Test cell temperature for one-hour interval with error bar

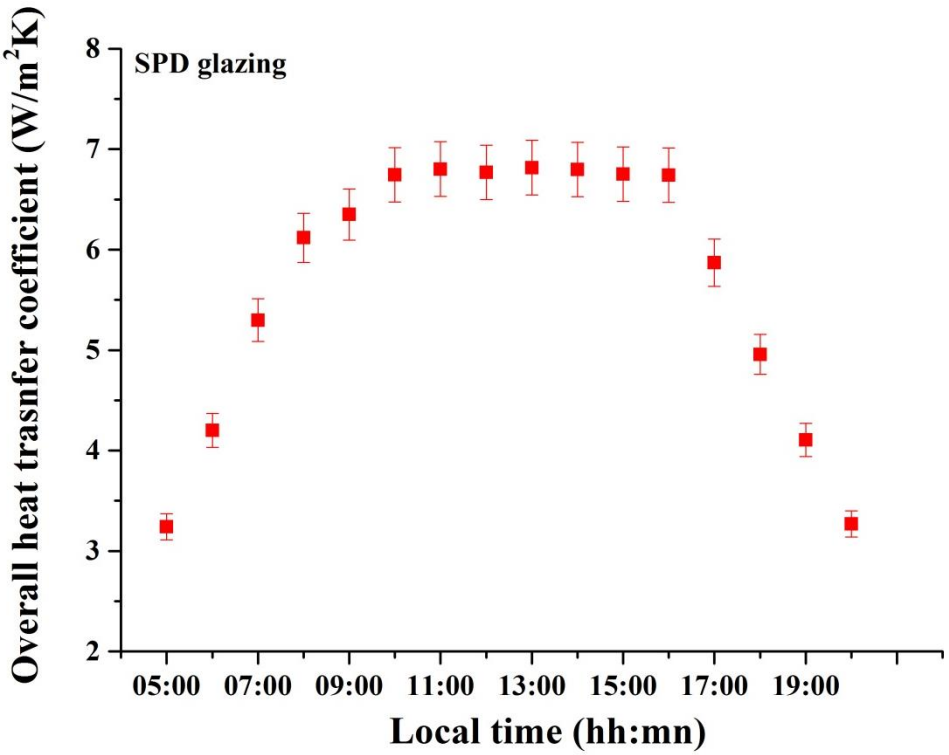

Figure 7- 24: Overall heat transfer coefficient for SPD single glazing with error bar

Overall heat transfer coefficient (U-value) can be written from equation 7-8

$$U = \frac{Q_g}{A_w(T_{in,tc} - T_{out,tc})}$$

where

$$Q_g = I_v(t)A_w\tau_v(\theta)\alpha - M_{tc}C_{tc}\frac{dT_{in,tc}}{dt}$$

Error for *U*-value will be ΔU and can be written as equation 7-16

$$\frac{\Delta U}{U} = \sqrt{\left(\frac{\Delta I}{I}\right)^2 + \left(\frac{\Delta T_{in,tc}}{T_{in,tc}}\right)^2 + \left(\frac{\Delta T_{out,tc}}{T_{out,tc}}\right)^2} \quad (7\text{-}16)$$

For SPD single glazing overall heat transfer coefficients, using the error range and reference values in Table 3-3 of Chapter 3 can be found from equation 7-16

$$\Delta U = \sqrt{\left(\frac{2}{900}\right) + \left(\frac{0.4}{37}\right) + \left(\frac{0.4}{20}\right)} \times 5.9$$

$$\Delta U = \pm 0.02 \times 5.9$$

$$\Delta U = 5.9 \pm 0.13$$

With an overall heat transfer coefficient, 5.9 W/m^{2}K the error range is ± 0.13 or 0.33%.

Calculated *U*-value for SPD single glazing was 5.9±0.13 at 97% confidence level.

7.7. Summary

Thermal characterisation of an SPD glazing was investigated using outdoor test cells. Suspended particle inside the SPD glazing absorb solar radiation irrespective of its stats (opaque and transparent) which increased the test cell temperature in similar way and the glazing surface temperature. It was also found that SPD glazing in both "opaque" and "transparent" conditions limits the temperature rise inside the test cell

due to transmission of the SPD in “transparent” and “opaque” being 55% and 5%, respectively compare to a double glazing at 78%. From the experimental results, an overall heat transfer coefficients (U_{spd}) value for SPD of 5.9 W/m^{2}K was found while for the double-glazing (U_{double}) it was 2.98 W/m^{2}K. Thus SPD switchable glazing can be considered as is a variable transparency single glazing.

To understand the cooling load reduction from SPD transparent to SPD opaque state one water flow heat exchanger was employed. A significant drop in the test cell temperature was found due to 0.016 kg/s water mass flow inside the test cell. The maximum test cell temperatures for SPD transparent and opaque states were found to be 25 ^{0}C and 22 ^{0}C respectively. From the experiment, it can be concluded that 61% cooling load reduction is possible for the SPD in its opaque state compared to its transparent state. Yearly CO_2 saving using SPD opaque state will be 1798 kg.

Chapter 8. Thermal and daylighting performance analysis of an evacuated glazing

8.1. Introduction

The goal of this chapter is to investigate the thermal analysis of evacuated (vacuum) type glazing.

Specific objectives are

- Analysing thermal behaviour of vacuum glazing using test cell;
- Calculation of overall heat transfer coefficient of vacuum glazing.

Thermal behaviour and overall heat transfer coefficient of vacuum glazing have been studied using hotbox calorimeter (Collins et.al. 1993; Fang et.al. 2006). Outdoor characterisation of vacuum glazing has only been performed once to (Lenzen and Collins 1997) look at the effects of a known periodically applied temperature difference on the long-term mechanical and thermal integrity performance of the glazing (Lenzen and Collins 1997).

8.2. Calculation of thermal and daylighting properties

Thermal and daylighting properties for evacuated glazing were calculated using the equations described in chapters 7 and 5 respectively. Overall heat transfer coefficient was calculated using equation 7-8 of Chapter 7.

Daylight factor was calculated using equation 5-2 of Chapter 5.

8.3. Experimental procedure

The experiment was performed on June 2014 on the roof of Kevin Street building DIT, Ireland (53.34 ^{0}N, 6.25 ^{0}W). Details of experiment set up and data logging and

monitor process are mentioned in Chapter 3. A photographic view of experimental set up is shown in Figure 8-1.

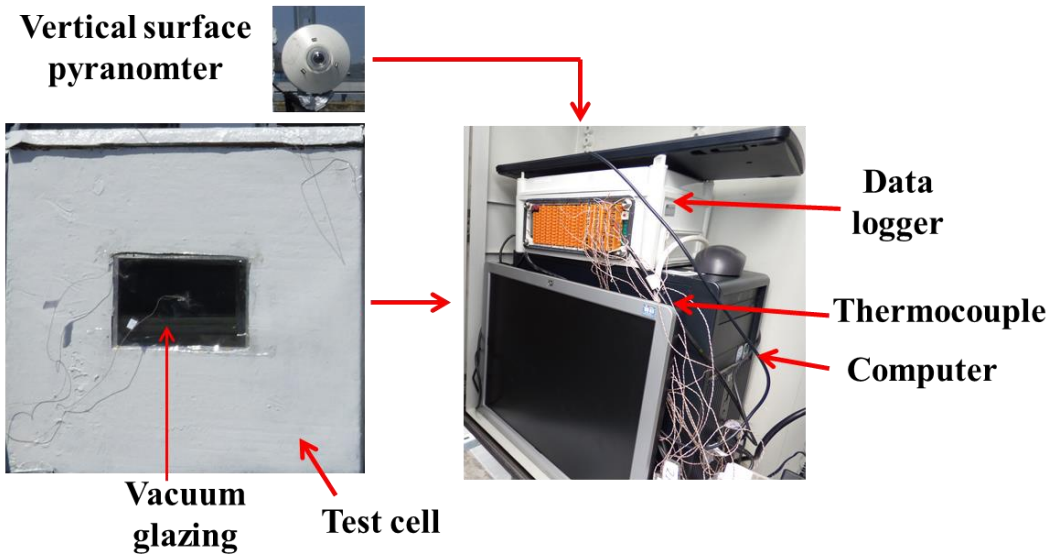

Figure 8-1: Test cell experimental set up.

8.4. Results

8.4.1. Test cell experimental results

Figure 8-2 indicates the diurnal variation of vacuum glazing inside and outside surface temperature and the vacuum glazing test cell inside temperature and ambient temperature for a clear sunny day, intermittent cloudy day and overcast cloudy day.

For clear sunny day, maximum test cell temperature was recorded 35 ^{0}C while the maximum inside surface temperature was 40 ^{0}C and outside was 34.1 ^{0}C. Between 8 am to 12 pm test cell temperature increased 3 ^{0}C/h whereas the ambient temperature increased at the rate of 1.5 ^{0}C/h. Slow rate of heat loss from the test cell occurred compared to inside, outside and ambient temperature reduction.

Test cell temperature was higher than ambient after the sun set (no solar radiation) clearly showing the thermal insulation properties of vacuum glazing. Recorded

maximum temperature for vacuum glazing inside, outside surface, test cell and ambient temperature are listed in Table 8-1. Table 8-2 illustrates the rate for temperature increased from 8 am to 12 pm for vacuum glazing inside surface, outside surface, test cell and ambient temperature. Table 8-3 indicates the decrease rate (^{0}C/h) of temperature for vacuum glazing surfaces, test cell and ambient. Negative sign in table 8-3 signifies the higher temperature at 4 pm compare to 12 pm measurement. Test cell inside temperatures for all three days were found higher between 15:00 hh (sunny day) to 16:00 hh (intermittent and overcast days) which offered always a negative values of temperature decrement.

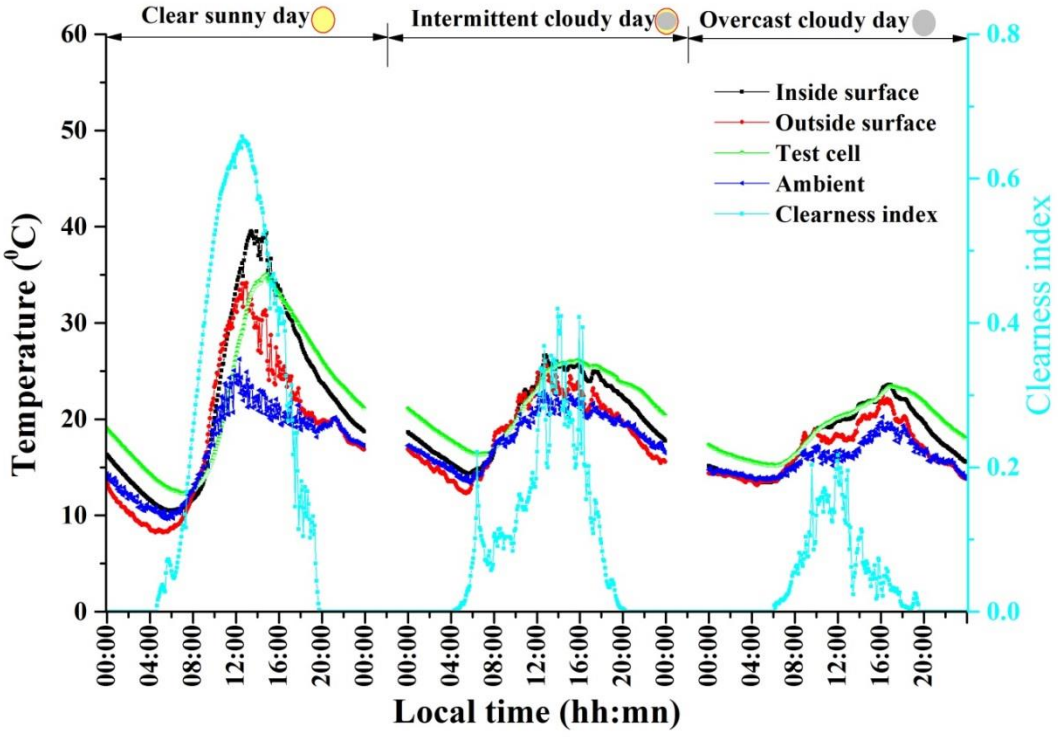

Figure 8-2: Diurnal variation of vacuum glazing outside, inside surface, test cell temperature, ambient temperature and solar radiation for a clear sunny day, intermittent cloudy day and overcast cloudy day.

Table 8-1: Maximum temperature of vacuum glazing surfaces and test cell for three different days.

		Maximum ambient temperature (^{0}C)	Maximum test cell temperature (^{0}C)	Maximum inside surface temperature (^{0}C)	Maximum outside surface temperature (^{0}C)
Type of sky	Sunny day	26.2	35	40	34.1
	Intermittent sunny day	22.5	26.1	26.6	26.1
	Overcast day	18.8	23.3	23.5	22

Table 8-2: Rate of temperature increment per hour from 8 am to 12 pm for vacuum glazing.

		Increased ambient temperature (^{0}C/h)	Increased test cell temperature (^{0}C/h)	Increased inside surface temperature (^{0}C/h)	Increased outside surface temperature (^{0}C/h)
Type of sky	Sunny day	1.5	3	5	5.02
	Intermittent sunny day	1.1	1.5	1.8	1.44
	Overcast day	0.335	0.9525	0.9875	0.5975

Table 8-3: Rate of temperature decrement per hour from 12 pm to 4 pm for vacuum glazing.

		Increased ambient temperature (^{0}C/h)	Increased test cell temperature (^{0}C/h)	Increased inside surface temperature (^{0}C/h)	Increased outside surface temperature (^{0}C/h)
Type of sky	Sunny day	1.5	-1.64	0.1475	1.96
	Intermittent sunny day	0.03	-0.79	-0.405	0.2525
	Overcast day	-0.9025	-0.59	-0.7175	-0.835

8.4.2. Transmitted solar energy

Figure 8-3 shows the diurnal variation of calculated clearness index, diffuse factor and anisotropic index, transmitted solar energy through vacuum glazing and measured vertical surface solar radiation for clear sunny, intermittent cloudy and overcast cloudy day. Transmitted solar energy was calculated using equation 7-13.

Clearness index was achieved maximum 0.8 at mid-day period for a clear sunny day. Anisotropic index represents transmittance of the atmosphere for the direct solar radiation whereas cleanness index indicates the global solar radiation transmission. For a clear sunny day, mid-day period shows higher values of anisotropic index and higher clearness index indicates the global radiation is mostly direct solar radiation. At this time diffuse factor values are low nearly 0.3. This indicates the diffuse radiation at this time was lower compare to direct solar radiation. For intermittent and overcast day lower clearness index and lower anisotropic index was achieved where as higher values of diffuse factor was obtained. Maximum transmitted solar energy was 482 W/m^2 while solar radiation was 955 W/m^2 for clear sunny day.

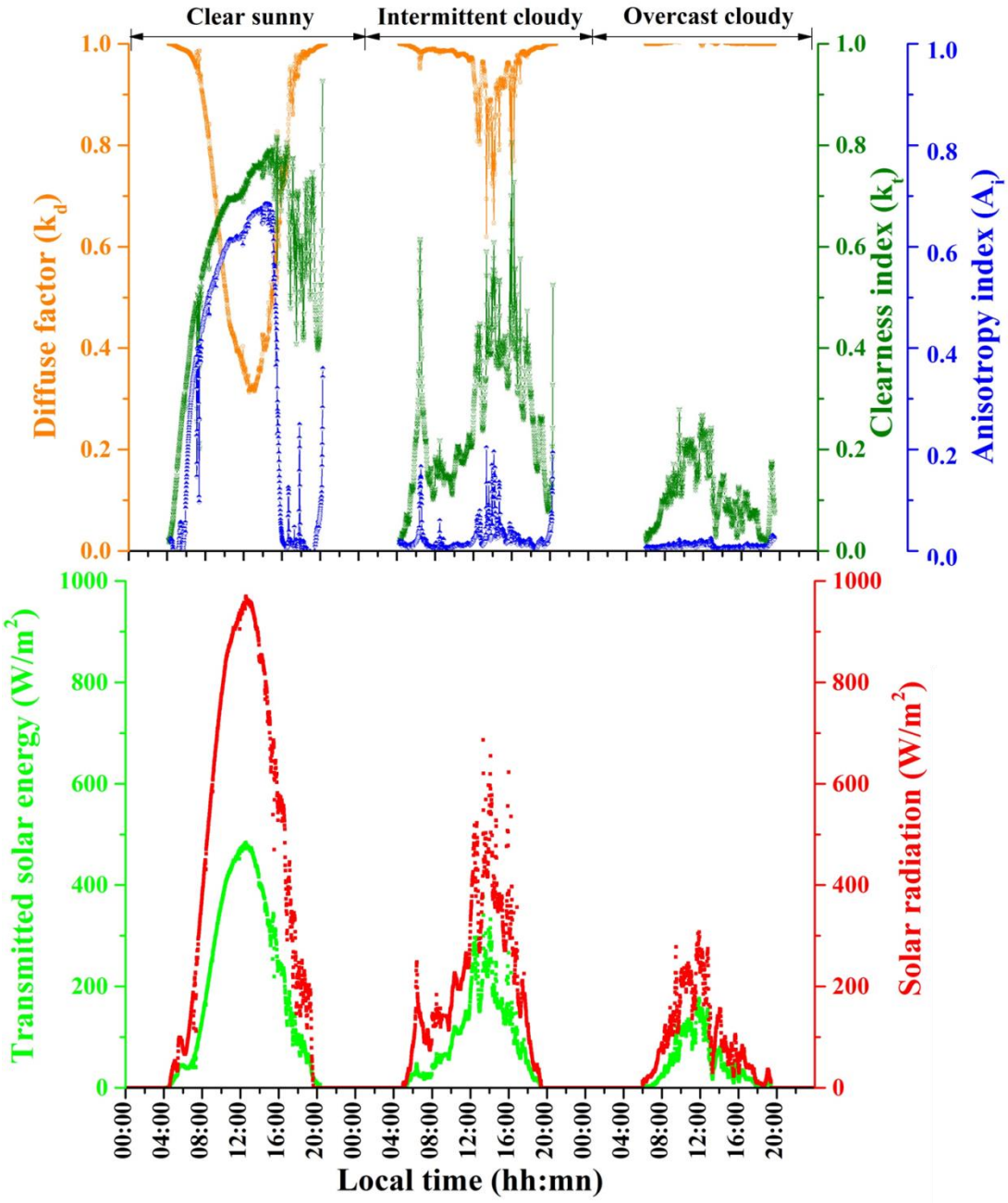

Figure 8- 3: Diurnal variation of calculated clear ness index, diffuse factor, anisotropy index and transmitted solar energy through vacuum glazing and measured vertical surface solar radiation for clear sunny, intermittent cloudy and overcast cloudy day.

8.4.3. Solar heat gain coefficients

Figure 8-4 shows the solar heat gain coefficients (SHGC) and vacuum glazing angular transmittance variation with incidence angle. SHGC was calculated from equation 7-15 discussed in Chapter 7. SHGC varied between 0.58 and 0.35.

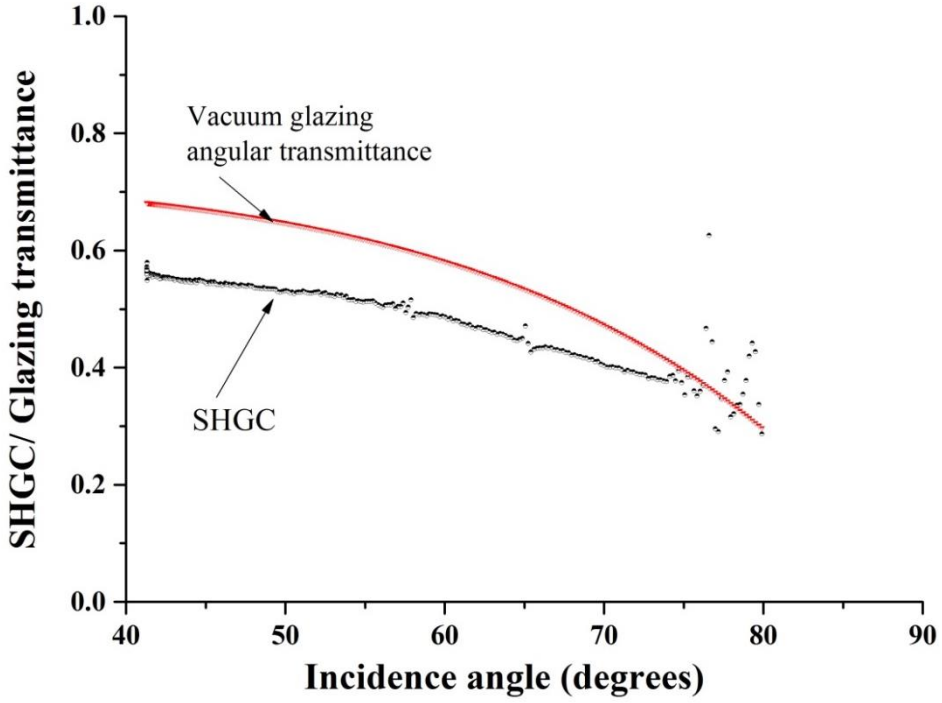

Figure 8-4: Variation of solar heat gain coefficient and angular transmittance of vacuum glazing with incidence angle.

8.4.4. Overall heat transfer coefficient of vacuum glazing

Overall heat transfer coefficient of vacuum glazing was calculated using equation 7-8 of Chapter 7. Overall heat transfer coefficient of 1.4 W/m^2K was found for vacuum glazing.

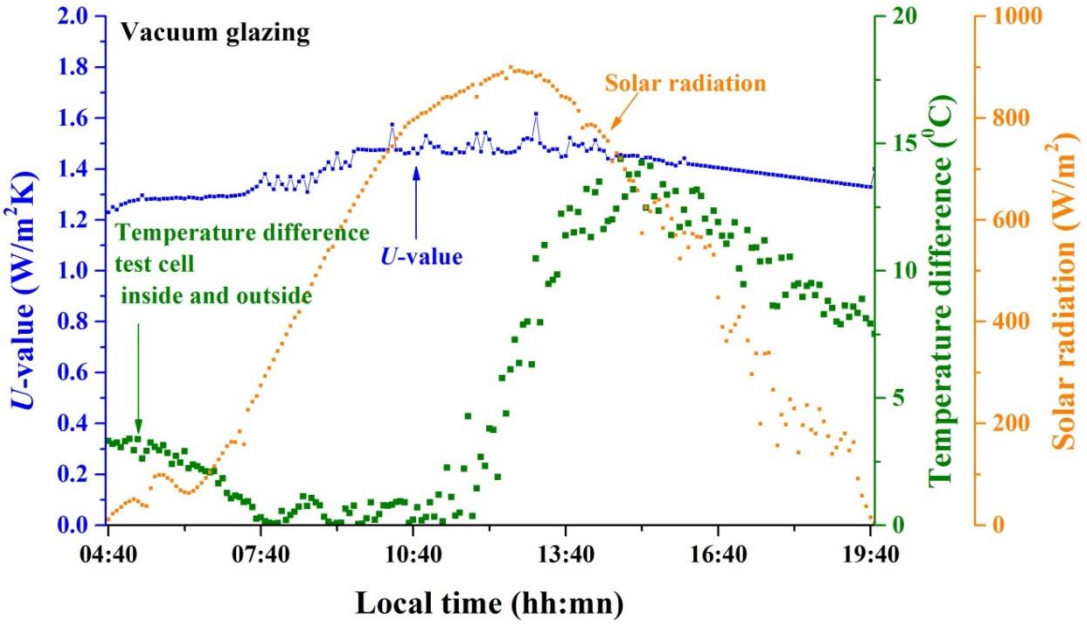

Figure 8-5: Diurnal variation of the overall heat transfer coefficient of vacuum glazing, vertical surface solar radiation and temperature difference between test cell inside and outside ambient temperature.

8.4.5. Illuminance of vacuum glazing

Figure 8-6 indicates the location of illuminance measuring point inside test cell for vacuum glazing. The location was on a working plane 27 cm away and 20 cm above from the ground for vacuum glazing and double-glazing. It also illustrates the measured outside illuminance and measured inside illuminance for clear sunny, intermittent cloudy and overcast cloudy day for vacuum and double-glazing. Variation of inside illuminance was found which was due to the transmission variation of double-glazing (78%) and vacuum glazing (72%).

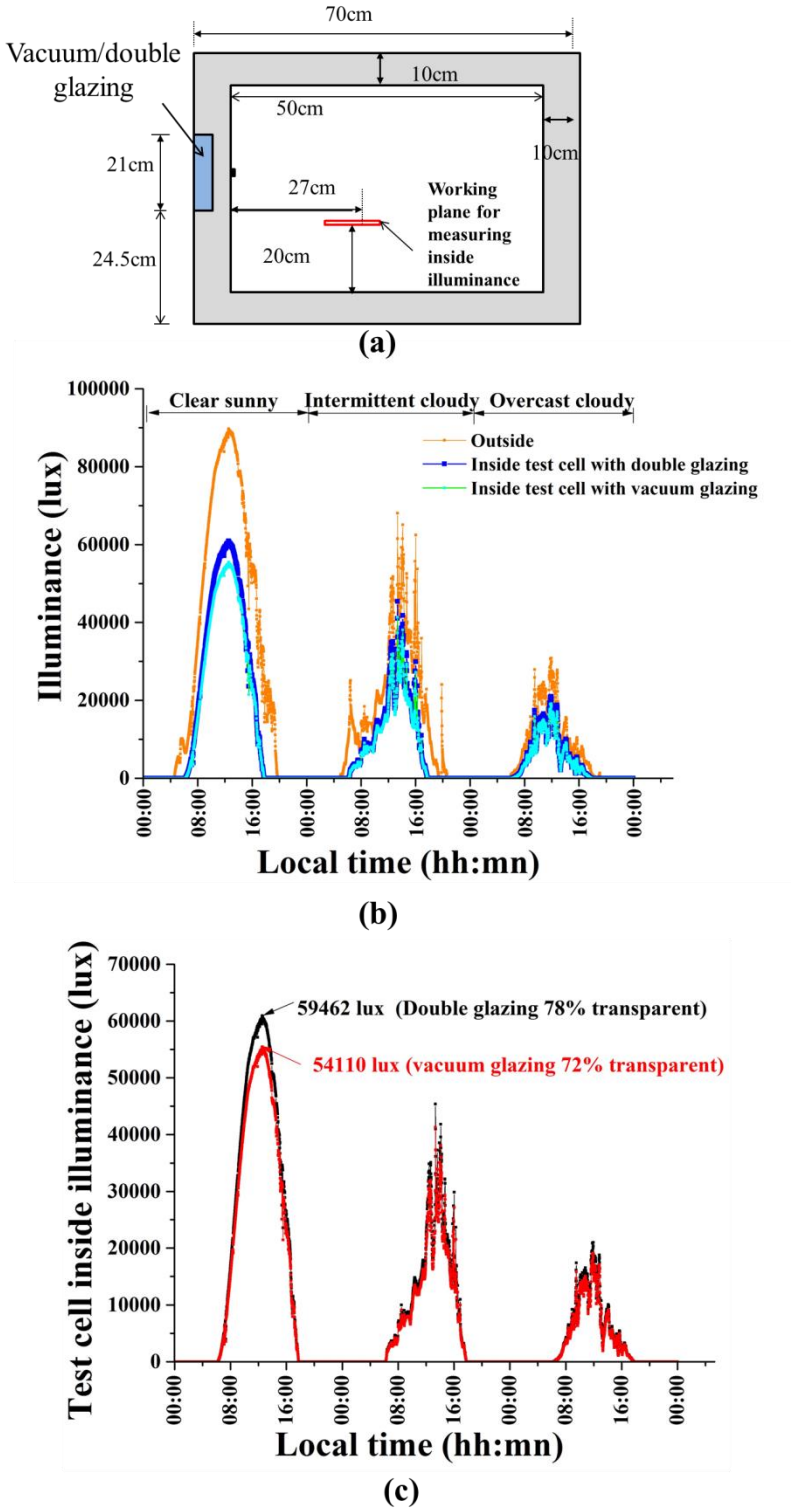

Figure 8-6: (a) Illuminance sensor location inside test cell for glazing on a working plane 27 cm away and 20 cm above from the ground (b) Outside illuminance and inside illuminance for clear sunny day, intermittent cloudy day and overcast cloudy day of vacuum double glazing and (c) inside illuminance inside test cell for vacuum and double glazing.

Presence of pillars inside the vacuum glazing did not create an obstacle for viewing. The vacuum glazing consists of a total of 170 pillars having 0.3 mm diameter. Total area ($A_{pillars}$) occupied by pillars were

$$A_{pillars} = 170 \times \pi \left(\frac{0.3}{2 \times 1000} \right)^2 = 24.021 \times 10^{-6} m^2$$

Vacuum glazing area was A_{vacuum},

$$A_{vacuum} = 0.35 \times 0.2 = 0.07 m^2$$

The pillars inside vacuum glazing occupied negligible area. Maximum illuminance inside vacuum glazing and double-glazing for a clear sunny day were 59462 lux and 54110 lux respectively. Ratio of these two illuminance (59462/54110 = 1.08) is similar to the ratio of the average transmittance (78/72 = 1.08) of glazing. This clearly indicates that vacuum glazing pillars does not create any blockages and offer high illuminance.

8.5. Summary

Outdoor characterisation of a vacuum glazing was performed using a test cell. Vacuum glazing inside surface, outside surface, test cell and ambient temperatures were recorded. For an intermittent and an overcast day, surface temperatures were higher due to higher solar radiation after 12 pm. The inside surface of the vacuum glazing was always higher than the outside surface as entering solar radiation was absorbed by the low-e coating. During the night, vacuum glazing will reduce the heat losses from the room and also keep the room warm due to heat retained from sunshine period. Diurnal overall heat transfer coefficient was calculated using the recorded solar radiation and temperature data. Average overall heat transfer coefficient was found to be 1.4 W/m^2K. Vacuum glazing thus can be a suitable

alternative compared to double-glazing as it has very low overall heat transfer rate (double-glazing *U*-value 2.98 W/m^{2}K from Chapter 7). It is suitable for reduction of heating load and has nearly same transparency level as double-glazing.

Chapter 9. Thermal performance analysis of low heat loss SPD switchable glazing

9.1. Introduction

From SPD glazing thermal analysis result (Chapter 7), it was evident that the SPD glazing's overall heat transfer coefficient was higher than double-glazing. In this chapter, addition of double-glazing with SPD glazing was monitored to achieve an improved low thermal heat loss glazing. Vacuum glazing has higher potential to achieve low thermal heat loss compare to double-glazing. SPD vacuum glazing can be a promising novel glazing system, which will allow maximum low heat loss with addition of switchable transparency. These two types of system components were examined in this chapter.

9.2. Calculation of thermal properties

Thermal properties for low heat loss SPD glazing were calculated using the equations described in Chapter 7. Overall heat transfer coefficient was calculated using equation 7-8 and solar heat gain coefficient was calculated using equation 7-15 of Chapter 7.

9.3. Experimental procedure

The experiment was performed from April 2015 to August 2015 on the roof of Kevin Street building DIT, Ireland (53.34 ^{0}N, 6.25 ^{0}W). Details of experiment set up and data logging and monitor process are mentioned in section 3.3.1 of Chapter 3.

9.4. Results of SPD double-glazing

9.4.1. Overall heat transfer coefficient of SPD double glazing

The combined double and SPD switchable single glazing achieved a low total average *U*-value ($U_{spd-double}$) 1.99 W/m^{2}K for a sunny day in Dublin shown in Figure

9-1. This system was compared with another set of double-glazing unit attached a single on the one side of it. This system gave a total average *U*-value of 1.8 W/m^{2}K shown in Figure 9-2.

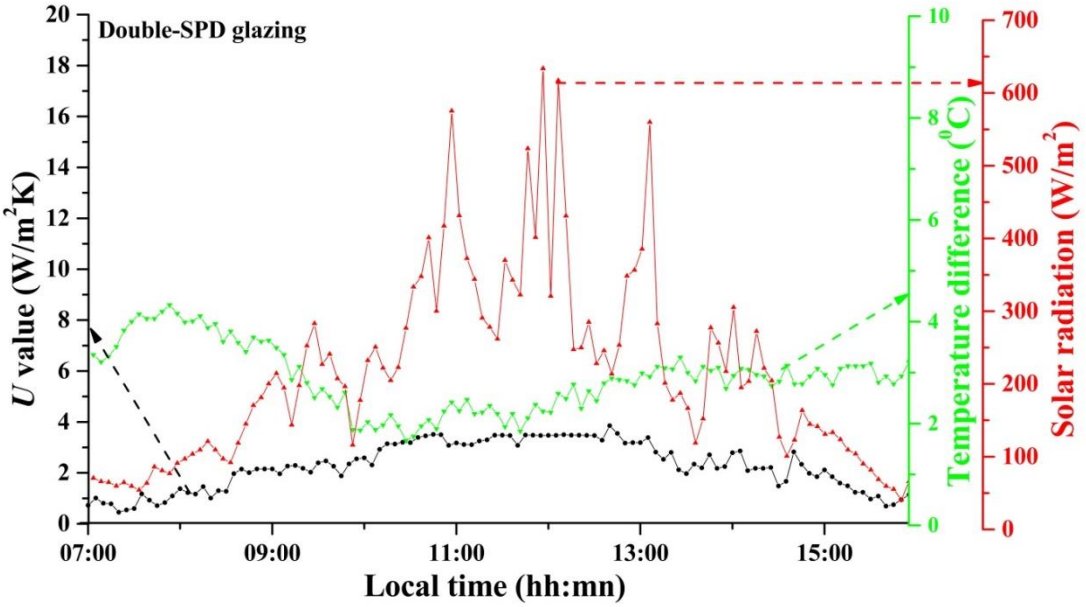

Figure 9-1: Diurnal variation of the overall heat transfer coefficient of SPD switchable double-glazing, solar radiation and temperature difference between test cell inside and outside ambient temperature.

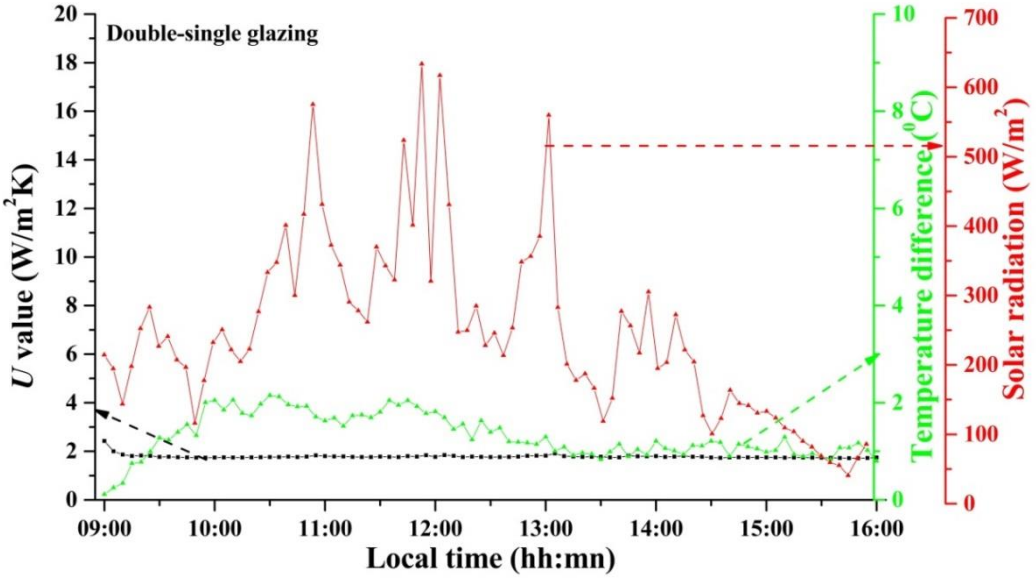

Figure 9-2: Diurnal variation of the overall heat transfer coefficient of double-single glazing, solar radiation and temperature difference between test cell inside and outside ambient temperature.

9.5. Results of SPD vacuum glazing

9.5.1. Combined SPD vacuum glazing window with the SPD transparent

Figure 9-3 shows the diurnal thermal behaviour of SPD vacuum glazing window when the SPD was in transparent state for clear sunny day, intermittent day and overcast day. Outside surface (SPD glazing glass pane) temperature was found to be higher than inside surface temperature (vacuum glazing glass pane) for clear sunny day. SPD particle inside the SPD glazing absorb solar radiation, which increased the surface temperature. For clear sunny day maximum test cell temperature of 31.4 ^{0}C was recorded at 14:46 hh. Outside surface temperature (SPD glazing glass pane) increased at the rate of 4.2 ^{0}C/h from 09:00 to 12:00 and maximum surface temperature was recorded 41.6 ^{0}C at 13:00 hh. Thermal swing of test cell internal temperature between 04:00 to 14:00 was 15 ^{0}C. Maximum inside surface temperature was 34.9 ^{0}C at 13:56 hh. Maximum test cell temperatures of SPD vacuum glazing for intermittent sunny and overcast days were 27 ^{0}C and 24.1 ^{0}C respectively.

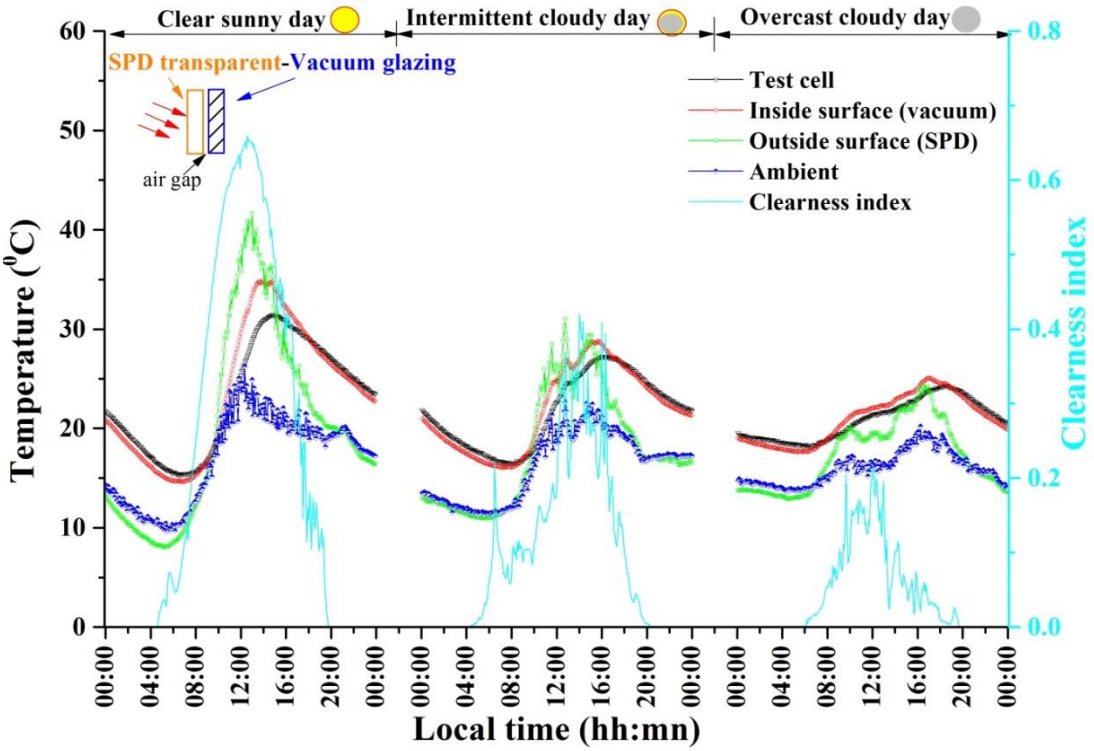

Figure 9-3: Diurnal variation of temperature for a combined suspended particle device (SPD) vacuum glazing window with the SPD transparent for a typical clear sunny day, intermittent day and overcast day in Dublin.

9.5.2. Combined SPD vacuum glazing window with the SPD opaque

Figure 9-4 illustrates the diurnal variation of SPD vacuum glazing in its 2% transparent condition. In this case, the outside surface (SPD glazing) temperature was found higher same as Figure 9-3. Maximum outside surface temperature was 37 ^{0}C. This surface temperature increased at the rate of 6.5 ^{0}C/h. Maximum test cell temperature was recorded 22 ^{0}C at 16:00 h. Nearly 9 ^{0}C maximum test cell temperature difference was found between Figure 9-3 and 9-4. Thermal swing of test cell internal temperature between 04:00 to 14:00 was 9 ^{0}C.

Maximum test cell temperatures of SPD vacuum glazing for intermittent sunny and overcast days were 15.4 ^{0}C and 12.6 ^{0}C respectively.

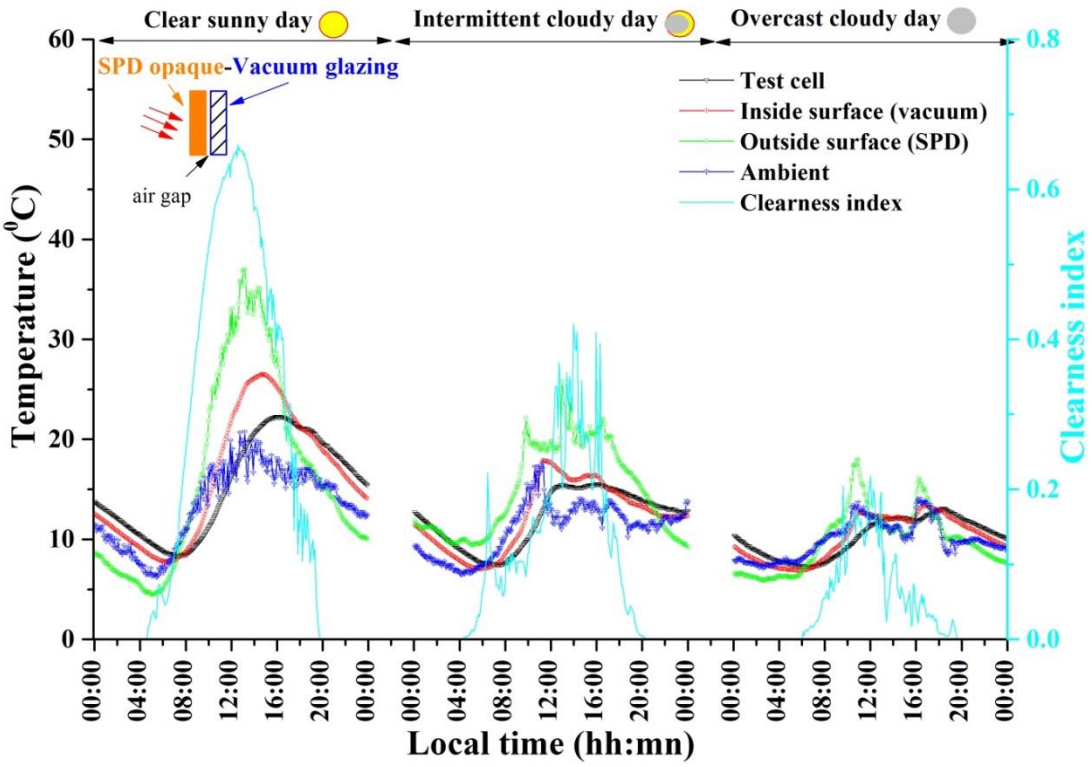

Figure 9-4: Diurnal variation of temperature for a combined suspended particle device (SPD) vacuum glazing window with the SPD opaque for a typical clear sunny day, intermittent day and overcast day in Dublin.

9.5.3. Combined vacuum SPD glazing window with the SPD transparent

Figure 9-5 illustrates the combined vacuum SPD glazing in its transparent condition for a clear sunny day. In this case, vacuum glazing was facing outside ambient (outside surface) and SPD glazing (inside surface) was facing inside test cell. Comparing Figure 9-3, variation of the test cell temperature was nearly 4 ^{0}C (27 ^{0}C for vacuum SPD, 31.4 ^{0}C for SPD vacuum). Maximum inside surface temperature (SPD glazing) for vacuum SPD combination was recorded 37.5 ^{0}C at 13:15 hh. Maximum test cell temperature, surface temperature between two glazing and ambient temperature for vacuum – SPD combination were recorded 27 ^{0}C, 31 ^{0}C, and 40.4 ^{0}C respectively. Inside surface temperature (SPD glazing glass pane) increased at the rate of 5.4 ^{0}C/h from 09:00 to 12:00.

For intermittent day and overcast day, maximum test cell temperatures were found to be 22.9 ^{0}C and 20.9 ^{0}C respectively.

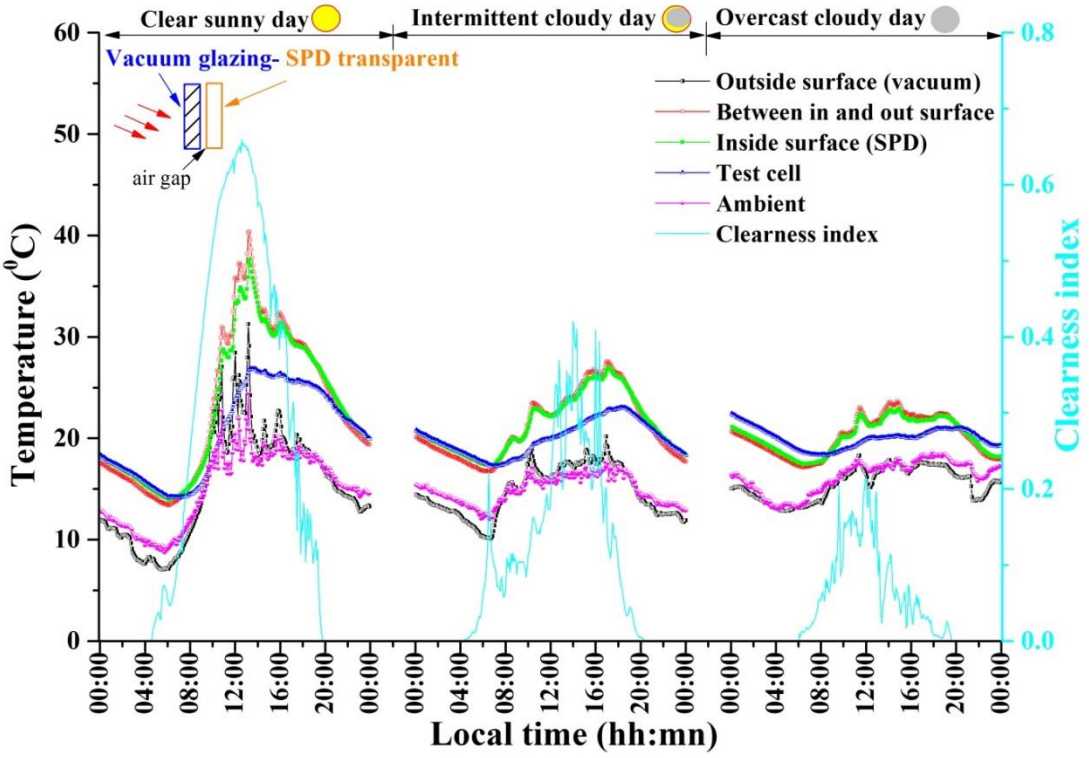

Figure 9-5: Diurnal variation of temperature for a combined vacuum suspended particle device (SPD) glazing window with the SPD transparent for a typical clear sunny day, intermittent day and overcast day in Dublin.

9.5.4. Combined vacuum SPD glazing window with the SPD opaque

Figure 9-6 illustrates the diurnal variation of temperature for a combined vacuum suspended particle device (SPD) glazing window with the SPD opaque for a typical sunny day in Dublin. In this case temperature between vacuum and SPD glazing was found higher than the inside (SPD glazing) and outside surface temperature (vacuum). This was due to the presence of low-e coating of vacuum glazing.

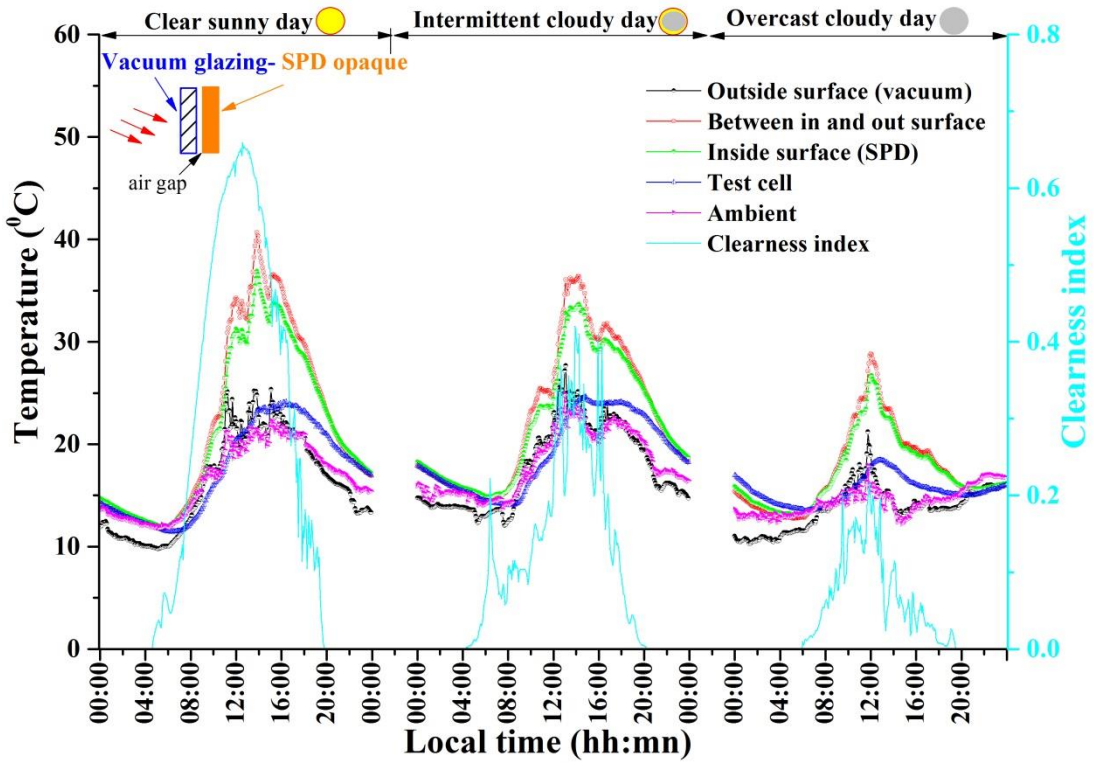

Figure 9-6: Diurnal variation of temperature for a combined vacuum suspended particle device (SPD) glazing window with the SPD opaque for a typical clear sunny day, intermittent day and overcast day in Dublin.

Common observation from these four different type characterisations-

- Test cell temperatures were always higher than any glazing surface temperature under no sun condition, which indicates the heat insulation property of vacuum glazing. Using only SPD glazing it was found that test cell temperature decreased similar with the ambient temperature after sun set period.
- SPD glazing facing the indoor test cell environment or facing the outdoor ambient environment, had less impact on the glazing surface temperature and test cell inside temperature.
- SPD glazing surface temperature was always higher than the surface temperature of vacuum glazing.

9.5.5. Overall heat transfer coefficient

Overall heat transfer coefficients (*U*-value) of SPD vacuum glazing for both transparent and opaque conditions have been calculated using the *U*-value equation 7-8. Figure 9-7 and 9-8 illustrate the diurnal change of overall heat transfer coefficient calculated using equation 7-8 for the combined glazing when SPD was facing outside ambient environment for its transparent and opaque states. Average overall heat transfer coefficient for combined SPD vacuum glazing was 1.16 W/m^{2}K and 1.01 W/m^{2}K for SPD transparent and opaque state respectively.

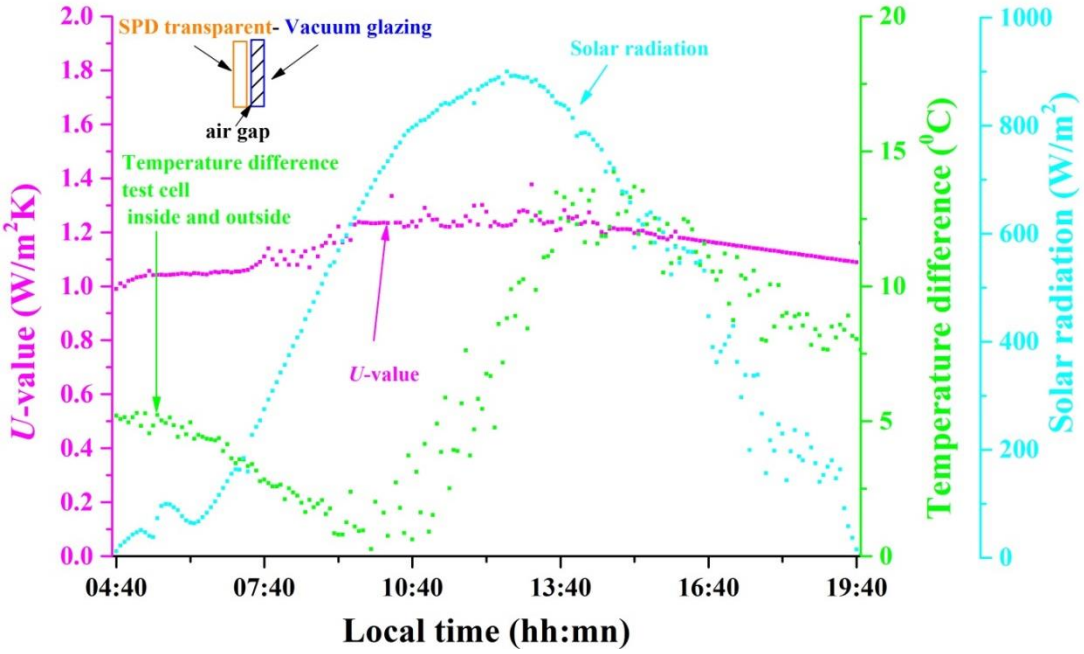

Figure 9-7: Diurnal variation of the overall heat transfer coefficient of SPD transparent vacuum glazing, vertical surface solar radiation and temperature difference between test cell inside and outside ambient temperature.

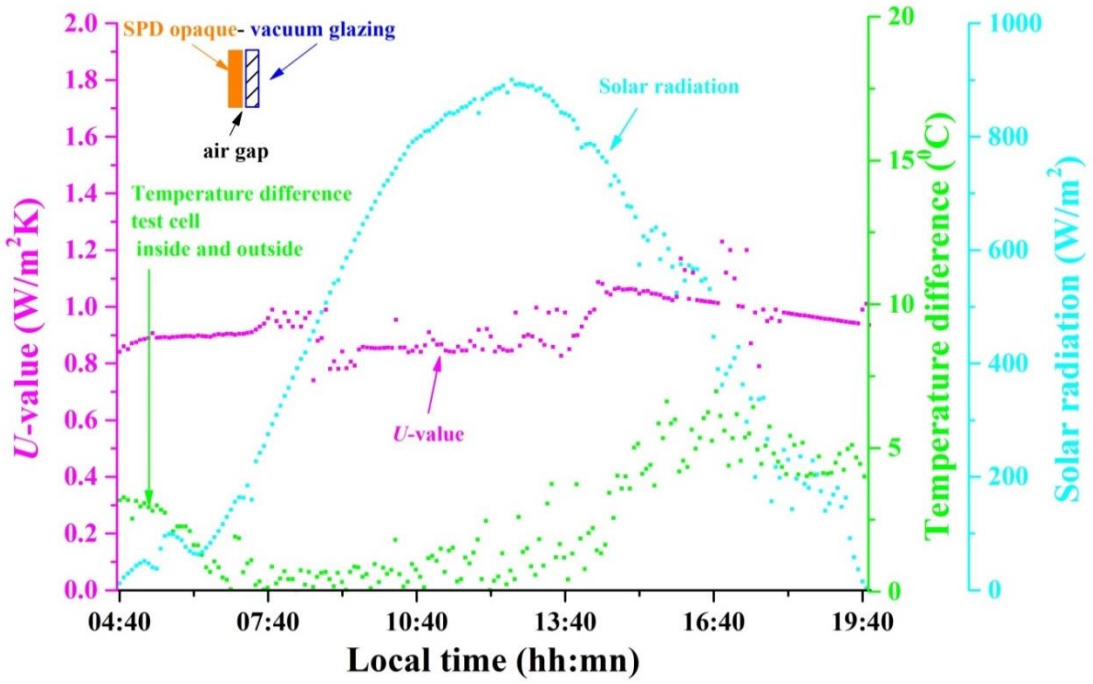

Figure 9-8: Diurnal variation of the overall heat transfer coefficient of SPD switchable double glazing, vertical surface solar radiation and temperature difference between test cell inside and outside ambient temperature.

Figure 9-9 and 9-10 illustrate the diurnal change of overall heat transfer coefficient calculated using equation **7-8** for the combined glazing when SPD was facing inside test cell environment for its transparent and opaque states.

Average overall heat transfer coefficient for combined vacuum SPD glazing was 1.14 W/m^{2}K and 1.00 W/m^{2}K for SPD transparent and opaque state respectively. The difference of overall heat transfer coefficient was due to the opaque SPD, which admitted less solar radiation that controlled the rise of temperature difference between inside and outside the test cell.

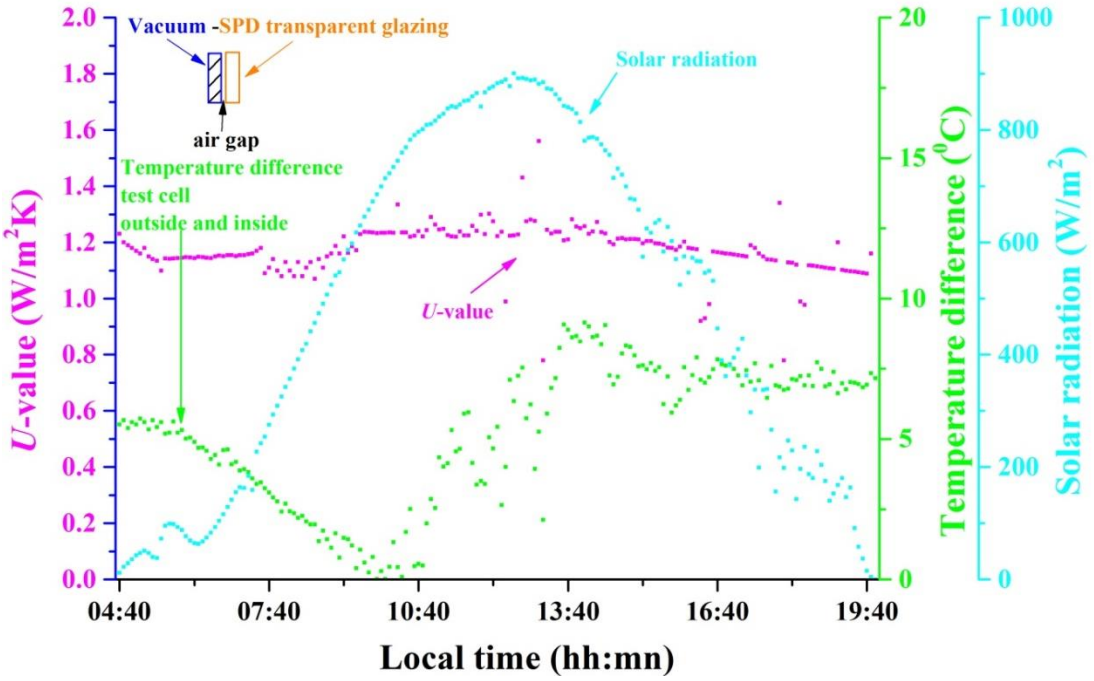

Figure 9-9: Diurnal variation of the overall heat transfer coefficient of Vacuum SPD transparent glazing, vertical surface solar radiation and temperature difference between test cell inside and outside ambient temperature.

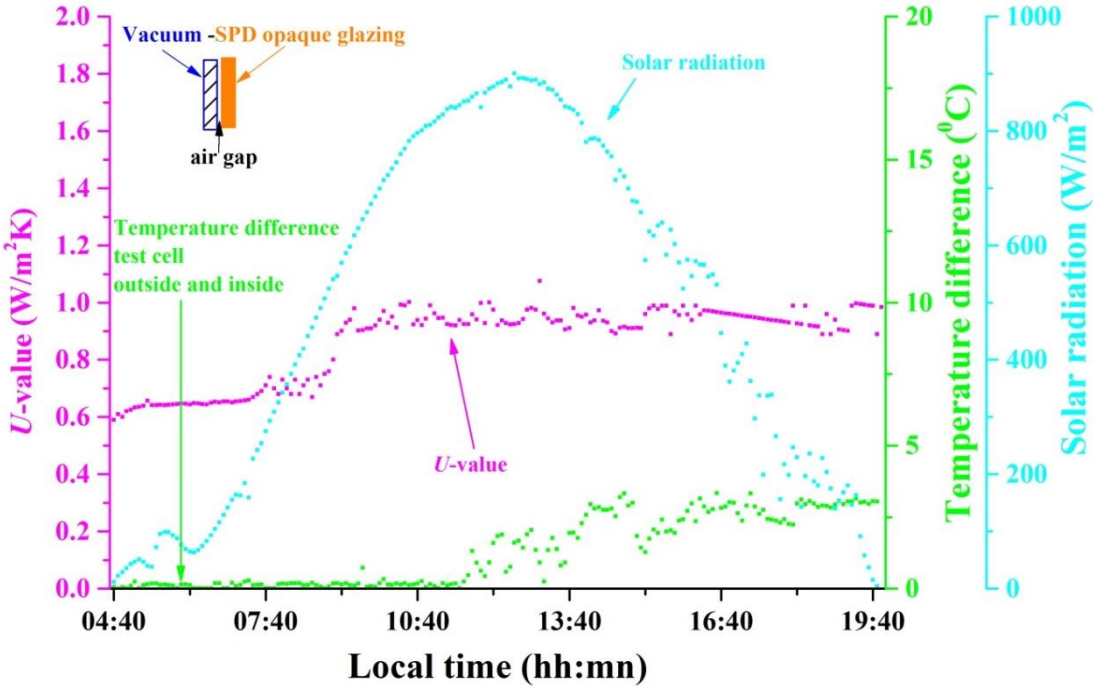

Figure 9-10: Diurnal variation of the overall heat transfer coefficient of Vacuum SPD opaque glazing, vertical surface solar radiation and temperature difference between test cell inside and outside ambient temperature.

9.5.6. Solar heat gain coefficient

SHGC of this SPD vacuum glazing was evaluated using equation 7-15. SPD transparent and opaque both conditions were considered. Figure 9-11 illustrates SHGC of SPD vacuum glazing for SPD transparent condition. SGHC varied from 0.27 to 0.15 and changes were observed with the change of incidence angle. Figure 9-12 illustrates the SHGC for this combined SPD vacuum glazing while SPD was in opaque state. 0.06 SHGC was found for this case during mid-day (12:00) period.

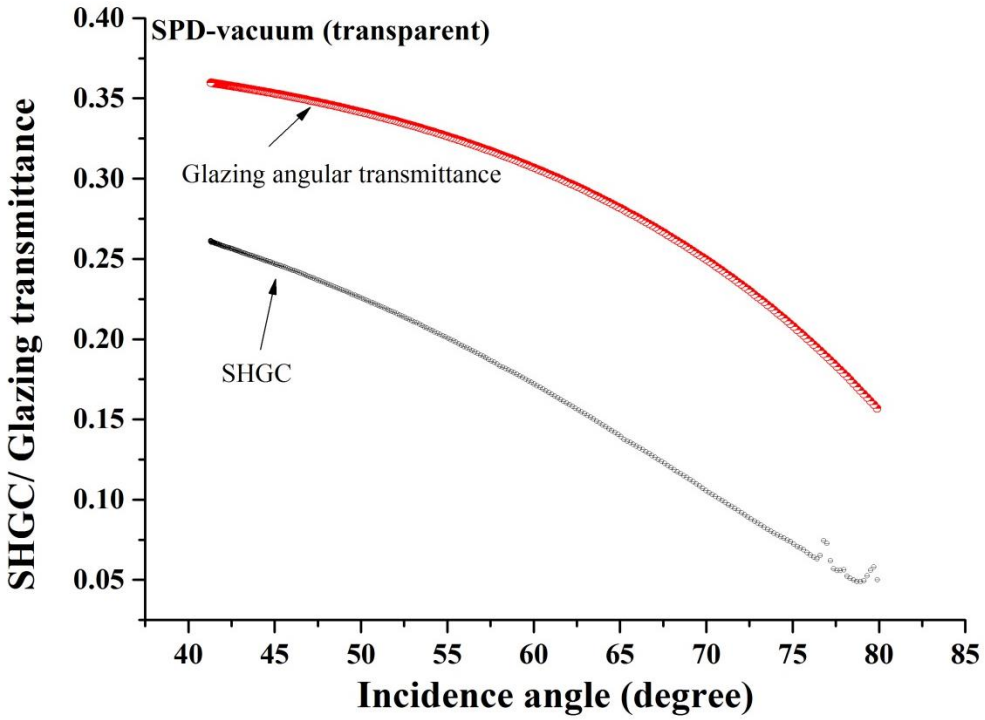

Figure 9-11: Change of solar heat gain coefficient and transparent state angular transmittance of combined glazing for different incidence angle.

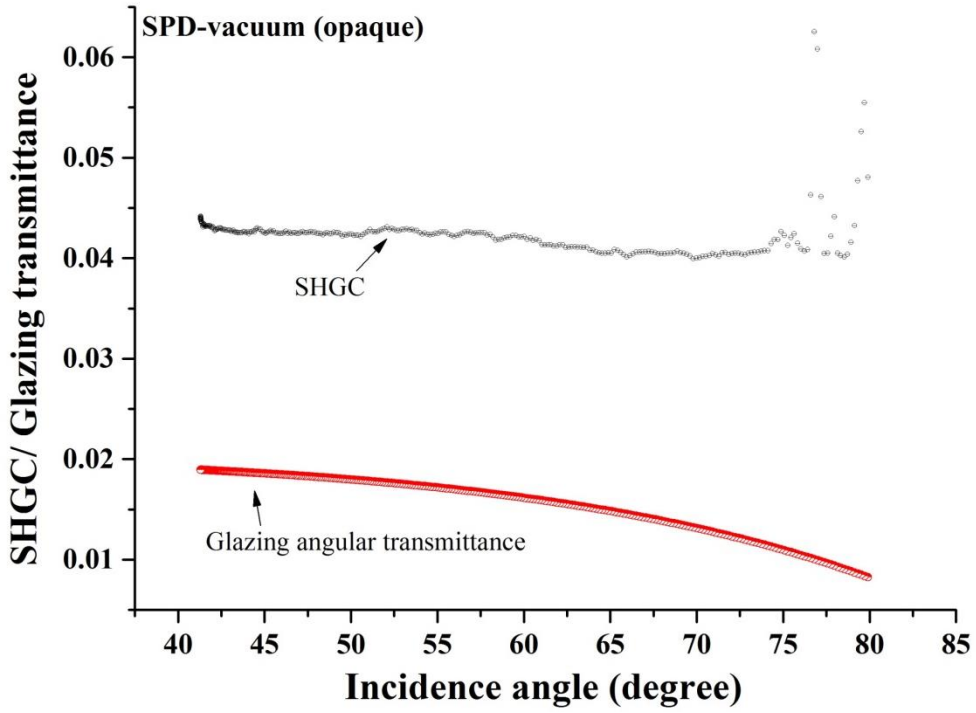

Figure 9-12: Change of solar heat gain coefficient and opaque state angular transmittance of combined glazing for different incidence angle.

9.6. Summary

Thermal performance of a combined SPD – vacuum glazing system was characterised using an outdoor test cell. Due to SPD glazing higher absorption property and presence of low e coating in vacuum glazing, the surface temperature of SPD glazing was found always higher than the vacuum glazing. SPD glazing facing the ambient environment and the test cell indoor environment had negligible impact on the surface temperature. Due to SPD glazing transparent and opaque state, variation of test cell temperature and the inside and outside surface temperature of the combined glazing was found. Under no solar radiation condition, test cell temperature was always higher than glazing surface temperatures. This indicates the heat insulation for the vacuum glazing present in the combined glazing. Low *U*-value (1.0 - 1.14 W/m^2K) was achieved using this combined glazing, which can be considered as switchable vacuum glazing or low heat loss SPD glazing. Due to its

switchable property, two different types of SHGC values were possible during mid-day period, which are advantageous for modern building application.

This combined glazing offered a low thermal swing range of 6 to 11 ^{0}C between 04:00 to 14:00 hh for SPD opaque and transparent state. SPD single glazing transparent and double-glazing had nearly 20 ^{0}C and 25 ^{0}C thermal swing respectively. Low thermal swing is advantageous for reduction of building heating and cooling energy consumption.

For modern net zero or retrofit building application, this type of glazing can be a solution for both in summer and in winter. In summer during mid-day period, this glazing can be kept at an opaque sate, which will reduce the heat gain and cooling load. Presence of vacuum glazing in this combined glazing, will store low temperature inside the room for longer period and will offer thermal comfort and reduce the cooling load. In winter during the mid-day period, glazing can be kept at transparent state allowing heat gain and this heat will be again stored due to vacuum glazing and will reduce the heating load demand of building.

Chapter 10. Cost analysis of a PV powered SPD switchable vacuum glazing system

10.1. Introduction

The aim of this chapter is to conduct cost of a PV powered SPD vacuum glazing. Using loss of power supply probability (LPSP) minimum PV device area was found to switch the 1 m^2 SPD glazing to achieve allowable glare. To achieve dynamic behaviour of PV, battery and inverter, model had been carried out in MATLAB. Different components results were validated from the recorded data described in Chapter 6.

10.2. Using LPSP method PV area determination for SPD switching

In the literature, (Borowy and Salameh 1996; Diaf et.al. 2007; Shen 2009; Bakelli et.al. 2011; Maleki and Pourfayaz 2015) loss of power supply probability (LPSP) concept was introduced for finding the reliability of power supply to load. It is defined as the ratio of the number of hours that the system fails to supply a load to the total number of hours required by the load. A LPSP of 0 refers to the power can fully meet load demand, whereas a LPSP of 1 is referred to the power can never meet load demand. A LPSP from 0 to 1 is referred to the power cannot fully supply to the load when the solar power is not enough while the battery has been in the allowable maximum depth of discharge (DOD) or the allowable minimum state of charge (SOC). The purpose of the size optimization of solar array and battery is to match the load demand at the desired LPSP with the preset allowable minimum battery SOC at the minimum cost of the system.

LPSP model was employed to find out the required PV material for SPD vacuum glazing switching.

Assumption for this model

- $1m^2$ SPD glazing is in switch on condition for 24 hours and 365 days. From chapter 5 it was found that this SPD glazing requires 0.4 W for $1m^2$ area of size.
- For simulation 0.34 m^2 PV area was considered number 1.
- High sizing ratio inverter and battery as mentioned in Chapter 6 is used in this model.

10.2.1. Solar radiation model

Perez model has been used in this work, details of this model has been discussed in Chapter 4.

10.2.2. PV modelling

There are one-diode (Walker 2001; Soto et.al. 2006) and two-diode models (Sah et. al. 1957, Zegaoui et.al. 2011) to evaluate the maximum power output from a PV cell. In case of two-diode model, the extra diode represents recombination carriers.

An equivalent circuit of a two-diode model (Ishaque.et. al. 2011) of PV device is shown in Figure 10-1 where both diode saturation currents were considered same in magnitude. K_i and K_v are the short circuit current and open circuit voltage coefficient, respectively. Diode ideality factor a_1 and a_2 represent the diffusion and recombination current components and both were considered to be 1 from Shockley's diffusion theory (Sah et al. 1957).

Here I_{pv} and I_0 are the photovoltaic and saturation current while equation 10-3 represents the thermal voltage.

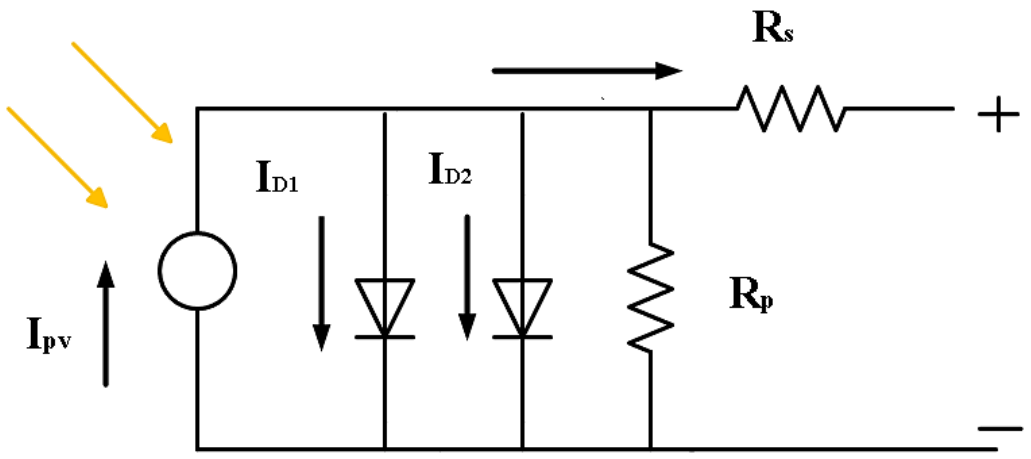

Figure 10-1: Equivalent circuit diagram of a two-diode model of PV cell

$$I = I_{PV} - I_{D1} - I_{D2} - I_P \qquad (10\text{-}1)$$

$$I = I_{PV} - I_{01}\left[\exp\left(\frac{V + IR_S}{a_1 V_{T1}}\right) - 1\right] - I_{02}\left[\exp\left(\frac{V + IR_S}{a_2 V_{T2}}\right)\right] - \left(\frac{V + IR_S}{R_P}\right) \qquad (10\text{-}2)$$

$$V_T = \frac{N_s KT}{q} \qquad (10\text{-}3)$$

$$I_0 = I_{01} = I_{02} = \frac{\left(I_{scn} + K_i\right)\Delta T}{\exp\left[\frac{V_{ocn} + K_v \Delta T}{a V_T}\right] - 1} \qquad (10\text{-}4)$$

$$I_{PV} = \left(I_{scn} + K_i\right)\frac{G}{G_n} \qquad (10\text{-}5)$$

10.2.3. Inverter output modelling

In some previous work, inverter was considered as a constant value. In real time operation, inverter efficiency actually varies as a function of an inverter input power (Peippo and Lund 1994).

$$P_{invout} = P_{inv,norm,out} P_{inv,rate} \qquad (10\text{-}6)$$

$$P_{inv,norm,out} = v_0 + v_1 P_{inv,norm,in} + v_2 P_{inv,norm,in}^2 \qquad (10\text{-}7)$$

$$P_{inv,norm,in} = \frac{P_{pv}}{P_{inv,rate}} \tag{10-8}$$

Instantaneous inverter efficiency

$$\eta_{inv} = \frac{P_{inv,norm,out}}{P_{inv,norm,in}} \tag{10-9}$$

Here P_{invout} is the inverter output, $P_{inv,norm,out}$ is the normalised inverter output, $P_{inv,rate}$ inverter rated input (DC), $P_{inv,norm,in}$ inverter normalised input, P_{pv} Is the inverter input from PV. v_0 is the normalized self-consumption loss, v_1 is the linear efficiency coefficient, v_2 is the coefficient for losses proportional to input power squared.

10.2.4. Battery model

For Lead acid battery storage, a nonlinear model was employed in this work (Joyesh et.al. 2001; Chen et.al. 2007).

$$V_b = \varepsilon_0 + \left(a \times SOC\right) + \left(R_{\text{int}} \times I_{bat}\right) \tag{10-10}$$

Here V_b is the battery voltage for one element is the battery equilibrium voltage, SOC is the state of charge of the battery, the parameter relates the voltage with the state of charge. For accurate calculation, knowledge of the SOC of a battery is necessary (Piller et.al. 2001). At the starting where SOC_0 is the battery SOC of the starting point; t0 and t are the time of the starting point and the time of interest, respectively, C_{bat} is the battery capacity, I_{bat} is the battery current. Equation 10-11 represents the battery SOC for ideal batteries.

$$SOC = SOC_0 + \int_{t_0}^{t} \frac{I_{bat}}{C_{bat}} d\tau \tag{10-11}$$

10.2.5. Loss of power supply probability (LPSP) model

In hybrid energy systems, for having a reliable system the concept of the loss of power supply probability (LPSP) should be regarded. LPSP is defined by a number between 0 and 1. LPSP of 1 means that the load will never be satisfied and the LPSP of 0 means that the load will be always satisfied. For a specified period T (1 year in this study), LPSP is defined by the following equation:

$$LPSP(t) = \frac{\sum_{t=1}^{T} LPS(t)}{\sum_{t=1}^{T} E_L(t)} \tag{10-12}$$

where LPS is the loss of power supply when the generated energy, EGen, is less than the load demand energy. Figure 10-2 shows the flow diagram of LPSP model.

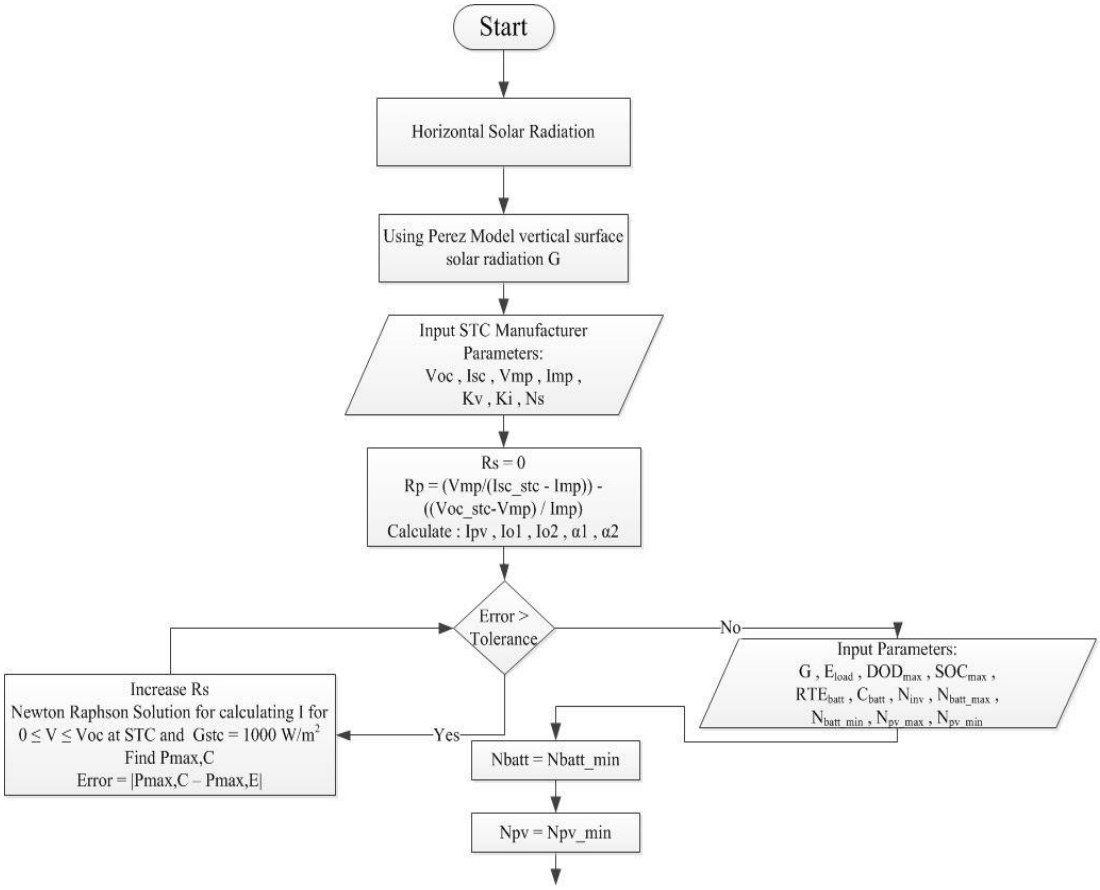

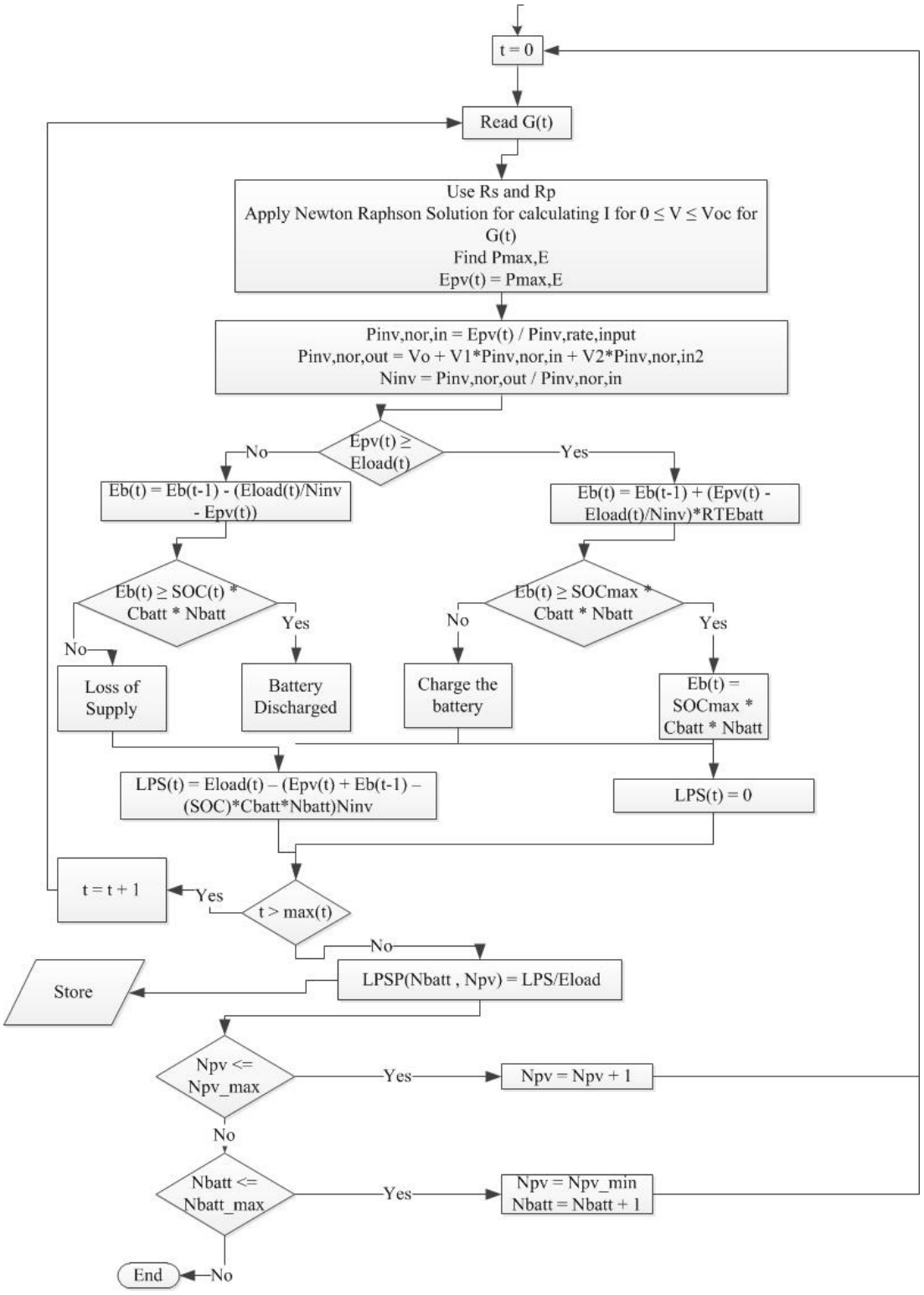

Figure 10-2: Flow diagram for LSPP model.

10.3. Results

10.3.1. Modelling validation results

10.3.1.1. Solar radiation

Solar radiation model was discussed in Chapter 4. Perez solar radiation model was used for this simulation.

10.3.1.2. PV output

To validate the PV power output result was compared with the 40 W PV power output from chapter 6. Measured south facing vertical solar radiation was employed as input. From the Figure it is clear that PV double diode PV model completely match with the experimental result.at 12:00 pm maximum PV output was 32.61 W by simulation and experimentally it was 32.28 W.

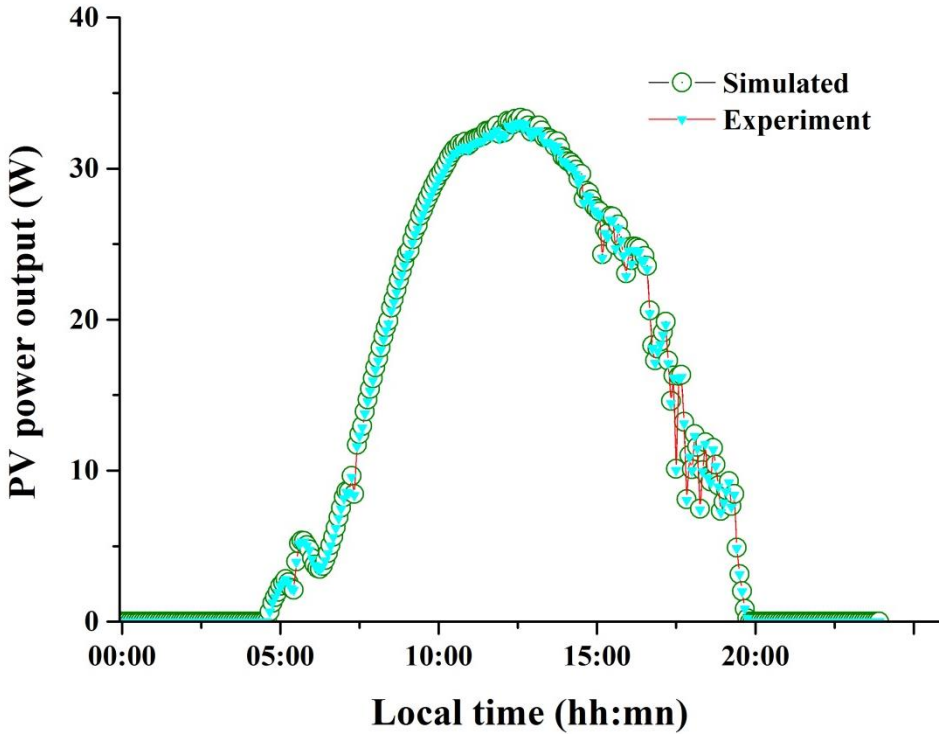

Figure 10-3: PV output power from simulation and experiment.

10.3.1.3. Inverter output

Output of PV power was used as an input in to the inverter. Using inverter equation simulated inverter output was achieved. These results were validated using data recorded from the experiment discussed in Chapter 6.

Maximum inverter output at 12:25 pm was 19.76 W by simulation and 19.25 W by experimentally. v_0,v_1,v_2 values were -0.05, 0.915,-0.15 respectively which offered the best fit .

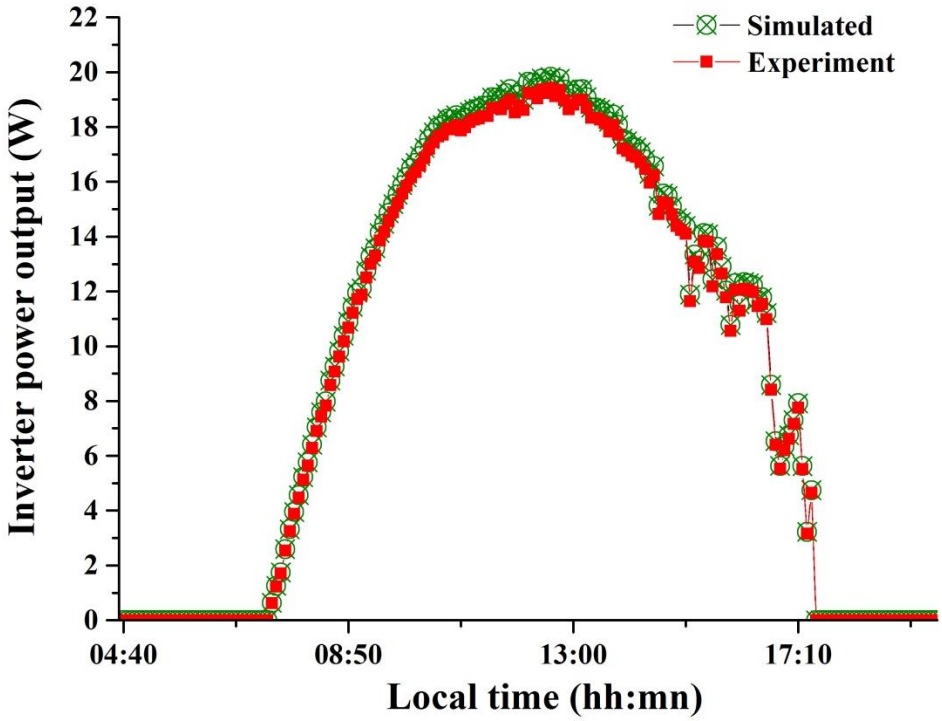

Figure 10-4: Inverter output from simulation and experiment.

10.4. LPSP results

Figure 10-5 illustrates the number of PV and battery combination for different LSPSP level. LPSP was shown to be high nearly 0.6 to 0.74, due to the poor performance of inverter. Inverter diurnal power output enhanced huge power losses.

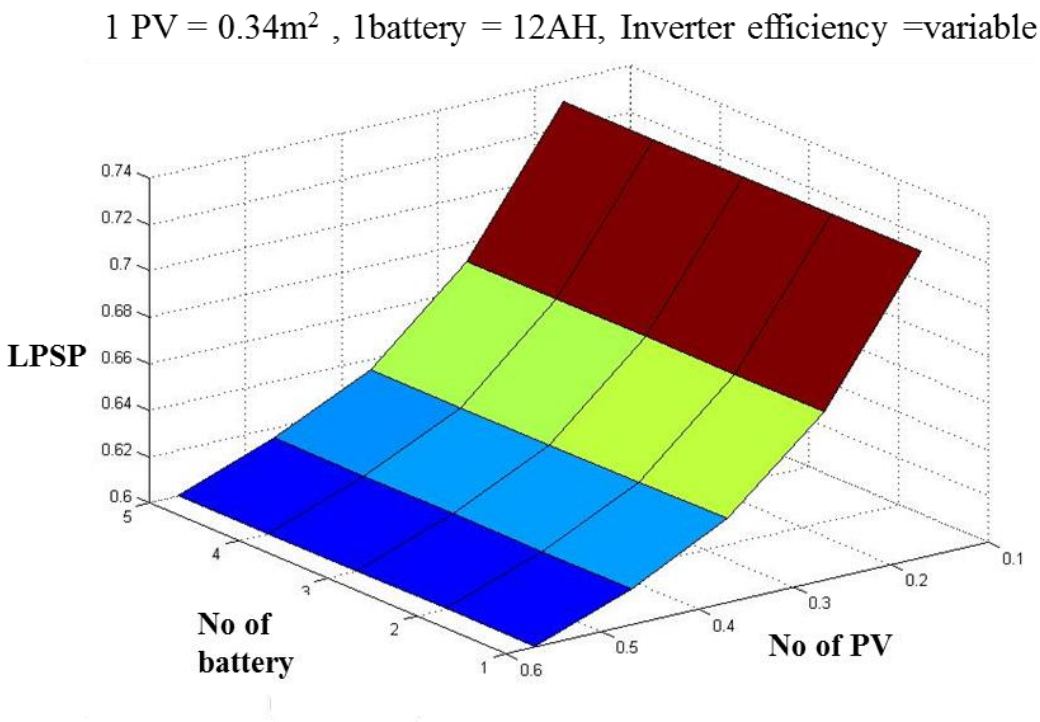

Figure 10-5: Variable LPSP values for different area of PV and different number of battery (variable inverter)

Figure 10-6 shows the PV and battery combination for different LPSP. Inverter was considered here having constant 90% efficiency. Constant efficiency inverter always provided higher output, which offered to fulfil the SPD glazing power requirement demand, and less LPSP was found. Compare to Figure 10-5 and Figure 10-6 number of PV and battery was equal though LPSP varied. This was due to inverter performance.

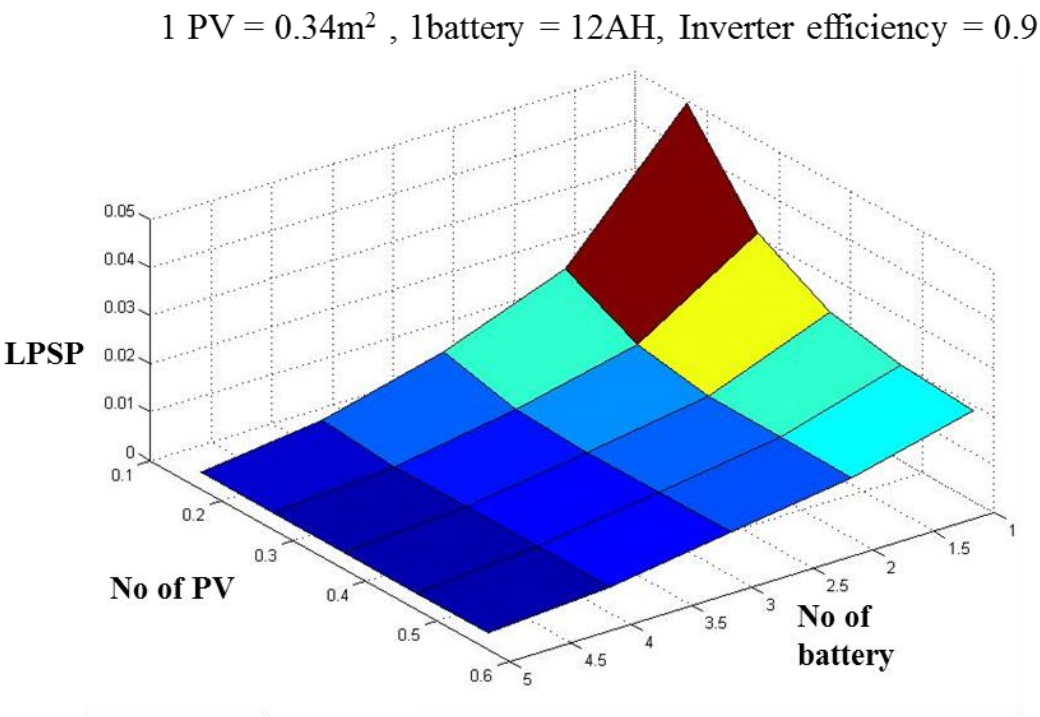

Figure 10-6: Variable LPSP values for different area of PV and different number of battery (constant inverter efficiency 90%)

Figure 10-7 illustrates the LPSP for 100% efficient inverter. Less difference was found between Figure 10-6 and Figure 10-7. Due to 100% efficient it can be considered that PV power output was applied directly to the SPD glazing as no losses was found. As SPD worked with only AC and 100% inverter efficiency is not possible, this glazing can be considered as DC powered glazing.

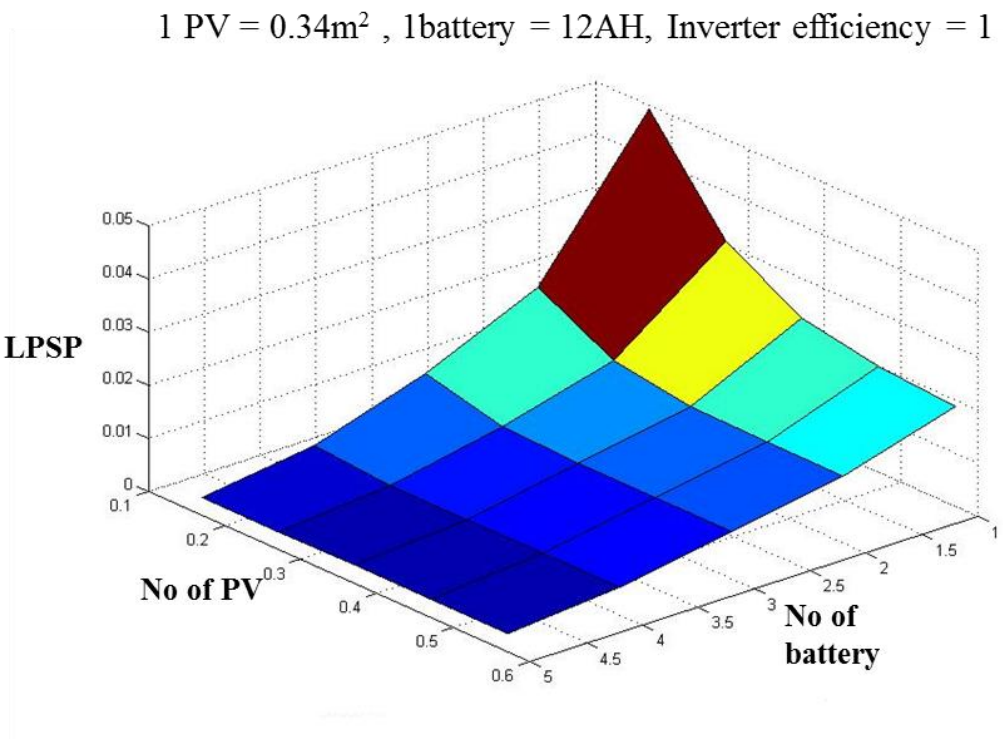

Figure 10-7: Variable LPSP values for different area of PV and different number of battery (constant inverter efficiency 100% or for DC glazing)

10.5. Cost of PV powered SPD glazing

A simple cost analysis was employed to understand the variation of total system cost for different LPSP level. Cost of different device is mentioned in Table 10-5.

Table 10-1: Cost of different device

Device	Cost
PV	550(€) for 0.34 m^2
Inverter	150 (€)
Battery	35 (€)
Glazing	100 (€)/1m^2

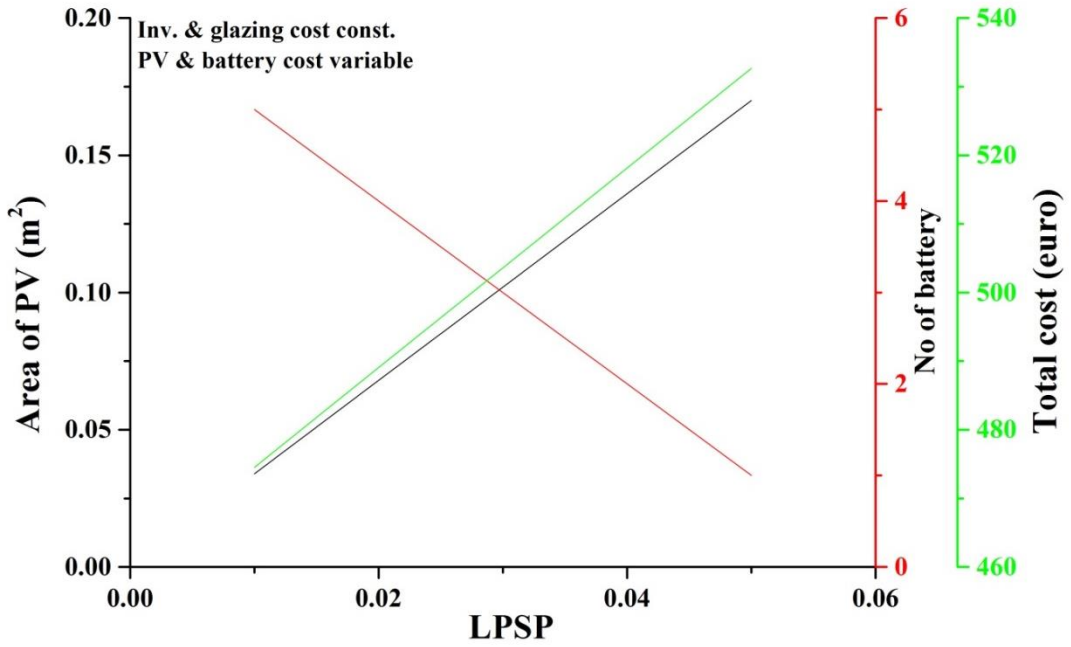

Figure 10-8: Variation of PV powered SPD glazing for different LPSP.

Figure 10-8 illustrates the variation of total cost based on different LPSP. To find out total cost only material cost has been included

$$\text{Cost}_{\text{total}} = C_{PV} + C_{bat} + C_{inv} + C_{glazing} \tag{10-13}$$

To achieve lower LPSP, lower PV device area and higher number of battery is essential. SPD was powered continuously only from PV during daytime and from battery device during night-time. Thus, higher PV device area is not able to reduce the losses but increase the total system cost.

10.6. Summary

PV powered switchable SPD-vacuum glazing can contribute to building for building energy consumption reduction. The LPSP method offered a variable method to determine the required PV area to keep the SPD glazing continuously switched on for all the year. As PV devices only generate electricity under sunlight, a battery storage system is an essential for operating this type of glazing over 24 hours.

Chapter 11. Conclusions and Recommendation for Future Work

11.1. Conclusions

Electrically actuated switchable glazing changes its transparency from opaque to transparent in the presence of applied power. Advantage of being electrically switchable over being non-electrically switchable is that the transparency can be changed based on building-occupant demand. Electrically switchable SPD glazing was evaluated in this project. Though electrically actuated electrochromic (EC) glazing has been researched for past 30 years, slow switching speed and low durability has made it less applicable commercially. SPD glazing has fast switching compared to EC glazing. SPD glazing was patented in 2001 and very few published works are available.

Prior to this research there had been no measurements for SPD glazing overall heat transfer coefficient, solar heat gain coefficient and glare control potential. As this glazing has potentially widespread use, measurements of all these parameters are a key contribution to knowledge enabling its inclusion in building design calculations. Combining SPD and vacuum glazing was also an unexplored area. Realising and characterising a self-powered SPD via the addition of a PV device is a new research initiated in this PhD.

Outdoor test cell experimental methodology was selected over indoor hotbox calorimeter as test cell offers a real time experimental facility. From the field measurement three main parameters, solar radiation, temperature and illuminance were recorded.

Using an one-dimensional semi empirical heat transfer model, it was found that SPD glazing has overall heat transfer coefficient (*U*-value) of 5.9 W/m^2K. This glazing can be considered as a switchable single glazing. To reduce the high *U*-value of SPD

glazing, a same area of double-glazing was attached with it. This combined switchable SPD double-glazing had a *U*-value of 2.9 W/m^{2}K. To reduce its *U* value further a vacuum glazing was attached. *U*-value of this combination was 1.14 W/m^{2}K. The conception realisation and characterisation of these combinations is totally original to this research.

Solar heat gain coefficients for SPD in a transparent state changed from 0.37 to 0.1 from midday period to afternoon time. Less change of SHGC was found for SPD in the opaque state, as direct solar radiation was not transmitted during SPD opaque state. This clearly indicates that SPD glazing can successfully control glare, which arises from direct solar radiation.

From daylighting experiment, the hypothesis was confirmed that SPD glazing can control interior illuminance and glare. SPD glazing has variable transmission for variable applied voltage. For a particular representative room configuration, SPD glazing with 30% transmission was found best for glare and maintained the DF at a required level.

PV powered SPD glazing experiment was promising candidate for autonomous electrically -actuated glazing. 0.03588 m^2 SPD glazing changes its transparency from 5% to 55% in the presence of 0.07 W PV power. As an SPD glazing requires an AC power supply, an inverter was connected between the PV panel and SPD glazing. Optimising the sizing ratio between the inverter and the PV is crucial as an inappropriately high sizing ratio gives low power output from PV-inverter combination.

Using field data of PV powered SPD, modelling was done to determine the PV material requirement to switch a 1 m^2 SPD glazing using LPSP method. The results showed that storage is essential to obtain continuous power for SPD battery energy.

To achieve less mismatch between generation and demand, battery storage and photovoltaic system sizes need to be co-optimised to ensure minimal total system cost.

Use of SPD glazing can mitigate global CO_2 emission. A 1 m^2 glazing in its opaque state over 1 year can save 1797.7 kg CO_2 from cooling load reductions and 150 kg of CO_2 from lighting energy saving. As this glazing requires very low power consumption to operate, only 4.8 kg CO_2 is generated over a year for continuous switching. It clearly indicates that this SPD glazing has potential to be an energy saving and decarbonizing glazing system. Results from daylighting and thermal experiment proved that SPD glazing is a strong candidate for adaptive façade application.

11.2. Recommendation for future work

- Using energy plus software with SPD and SPD vacuum glazing *U*-value and SHGC the potential building energy saving in various countries can be estimated.
- Two-dimensional (2d) and three-dimensional (3d) finite element heat transfer model can be established to validate the experimental results.
- A complete dynamic thermo-optical model can be established to find out thermal comfort for building occupants.
- For small-scale PV powered application, low power rated inverter need to be developed.

References

Ahern C., Griffiths P., O'Flaherty M., (2013), State of the Irish housing stock—Modelling the heat losses of Ireland's existing detached rural housing stock & estimating the benefit of thermal retrofit measures on this stock, Energy Policy, 55, 139–151

Ahmad J.A., Tiwari G.N., (2010), Estimation of luminous efficacy of daylight and illuminance for composite climate, International Journal of Energy and Environment, 1, 257-276

Ahn K.S., Yoo S.J., Kang M.S., Lee J.W., Sung Y.E., (2007), Tandem dye sensitized solar cell powered electrochromic devices for the photovoltaic powered smart window, Journal of Power Sources, 168, 533–536

Ahwide F., Spena A., El-Kafrawy A., (2013), Correlation for the average daily diffuse fraction with clearness index and estimation of beam solar radiation and possible sunshine hours fraction in Sabha, Ghdames and Tripoli – Libya, APCBEE Procedia, 5, 208 – 220

Alvarez G., Palacios M.J., Flores J.J., (2000), A test method to evaluate the thermal performance of window glazings, Applied Thermal Engineering, 20, 803-812

Aleo F., Pennisi A., Scalia S., Simone F., (2001), Optical and energetic performances of an electrochromic window tested in a ''PASSYS'' cell, Electrochimica Acta, 46, 2243–2249

Andersen M., Rubin M., Scartezzini J.L., (2003), Comparison between ray-tracing simulations and bi-directional transmission measurements on prismatic glazing, Solar Energy, 74, 157–173

Anjaneyulu Y., Yoon D.W., (1986), A PCGH Liquid crystal window to control solar energy, Solar Energy Materials, 14, 223-232

Aranda L.L., (2001), Silica Aerogel, IEEE, 20, 12-15

Arici M., Karabay H., (2010), Determination of optimum thickness of double-glazed windows for the climatic regions of Turkey, Energy and Building, 42, 1773–1778

Armstrong S., Hurley W.G., (2010), A thermal model for photovoltaic panels under varying atmospheric conditions, Applied Thermal Engineering, 30, 1488–1495

Arno S., Hans-Rainer H., (1996), The optical behavior of lyotropic liquid crystalline polymer gel networks: dependence on temperature, Advanced Material, 8, 408–411

Ashina S., Nakata T., (2008), Energy-efficiency strategy for CO_2 emissions in a residential sector in Japan, Applied Energy, 85, 101–114

Ashrit M.K., Girouard F.E., Truong V.V., (1996), Fabrication and testing of an all solid state system for smart window application, Sold State Ionics, 89, 65-73

Aste N., Tagliabue L.C., Del Pero C., Testa D., Fusco R., (2015), Performance analysis of a large-area luminescent solar concentrator module, Renewable Energy, 76, 330-337

ASTM C1199-00 Standard, Test Method for Measuring the Steady-State Thermal Transmittance of Fenestration Systems Using Hot Box Methods

ASTM C518-04 Standard, Test Method for Steady-State Thermal Transmission Properties by Means of the Heat Flow Meter Apparatus

Atif M.R., Galasiu A.D., (2003), Energy performance of daylight-linked automatic lighting control systems in large atrium spaces: report on two field-monitored case studies, Energy and Buildings, 35, 441–461

Australian Energy Market Operator (AEMO), 2014. Carbon Dioxide Equivalent Intensity Index [Online]. Available at: http://www.sciencedirect.com/science?_ob=DownloadURL&_method=finish&_eidkey=1-s2.0S0301421513007398&count=1&_docType=FLA&md5=8959fea5e228d3f59139f9f67d8cd7b9〉 (accessed 11.10.14).

Aydin O., (2000), Determination of optimum air-layer thickness in double-pane windows, Energy and Buildings, 32, 303–308

Aydin O., (2006), Conjugate heat transfer analysis of double pane windows, Building and Environment, 41, 109–116

Ayodele T.R., Ogunjuyigbe A.S.O., (2015), Prediction of monthly average global solar radiation based on statistical distribution of clearness index, Energy, 90, 1733–1742

Baetens R., Jelle B.P., Gustavsen A., (2010), Properties, requirements and possibilities of smart windows for dynamic daylight and solar energy control in buildings: A state-of-the-art review, Solar Energy Materials & Solar Cells, 94, 87–105

Baetens R., Jelle B.P., Gustavsen A., (2010), Phase change materials for building applications: A state-of-the-art review, Energy and Buildings, 42, 1361–1368

Bahaj A.S., James P.A.B., Jentsch M.F., (2008), Potential of emerging glazing technologies for highly glazed buildings in hot arid climates, Energy and Buildings, 40, 720–731

Baig H., Sellami N., Mallick T.K., (2015), Performance modeling and testing of a Building Integrated Concentrating Photovoltaic (BICPV) system, Solar Energy Materials & Solar Cells, 134, 29–44

Baker P.H., McEvoy M., (2000), Test cell analysis of the use of a supply air window as a passive solar component, Solar Energy, 69, 113–130

Baker N., Fanchiotti A., Steemers K., (1993), Light and Human Requirements, Daylighting in Architecture, James & James for the Commission of the European Communities, Brussels

Borowy B.S., Salameh Z.M., (1996), Methodology for optimally sizing the combination of a battery bank and PV array in a wind/PV hybrid system, IEEE Transaction on Energy Conversion, 11, 367–375

Bakelli Y., Arab H.A., Azoui B., (2011), Optimal sizing of photovoltaic pumping system with water tank storage using LPSP concept, Solar Energy, 85, 288–294

Baker N., Pande A., Ander G., Melnyk J., (2004), Effectiveness of photocontrols with skylighting, 1-18

Baker P.H., McEvoy M., (2000), Test cell analysis of the use of a supply air window as a passive solar component, Solar Energy, 69, 113–130

Baker P.H., van Dijk H.A.L., (2008), PASLINK and dynamic outdoor testing of building components, Building and Environment, 43, 143–151

Balaras C.A., Droutsa K., Argiriou A.A., Asimakopoulos D.N., (2000), Potential for energy saving in apartment buildings, Energy and Buildings, 31, 143–154

Band Y.B., (2010), Light and Matter: Electromagnetism, Optics, Spectroscopy and Lasers. John Wiley & Sons

Barnham K.W.J., Marques J.L., Hassard J., O'Brien P., (2000), Quantum dots concentrator and thermodynamic model for the global red shift, Applied Physical Letters, 76, 1197-1199

Barrios D., Vergaz R., Pena J.M.S.N., Granqvist C.G., Niklasson G.A., (2013), Toward a quantitative model for suspended particle devices: optical scattering and absorption coefficients, Solar Energy Materials & Solar Cells, 111, 115–122

Barrios D., Vergaz R., Pena J.M.S.N., Cámara B.G., Granqvist C.G., Niklasson GA., (2015), Simulation of the thickness dependence of the optical properties of suspended particle devices, Solar Energy Materials & Solar Cells, 143, 613-622

Batchelder J.S., Zewail A.H., Cole T., (1979), Luminescent solar concentrators Part 1 Theory of operation and techniques for performance evaluation, Applied Optics, 18, 3090–3110

Bechinger C., Ferrere S., Zaban A., Sprague J., Gregg B.A., (1996), Photoelectrochromic windows and displays, Nature, 383, 608–610

Benson D.K., Branz H.M., (1995), Design goals and challenges for a photovoltaic powered electrochromic window covering, Solar Energy Material & Solar Cells, 39, 203–211

Bird R.E., Hulstrom R.L., (1983), Terrestrial solar spectral data sets, Solar Energy, 30, 563-573

Bodart M., De Herde A., (2002), Global energy savings in offices buildings by the use of daylighting, Energy and Buildings, 34, 421–429

Borowy B.S., Salameh Z.M., (1996), Methodology for optimally sizing the combination of a battery bank and PV array in a wind/PV hybrid system, IEEE Transaction on Energy Conversion, 11, 367–375

Boubekri M., Boyer L.L., (1992), Effect of window size and sunlight presence on glare, Lighting Research and Technology, 24, 69-73

Boyce P., Beckstead J., (1991), Influences on discomfort glare ratings, in: Proceedings of the 1st International Symposium on Glare, Lighting Research Institute, Orlando, FL, 93-100

Branz H.M., Crandall R.S., Tracy C.E., (1994), US Patent 5,377,037: Electrochromic-Photovoltaic Film for Light-Sensitive Control of Optical Transmittance

Bullock J.N., Bechinger C., Benson D.K., Branz H.M., (1996), Semi-transparent a-Si C:H solar cells for self-powered photovoltaic-electrochromic devices, Journal of Non-Crystalline Solid, 198–200, 1163–1167

Bülow-Hübe H., (2001), Energy-efficient window systems: effects on energy use and daylight in buildings, PhD thesis, Division of Energy and Building Design, Department of Construction and Architecture, Lund University, Lund (Sweden)

Bülow-Hübe H., (1995), Subjective reactions to daylight in rooms: effect of using low-emittance coatings on windows, Lighting Research and Technology, 27, 37–44

Buratti C., Moretti E., (2012), Experimental performance evaluation of aerogel glazing systems, Applied Energy, 97, 430–437

Buratti C., Moretti E., (2012), Glazing systems with silica aerogel for energy savings in buildings, Applied Energy, 98, 396–402

Bodart M., Herde A.D., (2002), Global energy savings in offices buildings by the use of daylighting, Energy and Buildings, 34, 421–429

Borowy B.S., Salameh Z.M., (1996), Methodology for optimally sizing the combination of a battery bank and PV array in a wind/PV hybrid system, IEEE Transaction on Energy Conversion, 11, 367‑375

Brandemuehl, M.J., Beckman, W.A., (1980), Transmission of diffuse radiation through CPC and flat-plate collector glazings, Solar Energy, 24, 511–513

Brophy V., Clinch J.P., Convery F., Healy J., King C., Lewis J.O., (1999), Homes for the 21st Century: Energy Action

Browne M.C., Norton B., McCormack S.J., (2015), Phase change materials for photovoltaic thermal management, Renewable and Sustainable Energy Reviews, 47, 762–782

Cabeza L.F., Rincón L., Vilariño V., Pérez G., Castell A., (2014), Life cycle assessment (LCA) and life cycle energy analysis (LCEA) of buildings and the building sector: A review, Renewable and Sustainable Energy Reviews, 29, 394–416

Carmody J., Selkowitz S., Heshong L., (1996), Residential Windows: A guide to new technology and energy performance, 1st ed, NY, USA, 214

Carroll J.J., (1985), Global transmissivity and diffuse fraction of solar radiation for clear and cloudy skies as measured and as predicted by bulk transmissivity models, Solar Energy, 35, 105-118

Cesaratto P.G., Carli M.D., (2013), A measuring campaign of thermal conductance in situ and possible impacts on net energy demand in buildings, Energy Building, 59, 29–36

Chae Y.T., Kim J., Park H., Shin B., (2014), Building energy performance evaluation of building integrated photovoltaic (BIPV) window with semi-transparent solar cells, Applied Energy, 129, 217–227

Chakrapani S., Slovak S.M., Saxe R.L., Fanning B., (2002), SPD films and light valves comprising same, U.S. Patent No.6416827

Chan C.C., Hsu W.C., Chang C.C., Hsu C.S., (2010), Preparation and characterization of gasochromic Pt/WO_3 hydrogen sensor by using the Taguchi design method, Sensors and Actuators B: Chemical, 145, 691–697

Chandrasekhar Y.S., (1992), Liquid Crystals, Cambridge University Press

Chang C.Y., Chen P.K., (2005), Human response to window views and indoor plants in the workplace, Hort Science, 40, 1354–1359

Charron R., Athienitis A.K., (2006), Optimization of the performance of double-facades with integrated photovoltaic panels and motorized blinds, Solar Energy, 80, 482–491

Chau J.L.H., Chen R.T., Hwang G.L., Tsai P.Y., Lin C.C., (2010), Transparent solar cell window module, Solar Energy Materials & Solar Cells, 94, 588-591

Chauvel P., Collins J.B., Dogniaux R., Longniore J., (1980), Glare from windows: current views of the problem, in: Proceedings of the Symposium on Daylight, Commission Internationale de l'Eclairage, Berlin, Germany, 294-302

Chauvel P., Collins J.B., Dogniaux R., Longmore J., (1982), Glare from windows: current view of problem, Lighting Research and Technology, 14, 31–46

Chel A., Tiwari G.N., Chandra A., (2009), A model for estimation of daylight factor for skylight: An experimental validation using pyramid shape skylight over vault roof mud-house in New Delhi (India), Applied Energy, 86, 2507–2519

Chel A., Tiwari G.N., (2010), Stand-alone photovoltaic (PV) integrated with earth to air heat exchanger (EAHE) for space heating/cooling of adobe house in New Delhi (India), Energy Conversion and Management, 51, 393–409

Chemisana D., (2011), Building Integrated Concentrating Photovoltaics: A review, Renewable and Sustainable Energy Reviews, 15, 603–611

Chen F.,Wittkopf S.K., Ng P.K., Du H., (2012), Solar heat gain coefficient measurement of semi-transparent photovoltaic modules with indoor calorimetric hot box and solar simulator Energy and Buildings, 53, 74–84

Chen H.C., Jan D.J., Chen C.H., Huang K.T., (2013), Bond and electrochromic properties of WO_3 films deposited with horizontal DC, pulsed DC and RF sputtering, Electrochimica Acta, 93, 307– 313

Cheng J., Boyd G.D., (1982), Reduction of threshold voltage for bistable liquid crystal switching using a priming voltage, IEEE Transactions on Electron Devices, 29, 1853-1856

Cheng V., Ng E., Givoni B., (2005), Effect of envelope colour and thermal mass on indoor temperatures in hot humid climate, Solar Energy, 78, 528–534

Chiba K., Takahashi T., Kageyama T., Oda H., (2005), Low-emissivity coating of amorphous diamond-like carbon/Ag-alloy multilayer on glass, Applied Surface Science, 246, 48–51

Chow K.K., Fong K.F., He W., Lin Z., Chan A.L.S., (2007), Performance evaluation of a PV ventilated window applying to office building of Hong Kong, Energy and Buildings, 39, 643–650

Chow T.T., Qiu Z., Li C., (2009), Potential application of ‘‘see-through’’ solar cells in ventilated glazing in Hong Kong, Solar Energy Materials & Solar Cells, 93, 230–238

Chow T.T., Li C., Lin Z., (2011a), The function of solar absorbing window as water-heating device, Building and Environment, 46, 955-960

Chow T.T., Li C., Lin Z., (2010), Innovative solar windows for cooling-demand climate, Solar Energy Materials & Solar Cells, 94, 212–220

Chow T.T., Li C., Lin Z., (2011b), Thermal characteristics of water-flow double-pane window, International Journal of Thermal Sciences, 50, 140-148

Chow T.T., Li C., (2013), Liquid-filled solar glazing design for buoyant water-flow, Building and Environment, 60, 45-55

Chung T.M., (1992), A study of luminous efficacy of daylight in Hong Kong, Energy and Buildings, 19, 45–50

Clancy J.M., Gaffney F., Deane J.P., Curtis J., Ó Gallachóir B.P., (2015), Fossil fuel and CO_2 emissions savings on a high renewable electricity system – A single year case study for Ireland, Energy Policy, 83, 151–164

Clift R., (2007), Climate change and energy policy: the importance of sustainability arguments, Energy, 32, 262–268

Cogan S.F., Rauh R.D., Nguyen N.M., Plante T.D., (1996), Stability and switching of Li-based electrochromic coatings, Presented at IME-2, San Diego, CA, 30 September–2 October

Collares-Pereira M., Rabl A., (1979), Correlations between diffuse and hemispherical and between daily and hourly insolation values, Solar Energy, 22, 155-164

Colclough S.M., Griffiths P.W., Hewitt N.J., (2011), A year in the life of a passive house with solar energy store, ICSES Energy Storage Conference, Belfast, UK

Collins R., Robinson S.J., (1991), Evacuated glazing, Solar Energy, 47, 27-38

Collins R.E., Cripps A.C.F., Tang J.Z., (1992), Transparent evacuated insulation, Solar Energy, 49, 333

Collins R.E., Davis C.A., Dey C.J., Robinson S.J., Tang J.Z., Turner G.M., (1993), Measurement of local heat flow in flat evacuated glazing, International Journal of Heat and Mass Transfer, 36, 2553–2563

Collins R.E, Simko T.M., (1998), Current status of the science and technology of vacuum glazing, Solar Energy, 62, 189-213

Collins R.E., Turner G.M., Fischer–crips A.C., Tang J.Z., Simko T.M., Dey C. J., Clugston D. A., Zhang Q.C., Garrison J.D., (1995), Vacuum glazing- a new component for insulating windows, Building and Environment, 30, 459-492

Collings P.J., Hird M., (2004), Introduction to liquid crystals, London, Taylor & Francis

Copppolino S., (1990), A new model for estimating diffuse solar radiation in Italy from clearness index and minimum air mass, Solar & Wind Technology, 7, 549-553

Cupelli D., Nicoletta F.P., Manfredi S., DeFilpo G., Chidichimo G., (2009), Electrically switchable chromogenic materials for external glazing, Solar Energy Materials & Solar Cells, 93, 329–333

Cupelli D., Nicoletta F.P., Manfredi S., Vivacqua M., Formoso P., DeFilpo G., Chidichimo G., (2009), Self-adjusting smart windows based on polymer-dispersed liquid crystals, Solar Energy Materials & Solar Cells, 93, 2008–2012

Coates D., Crossland W.A., Morrissy J.H., Needham B., (1978), Electrically induced scattering textures in smectic A phases and their electrical reversal, Journal of Applied Physics D, 11, 2025–2034

Daneshyar M., (1978), Solar radiation statistics for Iran, Solar Energy, 21, 345–349

Davidsson H., Perers B., Karlsson B., (2010), Performance of a multifunctional PV/T hybrid solar window, Solar Energy, 84, 365–372

Davidsson H., Perers B., Karlsson B., (2012), System analysis of a multifunctional PV/T hybrid solar window, Solar Energy, 86, 903–910

Daly D., Cooper P., Ma Z., (2014), Implications of global warming for commercial building retrofitting in Australian cities, Building and Environment, 74, 86-95

Deb S.K., (1969), Applied optics, Supply 3 on electrophotography, 192-195

Deb S.K., Lee S.H., Tracy C.E., Pitts J.R., Gregg B.A., Branz H.M., (2001), Standalone photovoltaic powered electrochromic smart window, Electrochimica Acta, 46, 2125–2130

DeBerry D.W., Viehbeck A., (1983), Photoelectrochromic behaviour of Prussian blue modified TiO_2 electrodes, Journal of Electrochemical Society, 130, 249–251

De Gennes P.G., Prost J., (1995), The physics of liquid crystals, Oxford University Press

Del Re M., Gouttebaron R., Dauchot J.P., Hecq M., (2004), Study of the optical properties of AlN/ZrN/AlN low-e coating, Surface Coating Technology, 180–181, 488–495

DeForest N., Shehabi A., Garcia G., Greenblatt J., Masanet E., Lee E.S., Selkowitz S., Milliron D.J., (2013), Regional performance targets for transparent near-infrared switching electrochromic window glazings, Building and Environment, 61, 160-168

DeForest N., Shehabi A., O'Donnell J., Garcia G., Greenblatt J., Lee E.S., Selkowitz S., Milliron D.J., (2015), United States energy and CO_2 savings potential from deployment of near-infrared electrochromic window glazings, Building and Environment, 89, 107-117

Deng S., Wang R.Z., Dai Y.J., (2014), How to evaluate performance of net zero energy building - A literature research, Energy, 71, 1-16

Diaf S., Diaf D., Belhamel M., Haddadi M., Louche A., (2007), A methodology for optimal sizing of autonomous hybrid PV/wind system, Energy Policy, 35, 5708–5718

Didoné E.L., Wagner A., (2013), Semi-transparent PV windows: A study for office buildings in Brazil, Energy and Buildings, 67, 136–142

Dorcheh A.S., Abbasi M.H., (2008), Silica aerogel synthesis, properties and characterization, Journal of Materials Processing Technology, 199, 10–26

Duer K., Svendsens S., (1998), Monolithic silica aerogel in super insulating glazings, Solar Energy, 63, 259–267

Duffie J.A., Beckman W.A., (2013), Solar Engineering of Thermal Processes (fourth ed.)Wiley, New York

Dyer A.L., Bulloch R.H., Zhou Y., Kippelen B., Reynolds J.R., Zhang F., (2014), A vertically integrated solar-powered electrochromic window for energy efficient buildings, Advanced Materials, 26, 4895-4900

Dimitrov I., Trzebicka B., Muller A.H.E., Dworak A., Tsvetanov C.B., (2007), Thermosensitive water-soluble copolymers with doubly responsive reversibly interacting entities, Progress in Polymer Science, 32, 1275–1343

Eames P.C., (2008), Vacuum glazing: current performance and future prospects, Vacuum, 82, 717–722

Einhorn H.D., (1969), A new method for the assessment of discomfort glare, Lighting Research and Technology, 1, 235–247

Einhorn H.D., (1979), Discomfort glare: a formula to bridge differences, Lighting Research and Technology, 11, 90–94

EIA., (2011), Voluntary Reporting of Greenhouse Gases Program Fuel Carbon Dioxide Emission Coefficients, http://205.254.135.7/oiaf/1605/coefficients.html [accessed 20.05.14]

Erbs D.G., Klein S.A., Duffie J.A., (1982), Estimation of the diffuse radiation fraction for hourly, daily and monthly-average global radiation, Solar Energy, 28, 293–302

Eriksson T.S., Granqvist C.G., Karlsson J., (1987), Transparent thermal insulation with infrared-absorbing gases, Solar Energy Materials, 16, 243-253

European Commission, (2011), A Roadmap for moving to a competitive low carbon economy in 2050

European Commission, (2014), Communication from the Commission to the European Parliament, the Council, the European Economic and Social Committee and the Committee of the Regions – A policy framework for climate and energy in the period from 2020 to 2030. Brussels, 22/1/ 2014. (available at: Retrieved from http://ec.europa.eu/ clima/policies/2030/documentation_en.htm).

European Standard EN410, Glass in building – Determination of luminous and solar characteristics of glazing (1998)

Fang Y., Eames P.C., Norton B., (2000), Influence of insolation level and glass thickness on the thermal performance of evacuated glazing, In: Proceedings World Renewable Energy Congress VI (WREC 2000), Brighton, UK, 1878–1881

Fang Y., Eames P.C., Hyde T.J., Norton B., (2005), Complex multimaterial insulating frames for windows with evacuated glazing, Solar Energy, 79, 245-261

Fang Y., Eames P.C., Norton B., Hyde T.J., (2006), Experimental validation of numerical model for heat transfer in vacuum glazing, Solar Energy, 80, 564-577

Fang Y., Hyde T.J., Hewitt N., (2010), Predicted thermal performance of triple vacuum glazing, Solar Energy, 84, 2132-2139

Fang Y., Eames P C., (2006), Thermal performance of an electrochromic vacuum glazing, Energy Conversion and Management, 47, 3602–3610

Fang Y., Eames P. C., (2006), The effect of glass coating emittance and frame rebate on heat transfer through vacuum and electrochromic vacuum glazed windows, Solar Energy Materials & Solar Cells, 90, 2683–2695

Fang Y., Eames P.C., Norton B., Hyde T., Huang Y., Hewitt N., (2008), The thermal performance of an electrochromic vacuum glazing with selected low-emittance coatings, Thin Solid Films, 516, 1074–1081

Fang Y., Eames P.C., Norton B., (2007), Effect of glass thickness on the thermal performance of evacuated glazing, Solar Energy, 81, 395-404

Fang Y., Hyde T., Eames P.C., Hewitt N., (2009a), Theoretical and experimental analysis of the vacuum pressure in a vacuum glazing after extreme thermal cycling, Solar Energy, 83, 1723–1730

Fang Y., Hyde T., Hewitt N., Eames P.C., Norton B., (2009b), Comparison of vacuum glazing thermal performance predicted using two- and three-dimensional models and their experimental validation, Solar Energy Materials and Solar Cells, 93, 1492–1498

Fang Y., Hyde T., Hewitt N., Eames P.C., Norton B., (2010), Thermal performance analysis of an electrochromic vacuum glazing with low emittance coatings, Solar Energy, 84, 516–525

Fang Y., Hyde T.J., Hewitt N., (2010), Predicted thermal performance of triple vacuum glazing, Solar Energy, 84, 2132-2139

Fang Y., Hyde T.J., Arya F., Hewitt N., Wang R., Dai Y., (2015), Enhancing the thermal performance of triple vacuum glazing with low-emittance coatings, Energy and Buildings, 97, 186–195

Farret F.A., Simoes M.G., (2006), Integration of Alternative Energy Sources of Energy, John Wiley & Sons, Hoboken

Fernandes L.L., Lee E.S., Ward G., (2013), Lighting energy savings potential of split-pane electrochromic windows controlled for daylighting with visual comfort, Energy and Buildings, 61, 8–20

Fuls E.N., Hensler D.H., Ross D.H., (1967), Reactively sputtered vanadium dioxide thin films, Applied Physics Letter, 10, 199

Fung T.Y.Y., Yang H., (2008), Study on thermal performance of semi-transparent building-integrated photovoltaic glazings, Energy and Buildings, 40, 341–350

Fischer-Cripps A.C., Collins R.E., Turner G.M., Bezzel E., (1995), Stresses and fracture probability in evacuated glazing, Building and Environment, 30, 41–59

Gao W., Liu P., Crandall R.S., Lee S.H., Benson D.K., (2000), Approaches for large area a-Si C:H photovoltaic-powered electrochromic window coatings, Journal of Non-Crystalline Solids, 266–269, 1140–1144

Gao W., Lee S. H., Bullock J., Xu Y., Benson D. K., Morrison S., Branz H.M., (1999), First a-Si C:H photovoltaic powered monolithic tandem electrochromic smart window device, Solar Energy Materials & Solar Cells, 59, 243–254

Gardiner D.J., Morris S.M., Coles H.J., (2009), High-efficiency multistable switchable glazing using smectic A liquid crystals, Solar Energy Materials & Solar Cells, 93, 301–306

Georg A., Georg A., (2009), Electrochromic device with a redox electrolyte, Solar Energy Materials & Solar Cells, 93, 1329–1337

Georg A., Graf W., Neumann R., Wittwer V., (2000), Mechanism of the gasochromic coloration of porous WO_3 films, Solid State Ionics, 127, 319-328

Georg A., Graf W., Schweiger D., Wittwer V., Nitz P., Wilson H.R., (1998), switchable glazing with a large dynamic range in total solar energy transmittance (TEST), Solar Energy, 62, 215-228

Georg A., Georg A., Graf W., Wittwer V., (2008), Switchable windows with tungsten oxide, Vacuum, 82, 730- 735

Georg A., Graf W., Neumann R., Wittwer V., (2001), The role of water in gasochromic WO_3 films, Thin Solid Films, 384, 269 -275

Georg A., Graf W., Neumann R., Wittwer V., (2000), Stability of gasochromic WO_3 films, Solar Energy Materials & Solar Cells, 63, 165-176

Ghosal M.K., Tiwari G.N., Srivastava N.S.L., (2004), Thermal modelling of a greenhouse with an integrated earth to air heat exchanger: an experimental validation, Energy and Buildings, 36, 219–227

Gladen A.C., Davidson J.H., Mantell S.C., (2014), Selection of thermotropic materials for overheat protection of polymer absorbers, Solar Energy, 104, 42–51

Goetzberger A., (1978), Fluorescent solar collector: operating condition with diffuse light, Applied Physics, 16, 399-404

Goetzberger A., Wittwer V., (1979), Fluorescent planar collector concentrators for solar energy conversion, Festkorperprobleme, XIX, 427–450

Goetzberger A., Greubel W., (1977), Solar energy conversion with fluorescent collectors, Applied Physics, 14, 123-139

Goetzberger A., Heidler K., Wittwer V., Zastrow A., Baur G., Sah E., (1979), in Proceedings, Second E. C. Photovoltaic Solar Energy Conference, Berlin, 515

Goia F., (2012), Thermo-physical behaviour and energy performance assessment of PCM glazing system configurations: A numerical analysis, Frontiers of Architectural Research, 1, 341–347

Goia F., Zinzi M., Carnielo E., Serra V., (2015), Spectral and angular solar properties of a PCM-filled double glazing unit, Energy and Buildings, 87, 302–312

Goia F., Perino M., Serra V., (2014), Experimental analysis of the energy performance of a full-scale PCM glazing prototype, Solar Energy, 100, 217–233

Goia F., Perino M., Serra V., (2013), Improving thermal comfort conditions by means of PCM glazing systems, Energy and Buildings, 60, 442–452

Goldner L.B., Rauh D.R., (1984) Electrochromic materials for controlled radiant energy transfer in buildings, Solar Energy Materials, 11, 177-185

Goldner R.B., Chapman R.L., Foley G., Goldner E.L., Haas T., Norton P., Seward G., Wonger K.K., (1986), Recent research related to the development of electrochromic windows, Solar Energy Materials, 14, 195-203

Gopinathan K.K., (1988), Computing the monthly mean daily diffuse radiation from clearness index and percent possible sunshine, Solar Energy, 41, 379–385

Granqvist C.G., (1995), Handbook of Inorganic Electrochromic Materials Elsevier, Amsterdam

Granqvist C.G., (2000), Electrochromic tungsten oxide films: Review of progress 1993-1998, Solar Energy Materials & Solar Cells, 60, 201- 262

Granqvist C.G., (2005), Electrochromic devices, Journal of the European Ceramic Society, 25, 2907–2912

Granqvist C.G., Green S., Niklasson G.A., Mlyuka N.R., Kræmer S. V., Georén P., (2010), Advances in chromogenic materials and devices, Thin Solid Films, 518, 3046–3053

Granqvist C.G., (2012), Oxide electrochromics: An introduction to devices and materials, Solar Energy Materials & Solar Cells, 99, 1–13

Granqvist C.G., Avendan E, Azens A., (2003), Electrochromic coatings and devices: survey of some recent advances, Thin Solid Films, 442, 201–211

Granqvist C.G., Wittwer V., (1998), Materials for solar energy conversion: An overview, Solar Energy Materials & Solar Cells, 54, 39-48

Gratia E., Herde A.D., (2003), Design of low energy office building, Energy and Buildings, 35, 475-491

Griessen R., Huiberts J.N., Kremers M., Van Gogh A.T.M., Koeman N.J., Dekker J.P., Notten P.H.L., (1997), Yttrium and lanthanum hydride films with switchable optical properties, Journal of Alloys and Compounds, 253–254, 44

Griffiths P.W., Leo Di. M., Cartwright P., Eames P.C., Yianoulis P., Leftheriotis G., Norton B., (1998), Fabrication of evacuated glazing at low temperature, Solar Energy, 63, 243–249

Griffiths P.W., Eames P.C., Hyde T.J., Fang Y., Norton B., (2006), Experimental characterization and detailed performance prediction of a vacuum glazing system fabricated with a low temperature metal edge seal, using a validated computer model, Journal of Solar Energy Engineering Transactions of ASME, 128, 199–203

Grimmer D.P., McFarlan R.D., Balcomb J.D., (1979), Initial experimental tests on the use of small passive-solar test-boxes to model the thermal performance of passively solar-heated building designs, Solar Energy, 22, 351‑354

Gueymard C., DuPont W., (2009), Spectral effects on the transmittance, solar heat gain, and performance rating of glazing systems, Solar Energy, 83, 940–953

Guth S.K., (1966), Outline of a standard procedure for computing visual comfort ratings for interior lighting, Illuminating Engineering, 61, 634–642

Hahne E., Pfluger R., (1996), Improvements on PASSYS test cell, Solar Energy, 58, 239-246

Hale J.S., Woollam J.A., (1999), Prospects for IR emissivity control using electrochromic structures, Thin Solid Films, 339, 174-180

Hammarberg E., Roos A., (2003), Antireflection treatment of low-emitting glazings for energy efficient windows with high visible transmittance, Thin Solid Films, 442, 222–226

Han J., Lu L., Yang H., (2009), Thermal behaviour of a novel type see-through glazing system with integrated PV cells, Building and Environment, 44, 2129–2136

Han J., Lu L., Yang H., (2010), Numerical evaluation of the mixed convective heat transfer in a double-pane window integrated with see-through a-Si PV cells with low-e coatings, Applied Energy, 87, 3431–3437

Han J., Lu L., Peng J., Yang H., (2013), Performance of ventilated double-sided PV façade compared with conventional clear glass façade, Energy Building, 56, 204–209

Hara K., Uwasu M., Kishita Y., Takeda H., (2015), Determinant factors of residential consumption and perception of energy conservation: Time-series analysis by large-scale questionnaire in Suita, Japan, Energy Policy, 87, 240–249

Harrison S.J., Dubrous F.M., (1992), Uncertainties in the evaluation of window SHGC and U-values measured using an indoor solar simulator facility, ASHRAE Transactions, 98, 638–645

Harrison S.J., Wonderen S.J.V., (1994), A test method for the determination of window solar heat gain coefficient, ASHRAE Transactions, 100, 1057–1064

Hartmann J., Rubin M., Arasteh D., (1987), Thermal and solar optical properties of silica aerogel for use in insulated window, 12th Annual Passive Solar conference, Portland, July, 12-16

Harrestrup M., Svendsen S., (2015), Full-scale test of an old heritage multi-storey building undergoing energy retrofitting with focus on internal insulation and moisture, Building and Environment, 85, 123-133

Hay J.E., Davies J.A., (1980), Calculation of the Solar Radiation Incident on an Inclined Surface, Proc. of the First Canadian Solar Radiation Data Workshop, Toronto, 59–72.

Hauch A., Georg A., Baumgartner S., Kraover U.O., Orel B., (2001), New photoelectrochromic device, Electrochimica Acta, 46, 2131–2136

He W., Zhang Y.X., Sun W., Hou J.X., Jiang Q.Y., Ji J., (2011), Experimental and numerical investigation on the performance of amorphous silicon photovoltaics window in East China, Building and Environment, 46, 363-369

Heckner K.H., Kraft A., (2002), Similarities between electrochromic windows and thin film batteries, Solid State Ionics, 152– 153, 899– 905

Hollands K.G.T., Wright J.L., Granqvist C.G., (2001), Solar Energy-The state of art, James and James ltd, London, UK (chapter 2)

Ho K.C., (1999), The influence of charge capacity ratio on the performance of a complementary electrochromic system, Solar Energy Materials & Solar Cells, 56, 271-280

Hopkinson R.G., (1957), Evaluation of glare, Illuminating Engineering, XII, 305-316

Hopkinson R.G., (1970), Glare from windows, Construction Research and Development Journal, 98–105, 169–175

Hopkinson R.G., (1972), Glare from daylighting in buildings, Applied Ergonomics, 3, 206–215

Hove T., Manyumbu E., Rukweza G., (2014), Developing an improved global solar radiation map for Zimbabwe through correlating long-term ground- and satellite-based monthly clearness index values, Renewable Energy, 63, 687–697

Howley M., Gallachóir B. Ó., (2008), Energy statistics 1990-2007: 2008 report, Energy Policy Statistical Support Unit, Sustainable Energy Ireland, December

Hsu C.Y., Lee K.M., Huang J.H., Thomas K.R.J., Lin J.T., Ho K.C., (2008), A novel photoelectrochromic device with dual application based on poly (3, 4-alkyle-nedioxythiophene) thin film and an organic dye, Journal of Power Sources, 185, 1505–1508

Huang Y., Niu J.L., (2015), Application of super-insulating translucent silica aerogel glazing system on commercial building envelope of humid subtropical climates - Impact on space cooling load, Energy, 83, 316-325

Huang L.M., Hu C.W., Liu H.C., Hsu C.Y., Chen C. H., Ho K.C., (2012a), Photovoltaic electrochromic device for solar cell module and self-powered smart glass applications, Solar Energy Materials & Solar Cells, 99, 154–159

Huang L.M., Kung C.P., Hu C.W., Peng C.Y., Liu H.C., (2012b), Tunable photovoltaic electrochromic device and module, Solar Energy Materials & Solar Cells, 107, 390–395

Huang Z., Chen S., Wang B., Huang Y., Liu N., Xu J., Lai J., (2011), Vanadium dioxide thin film with low phase transition temperature deposited on borosilicate glass substrate, Thin Solid Films, 519, 4246–4248

Hunt D.R.G., (1979), The use of artificial lighting in relation to daylight levels and occupancy, Building and Environment, 14, 21–33

Hyde T.J., Griffiths P.W., Eames P.C., Norton B., (2000), Development of a novel low-emittance multiple coatings for glazing applications In: Proceedings World Renewable Energy Congress VI (WREC2000), Brighton, UK, 271–274

Ishaque K., Salam Z., (2011), An improved modeling method to determine the model parameters of photovoltaic (PV) modules using differential evolution (DE), Solar Energy, 85, 2349–2359

IEA, CO_2 emissions from fuel combustion: Highlights, 2010

IESNA, IES Lighting Handbook, 9th edition, Illuminating Engineering Society of North America, New York, USA (2000).

IES Committee on Recommendations for Quality and Quantity of Illumination, (1996), Subcommittee on Direct Glare, "Outline of a standard procedure for computing visual comfort ratings for interior lighting: Report no. 2", Illuminating Engineering, 61, 643-666

Ihara T., Gao T., Grynning S., Jelle B.P., Gustavsen A., (2015), Aerogel granulate glazing facades and their application potential from an energy saving perspective, Applied Energy, 142, 179–191

ISO/FDIS 9050 Glass in building – Determination of light transmittance, solar direct transmittance, total solar energy transmittance, ultraviolet transmittance and related glazing factors (2003)

Ihara T., Grynning S., Gao T., Gustavsen A., Jelle B.P., (2015), Impact of convection on thermal performance of aerogel granulate glazing systems, Energy and Buildings, 88, 165–173

Inanuma M., Takeda H., (2002), A study on luminous efficacy of each of direct, diffuse and global illuminance of daylight based on long-term observation data, Journal of Architecture, 560, 7–13

Ismail K.A.R., Henríquez J.R., (2002), Parametric study on composite and PCM glass system, Energy Conversion and Management, 43, 973–993

Ismail K.A.R., Henríquez J.R., (2005), Two-dimensional model for the double glass naturally ventilated window, International Journal of Heat and Mass Transfer, 48, 461–475

Ismail K.A.R., Salinas C.T., Henríquez J.R., (2008), Comparison between PCM filled glass windows and absorbing gas-filled windows, Energy and Buildings, 40, 710–719

Ismail K.A.R., Salinas C.T., Henríquez J.R., (2009), A comparative study of naturally ventilated and gas filled windows for hot climates, Energy Conversion and Management, 50, 1691–1703

ISO standard 8301-1991, Thermal insulation – determination of steady-state thermal resistance and related properties – heat flow meter apparatus.

ISO standard 8302-1991, Thermal insulation – determination of steady-state thermal resistance and related properties – guarded hot plate apparatus.

ISO standard 8990-1994, Thermal insulation – determination of steady-state thermal resistance and related properties – calibrated and guarded hot box.

ISO12567-1:2010 – Thermal performance of windows and doors – determination of thermal transmittance by the hot-box method – Part 1: complete windows and doors.

Isomura M., Sakai S., Sayama K., Hishikawa Y., Matsumi S., Haku H., Wakisaka K., Tanaka M., Kiyama S., Tsuda S., Nakano S., (1996), Efficiency evaluation of a-si and c-si solar cells for outdoor use, Photovoltaic Specialists Conference, Conference Record of the Twenty-Fifth IEEE, 13–17 May

Ishaque K., Salam Z., Taheri H., Syafaruddin., (2011), Modelling and simulation of photovoltaic (PV) system during partial shading based on a two –diode model, Simulation Modelling Practice and Theory, 19, 1613-1626

Iwata T., Tokura M., (1998), Examination of the limitations of predicted glare sensation vote (PGSV) as a glare index for a large source: towards a comprehensive development of discomfort glare evaluation, Lighting Research Technology, 30, 81-88

Iwata T., Shukuya M., Somekawa N., Kimura K., (1992), Experimental study on discomfort glare caused by windows, Part 2. Subjective response to glare from actual windows, Journal of Architecture Plan Environment Engineering, Nr 439, 19-31

Iwata T., Shukuya M., Somekawa N., Tokura M., (1991), Subjective response on discomfort glare caused by windows, in: Proceedings of the CIE 22nd Session

Jelle B.P., Hynd A., Gustavsen A., Arasteh D., Goudey H., Hart R., (2012), Fenestration of today and tomorrow: A state-of-the-art review and future research opportunities, Solar Energy Materials & Solar Cells, 96, 1–28

Jensen K.I., Schultz J.M., Kristiansen F.H., (2004), Development of windows based on highly insulated aerogel glazings, Journal of Non-Crystalline Solids, 350, 351-357

Jiménez M.J., Madsen H., (2008), Models for describing the thermal characteristics of building components, Building and Environment, 43,152–162

Jiménez M.J., Madsen H., Andersen K.K., (2008), Identification of the main thermal characteristics of building components using MATLAB, Building and Environment, 43, 170–180

Jin X., Medina M.A., Zhang X., (2013), On the importance of the location of PCMs in building walls for enhanced thermal performance, Applied Energy, 106, 72–78

Johnson T.E., (1991), Low-e glazing design guide Butterworth-Heinemann, USA

Jones G.F., Jones R.W., (1999), Steady-state heat transfer in an insulated, reinforced concrete wall: theory, numerical simulations, and experiments, Energy Building, 29, 293–305

Joshi M., Sawhney R.L., Buddhi D., (2007), Estimation of luminous efficacy of daylight and exterior illuminance for composite climate of Indore city in Mid-Western India, Renewable Energy, 32, 1363–1378

Joyce A., Rodrigues C., Manso R., (2001), Modelling a PV system, Renewable Energy, 22, 275-280

Klainsek J., Bedoya C., Neila J., (1996), The effect of glazing shape upon the thermal performance of buildings, Renewable Energy, 8, 182–185

Kahn K.A., Niklasson G.A., Granqvist C.G., (1998), Optical properties at the metal–insulator transition in thermochromic $VO_{2-}xFx$ thin films, Journal of Applied Physics, 64, 3327–3329

Khan K.A., Granqvist C.G., (1989), Thermochromic sputter-deposited vanadium oxyfluoride coatings with low luminous absorptance, Applied Physics Letters, 55, 4-6

Khedari J., Waewsak J., Supheng W., Hirunlabh J., (2004), Experimental investigation of performance of a multi-purpose PV-slat window, Solar Energy Materials & Solar Cells, 82, 431–445

Kim G.S., Hyun S.H., (2003), Synthesis of window glazing coated with silica aerogel films via ambient drying, Journal of Non –Crystalline Solids, 320, 125-132

Klems J.H., Selkowitz S., Horowitz S., (1982), A mobile Facility for measuring net energy performance of windows and skylights, 3rd international Symposium on energy conservation in the built environment, Dublin, Ireland, march 30-April1

Klems J.H., (1984), Measurement of fenestration performance under realistic conditions, Report LBL-17429, Lawrence Berkeley Laboratory, Berkeley, CA

Klems J., Keller H., (1987), Measurement of single and double glazing thermal performance under realistics condition using the mobile window thermal test (MoWiTT) facility, ASME Solar Energy Division Conference, Honolulu, HI, March 22-27

Klems J.H., (2001), Net energy performance measurements on electrochromic skylights, Energy and Buildings, 33, 93-102

Klucher T.M., (1979), Evaluation of models to predict insolation on tilted surfaces, Solar Energy, 23, 111–114

Koebel M.M., Manz H., Mayerhofer K.M., Keller B., (2010), Service-life limitations in vacuum glazing: A transient pressure balance model, Solar Energy Materials & Solar Cells, 94, 1015–1024

Kolokotsa D., Rovas D., Kosmatopoulos E., Kalaitzakis E., (2011), Roadmap towards intelligent net zero- and positive-energy buildings, Solar Energy, 85, 3067–3084

Kong H.J., Kim J.T., (2013), Modeling luminous efficacy of daylight for Yongin, South Korea, Energy and Buildings, 62, 550–558

Krauter S., Araujo R.G., Schroer S., Hanitsch R., Salih M.J., Triebel C., Lemoine R., (1999), Combined photovoltaic and solar thermal systems for facade integration and building insulation, Solar Energy, 67, 239–248

Krüger E.L., Adriazola M., Matoski A., Iwakiri S., (2009), Thermal analysis of wood–cement panels: Heat flux and indoor temperature measurements in test cells Construction and Building Materials, 23, 2299–2305

Krüger E.L., Adriazola M., (2010), Thermal analysis of wood-based test cells, Construction and Building Materials, 24, 999–1007

Kubo T., Shinadaa T., Kobayashi Y., Imafuku H., Toya T., Akita S., Nishikitani Y., Watanabe H., (2003), Current state of the art for NOC-AGC electrochromic windows for architectural and automotive applications, Solid State Ionics, 165, 209 – 216

Kuhn T.E., Buhler C., Platzer W.J., (2000), Evaluation of overheating protection with sun-shading systems, Solar Energy, 69, 59–74

Kuhn T.E., (2014), Calorimetric determination of the solar heat gain coefficient g with steady-state laboratory measurements, Energy and Buildings, 84, 388–402

Lampert C. M., (1984), Towards large-area photovoltaic nanocells: experiences learned from smart window technology, Solar Energy Material & Solar cells, 11, 1–27

Lampert C.M., (1998), Smart switchable glazing for solar energy and daylight control, Solar Energy Materials & Solar Cells, 52, 207–221

Lampert C.M., (1984), Electrochromic materials and devices for energy efficient windows, Solar Energy Materials & solar Cells, 11, 1-27

Lampert C.M., Agarwal A., Baertlien C., Nagai J., (1999), Durability evaluation of electrochromic devices - an industry perspective, Solar Energy Materials & Solar Cells, 56, 449- 463

Lampert C.M., (2003), Large-area smart glass and integrated photovoltaics, Solar Energy Materials & Solar Cells, 76, 489–499

Lampert C.M., (1993), Optical switching technology for glazings, Thin Solid Films, 236, 6–13

Lampert C.M., (2004), Chromogenic smart materials, Materials Today, 7, 28-35

Lam J.C., Li D.H.W., (1999), An analysis of daylighting and solar heat for cooling-dominated office buildings, Solar Energy, 65, 251–262

Lam J.C., Li D.H.W., Cheung S.O., (2003), An analysis of electricity end-use in air-conditioned office buildings in Hong Kong, Building and Environment, 38, 493–498

Land E.H., (1934), Light valve and method of operation, U.S. Patent No. 1,955,923

Lawrence S.A., Tiwari G.N., (1990), Theoretical evaluation of solar distillation under natural circulation with heat exchanger, Energy Conversion and Management, 30, 205–213

Lapillonne B., Sebi C., Pollier K., (2012), Energy Efficiency Trends for Households in the EU, Enerdata—An Analysis Based on the ODYSSEE Database

Lee E.S., Pang X., Hoffman S., Goudey H., Thanachareonkit A., (2013), An empirical study of a full-scale polymer thermochromic window and its implications on material science development objectives, Solar Energy Materials & Solar Cells, 116, 14–26

Lee E.S., DiBartolomeo D.L., Selkowitz S.E., (2006), Daylighting control performance of a thin-film ceramic electrochromic window: Field study results, Energy and Buildings, 38, 30–44

Lee M.H., (2002), Thermochromic glazing of windows with better luminous solar transmittance, Solar Energy Materials & Solar Cells, 71, 537–540

Lee E.S., DiBartolomeo D.L., Rubinstein F.M., Selkowitz S.E. (2004), Low-cost networking for dynamic window systems, Energy and Buildings, 36, 503–513

Lee J.W., Jung H.J., Park J.Y., Lee J.B., Yoon Y., (2013), Optimization of building window system in Asian regions by analyzing solar heat gain and daylighting elements, Renewable Energy, 50, 522–531

Leftheriotis G., Yianoulis P., (1999), Characterisation and stability of low-emittance multiple coatings for glazing applications, Solar Energy Materials & Solar Cells, 58, 185-197

Lenzen M., Collins R.E., (1997), Long-term field tests of vacuum glazing, Solar Energy, 61, 11–15

Levermore G.J., (2008), A review of the IPCC assessment report four, part 1: the IPCC process and greenhouse gas emission trends from buildings worldwide, Building Service Engineering Research Technology, 29, 349–361

Littlefair P.J., (1985), The luminous efficacy of daylight: a review, Lighting Research and Technology, 17, 162–182

Littlefair P.J., (1987), Prediction of reflected solar dazzle from sloping facades, Building and Environment, 22, 285-291

Littlefair P. J., (1988), Average daylight factor: a simple basis for daylight design. BRE Information Paper IP15 /88, CRC, Garston

Littleefair P.J., (1990), Predicting annual lighting use in daylit buildings, Building and Environment, 25, 43-53

Littlefair P.J., Aizlewood M.E., Birtles A.B., (1994), The performance of innovative daylighting systems, Renewable Energy, 5, 920-934

Littlefair P.J., (2001), Daylight, sunlight and solar gain in the urban environment, Solar Energy, 70, 177–185

Littlefair P.J., (2002), Daylight prediction in atrium buildings, Solar Energy, 73, 105–109

Li D.H.W., (2010), A review of daylight illuminance determinations and energy implications, Applied Energy, 87, 2109–2118

Li D.H.W., Lam J.C., (2000), Vertical solar radiation and daylight illuminance data for Hong Kong, Lighting Research and Technology, 32, 93–98

Li D.H.W., Lam J.C., (2001), Analysis of solar heat gain factors using sky clearness index and energy implications, Energy Conversion and Management, 42, 555-571

Lombard L.P., Ortiz J., Pout C., (2008), A review on buildings energy consumption information, Energy and Building, 40, 394–398

Long L., Ye H., (2014), Discussion of the performance improvement of thermochromic smart glazing applied in passive buildings, Solar Energy, 107, 236–244

Lopez T.G., Molina C.G., (2013), Influence of double glazing with a circulating water chamber on the thermal energy savings in buildings, Energy and Buildings, 56, 56–65

Lopez T.G., Molina C.G., (2013), Environmental, economic and energy analysis of double glazing with a circulating water chamber in residential buildings, Applied Energy, 101, 572–581

Lorenz W., (2001), A glazing unit for solar control, daylighting and energy conservation, Solar Energy, 70, 109–130

Loutzenhiser P.G, Manz H., Carl S., Simmler H., Maxwell G.M., (2008), Empirical validations of solar gain models for a glazing unit with exterior and interior blind assemblies, Energy Building, 40, 330–340

Lynn N., Mohanty L., Wittkopf S., (2012), Color rendering properties of semi-transparent thin-film PV modules, Building and Environment, 54, 148–158

Ma A., Cooper P., Daly D., Ledo L., (2012), Existing building retrofits: methodology and state-of-the-art, Energy and Building, 55, 889–902

Macht B., Turrion M., Barkschat A., Salvador P., Ellmer K.,Tributsch H., (2002), Patterns of efficiency and degradation in dye sensitization solar cells measured with imaging techniques, Solar Energy Material & Solar Cells, 73, 163–173.

Maghrabi A.H., (2009), Parameterization of a simple model to estimate monthly global solar radiation based on meteorological variables, and evaluation of existing solar radiation models for Tabouk, Saudi Arabia, Energy Conversion and Management, 50, 2754–2760

Maleki A., Pourfayaz F., (2015), Optimal sizing of autonomous hybrid photovoltaic/wind/battery power system with LPSP technology by using evolutionary algorithms, Solar Energy, 115, 471–483

Mallick T.K., Eames P.C., Hyde T.J., Norton B., (2004), The design and experimental characterisation of an asymmetric compound parabolic photovoltaic concentrator for building facade integration in the UK , Solar Energy, 77, 319–327

Mallick T.K., Eames P.C., Norton B., (2006), Non-concentrating and asymmetric compound parabolic concentrating building façade integrated photovoltaics: An experimental comparison, Solar Energy, 80, 834–849

Maleki A., Pourfayaz F., (2015), Optimal sizing of autonomous hybrid photovoltaic/wind/battery power system with LPSP technology by using evolutionary algorithms, Solar Energy, 115, 471–483

Manz H., Egolf P.W., Suter P., Goetzberger A., (1997), TIM–PCM External wall system for solar space heating and daylighting, Solar Energy, 61, 369–379

Manz H., Menti U.P., (2012), Energy performance of glazings in European climates, Renewable Energy, 37, 226–232

Manz H., Brunner S., Wullschleger L., (2006), Triple vacuum glazing: Heat transfer and basic mechanical design constraints, Solar Energy, 80, 1632-1642

Mara T.A., Garde F., Boyer H., Mamode M., (2000), Emipirical validation of the thermal model of a passive solar test cell, Energy and Building, 33, 589-599

Marcelli G., (1998), Electrochromic windows, Renewable Energy, 15, 306-311

Marinoski D.L., Güths S., Lamberts R., (2012), Development of a calorimeter for determination of the solar factor of architectural glass and fenestrations, Building and Environment, 47, 232-242

Marks A.M., (1969), Electrooptical characteristics of dipole suspensions, Applied Optics, 8, 1397–1412

Martins A.M.T., Carlos J.S., (2014), The retrofitting of the bernardas' convent in Lisbon, Energy and Buildings, 68, 396–402

Masetti E., Dini D., Decker F., (1995), The electrochromic response of tungsten bronzes M_xWO_3 with different ions and insertion rates, Solar Energy Materials & Solar Cells, 39, 301-307

Matthews J.P., Bell J.M., Skryabin I.L., (1999), Effect of temperature on electrochromic device switching voltages, Electrochimica Acta, 44, 3245-3250

Matthews J.P., Bell J.M., Skryabin I.L., (2001), Simulation of electrochromic switching voltages at elevated temperatures, Electrochimica Acta, 46, 1957–1961

Maurizio Cellura M., Guarino F., Longo S., Mistretta M., (2015), Different energy balances for the redesign of nearly net zero energy buildings: An Italian case study, Renewable and Sustainable Energy Reviews, 45, 100–112

McEvoy M.E., Southall R. G., Baker P.H., (2003), Test cell evaluation of supply air windows to characterise their optimum performance and its verification by the use of modelling techniques, Energy and Buildings, 35, 1009–1020

McHugh J., Pande A., Ander G.D., Melnyk J., (2004), Effectiveness of photocontrols with skylighting, Presented at the IESNA Annual Conference in Tampa, Florida July 25- 28

Mescher J., Kettlitz S.W., Christ N., Klein M.F.G., Puetz A., Mertens A., Colsmann A., Lemmer U., (2014), Design rules for semi-transparent organic tandem solar cells for window integration, Organic Electronics, 15, 1476–1480

Miao H., Shan X., Zhang J., Sun J., Wang H., (2015), Effect of sealing temperature on the sealing edge performance of vacuum glazing, Vacuum, 116 , 7-12

Mitsumata T., Kawada H., Takimoto J.I., (2007), Thermosensitive solutions and gels consisting of poly(vinyl alcohol) and sodium silicate, Material Letters, 61, 3878–3881

Miyazaki T., Akisawa A., Kashiwagi T., (2005), Energy savings of office buildings by the use of semi-transparent solar cells for windows, Renewable Energy, 30, 281–304

Mlyuka N.R., Niklasson G.A., Granqvist C.G., (2009), Mg doping of thermochromic VO_2 films enhances the optical transmittance and decreases the metal–insulator transition temperature, Applied Physics Letters, 95, 17

Moeck M., Lee E.S., Rubin M.D., Sullivan R.T., Selkowitz S.E., (1998), Visual quality assessment of electrochromic and conventional glazings, Solar Energy Materials & Solar Cells, 54, 157-164

Mondol J.D., Yohanis Y.G., Norton B., (2008), Solar radiation modelling for the simulation of photovoltaic systems, Renewable Energy, 33, 1109–1120

Morelli M., Ronby L., Mikkelsen S.E., Minzari MG., Kildemoes T., Tommerup H.M., (2012), Energy retrofitting of a typical old Danish multi-family building to a "nearly-zero" energy building based on experiences from a test apartment, Energy and Buildings, 54, 395–406

Morin F.J., (1959), Oxides which show a metal to insulator transition at the neel temperature, Physics Review Letters, 3, 34-36

Mortimer R.J., Dyer A.L., Reynolds J.R., (2006), Electro chromic organic and polymeric materials for display applications, Displays, 27, 2–18

Muneer T., Kinghorn D., (1997), Luminous efficacy of solar irradiance: improved models, Lighting Research and Technology, 29, 185–191

Muneer T., Kinghorn D., (1998), Luminous efficacy models: evaluation against UK data**,** Journal of the IES, 27, 163–170

Muneer T., (2004), Solar Radiation and Daylight Models: For the Energy Design of Buildings (second ed.) Elsevier Science and Technology Pub, UK

Nabil A., Mardaljevic J., (2006), Useful daylight illuminances: A replacement for daylight factors, Energy and Buildings, 38, 905–913

Nagai J., McMeeking G.D., Saitoh Y., (1999), Durability of electrochromic glazing, Solar Energy Materials & Solar Cells, 56, 309-319

Nagengast D.G., Van Gogh A.T.M., Kooij E.S., Dam B., Griessen R., (1999), Contrast enhancement of rare-earth switchable mirrors through microscopic shutter effect, Applied Physics Letters, 75, 2050

Nanoco Technology, http://www.nanocotechnologies.com.

National Fenestration Rating Council, NFRC 200-2010, Procedure for determining fenestration product solar heat gain coefficient and visible transmittance at normal incidence, 2010.

National Fenestration Rating Council, NFRC 300-2010, Test method for determining the solar optical properties of glazing materials and systems, 2010.

Nazzal A.A., (2001), A new daylight glare evaluation method Introduction of the monitoring protocol and calculation method, Energy and Buildings, 33, 257-265.

Nazzal, A.A., (2005), A new evaluation method for daylight discomfort glare, International Journal of Industrial Ergonomics, 35, 295–306

Nejat P., Jomehzadeh F., Taheri M.M.,Gohari M., Majid M.Z.A., (2015), global review of energy consumption, CO_2 emissions and policy in the residential sector (with an overview of the top ten CO_2 emitting countries), Renewable and Sustainable Energy Reviews, 43, 843–862

Ng P.K., Mithraratne N., Kuac H.W., (2013), Energy analysis of semi-transparent BIPV in Singapore buildings, Energy and buildings, 66, 274–281

Ng P.K., Mithraratne N., (2014), Lifetime performance of semi-transparent building-integrated photovoltaic (BIPV) glazing systems in the tropics, Renewable and Sustainable Energy Reviews, 31, 736–745

Ng N., Collins R.E., So L., (2005), Thermal and optical evolution of gas in vacuum glazing, Materials Science and Engineering B, 119, 258–264

Ng N., Collins R.E., So L., (2006), Thermal conductance measurement on vacuum glazing, International Journal of Heat and Mass Transfer, 49, 4877–4885

Ng N., Collins R.E., So L., (2007), Characterization of the thermal insulating properties of vacuum glazing, Materials Science and Engineering B, 138, 128–134

Nitz P., Hartwig H., (2005), Solar control with thermotropic layers, Solar Energy, 79, 573–582

Nishikitani Y., Asano T., Uchida S., Kubo T., (1999), Thermal and optical behaviour of electrochromic windows fabricated with carbon- based counter electrode, Electrochimica Acta, 44, 3211-3217

Nogueira V.C., Longo C., Nogueira A.F., Oviedo M.A.S., De Paoli M.A., (2006), Solid-state dye-sensitized solar cell: improved performance and stability using a plasticized polymer electrolyte, Journal of Photochemistry and Photobiology A: Chemistry, 181, 226–232

Nokki H.S., Kallioinen J., Tommola J.K., (2007), A dye-sensitized solar cell driven electrochromic device, Photochemical and Photobiological Science, 6, 63–66

Norton B., Probert S.D., (1984), Solar-energy stimulated, open-looped thermosyphonic air heaters, Applied Energy, 17, 217-234

Norton B., Probert S.D., (1982), Natural –circulation solar energy stimulated systems for heating water, Applied Energy, 11, 167 -196

Norton B., Eames P.C., Mallick T.K., Huang M.J., McCormack S.J., Mondol J.D., Yohanis Y.G., (2011), Enhancing the performance of building integrated photovoltaics, Solar Energy, 85, 1629–1664

Norton B., (2014), Harnessing Solar Heat, Springer, Dordrecht, Netherlands

Olivieri L., Caama˜no-Martina E., Olivieri F., Neila J., (2014), Integral energy performance characterization of semi-transparent photovoltaic elements for building integration under real operation conditions , Energy and Buildings, 68, 280–291

Olson R.W., Loring R.F., Fayer M.D., (1981), Luminescent solar concentrators and the re-absorption problem, Applied Optics, 20, 2934

O'Regan B., Gratzel M., (1991), A low-cost, high-efficiency solar-cell based on dye-sensitized colloidal TiO_2 films, Nature, 353, 727–740

Orgill J.F., Hollands K.G.T., (1977), Correlation equation for hourly diffuse radiation on a horizontal surface, Solar Energy, 19, 357–359

Osterhaus W.K.E., (2005), Discomfort glare assessment and prevention for daylight applications in office environments, Solar Energy, 79, 140–158

Papaefthimiou S., Leftheriotis G., Yianoulis P., Hyde T. J., Eames P.C., Fang Y., Pennarun P. Y., Jannasch P., (2006), Development of electrochromic evacuated advanced glazing, Energy and Buildings, 38, 1455–1467

Papaefthimiou S., Syrrakou E., Yianoulis P., (2009), An alternative approach for the energy and environmental rating of advanced glazing: An electrochromic window case study, Energy and Buildings, 41, 17–26

Park K.E., Kang G.H., Kim H.I., Yu G.J., Kim J.T., (2010), Analysis of thermal and electrical performance of semi-transparent photovoltaic (PV) module, Energy, 35, 2681–2687

Park S., Hong J.W., (2009), Polymer dispersed liquid crystal film for variable-transparency glazing, Thin Solid Films, 517, 3183–3186

Péczely Gy., (1979), Éghajlattan—Climatology in Hungarian, Nemzeti Tankönyvkiadó, Budapest

Peippo K., Lund P.D., (1994), Optimal sizing of solar array and inverter in grid –connected photovoltaic systems, Solar Energy Materials & Solar Cells, 32, 95-114

Peng C., Huang Y., Wu Z., (2011), Building-integrated photovoltaics (BIPV) in architectural design in China, Energy and Buildings, 43, 3592–3598

Peng J., Lu L., Yang H., (2013), An experimental study of the thermal performance of a novel photovoltaic double-skin facade in Hong Kong, Solar Energy, 97, 293–304

Pennisi A., Simone F., Barletta G., Marco G. D., Lanza M., (1999), Preliminary test of a large electrochromic window, Electrochimica Acta, 44, 3237-3243

Pereira E.O.R., (1992), Luminious and thermal performance of windows shading and sunlight reflecting devices, PhD Thesis, School of Architectural Studies, University of Sheffield, UK, 301

Pereira F.O.R., Sharples S., (1991), The development of a device for measuring solar heat gain and shading coefficients of windows in scale model, Energy and Buildings, 17, 271-281

Perez R., Ineichen P., Seals R., Zelenka A., (1990), Making full use of the clearness index for parameterizing hourly insolation conditions, Solar Energy, 45, 111–114

Perez R., Seals R., Michalsky J., (1993), All-weather model for sky luminance distribuition-preliminary configuration and validation, Solar Energy, 50, 235–245

Petherbridge P., Hopkinson R.G., (1950), Discomfort glare and the lighting of buildings, Transactions of the Illuminating Engineering Society, 15, 29-79

Petti L., Mormile P., Blau W.J., (2003), Fast electro-optical switching and high contrast ratio in epoxy-based polymer dispersed liquid crystals, Optics and Lasers in Engineering, 39, 369-277

Piccolo A., Pennisi A., Simone F., (2009a), Daylighting performance of an electrochromic window in a small scale test-cell, Solar Energy, 83, 832–844

Piccolo A., Simone F., (2009b), Effect of switchable glazing on discomfort glare from windows, Building and Environment, 44, 1171–1180

Piccolo A., (2010), Thermal performance of an electrochromic smart window tested in an environmental test cell, Energy Building, 42, 1409–1417

Piller S., Perrin M., Jossen A., (2001), Methods for state-of-charge determination and their applications, Journal of Power Sources, 96, 113–20

Polo J., Zarzalejo L.F., Cony M., Navarro A.A., Marchante R., Martin L., Romero M., (2011), Solar radiation estimations over India using Meteosat satellite images, Solar Energy, 85, 2395–2406

Prabhakant, Tiwari G.N., (1991), Analytical study of heat exchanger design, Energy Conversion and Management, 32, 403–408

Quesada G., Rousse D., Dutil Y., Badache M., Hallé S., (2012), A comprehensive review of solar facades. Transparent and translucent solar facades, Renewable and Sustainable Energy Reviews, 16, 2643–2651

Qahtan A., Keumala N., Rao S.P., Abdul-Samad Z., (2011), Experimental determination of thermal performance of glazed façades with water film, under direct solar radiation in the tropics, Building Environment, 46, 2238–2246

Qahtan A., Rao SP., Keumala N., (2014), The effectiveness of the sustainable flowing water film in improving the solar-optical properties of glazing in the tropics, Energy and Buildings, 77, 247–255

Raicu A., Wilson H.R., Nitz P., Platzer W., Wittwer V., E. Jahns E., (2002), Façade systems with variable solar control using thermotropic polymer blends, Solar Energy, 72, 31–42

Rapp C.F., Boling N.L., (1978), Luminescent Solar Concentrator, proceedings of the 13th IEEE Photovoltaic Specialists Conference, 690-693

Raziemska E., (2003), The effect of temperature on the power drop in crystalline silicon solar cells, Renewable Energy, 28, 1–12

Rea M.S., (2000), The IESNA lighting handbook: Reference and application (9^{th} ed), Illuminating Engineering Society, New York

Reidinger M., Rydzek M., Scherdel C., Schuster M. A., Manara J., (2009), Low-emitting transparent coatings based on tin doped indiumoxide applied via a sol–gel routine, Thin Solid Films, 517, 3096–3099

Reim M., Beck A., Korner W., Petricevic R., Glora M., Weth M., Schliermann T., Fricke J., Schmidt C., Potter F.J., (2002), Highly insulating aerogel glazing for solar energy usage, Solar Energy, 72, 21–29

Reindl D.T., Beckman W.A., Duffie J.A., (1990), Diffuse fraction corrections, Solar Energy, 45, 1–7

Reisfeld R., (1983), Future technological applications of rare earth doped materials, Journal of the Less Common Metals, 93, 243–251

Reisfeld R., kalisky Y., (1981), Nd +3 and Yb+3 germanate and tellurite glasses for fluorescent solar energy collector, Chemical Physics Letters, 80, 178-183

Ren H., Gao W., Zhou W., Nakagami K., (2009), Multi-criteria evaluation for the optimal adoption of distributed residential energy systems in Japan, Energy Policy, 37, 5484–5493

Revel G.C., Martarelli M., Emiliani M., Celotti L., Nadalini R., De Ferrari A., Hermanns S., Beckers E., (2014), Cool products for building envelope – Part II: Experimental and numerical evaluation of thermal performances, Solar Energy, 105, 780–791

Richards B.S., Shavlav A., Crokish P., (2004), A low escape cone loss luminescent solar concentrator, 19th E.C Photovoltaic Solar Energy Conference, Paris, 113-116

Roche P.L., Milne M., (2004), Effects of window size and thermal mass on building comfort using an intelligent ventilation controller, Solar Energy, 77, 421–434

Roche P.L., Berardi U., (2014), Comfort and energy savings with active green roofs, Energy and Buildings, 82, 492–504

Robinson S.J., Collins R.E., (1989), Evacuated windows-theory and practice. In: ISES Solar World Congress, International Solar Energy Society, Kobe, Japan.

Robinson P., Littler J., (1993), Advanced glazing: Outdoor test room measurements, performance prediction and building thermal simulation, Building and Environment, 28, 145-152

Rodriguez U. E., Arranz B.A., Sánchez S. V., González F.J. N., (2013), Influence of the use of PCM drywall and the fenestration in building retrofitting, Energy and Buildings, 65, 464–476

Rohan P.K., (1975), The Climate of Ireland, The Stationery Office, Dublin

Rosencwaig A., Hildum E.A., (1981), Nd{3+} fluorescence quantum efficiency measurements with photoacoustics, Physical Review B, 23, 3301–3307

Rosseinsky D.R., Mortimer R.J., (2001), Electrochromic systems and the prospects for devices, Advanced Materials, 13, 783–793

Resch K., Wallner G.M., Lang R.W., (2008), Spectroscopic investigations of phase-separated thermotropic layers based on UV cured acrylate resins, Macromolecular symposia, 265, 49–60

Starovoytova L., Spevcek J., (2006), Effect of time on the hydration and temperature-induced phase separation in aqueous polymer solutions. 1 h NMR study, Polymer, 47, 7329–7334

Saeli M., Piccirillo C., Parkin I.P., Binions R., Ridley I., (2010), Energy modelling studies of thermochromic glazing, Energy and Buildings, 42, 1666–1673

Sah C.T., Noyce R.N., Shockley W., (1957), Carrier Generation and recombination in p-n junctions and p-n junction characteristics, Proceedings of IRE, 45, 1228-1243

Santamouris M., Balaras C.A., Dascalaki E., Argiriou A., Gaglia A., (1996), Energy saving and retrofitting potential in Hellenic hotels, Energy and Buildings, 24, 65–75

Santbergen R., Zolingen R.J.C.V., (2008), The absorption factor of crystalline silicon PV cells: A numerical and experimental study, Solar Energy Materials & Solar Cells, 92, 432–444

Sarmah N., Richards B.S., Mallick T.K., (2014), Design, development and indoor performance analysis of a low concentrating dielectric photovoltaic module, Solar Energy, 103, 390–401

Sarmah N., Mallick T.K., (2015), Design, fabrication and outdoor performance analysis of a low concentrating photovoltaic system, Solar Energy, 112, 361–372

Saxe R.L., (1979), Light valve containing liquid suspension including polymer-stabilizing systems, U.S. Patent No. 4273422

Saxe R.L., (1981), Light valve suspension containing fluorocarbon liquid, U.S. Patent No. US4407565

Sbar N.L., Podbelski L., Yang H.M., Pease B., (2012), Electrochromic dynamic windows for office buildings, International Journal of Sustainable Built Environment, 1, 125–139

Schmidt M., Schwertfeger F., (1998), Applications for silica aerogel products, Journal of Non- Crystalline Solids, 225, 364-368

Schultz J. M., Jensen K. I., (2008), Evacuated aerogel glazings, Vacuum, 82, 723-729

Schultz J. M., Jensen K. I., Kristiansen F.H., (2005), Super insulating aerogel glazing, Solar Energy Materials & Solar Cells, 89, 275-285

Schuster P.A., Nguyen D., Caporaaleti O., (1986), Solid state electrochromic infrared switchable windows, Solar Energy Materials, 13, 153-160

SEAI (2013), Energy in the Residential Sector, In: IRELAND, S.E. (Ed.) Dublin

SEAI (2013),
(http://www.seai.ie/Publications/Statistics_Publications/Energy_in_Ireland/Energy-in-Ireland-1990-2013-report.pdf)

Seeboth A., Schneider J., Patzak A., (2000), Materials for intelligent sun protecting glazing**,** Solar Energy Materials & Solar Cells, 60, 263–277

Sellami N., Mallick T.K., (2013), Optical characterisation and optimisation of a static window integrated concentrating photovoltaic system, Solar Energy, 91, 273–282

Seybold G., Wagenblast G., (1989), New perylene and violanthrone dyestuffs for fluorescent collectors, Dyes and Pigments, 11, 303–317

Shehabi A., DeForest N., McNeil A., Masanet E., Greenblatt J., Lee E.S., Masson G., Helms B.A., Milliron D.J., (2013), US energy savings potential from dynamic daylighting control glazings, Energy and Building, 66, 415–423

Shen W.X., (2009), Optimally sizing of solar array and battery in a standalone photovoltaic system in Malaysia, Renewable Energy, 34, 348–352

Silva T., Vicente R., Rodrigues F., Samagaio A., Cardoso C., (2015a), Performance of a window shutter with phase change material under summer Mediterranean climate conditions, Applied Thermal Engineering, 84, 246–256

Silva T., Vicente R., Rodrigues F., Samagaio A., Cardoso C., (2015b), Development of a window shutter with phase change materials: Full scale outdoor experimental approach, Energy Building, 88, 110–121

Simko T.M., Fischer-Cripps A.C., Collins R.E., (1998), Temperature-induced stresses in vacuum glazing: Modelling and experimental validation, Solar Energy, 63, 1–21

Skryabin I.L., Evans G., Frost D., Vogelman G., Bell J.M., (1999), Testing and control issues in large area electrochromic films and devices, Electrochimica Acta, 44, 3203-3209

Slovak S.M., Chakrapani S., Saxe R.L., (2005), Methods for laminating films for SPD light valves and SPD light valves incorporating such laminated films, U.S. Patent No. US20050227061

Smestad G., Ries R., Winston R., Yablonovitch E., (1990), The thermodynamic limits of light concentrators, Solar Energy Materials, 21, 99-111

So L., Ng N., Bilek M., (2007), Analysis of the internal glass surfaces of vacuum glazing, Materials Science and Engineering B, 138, 135–138

Somani P.R., Radhakrishnan S., (2002), Electro chromic materials and devices: present and future, Materials Chemistry and Physics, 77, 117–133

Soto W.D., Klein S.A., Beckman W.A., (2006), Improvement and validation of a model for photovoltaic array performance, Solar Energy, 80, 78-88

Southall R.G., McEvoy M.E., (2006), Investigations into the functioning of a supply air window in relation to solar energy as determined by experiment and simulation, Solar Energy, 80, 512–523

Smith G.B., (2004), Materials and systems for efficient lighting and delivery of daylight, Solar Energy Materials & Solar Cells, 84, 395–409

Smyth M., McGarrigle P., Eames P.C., Norton B., (2005), Experimental comparison of alternative convection suppression arrangements for concentrating integral collector storage solar water heaters, Solar Energy, 78, 223–233

Strachan P., (1993), Model validation using the PASSYS test cells, Building and Environment, 28, 153-165

Strachan P.A., Vandaele L., (2008), Case studies of outdoor testing and analysis of building components, Building Environment, 43, 129–142

Swedish Energy Agency, (2004), Technical Guidance Document, Building Regulations (2011), http://www.environ.ie/.

Szűcs A., (2013), Wind comfort in a public urban space—case study within Dublin docklands, Frontiers of Architectural Research, 2, 50–66

Tait D.B., (2006a), Solar heat gain coefficients for high-mass glazing blocks, ASHRAE Transactions, 112, 142–150

Tait D.B., (2006b), Solar Heat Gain Coefficient Measurements for Glazings with Indoor Window Attachment Products, 112, 116 -121

Taleb H.M., Pitts A.C., (2009), The potential to exploit use of building-integrated photovoltaics in countries of the gulf cooperation council, Renewable Energy, 34, 1092–1099

Takashi M., Shuichi H., Daisuke O., Masahiko T., Jun S., (2013), Improvement of thermal environment and reduction of energy consumption for cooling and heating by retrofitting windows, Frontiers of Architectural Research, 2, 1–10

Tiwari G.N., Lawrence S.A., (1991), A transient analysis of a closed loop solar thermosyphon water heater with heat exchangers, Energy Conversion and Management, 31, 505–508

Tokura M., Iwata I., Shukuya M., (1996), Experimental study on discomfort glare caused by windows, part 3, Development of a method for evaluating discomfort glare from a large light source. Journal of Architecture, Planning and Environmental Engineering, 489, 17–25

Towards nearly zero energy building. Definition of common principles under the EPBD final report, http://ec.europa.eu/, accessed 24.10.2013

Tonui J.K., Tripanagnostopoulos Y., (2007), Air-cooled PV/T solar collectors with low cost performance improvements, Solar Energy, 81, 498–511

Tracy C.E., Zhang J.G., Benson D.K., Czanderna A.W., Deb S.K., (1999), Accelerated durability testing of electrochromic windows, Electrochimica Acta, 44, 3195–3202

Trupke T., Green M.A., Würfel P., (2002), Improving solar cell efficiencies by down-conversion of high energy photons, Journal of Applied Physics, 92, 1668-1674

Tsikaloudaki K., (2005), A study on luminous efficacy of global radiation under clear sky conditions in Athens, Greece, Renewable Energy, 30, 551–563

U.S. Department of Energy (DOE), 2010 buildings energy data book

United Nations Environment Programme, (2007), Buildings and climate change: status, challenges and opportunities [Online]

US DOE, Building Technologies Program, Planned Program Activities for 2008–2012, Department Of Energy, US, http://www1.eere.energy.gov/, 2008 (downloaded 01/07/2013).

Van der Sluis P., Ouwerkerk M., Duine P.A.,(1997), Optical switches based on magnesium lanthanide alloy hydrides, Applied Physics Letters, 70 , 3356

Vandijk H.A.L., Vander G.P., (1993), The PASSYS method for testing passive solar components, Building and Environment, 28, 115-126

Vartiainen E., (2000), A comparison of luminous efficacy models with illuminance and irradiance measurements, Renewable Energy, 20, 265–277

Ven Steensel K., Ven de Burg F., Kooy C., (1967), Thin-film switching elements of VO_2, Philips Research Reports, 22, 170

Vergaz R., Pena J.M.S.N., Barrios D., Va´zquez C., Lallana P.C., (2008), Modelling and electro-optical testing of suspended particle devices, Solar Energy Materials & Solar Cells, 92, 1483–1487

Veeraboinaa P., Yesuratnam G., Sundar L.S., (2011), Estimation of Annual Solar Radiation from measured temperatures by using Temperature-based (TB) approach in different cities in India, Sustainable Cities and Society, 1, 187–194

Villalva M.G., Gazoli J.R., Filho E.R., (2009), Comprehensive approach to modelling and simulation of photovoltaic arrays, IEEE Transactions on Power Electronics, 24, 1198-1208

Waide P.A., Norton B., (2003), Variation of insolation transmission with glazing plane position and sky conditions, ASME Journal of Solar Energy Engineering, 125, 182–189

Walmsley M.R.W., Walmsley T.G., Atkins M.J., Kamp P.J.J., Neale J.R., (2014), Minimising carbon emissions and energy expended for electricity generation in New Zealand through to 2050, Applied Energy, 135, 656–665

Walker G., (2001), Evaluating MPPT converter topologies using a matlab PV model, Journal of Electrical and Electronics Engineering, 21, 49-55

Wang J., Eames P.C., Zhao J.F., Hyde T., Fang Y., (2007), Stresses in vacuum glazing fabricated at low temperature, Solar Energy Materials & Solar Cells, 91, 290–303

Wang J.Y., Yu C.M., Hwan S.C., Ho K.C., Chen L.C., (2008), Influence of coloring voltage on the optical performance and cycling stability of a polyaniline–indium hexacyanoferrate electrochromic system, Solar Energy Materials & Solar Cells, 92, 112–119

Wang L., Gwilliam J., Jones P., (2009), Case study of zero energy house design in UK, Energy and Buildings, 41, 1215–1222

Wang N., Magdassi S., Mandler D., Long Y., (2013), Simple sol–gel process and one-step annealing of vanadium dioxide thin films: synthesis and thermochromic properties, Thin Solid Films, 534, 594-598

Wang X., Chen D., Ren Z., (2010), Assessment of climate change impact on residential building heating and cooling energy requirement in Australia, Building and Environment, 45, 1663–1682

Wang X., Chen D., Ren Z., (2011), Global warming and its implication to emission reduction strategies for residential buildings, Building and Environment, 46, 871-883

Watanabe H., (1998), Intelligent window using a hydrogel layer for energy efficiency, Solar Energy Materials & Solar Cells, 54, 203-211

Weakliem H.A., Redfield D., (1979), Temperature dependence of the optical properties of silicon, Journal of Applied Physics, 50, 1491–1493

Weber W.H., Lambe J., (1976), Luminescent greenhouse collector for solar Radiation, Applied Optics, 15, 2299

Weinlader H., Beck A., Fricke J., (2005), PCM-facade-panel for daylighting and room heating, Solar Energy, 78, 177–186

Wienold J., Christoffersen J., (2006), Evaluation methods and development of a new glare prediction model for daylight environments with the use of CCD cameras, Energy and Buildings, 38, 743–757

Wienold J., (2009), Dynamic daylight glare, Eleventh International IBPSA Conference, Glasgow, Scotland, July 27-30

Wilde P.D., Voorden M.V.D., (2004), Providing computational support for the selection of energy saving building components, Energy and Buildings, 36, 749–758

Wilson C.F, Simko T.M., Collins R.E., (1998), Heat conduction through the support pillars in vacuum glazing, Solar Energy, 63, 393-406

Wilson L.R., Richards B.S., (2009), Measurement method for photoluminescent quantum yields of fluorescent organic dyes in polymethyl methacrylate for luminescent solar concentrators, Applied Optics, 48, 212–220

Witter V., (1981), Theory of fluorescent planer concentrator and experimental result, Journal of Luminance, 24/25, 873-876

Witter V., Datz M., Ell J., Georg A., Graf W., Walze G., (2004), Gasochromic windows, Solar Energy Materials & Solar Cells, 84, 305–314

Woodworth J.R., Thomas M.G., Stevens J.W., Harrington S.R., Dunlop J.P., Swamy M.R., Demetrius L., (1994), Evaluation of the Batteries and Charge controllers in Small Stand Alone Photovoltaics Systems, Presented at the 24th IEEE Photovoltaic Specialists Conference, Dec. 5-9, Hawaii

Wouters P., Vandaele L., Voit P., Fischt N., (1993), The use of outdoor test cells for thermal and solar building research within the PASSYS project, Building and Environment, 28, 107-113

Wright J.L., (1986), Effective U-values and shading coefficients of preheat/ supply air glazing systems, in: Proceedings of the Renewable Energy Conference, Winnipeg, Manitob

Wu J.J., Hsieh M.D., Liao W.P., Wu W.T., Chen J.S., (2009), Fast-switching photovoltachromic cells with tunable transmittance, ACS Nano, 3, 2297–2303.

Wullschleger L., Manz H., Wakili K.G., (2009), Finite element analysis of temperature-induced deflection of vacuum glazing, Construction and Building Materials, 23, 1378–1388

Xinga Y., Hewitt N., Griffiths P., (2011), Zero carbon buildings refurbishment—A Hierarchical pathway, Renewable and Sustainable Energy Reviews, 15, 3229–3236

Xu C., Liu L., Legenski S.E., Ning D., Taya M., (2004), Switchable window based on electrochromic polymers, Journal of Materials Research, 19, 2072-2080

Yadav Y.P., Tiwari G.N., Sucheta S., (1989), Analytical study of a ground collector integrated with heat exchanger Energy Conversion and Management, 29, 245–251

Yan F., Noble J., Peltola J., Wicks S., Balasubramanian S., (2013), Semitransparent OPV modules pass environmental chamber test requirements, Solar Energy Material & Solar Cells, 114, 214–218

Yao J., Zhu N., (2012), Evaluation of indoor thermal environmental, energy and daylighting performance of thermotropic windows, Building and Environment, 49, 283–290

Ye H., Meng X., Xu B., (2012), Theoretical discussions of perfect window, ideal near infrared solar spectrum regulating window and current thermochromic window, Energy and Buildings, 49, 164–172

Ye H., Long L., Zhang H., Xu B., Gao Y., Kang L., Chen Z., (2013), The demonstration and simulation of the application performance of the vanadium dioxide single glazing, Solar Energy Material & Solar Cells, 117, 168–173

Yildiz Y., Arsan Z.D., (2011), Identification of the building parameters that influence heating and cooling energy loads for apartment buildings in hot-humid climates, Energy, 36, 4287–4296

Yi H., (2015), Clean-energy policies and electricity sector carbon emissions in the U.S. states, Utilities Policy, 34, 19–29

Yoon J.H., Shim S.R., An Y.S., Lee K.H., (2013), An experimental study on the annual surface temperature characteristics of amorphous silicon BIPV window, Energy and Buildings, 62, 166–175

Yoshimura K., Yamada Y., Bao S., Tajima K., Okada M., (2009), Preparation and characterization of gasochromic switchable-mirror window with practical size, Solar Energy Materials & Solar Cells, 93, 2138–2142

Yuill G.K., (1987), Laminar airflow super window, Renewable Energy Branch, Energy Mines and Resources, Canada

Zacharopoulos A., Eames P.C., McLarnon D., Norton B., (2000), Linear dielectric non imaging concentrating covers for PV integrated building facades, Solar Energy, 68, 439–452

Zain-Ahmed A., Sopian K., Othman M.Y.H., Sayigh A.A.M., Surendran P.N., (2002), Daylighting as a passive solar design strategy in tropical buildings: a case study of Malaysia, Energy Conversion and Management, 43, 1725–1736

Zegaoui A., Petit P., Aillerie M., Sawicki J.P., Belarbi A.W., Krachai M.D., Charles J.P., (2011), Photovoltaic cell/panel/array characterizations and modelling considering both reverse and direct modes, Energy Procedia, 6, 695-703

Zhang W., Lin J., Yu T., Lin S., Yang D., (2003), Effect of electric field on phase separation of polymer dispersed liquid crystal, European Polymer Journal, 39, 1635–1640

Zhao Y., Meek G.A., Levine B.G., Lunt R.R., (2014), Near infra-red harvesting transparent LSC, Advanced Optical Material, 2, 606–611

Zhao J., Luo S., Zhang X., Xu W., (2013), Preparation of a transparent supporting spacer array for vacuum glazing, Vacuum, 93, 60-64

Zhao J.F., Eames P.C., Hyde T.J., Fang Y., Wang J., (2007), A modified pump-out technique used for fabrication of low temperature metal sealed vacuum glazing, Solar Energy, 81, 1072–1077

Zhuang L., Xu X., Shen H., (2003), A study on the gasochromic properties of WO_3 thin films, Surface and Coatings Technology, 167, 217–220

Zhou D., Zhao C.Y., Tian Y., (2012), Review on thermal energy storage with phase change materials (PCMs) in building applications, Applied Energy, 92, 593–605

Zoller F., (1924), Hollow pane of glass, German patent no 387655

Zuo J., Zhao Z.Y., (2014), Green building research–current status and future agenda: A review, Renewable and Sustainable Energy Reviews, 30, 271–281

Zrinyi M., Szilagyi A., Filipcsei G., (2001), Smart gel–glass based on the responsive properties of polymer gels, Polymer Advanced Technology, 12, 501–505

List of publications

Journal Publication

1. Ghosh A., Norton B., Duffy A., (2015), ***Measured overall heat transfer coefficient of a suspended particle device switchable glazing.*** Applied Energy, 159, 362-369

2. Ghosh A., Norton B., Duffy A., (2016), ***Measured thermal performance of a combined suspended particle switchable device evacuated glazing,*** Applied Energy, 169, 469-480

3. Ghosh A., Norton B., Duffy A., (2016), ***Daylighting performance and glare calculation of a suspended particle device switchable glazing,*** Solar Energy, 132, 114-128

4. Ghosh A., Norton B., Duffy A., ***First outdoor characterization of a PV powered suspended particle device switchable window,*** Applied Energy, (Under Review)

5. Ghosh A., Norton B., Duffy A., ***Measured thermal and daylighting performance of an evacuated glazing using an outdoor test cell*** , Applied Energy, (Under Review)

6. Ghosh A., Norton B., Duffy A., ***Dynamic thermal behaviour of a suspended particle device switchable glazing, in an outdoor test cell maintained at a constant temperature,*** Applied Energy (Under Review)

Conference Publication

1. Ghosh A., Norton B., Duffy A., (2014), Multifunctional Glazing System: Solution for Modern Smart Glazing. Sustainable habitat for developing societies: choosing the way forward: *Plea 2014*, CEPT University, Ahmedabad, India, December 15-18

2. Ghosh A., Norton B. Duffy A., (2013), Conceptualization of a Photovoltaic Powered Electrochromic Switching of a Multifunctional Glazing, *ISES Solar World Congress 2013*, Cancun, Mexico , November 3-9

3. Ghosh A, Norton B., Duffy A., (2013), Calculation of Colouration Voltage for a Multifunctional Glazing Powered by Photovoltaic, *28th EU PVSEC*, Paris, France, 30th September